Projections of Future Physical and Biogeochemical Conditions in the Northwest Atlantic from CMIP5 Global Climate Models

Lavoie, D., N. Lambert, S. ben Mustapha and A. van der Baaren

Fisheries and Oceans Canada
Pelagic and Ecosystem Science Branch
Maurice-Lamontagne Institute
C.P. 1000, 850 route de la mer
Mont-Joli (Québec)
G5H 3Z4

2013

Canadian Technical Report of Hydrography and Ocean Sciences 285

Fisheries and Oceans Canada   Pêches et Océans Canada

Canada

Canadian Technical Report of Hydrography and Ocean Sciences

Technical reports contain scientific and technical information of a type that represents a contribution to existing knowledge but which is not normally found in the primary literature. The subject matter is generally related to programs and interests of the Oceans and Science sectors of Fisheries and Oceans Canada.

Technical reports may be cited as full publications. The correct citation appears above the abstract of each report. Each report is abstracted in the data base *Aquatic Sciences and Fisheries Abstracts.*

Technical reports are produced regionally but are numbered nationally. Requests for individual reports will be filled by the issuing establishment listed on the front cover and title page.

Regional and headquarters establishments of Ocean Science and Surveys ceased publication of their various report series as of December 1981. A complete listing of these publications and the last number issued under each title are published in the *Canadian Journal of Fisheries and Aquatic Sciences*, Volume 38: Index to Publications 1981. The current series began with Report Number 1 in January 1982.

Rapport technique canadien sur l'hydrographie et les sciences océaniques

Les rapports techniques contiennent des renseignements scientifiques et techniques qui constituent une contribution aux connaissances actuelles mais que l'on ne trouve pas normalement dans les revues scientifiques. Le sujet est généralement rattaché aux programmes et intérêts des secteurs des Océans et des Sciences de Pêches et Océans Canada.

Les rapports techniques peuvent être cités comme des publications à part entière. Le titre exact figure au-dessus du résumé de chaque rapport. Les rapports techniques sont résumés dans la base de données *Résumés des sciences aquatiques et halieutiques.*

Les rapports techniques sont produits à l'échelon régional, mais numérotés à l'échelon national. Les demandes de rapports seront satisfaites par l'établissement auteur dont le nom figure sur la couverture et la page de titre.

Les établissements de l'ancien secteur des Sciences et Levés océaniques dans les régions et à l'administration centrale ont cessé de publier leurs diverses séries de rapports en décembre 1981. Vous trouverez dans l'index des publications du volume 38 du *Journal canadien des sciences halieutiques et aquatiques*, la liste de ces publications ainsi que le dernier numéro paru dans chaque catégorie. La nouvelle série a commencé avec la publication du rapport numéro 1 en janvier 1982.

Canadian Technical Report of
Hydrography and Ocean Sciences 285

2013

Projections of future physical and biogeochemical conditions in the Northwest Atlantic from CMIP5 Global Climate Models

by

Diane Lavoie, Nicolas Lambert, Sélima Ben Mustapha and Augustine van der Baaren

Fisheries and Oceans Canada
Pelagic and Ecosystem Science Branch
Maurice-Lamontagne Institute
C.P. 1000, 850 route de la mer
Mont-Joli (Québec)
G5H 3Z4

© Her Majesty the Queen in Right of Canada, 2013.

Cat. No. Fs 97-18/285E-PDF ISSN 1488-5417 (on-line version)

Correct citation for this publication:

Lavoie, D., N. Lambert, S. Ben Mustapha and A. van der Baaren. 2013. Projections of future physical and biogeochemical conditions in the Northwest Atlantic from CMIP5 Global Climate Models. Can. Tech. Rep. Hydrogr. Ocean Sci. 285: xiv + 156p.

Table of content

Table of content iii
List of Tables iv
List of Figures v
List of Appendices xi
Abstract xiii
Résumé xiv
1 Introduction 1
  1.1 Descriptions of models and experiments 1
    1.1.1 CanESM2 2
    1.1.2 GFDL-ESM2M 2
    1.1.3 HadGEM2-ES 2
    1.1.4 IPSL-CM5A-LR 3
    1.1.5 MPI-ESM-LR 3
  1.2 Method 4
2 Results 4
  2.1 Labrador Sea 4
    2.1.1 Historical trends 5
      2.1.1.1 Sea surface salinity 5
      2.1.1.2 Sea surface temperature 5
      2.1.1.3 Sea ice 6
      2.1.1.4 Mixed layer depth 6
      2.1.1.5 Nitrate 7
      2.1.1.6 Primary Production 7
      2.1.1.7 Chl a 8
      2.1.1.8 Oxygen 8
      2.1.1.9 Ocean acidification 9
    2.1.2 Future trends (next 50 years) 10
  2.2 Atlantic Northwest 12
    2.2.1 Historical trends 12
      2.2.1.1 Sea surface salinity 12
      2.2.1.2 Sea surface temperature 13
      2.2.1.3 Sea ice 13
      2.2.1.4 Mixed layer depth 13
      2.2.1.5 Nitrate 14
      2.2.1.6 Primary Production 14
      2.2.1.7 Chl a 15
      2.2.1.8 Oxygen 15
      2.2.1.9 Ocean acidification 15
    2.2.2 Future trends 16
3 Discussion and Conclusion 19
4 Acknowledgements 20
5 References 20
Appendix I 135
Appendix II: Figures of bidecadal changes 136

List of Tables

Table 1. Identification of the models and institutions that supplied the output data used in this study. 1

List of Figures

Figure 1. Regions selected for trend analysis with position of transects. The Labrador Sea transect corresponds to the ARW7 line. 28

Figure 2. Bathymetry of the Labrador Sea in the different models and bathymetry from the General Bathymetric Chart of the Oceans (GEBCO, www.gebco.net). 29

Figure 3. Mean simulated sea surface salinity in the Labrador Sea for the historical period (1960-2005) and annual sea surface salinity from the World Ocean Atlas (WOA; Antonov et al., 2010). 30

Figure 4. Average sea surface salinity trends (per decade) over the Labrador Sea (see box in Figure 1) for the historical period (1960-2005). 31

Figure 5. Sea surface salinity trends (in decade^{-1}) at each grid cell in the Labrador Sea for the historical period (1960-2005). 32

Figure 6. Mean simulated sea surface temperature in the Labrador Sea for the historical period (1960-2005) and annual sea surface temperature from the World Ocean Atlas (WOA; Locarnini et al., 2010). 33

Figure 7. Average sea surface temperature trends (°C/decade) over the Labrador Sea for the historical period (1960-2005). 34

Figure 8. Sea surface temperature trend (°C/decade) at each grid cell in the Labrador Sea for the historical period (1960-2005). 35

Figure 9 : Average sea ice concentration in the Labrador Sea for the months of November, March and June for the historical period (1979-2000) and for the 5 GCMs. The magenta line represents the median extent (15% limit) measured by Fetterer et al. (2009) for the same period. 36

Figure 10. Sea ice concentration trends (%/decade) at each grid cell in Labrador Sea for the months of November, March, and June for the historical period (1960-2005) and for the 5 GCMs. 37

Figure 11. Annual mean simulated mixed layer depth in the Labrador Sea for the historical period (1960-2005). 38

Figure 12. Annual mean mixed layer depth trends (m/decade) over the Labrador Sea for the historical period (1960-2005). 39

Figure 13. Ocean mixed layer thickness trends (m/decade) in the Labrador Sea for the historical period (1960-2005). 40

Figure 14. Annual mean simulated nitrate concentration at the surface of the Labrador Sea for the historical period (1960-2005) and nitrate concentration at the surface from the World Ocean Atlas (WOA; Garcia et al., 2010b). 41

Figure 15. Average nitrate concentration trends (mmol m^{-3}/decade) at the surface over the Labrador Sea for the historical period (1960-2005). 42

Figure 16. Average nitrate concentration trends (mmol m^{-3}/decade) at 100-400 m over the Labrador Sea for the historical period (1960-2005). 42

Figure 17. Nitrate concentration trends (mmol m^{-3}/decade) at the surface at each grid cell in the Labrador Sea for the historical period (1960-2005). 43

Figure 18. Nitrate concentration trends (mmol m^{-3}/decade) at 100-400 m at each grid cell in the Labrador Sea for the historical period (1960-2005). 44

Figure 19. Mean vertically integrated primary production in the Labrador Sea for the historical period (1960-2005). 45
Figure 20. Average vertically integrated primary production trends (mol C m^{-2}/yr) over the Labrador Sea for the historical period (1960-2005). 46
Figure 21. Vertically integrated primary production trend (mol C m^{-2}/decade) at each grid cell in the Labrador Sea for the historical period (1960-2005). 47
Figure 22. Mean simulated Chl a concentration from GCMs and Ch al data from SeaWiFS in the Labrador Sea for the 1998-2005 period. 48
Figure 23. Average Chl a concentration trends (mg m^{-3}/decade) at the surface over the Labrador Sea for the historical period (1960-2005). 49
Figure 24. Chl a concentration trends (mg m^{-3}/decade) at the surface at each grid cell in the Labrador Sea for the SeaWiFS period (1960-2005). 50
Figure 25. Mean simulated dissolved oxygen concentration in the Labrador Sea for the historical period (1960-2005) and dissolved oxygen concentration at the surface from the World Ocean Atlas (WOA; Garcia et al., 2010a). 51
Figure 26. Average dissolved oxygen concentration trends (mol m^{-3}/decade) at the surface over the Labrador Sea for the 1985-2005 period. 52
Figure 27. Average dissolved oxygen concentration trends (mol m^{-3}/decade) at 100-400 m over the Labrador Sea for the 1990-2005 period. 52
Figure 28. Dissolved oxygen concentration trends (mol m^{-3}/decade) at the surface at each grid cell in the Labrador Sea for the 1985-2005 period. 53
Figure 29. Dissolved oxygen concentration trends (mol m^{-3}/decade) at 100-400 at each grid cell in the Labrador Sea for the 1990-2005 period. 54
Figure 30. Mean simulated dissolved inorganic carbon concentration in the Labrador Sea for the historical period (1960-2005). 55
Figure 31. Average DIC concentration trends (mol m^{-3}/decade) at the surface over the Labrador Sea for the historical period (1960-2005). 56
Figure 32. Average DIC concentration trends (mol m^{-3}/decade) at 100-400 m over the Labrador Sea for the 1990-2005 period. 56
Figure 33. DIC concentration trends (mol m^{-3}/decade) at 100-400 m at each grid cell in the Labrador Sea for the 1990-2005 period. 57
Figure 34. Mean simulated pH at the surface of the Labrador Sea for the historical period (1960-2005). 58
Figure 35. Average surface pH trends (per decade) over the Labrador Sea for the historical period (1960-2005). 59
Figure 36. Average pH trends (per decade) at 100-400 m over the Labrador Sea for the 1990-2005 period. 59
Figure 37. Future sea surface salinity trends (per decade) in the Labrador Sea for the 2012-2062 period for RCPs 4.5 and 8.5. 60
Figure 38. Future salinity trends (per decade) at 100-400 m in the Labrador Sea for the 2012-2062 period for RCPs 4.5 and 8.5. 61
Figure 39. Future sea surface temperature trends (°C/decade) in the Labrador Sea for the 2012-2062 period for RCPs 4.5 and 8.5. 62
Figure 40. Future sea ice concentration trends (%/decade) in the Labrador Sea for the 2012-2062 period for RCP 4.5. 63

Figure 41. Future sea ice concentration trends (%/decade) in the Labrador Sea for the 2012-2062 period for RCP 8.5. 64
Figure 42. Future ocean mixed layer depth trends (m/decade) in the Labrador Sea for the 2012-2062 period for RCPs 4.5 and 8.5. 65
Figure 43. Future nitrate concentration trends (mmol m^{-3}/decade) at 50-100 m in the Labrador Sea for the 2012-2062 period for RCPs 4.5 and 8.5. 66
Figure 44. Future nitrate concentration trends (mmol m^{-3}/decade) at 100-400 m in the Labrador Sea for the 2012-2062 period for RCPs 4.5 and 8.5. 67
Figure 45. Future nitrate concentration trends (mmol m^{-3}/decade) at each grid cell at 100-400 m in the Labrador Sea for the 2012-2062 period for RCP 8.5. 68
Figure 46. Future vertically integrated primary production trends (mol C m^{-2}/decade) in the Labrador Sea for the 2012-2062 period for RCPs 4.5 and 8.5. 69
Figure 47. Future Chl a concentration trends (mg m^{-3}/decade) at the surface in the Labrador Sea for the 2012-2062 period for RCPs 4.5 and 8.5. 70
Figure 48. Future Chl a concentration trends (mg m^{-3}/decade) at 50-100 m in the Labrador Sea for the 2012-2062 period for RCPs 4.5 and 8.5. 71
Figure 49. Future oxygen concentration trends (mol m^{-3}/decade) at the surface in the Labrador Sea for the 2012-2062 period for RCPs 4.5 and 8.5. 72
Figure 50. Future oxygen concentration trends (mol m^{-3}/decade) at 100-400 m in the Labrador Sea for the 2012-2062 period for RCPs 4.5 and 8.5. 73
Figure 51. Future DIC concentration trends (mol m^{-3}/decade) at the surface in the Labrador Sea for the 2012-2062 period for RCPs 4.5 and 8.5. 74
Figure 52. Future DIC concentration trends (mol m^{-3}/decade) at 100-400 m in the Labrador Sea for the 2012-2062 period for RCPs 4.5 and 8.5. 75
Figure 53. Future pH trends (per decade) at the surface m in the Labrador Sea for the 2012-2062 period for RCPs 4.5 and 8.5. 76
Figure 54. Future pH trends (per decade) at 100-400 m in the Labrador Sea for the 2012-2062 period for RCPs 4.5 and 8.5. 77
Figure 55. Future aragonite saturation horizon depth in the Labrador Sea for the 2012-2062 period for RCPs 4.5 and 8.5. 78
Figure 56. Bathymetry of the AtlNW region (see Figure 1) in the different models and bathymetry from the General Bathymetric Chart of the Oceans (GEBCO). 79
Figure 57. Mean simulated sea surface salinity in the AtlNW region for the historical period (1960-2005) compared with sea surface salinity from the World Ocean Atlas (WOA; Antonov et al., 2010). 80
Figure 58. Average sea surface salinity trends (per decade) over the AtlNW region for the historical period (1960-2005). 81
Figure 59. Sea surface salinity trends (per decade) at each grid cell in the AtlNW region for the historical period (1960-2005). 82
Figure 60. Mean simulated sea surface temperature in the AtlNW region for the historical period (1960-2005) compared with sea surface temperature from the World Ocean Atlas (WOA; Locarnini et al., 2010). 83
Figure 61. Average sea surface temperature trends (°C/decade) over the AtlNW region for the historical period (1960-2005). 84
Figure 62. Sea surface temperature trends (°C/decade) at each grid cell in the AtlNW region for the historical period (1960-2005). 85

Figure 63. Average sea ice concentration in the Atlantic Northwest for the months of January, March and April for the historical period (1971-2000) and for the 5 GCMs. The purple line represents the median extent (15% limit) measured by Fetterer et al. (2009) for the same period. 86
Figure 64. Sea ice concentration trends (%/decade) at each grid cell in Labrador Sea for the months of January, March, and April for the historical period (1960-2005) and for the 5 GCMs. 87
Figure 65. Annual mean mixed layer depths in the AtlNW region for the historical period (1960-2005). Upper right corner around 800 m for MPI and 400 m for GFDL. 88
Figure 66. Annual mean mixed layer depth trends (m/decade) over the AtlNW region for the historical period (1960-2005). 89
Figure 67. Annual mean mixed layer depth trends (m/decade) at each grid cell in the AtlNW region for the historical period (1990-2005). 90
Figure 68. Mean simulated nitrate concentration at the surface in the AtlNW region for the historical period (1960-2005) compared with nitrate concentration at the surface from the World Ocean Atlas (Garcia et al., 2010b). 91
Figure 69. Mean simulated nitrate concentration at 100-400 m in the AtlNW region for the historical period (1960-2005) compared with nitrate concentration at 100-400 m from the World Ocean Atlas (Garcia et al., 2010b). 92
Figure 70. Average nitrate concentration trends (mmol m^{-3}/decade) at the surface over the AtlNW region for the historical period (1960-2005). 93
Figure 71. Average nitrate concentration trends (mmol m^{-3}/decade) at 100-400 m over the AtlNW region for the historical period (1960-2005). 93
Figure 72. Nitrate concentration trends (mmol m^{-3}/decade) at the surface at each grid cell in the AtlNW region for the historical period (1960-2005). 94
Figure 73. Nitrate concentration trends (mmol m^{-3}/decade) at 100-400 at each grid cell in the AtlNW region for the historical period (1960-2005). 95
Figure 74. Mean vertically integrated primary production in the AtlNW region for the historical period (1960-2005). Saturated value with CanESM2 range between 35-40 molC m^{-2} $year^{-1}$. 96
Figure 75. Average vertically integrated primary production trends (mol C m^{-2}/decade) at the surface in the AtlNW region for the historical period (1960-2005). 97
Figure 76. Vertically integrated primary production trends (mol C m^{-2}/decade) at each grid cell in the AtlNW region for the historical period (1960-2005). 98
Figure 77. Mean simulated Chl a concentrations and Chlorophyll data from SeaWiFS in the AtlNW region for the historical period (1998-2005). 99
Figure 78. Average Chl a concentration trends (mg m^{-3}/decade) at the surface in the AtlNW region for the historical period (1960-2005). 100
Figure 79. Surface Chl a concentration trends (mg m^{-3}/decade) at each grid cell in the AtlNW region for the SeaWiFS period (1960-2005). 101
Figure 80. Mean simulated dissolved oxygen concentration at the surface in the AtlNW region for the historical period (1960-2005) and dissolved oxygen concentration at the surface from the World Ocean Atlas (Garcia et al., 2010a). 102
Figure 81. Mean simulated dissolved oxygen concentration at 100-400 m in the AtlNW region for the historical period (1960-2005) and dissolved oxygen concentration at 100-400 m from the World Ocean Atlas (Garcia et al., 2010a). 103

Figure 82. Average oxygen concentration trends (mol m^{-3}/decade) at the surface in the AtlNW region for the historical period (1960-2005). 104
Figure 83. Average oxygen concentration trends (mol m^{-3}/decade) at 100-400 m in the AtlNW region for the historical period (1960-2005). 104
Figure 84. Surface oxygen concentration trends (mol m^{-3}/decade) at each grid cell in the AtlNW region for the 1980-2005 period. 105
Figure 85. Oxygen concentration trends (mol m^{-3}/decade) at 100-400 m at each grid cell in the AtlNW region for the 1980-2005 period. 106
Figure 86. Mean simulated dissolved inorganic carbon concentration in the AtlNW region for the historical period (1960-2005). 107
Figure 87. Average DIC concentration trends (mol m^{-3}/decade) at the surface in the AtlNW region for the historical period (1960-2005). 108
Figure 88. Dissolved inorganic carbon concentration trends (mol m^{-3}/decade) at the surface at each grid cell in the AtlNW region for the historical period (1960-2005). 109
Figure 89. Mean simulated surface pH in the AtlNW region for the historical period (1960-2005). 110
Figure 90. Average pH trends (mol m^{-3}/decade) at the surface in the AtlNW region for the historical period (1960-2005). 111
Figure 91. Average aragonite saturation horizon depth trends (m/decade) in the AtlNW region for the historical period (1960-2005). 111
Figure 92. Future sea surface salinity trends (per decade) in the AtlNW region for the 2012-2062 period for RCPs 4.5 and 8.5. 112
Figure 93. Future sea surface salinity trends (per decade) at each grid cell in the AtlNW region for the 2012-2062 period for RCP 4.5. 113
Figure 94. Future sea surface salinity trends (per decade) at each grid cell in the AtlNW region for the 2012-2062 period for RCP 8.5. 114
Figure 95. Future sea surface temperature trends (°C/decade) in the AtlNW region for the 2012-2062 period for RCPs 4.5 and 8.5. 115
Figure 96. Future sea surface temperature trends (°C/decade) at each grid cell in the AtlNW region for the 2012-2062 period for RCP 8.5. 116
Figure 97. Future sea ice concentration trends (%/decade) in the Labrador Sea for the 2012-2062 period for RCP 4.5. 117
Figure 98. Future sea ice concentration trends (%/decade) in the Labrador Sea for the 2012-2062 period for RCP 8.5. 118
Figure 99. Future mixed layer depth trends (m/decade) in the AtlNW region for the 2012-2062 period for RCPs 4.5 and 8.5. 119
Figure 100. Future mixed layer depth trends (m/decade) per grid cell in the AtlNW region for the 2012-2062 period for RCP 8.5. 120
Figure 101. Future nitrate concentration trends (mmol m^{-3}/decade) at 50-100 m in the AltNW region for the 2012-2062 period for RCPs 4.5 and 8.5. 121
Figure 102. Future nitrate concentration trends (mmol m^{-3}/decade) at 50-100 m at each grid cell in the AtlNW for the 2012-2062 period for RCP 4.5. 122
Figure 103. Future nitrate concentration trends (mmol m^{-3}/decade) at 50-100 m at each grid cell in the AtlNW for the 2012-2062 period for RCP 8.5. 123

Figure 104. Future nitrate concentration trends (mmol m^{-3}/decade) at 100-400 m at each grid cell in the AtlNW for the 2012-2062 period for RCP 8.5. 124
Figure 105. Future vertically integrated primary production trends (mol C m^{-2}/decade) in the AltNW region for the 2012-2062 period for RCPs 4.5 and 8.5. 125
Figure 106. Future Chl a concentration trends (mg m^{-3}/decade) at the surface in the AtlNW region for the 2012-2062 period for RCPs 4.5 and 8.5. 126
Figure 107. Future Chl a concentration trends (mg m^{-3}/decade) at 50-100 m in the AtlNW region for the 2012-2062 period for RCPs 4.5 and 8.5.. 127
Figure 108. Future oxygen concentration trends (mol m^{-3}/decade) at the surface in the AtlNW region for the 2012-2062 period for RCPs 4.5 and 8.5. 128
Figure 109. Future oxygen concentration trends (mol m^{-3}/decade) at 100-400 m in the AtlNW region for the 2012-2062 period for RCPs 4.5 and 8.5. 129
Figure 110. Future DIC concentration trends (mol m^{-3}/decade) at the surface in the AtlNW region for the 2012-2062 period for RCPs 4.5 and 8.5. 130
Figure 111. Future DIC concentration trends (mol m^{-3}/decade) at 100-400 m in the AtlNW region for the 2012-2062 period for RCPs 4.5 and 8.5. 131
Figure 112. Future pH trends (per decade) at the surface in the AtlNW region for the 2012-2062 period for RCPs 4.5 and 8.5. 132
Figure 113. Future pH trends (per decade) at 100-400 m in the AtlNW region for the 2012-2062 period for RCPs 4.5 and 8.5. 133
Figure 114. Future aragonite saturation depth trends (m/decade) in the AtlNW region for the 2012-2062 period for RCPs 4.5 and 8.5.. 134

List of Appendices

Appendix I-1. Multi-model ensemble mean trends over the next 50 years for the different variables at the surface, in the 50-100 m layer, and in the 100-400 m layer for the two scenarios (RCPs 4.5 and 8.5). 135

Figure II- 1. Mean simulated nitrate concentration along the Labrador Sea transect for the historical period (1986-2005). 136
Figure II- 2. Bidecadal changes (2046-2065 average minus 1986-2005 average) in nitrate concentration along the Labrador Sea transect for RCP 8.5. 136
Figure II- 3. Mean simulated Chl a concentration (mg m^{-3}) along the Labrador Sea transect for the historical period (1986-2005). 137
Figure II- 4. Bidecadal changes (2046-2065 average minus 1986-2005 average) in Chl a concentration along the Labrador Sea transect for RCP 8.5. 137
Figure II- 5. Mean simulated dissolved oxygen concentration along the Labrador Sea transect for the historical period (1986-2005). 138
Figure II- 6. Bidecadal changes (2046-2065 average minus 1986-2005 average) in dissolved oxygen concentration along the Labrador Sea transect for RCP 8.5. 138
Figure II- 7. Mean simulated dissolved inorganic carbon concentration along the Labrador Sea transect for the historical period (1986-2005). 139
Figure II- 8. Bidecadal changes (2046-2065 average minus 1986-2005 average) in dissolved inorganic carbon concentration along the Labrador Sea transect for RCP 8.5. 139
Figure II- 9. Mean simulated pH along the Labrador Sea transect for the historical period (1960-2005). 140
Figure II- 10. Bidecadal changes (2046-2065 average minus 1986-2005 average) in pH along the Labrador Sea transect for RCP 8.5. 140
Figure II- 11. Mean simulated nitrate concentration along the AtlNW transect for the historical period (1986-2005). 141
Figure II- 12. Bidecadal changes (2046-2065 average minus 1986-2005 average) in nitrate concentration along the AtlNW region transect for RCP 8.5. 141
Figure II- 13. Mean simulated Chl a concentration along the AtlNW region transect for the historical period (1986-2005). 142
Figure II- 14. Bidecadal changes (2046-2065 average minus 1986-2005 average) in Chl a concentration along the AtlNW region transect for RCP 8.5. 142
Figure II- 15. Mean simulated dissolved oxygen concentration along the AtlNW transect for the historical period (1986-2005). 143
Figure II- 16. Bidecadal changes (2046-2065 average minus 1986-2005 average) in dissolved oxygen concentration along the AtlNW region transect for RCP 8.5. 143
Figure II- 17. Mean simulated dissolved inorganic carbon concentration along the AtlNW transect for the historical period (1986-2005). 144
Figure II- 18. Bidecadal changes (2046-2065 average minus 1986-2005 average) in dissolved inorganic carbon concentration along the AtlNW region transect for RCP 8.5. 144
Figure II- 19. Mean simulated pH along the AtlNW transect for the historical period (1986-2005). 145

Figure II- 20. Bidecadal changes (2046-2065 average minus 1986-2005 average) in pH along the AtlNW region transect for RCP 8.5. 145
Figure II- 21. Bidecadal means (1966-1985 to 2066-2085) of simulated nitrate concentration at the surface with CanESM2 for the RCP 8.5 scenario. 146
Figure II- 22. Bidecadal means (1966-1985 to 2066-2085) of simulated nitrate concentration at the surface with GFDL for the RCP 8.5 scenario. 147
Figure II- 23. Bidecadal means (1966-1985 to 2066-2085) of simulated nitrate concentration at the surface with HadGEM2 for the RCP 8.5 scenario. 148
Figure II- 24. Bidecadal means (1966-1985 to 2066-2085) of simulated nitrate concentration at the surface with IPSL for the RCP 8.5 scenario. 149
Figure II- 25. Bidecadal means (1966-1985 to 2066-2085) of simulated nitrate concentration at the surface with MPI for the RCP 8.5 scenario. 150
Figure II- 26. Bidecadal means (1966-1985 to 2066-2085) of simulated pH at the surface with CanESM2 for the RCP 8.5 scenario. 151
Figure II- 27. Bidecadal means (1966-1985 to 2066-2085) of simulated pH at the surface with GFDL for the RCP 8.5 scenario. 152
Figure II- 28. Bidecadal means (1966-1985 to 2066-2085) of simulated pH at the surface with HadGEM2 for the RCP 8.5 scenario. 153
Figure II- 29. Bidecadal means (1966-1985 to 2066-2085) of simulated pH at the surface with IPSL for the RCP 8.5 scenario. 154
Figure II- 30. Bidecadal means (1966-1985 to 2066-2085) of simulated pH at the surface with MPI for the RCP 8.5 scenario. 155
Figure II- 31. Bidecadal means (1966-1985 to 2066-2085) of aragonite saturation horizon depth with CanESM2 for the RCP 8.5 scenario. 156

Abstract

Lavoie, D., N. Lambert, S. Ben Mustapha and A. van der Baaren. 2013. Projections of future physical and biogeochemical conditions in the Northwest Atlantic from CMIP5 Global Climate Models. Can. Tech. Rep. Hydrogr. Ocean Sci. 285: xiv + 156 p.

Results from the new generation of global climate models were made available for the fifth assessment report (AR5) of the Intergovernmental Panel on Climate Change (IPCC) through the Coupled Model Intercomparison Project Phase 5 (CMIP5) archive. The outputs from five of these models were analyzed as a contribution to the climate change risk assessment analysis for the Atlantic Large Aquatic Basin (LAB) as part of the Aquatic Climate Change Adaptation Services Program (ACCASP). A comparison of simulated and observed trends was made for the historical period (between 1960 and 2005) when possible for sea surface temperature, sea surface salinity, mixed layer depth, sea ice concentration, nitrate concentration, primary production, chlorophyll a, dissolved oxygen, dissolved inorganic carbon, pH, and aragonite and calcite saturation horizon depths. Multi-model ensemble mean projections were then calculated for the next 50 years with two different scenarios (RCP 4.5 and RCP 8.5). The models present consistent future trends for dissolved inorganic carbon (increase), dissolved oxygen (decrease), pH (decrease), and variable trends for nitrate concentration although negative in general (leading us to conclude to a possible decrease), while for chlorophyll a and primary production, no firm conclusions can be drawn in the regions under study due to large differences in the trends from one model to another.

Résumé

Lavoie, D., N. Lambert, S. Ben Mustapha and A. van der Baaren. 2013. Projections of future physical and biogeochemical conditions in the Northwest Atlantic from CMIP5 Global Climate Models. Can. Tech. Rep. Hydrogr. Ocean Sci. 285: xiv + 156 p.

Les résultats de la nouvelle génération de modèles climatiques globaux sont maintenant disponibles pour la préparation du Cinquième Rapport d'Évaluation (AR5) du Groupe d'experts Intergouvernemental sur l'Évolution du Climat (GIEC) sur le site du 5° Projet d'Inter-Comparaison de Modèles Couplés (CMIP5). Les simulations de cinq modèles ont été analysées en vue de contribuer à l'évaluation des risques liés aux changements climatiques dans le bassin Atlantique pour le Programme sur les Sciences Aquatiques en lien avec l'Adaptation aux Changements Climatiques (PSAACC) de Pêches et Océans Canada. Une comparaison de l'évolution de différentes variables océanographiques simulées et observées a été faite sur la période historique de 1960 à 2005 (lorsque possible), notamment pour la salinité de surface, la température de surface, la profondeur de la couche de mélange, les concentrations de glace de mer, les concentrations de nitrate, d'oxygène dissous, et de carbone inorganique dissous, la production primaire et la chlorophylle a, le pH, et les profondeurs de la lysocline de l'aragonite et de la calcite. Les projections moyennes obtenues à partir de l'ensemble des cinq modèles climatiques ont étés calculés pour les 50 prochaines années avec deux des nouveaux scénarios de forçage du GIEC (RCP 4.5 et RCP 8.5). Les résultats des modèles montrent des tendances futures évidentes pour le carbone inorganique dissous (hausse), l'oxygène dissous (baisse), le pH (baisse), des tendances variables pour les nitrates quoique à la baisse en général, alors que pour la chlorophylle a et la production primaire de larges différences ont été observées d'un modèle à un autre dans les régions à l'étude, nous empêchant de poser un diagnostic fiable.

1 Introduction

This report is a contribution to the climate change risk assessment for the Atlantic Large Aquatic Basin (LAB) requested by Fisheries and Oceans Canada as part of the Aquatic Climate Change Adaptation Services Program (ACCASP). Numerical models are essential tools for obtaining projections of future physical and biochemical conditions in the ocean. Except for the Gulf of St. Lawrence – Scotian Shelf – Gulf of Maine (GSL-SS-GoM) area, regional climate models are not yet available, and we need to rely on Global Climate Models (GCMs) to obtain projections of ocean conditions. GCM projections have formed the basis of the Intergovernmental Panel on Climate Change Fourth Assessment Report (IPCC AR4) and are archived as part of phase 3 of the Coupled Model Intercomparison Project (CMIP3) Project. Many scientific papers have been written with these models' output up to now. However, the simulations produced for the IPCC AR4 do not include biogeochemical components. Simulations from coupled physical-biogeochemical models are now available for the IPCC fifth assessment report (AR5) and are archived as part of CMIP5. The outputs of five models that have a biogeochemical component were available when we undertook this study. We know from the CMIP3 experiment that GCMs have difficulty reproducing the complex dynamics of the Northwest Atlantic and Canadian Arctic Archipelago. However, we will attempt to determine if one or more of these models perform better than others in the regions under study in this report and, although they might produce different absolute values, if the projected trends are similar. We also calculated the multi-model ensemble mean projections for the next 50 years (2012 to 2062).

1.1 Descriptions of models and experiments

We used the CMIP5 multi-model ensemble (http://www-pcmdi.llnl.gov/) that had biochemical components and that were available in spring 2012 (see Table 1).

Table 1. Identification of the models and institutions that supplied the output data used in this study.

Modeling Center (or Group)	Model Name
Canadian Centre for Climate Modelling and Analysis	CanESM2
NOAA Geophysical Fluid Dynamics Laboratory	GFDL-ESM2M
Met Office Hadley Centre	HadGEM2-ES
Institut Pierre-Simon Laplace	IPSL-CM5A-LR
Max Planck Institute for Meteorology	MPI-ESM-LR

Two types of experiments are available under CMIP5 (Taylor et al., 2012): 1) near-term simulations (10- to 30-years), some of which were initialized with observed ocean state and sea ice data, and 2) long-term (out to 2100 and beyond) simulations initialized from the end of freely evolving simulations of the historical period (1850-2005). We use the long-term simulations (2006-2100) of the ensemble member r1i1p1, forced with specified concentrations consistent with a high emissions scenario (RCP 8.5) and a moderate mitigation scenario (RCP 4.5). In the RCP 4.5 scenario, radiative forcing stabilizes at ~4.5W m^{-2} after 2100, while it stabilizes at ~8.5W m^{-2} in the RCP 8.5 scenario. In the rest of the text, the following short names will be used to identify the models: CanESM2, GFDL, HadGEM2, IPSL, and MPI.

1.1.1 CanESM2

The physical ocean component of CanESM2 has 40 levels with approximately 10 m resolution in the upper ocean (Arora et al., 2011). The horizontal resolution of the physical ocean is approximately 1.41° (longitude) × 0.94° (latitude) in CanESM2, compared to 1.87° × 1.87° in CanESM1. The K-profile parameterization of Large et al. (1994) and a tidally-driven mixing parameterization are used. Horizontal friction is represented by the anisotropic viscosity of Large et al. (2001). The sea ice component of CanESM2 uses the atmospheric horizontal grid with a resolution of 2.81°. The sea ice is divided in two vertical layers, one layer of ice and one layer of snow. The growth and melt of the ice is governed by the thermodynamic energy balance (Flato et al., 2000). The Canadian Model of Ocean Carbon (CMOC), the ocean carbon cycle component of CanESM2, incorporates an inorganic chemistry module (solubility pump) and a simple NPZD ecosystem model (organic and carbonate pumps) for simulating the ocean-atmosphere exchange of CO2 (Christian et al., 2010; Zahariev et al., 2008). Dissolved inorganic carbon (DIC) and total alkalinity are prognostic variables while chlorophyll is semi-prognostic.

1.1.2 GFDL-ESM2M

The physical climate formulation and simulation characteristics of GFDL-ESM2M are described by Dunne et al. (2012). This GCM includes different components for each major system (land, atmosphere, ocean, sea ice, and iceberg). The ocean component of GFDL-ESM2M uses a 1° horizontal grid and a tripolar grid above 65°N with 50 verticals levels and a surface layer of 10 m (Griffies et al., 2005). The model uses a K-profile parameterization based on Danabasoglu et al. (2006). GFDL-ESM2M was updated from the previous version by using an isotropic Laplacian friction instead of a horizontal anisotropic friction scheme (Large et al., 2001). The sea ice component of GFDL-ESM2M uses the same horizontal grid as the ocean component with three vertical layers (two ice and one snow layer; Winton, 2000). The ocean biogeochemical component is TOPAZ2 (Tracers of Ocean Phytoplankton with Allometric Zooplankton); a detailed description was made by Dunne et al. (2013). TOPAZ2 simulates biogeochemical cycles (carbon, nitrogen, phosphorus, silicon, iron, oxygen and alkalinity) using 30 prognostic tracers. Three phytoplankton groups are used to define primary production with their own growth functions and limiting factors: small (prokaryotic picoplankton and nanoplankton), large (diatoms) and diazotrophic (nitrogen fixers). Finally, calcite and aragonite formation in TOPAZ2 are diagnostic variables.

1.1.3 HadGEM2-ES

The HadGEM2-ES model and all the HadGEM2 family are described by Johns et al. (2006) and Martin et al. (2011). HadGEM2-ES includes different components (troposphere, land surface and hydrology, aerosols, ocean and sea ice, terrestrial carbon cycle, and ocean biogeochemistry) coupled every day. The ocean component of HadGEM2-ES uses a latitude–longitude grid with a zonal resolution of 1° everywhere and meridional resolution of 1° between the poles and 30° of latitude, after which it changes smoothly to 1/3° at the equator. There are 40 vertical layers with thicknesses of 10 m near the surface. An anisotropic Laplacian viscosity is used (Large et al., 2001). The sea ice model component of HadGEM2-ES uses the same grid as the ocean component and the sea ice is divided into five thickness categories (Hunke and Lipscomb, 2004). The carbon cycle model used by HadGEM2-ES is Diat-HadOCC (Collins et al., 2011). This model is similar to the model described by Palmer and Totterdell (2001) except for the phytoplankton component which was divided into two compartments: diatoms and other phytoplankton. Phytoplankton growth is simulated by a NPZD model that uses nitrogen, iron, and silicon (diatoms) as the limiting nutrients. The aragonite and calcite saturation state are diagnostic variables.

1.1.4 IPSL-CM5A-LR

The different components of IPSL-CM5A-LR are described by Dufresne et al. (2013): atmosphere (LMDZ), ocean (NEMO/OPA), sea ice (NEMO/LIM2), land (ORCHIDEE), chemistry and aerosol (INCA), and stratospheric chemistry (REPROBUS). The OASIS coupler is used to exchange fields between the different components of the model (Dufresne et al., 2013). The ocean model uses a tri-polar global grid (Madec and Imbard, 1996) with a resolution of 2° for most of the grid (a latitudinal grid refinement of 0.5° is used in the tropics) and 31 vertical levels (with thicknesses of 10 m near the surface to 500 m at 5000 m). The sea ice model uses the same horizontal grid as the ocean model with three vertical layers. The biogeochemistry of the ocean is simulated by the PISCES model (Pelagic Interaction Scheme for Carbon and Ecosystem Studies; Aumont and Bopp, 2006). It has 24 compartments, including two phytoplankton groups (nanophytoplankton and diatoms) and five nutrients (nitrate, ammonium, phosphate, silicate and iron).

1.1.5 MPI-ESM-LR

MPI-ESM-LR uses different components to simulate the atmosphere (ECHAM6), the ocean (MPIOM; Marsland et al., 2003), the land surface (JSBACH) and the oceanic biogeochemistry processes (HAMOCC). These components are coupled with the OASIS3 coupling program. The ocean model horizontal grid is an orthogonal curvilinear grid with an arbitrary placement of the grid poles (North Pole shifted to Greenland and the South Pole moved toward the centre of the Antarctic continent). The grid spacing is 15 km (0.14°) at minimum (around Greenland) and 184 km (1.65°) at maximum (in the Pacific) (Jungclaus et al., 2006). There are 40 unevenly spaced vertical levels with thicknesses between 10 m and 600 m. The sea ice model uses the same horizontal grid as the ocean model and the effect of snow accumulation on sea ice is included. The HAMOCC ocean biogeochemistry model (Hamburg Ocean Carbon Cycle Model) is part of the MPI-ESM-LR global model (Ilyina et al., 2013). HAMOCC uses 17 state variables in the water column (including only one group of phytoplankton but three nutrients: phosphate, nitrate and iron) and 12 variables in the sediment.

1.2 Method

Two different regions (the Labrador Sea and the Northwest Atlantic Shelf) were selected for trend analysis (Figure 1) due to the different hydrodynamic conditions prevailing in each area. We first looked at the representativeness of different simulated physical (temperature, salinity, sea ice, mixed layer depth) and biogeochemical (nitrate, chlorophyll *a* (Chl a), primary production, oxygen, dissolved inorganic carbon (DIC), pH, and aragonite and calcite saturation horizon depths) variables for each region by comparing them with observed values (range of values and distribution). We also compared the trends simulated over the historical period (1960-2005) with available observed trends. The period over which the trend was calculated was sometimes shortened to better compare with available observations. In a second step, we calculated future trends over a 50-year period (2012-2062) for each model as well as the mean trend of the multi-model ensemble. The mean trend over each region was calculated as well as the trend over each grid cell within each region to analyze spatial variability in the trends. Past and future bi-decadal distribution, from 1966-1985 to 2066-2085 were also calculated for each variable for the RCP 4.5 and 8.5 scenarios, at the surface and along some transects (vertical distribution) depicted in Figure 1. Figures of these results are available on demand, and some of the figures can also be found in Appendix II. Finally, trends and projections for the physical variables are also presented in Loder and van der Baaren (2013).

2 Results

2.1 Labrador Sea

The Labrador Sea has a large impact on global ocean physics and biogeochemistry. It is an important region of deep water formation. Deep convection occurring there provides an important pathway for atmospheric gases, such as oxygen and carbon dioxide (CO_2), and biogenic matter to pass from the surface mixed layer to intermediate depths (Hendry and Harrison, 2007; Strutton et al., 2011 and references therein), while it replenishes the surface layer with nutrients present in the deeper layers.

Freshwater exiting the Arctic ocean through the Canadian Arctic Archipelago (CAA) has an important effect on convection in the Labrador Sea and thus on the Atlantic meridional overturning circulation (AMOC) and the global climate system (see McGeehan and Maslowski, 2011 and references therein). The bathymetry of the region is shown in Figure 2.

2.1.1 Historical trends

2.1.1.1 Sea surface salinity

Salinity variations in the Labrador Sea are controlled by changes in local precipitation and evaporation, by changes in the salinity and advection of remote sources of freshwater and salt from the Arctic and the North Atlantic, as well as by changes in mixing and convection depth (e.g., Hendry et al., 2003). Waters flowing from the Arctic along the Labrador coast are fresher, while waters originating from the Irminger Current entering at the southern tip of Greenland are more saline. The World Ocean Atlas (WOA) shows salinities varying from 32 along the Labrador coast to 34.6 south of Greenland (Figure 3, bottom right panel). CanESM2 has high values in the north-west, suggesting no freshwater inflow through the CAA (Figure 3). On the other hand, the outflow from the CAA and Hudson Bay is too fresh in HadGEM2 and MPI, although they have the best representation of the saltier surface water in the central Labrador Sea. The spatial pattern of IPSL sea surface salinities is good but salinities are slightly fresh. Overall, GFDL appears to better represent the sea surface salinity, although salinities are a little high in the northeast corner of the region.

Salt content in the 0-1000 m layer of the Labrador Sea is quite variable but shows a small increase since the early 1990s (Hendry and Harrison, 2007). The models show, on average, a decrease in sea surface salinity over the 1960-2005 period, except for HadGEM2, with a multi-model ensemble mean of -0.009±0.065 unit per decade (Figure 4). Three models display spatial variability, with fresher water from the Arctic and saltier water from the North Atlantic, while GFDL and MPI show a general sea surface salinity freshening (Figure 5).

2.1.1.2 Sea surface temperature

Most models represent the colder waters flowing from the Arctic along the Labrador coast (western shelf) and the warmer Irminger Current water entering at the tip of Greenland (Figure 6). However, IPSL and CanESM2 have a coarse resolution and do not represent well the warmer water in the central Labrador Sea. GFDL and MPI display appropriate sea surface temperature (SST) of the Arctic outflow but the central Labrador Sea is too warm. In contrast, HadGEM2 gives a good representation of SST in the central Labrador Sea but its Arctic outflow is too cold. MPI has the best resolution, and, although too warm, it displays all the oceanographic features of the region.

There has been a general warming of the Labrador Sea since 1990, both at the surface and down to 2000 m (Hendry and Harrison, 2007). Petrie et al. (2008) report an SST increase of about 2°C at different locations of the Labrador Sea between 1985 and 2007 (based on satellite imagery). HadGEM2 is the model that best represents the warming trend depicted in Petrie et al. (2008) over this 20-year period (Figure 7). Most models display an increasing trend over the 1960-2005 period, except for GDFL, with a multi-model ensemble mean of 0.13±0.16°C per decade. With MPI, warming is present mainly in the western part of the Labrador Sea (Figure 8).

2.1.1.3 Sea ice

The Labrador Sea is ice free in summer. Sea ice forms locally along the Canadian coast in the fall and is also advected from the North (e.g., Yao et al., 2000). The sea ice reaches its most southern limit in March, and the ice edge is located near the Labrador Current (about 200 km from the Labrador coast). In the eastern part of the sea, near the Greenland coast, the ocean never reaches the freezing point. Among the five Global Climate Models analyzed, MPI and HadGEM2 have a good representation of sea ice concentration in the Labrador Sea (Figure 9). In GFDL, the winter conditions are well represented but the model doesn't show enough ice in fall and in spring. In CanESM2 and IPSL, there is too much ice in winter and not enough in fall and spring.

Tivy et al. (2011a; b) show that the sea ice extent in the Labrador Sea has decreased over the 1968-2008 period. The decrease of the ice cover in the northern part of the sea (Davis Strait) is 14.2±3.9 % per decade while the decrease in the southern part of the sea is 17.8±4.8 % per decade. Parkinson and Cavalieri (2008) also found a decreasing trend of sea ice extent in the Labrador Sea and Baffin Bay for the 1979-2006 period equal to 9.2±2.5 % per decade. Figure 10 shows the sea ice concentration trend obtained with the GCMs over the historical period. All the GCMs show a global decrease of the sea ice concentration over the ice covered period (November to June), except for GFDL that shows an increase of ice concentration in March.

2.1.1.4 Mixed layer depth

Convection driven by winter cooling and wind mixing lead to a deep surface mixed layer in the Labrador Sea that can reach depths as great as 2000 m (Hendry et al., 2003; Hendry and Harrison, 2007; Yashayaev and Loder, 2009). Deep convective mixing was observed in the early 1990s. Afterward, a shallowing of the winter mixed layer was observed, with depths of about 1200 m, until deeper mixing occurred in 2008 (Stramma et al., 2004; Yashayaev and Loder, 2009). The North Atlantic Oscillation (NAO) would have an important influence on the hydrography of this region (Henson et al., 2009; Lu et al., 2007).

In the GCMs, the mixed layer depth is described by two different variables. The Mixed Layer Depth (MLD) is defined by the water density (σ_t) and the Maximum Mixed Layer Depth (MMLD) is based on the mixing scheme of the GCMs. The MLD is available with three models (Figure 11), CanESM2, GFDL, and MPI while the MMLD is available for these three models and with IPSL. The location of the deep convection area is better represented with MPI and GFDL, although MPI's MLD appears to be too deep, while GFDL's appears to be shallow. The three models that provided MLD show a decreasing trend over the historical period, with a multi-model ensemble mean trend of -11.3±9.7 m per decade (Figure 12). A decreasing mixed layer trend is observed over the whole region for GFDL, but with MPI, there are decreasing and increasing trends depending on the area. This suggests a displacement of the deep mixing area towards the north (Figure 13). A displacement of the deep convection area was observed by Stramma et al. (2004) during periods of deep and low convection.

2.1.1.5 Nitrate

The WOA shows annual mean surface nitrate concentrations between 2 and 10 mmol N m^{-3} in the Labrador Sea, with higher concentrations around the southern tip of Greenland and decreasing concentrations from the east towards the west (Figure 14, lower right panel). Average concentration would vary by about 8-10 mmol N m^{-3} between the winter maximum and the summer minimum (Harrison and Li, 2007; Louanchi and Najjar, 2001). Average surface nitrate concentration measured by Harrison and Li (2007) between 1994 and 2005 is close to the climatological mean (1962-2002, National Oceanographic Data Center) except on the Labrador Shelf where the values are higher. GFDL and MPI best represent this distribution, although GFDL nitrate concentration in the southeast area is higher than WOA values while MPI values are a little lower (Figure 14). Four models also show a surface inflow with higher nitrate concentration from Hudson and Baffin Bays. These higher concentrations are not apparent in surface nitrate concentration from the WOA but could be realistic. Strong tidal mixing in Hudson Strait replenishes surface nutrient concentration that could then be advected towards the Labrador Sea (Ferland et al., 2011). GFDL and MPI are also the models that best represent the MLD. Figure 3 of Azetsu-Scott and Yeats (2007) shows that nitrate concentration in the deep convection area ranges between 15.5 and 16 mmol N m^{-3}. Figure II- 1 and Figure 16 show that most models display lower concentration, while GFDL shows higher concentrations. CanESM2 and GFDL are the models that best represent the nitrate concentration in the vertical.

All models show an average decreasing trend over the region in all layers, except for HadGEM2 (Figure 15 to Figure 18). However, most models, except for CanESM2, point to an increasing trend near the boundary with Baffin Bay in the 100-400 m layer (Figure 18). These trends (away from Baffin Bay) are consistent with observation (Pepin et al., 2013 and references therein) that show decreasing nitrate concentrations on the Labrador Shelf (last two decades or so) in the 50-100 m layer, and more pronounced decline in the 100-400 m depth range for the Labrador Sea Basin.

2.1.1.6 Primary Production

The Labrador Sea and adjacent shelves (especially the West Greenland Shelf) represent a biologically productive high-latitude ecosystem (Harrison and Li, 2007; Vantrepotte and Mélin, 2011). Primary production in the Labrador Sea would be essentially light limited (e.g., Harrison and Li, 2007; Henson et al., 2009) and the timing of the spring bloom would be correlated with the mixed layer depth in sea ice free areas (Henson et al., 2009) and with sea ice melt and retreat in ice covered areas (eastern Greenland shelf and Canadian East Coast; Wu et al., 2007). The offshore advection of freshwater from Greenland by the West Greenland Current would also influence the timing of the spring bloom in the central Labrador Sea (Frajka-Williams and Rhines, 2010).

Most models show a greater primary production at the southern tip of Greenland (Figure 19). Three models show a lower primary production on the Labrador shelf, while CanESM2 and GFDL also display high primary production at the mouth of Hudson Strait and below. The models show divergent primary production trends over the historical period (Figure 20 and Figure 21).

2.1.1.7 Chl a

Although few primary production measurements are available for comparison with the models, we can compare surface Chl a data with satellite images. MPI is the model that best represents the SeaWiFS data record, with high Chl a values around the southern tip of Greenland and some high values on the Labrador Shelf (Figure 22). Both Vantrepotte and Mélin (2011) and Li et al. (2006) point to an increase in Chl a around the southern tip of Greenland in the last decade or so. Over the Labrador Shelf and Basin, Li et al. (2006) observed a decrease in spring followed by an increase in fall with no net change. Over the Greenland Shelf, an increase was observed in spring with no change in the fall. The SeaWiFS record is too short to allow a comparison of trends with the GCMs, so we display the trends obtained over the historical period. As for primary production, the models show divergent trends for Chl a over the historical period (Figure 23 and Figure 24).

2.1.1.8 Oxygen

Figures from the AR7W line between 2007 and 2010 (see recent conditions at http://www.iob.gc.ca/science/monitoring-monitorage/azomp-pmzao/labrador/chemical-chimique-fra.php) show surface oxygen concentration in May varying between 0.34 and 0.36 mol m^{-3} on the Labrador Shelf and between 0.32 and 0.33 mol m^{-3} in the Labrador Basin (using a conversion factor of 22.392 l/mol O_2; Hofmann et al., 2011). Values from the WOA range between 0.30 and 0.36 mol m^{-3} for the Labrador Sea region (Figure 25, bottom right panel). As for SST (section 2.1.1.2), the models do not give a perfect representation of surface oxygen concentrations. The highest concentrations are found in the cold Arctic outflow of HadGEM2, and the lowest in the warm surface water of GFDL (Figure 25). Although MPI also has oxygen concentrations that are a little high in its Arctic outflow, it has the best range of values in general. GFDL has the best range of values in the Arctic outflow on the western shelf.

Oxygen concentrations from MPI and IPSL show weak positive trends at the surface while GFDL and HadGEM2 clearly display decreasing O_2 concentration at the surface for the 1985-2005 period (Figure 26 and Figure 28). These trends reflect the sea surface temperature trends over the region (Figure 7). In the 100-400 m layer, all models show a decreasing trend for the 1990-2005 period (Figure 27 and Figure 29). The multi-model ensemble mean trend for the 100-400 m layer for the 1990-2005 period is -0.0035±0.0009 mol m^{-3} per decade. This is half the trend calculated from observations in the central Labrador Sea at 150-500 m for the same period (around -0.0072 mol m^{-3} per decade, http://www.bio.gc.ca/science/monitoring-monitorage/azomp-pmzao/labrador/chemical-chimique-eng.php).

2.1.1.9 Ocean acidification

Oceans have taken up a great part (~ 40%) of anthropogenic CO_2 emissions, thereby reducing climate warming caused by greenhouse gases (Zeebe et al., 2008). However, the increase of CO_2 in the oceans alters its chemistry, which can have potentially serious consequences for marine organisms, especially for calcifying organisms. When CO_2 gas enters the ocean, it decreases the seawater pH as well as the concentration of CO_3^{2-}, which lowers the saturation state of calcium carbonate ($CaCO_3$) minerals such as calcite and aragonite. This process is called ocean acidification.

2.1.1.9.1 DIC

Figures from the AR7W line between 2007 and 2010 (http://www.bio.gc.ca/science/monitoring-monitorage/azomp-pmzao/labrador/conditions-eng.php) show that surface DIC concentration in May are around 2.0 mol m^{-3} on the Labrador shelf and around 2.1 mol m^{-3} in the Labrador Basin, with values on the Greenland shelf sometimes approaching values similar to the Labrador Shelf. Thus CanESM2, MPI, and HadGEM2 appear to best represent surface DIC (Figure 30), although values in the Labrador Basin appear a little high with MPI (compared to the May observations). All the models show a similar positive trend at the surface, with IPSL and HadGEM2 showing the highest trends (Figure 31). Over the 100-400 m layer, the trends are similar with, again, IPSL and HadGEM2 showing higher trends. The multi-model ensemble mean trend (at 100-400 m) for the 1990-2005 period (4.9±2.0 mmol m^{-3} per decade, Figure 32) is about half the trend observed along the ARW7 line over the 1996-2012 period for the 150-500 m depth range (Figure 9 of Greenan et al., 2010).

2.1.1.9.2 pH

Surface pH values in the region vary between 8.08 and 8.2 (Azetsu-Scott et al., 2010). These measurements were made recently and it is well known that pH values have decreased in the recent decades, so the 1960-2005 average should be higher than the values reported above. The GLODAP database shows pH values between 8.2 and 8.25 in the Labrador Sea for 1995 (Feely et al., 2009). Model values range between 8.05 and 8.25, with the lowest values displayed by CanESM2 and the highest values displayed by HadGEM2 (Figure 34). Due to the lack of data, it is thus difficult to judge which model best represents pH in the Labrador Sea. However, all the models show a similar decreasing trend at the surface, with a multi-model ensemble mean of -0.016±0.002 unit per decade over the 1960-2005 period (Figure 35). The multi-model ensemble mean trend for the 100-400 m depth range over the 1990-2005 period (-0.017±0.01 per decade, Figure 36) is somewhat smaller than the observed trend along the ARW7 line for the 150-500 m depth range (-0.03 per decade, Figure 9 of Greenan et al., 2010).

2.1.1.9.3 Calcium carbonate saturation horizons

Azetsu-Scott et al. (2010) found that the aragonite saturation horizon depth along the ARW7 line corresponds approximately to the boundary between the Labrador Sea Water (LSW) and the North East Atlantic Deep Water (NEADW) at around 2300m. On the other hand, calcite is oversaturated, with a saturation state <1.2 at the bottom and 2.2-2.8 at the surface. However, at the northern limit of the region (Davis Strait), low saturation states, associated with the Arctic outflow, were observed. The aragonite saturation horizon shallows to <200 m on the Baffin Island side while calcite saturation states ≤ 1 were observed in a limited area on the western side of Davis Strait, at depths of about 400 m (Azetsu-Scott et al., 2010). For aragonite, GFDL and CanESM2 give the best representation of the saturation horizon at about 3200 m while HadGEM2 gives aragonite saturation states above 100% for the entire water column. GFDL, HadGEM2, and CanESM2 have oversaturated waters in the Labrador Sea with respect to calcite.

2.1.2 Future trends (next 50 years)

A summary table of future trends can be found in Appendix I.

- **Salinity**: All models display a decreasing trend for sea surface salinity in the Labrador Sea, except for IPSL (Figure 37). The multi-model ensemble mean trends are -0.06±0.10 and -0.12±0.11 unit per decade for RCPs 4.5 and 8.5, respectively. A sea surface salinity decrease is indeed expected with the intensification of the hydrological cycle (Carmack and McLaughlin, 2011 and references therein) and the melting of the Greenland ice sheet. For the 50-100 m layer, the multi-model ensemble mean trends are -0.022±0.017 and -0.07±0.06 unit per decade and for the 100-400 m layer, the multi-model ensemble mean trends are +0.001±0.033 and -0.014±0.019 unit per decade for RCP 4.5 and RCP 8.5, respectively (Figure 38).

- **Temperature:** All the models show an increasing trend for SST. The multi-model ensemble mean trends are 0.16±0.13 and 0.22±0.13°C per decade for RCP 4.5 and 8.5, respectively (Figure 39). This corresponds approximately to an increase of 0.8-1.1°C over the next 50 years. For the 50-100 m and 100-400 m layers, the temperature increases in all GCMs with both RCPs. For the 50-100 m layer, the multi-model ensemble mean trends are 0.14±0.14 and 0.19±0.14°C per decade and for the 100-400 m layer, the multi-model ensemble means trends are 0.16±0.08 and 0.24±0.09°C per decade for RCP 4.5 and RCP 8.5.

- **Sea Ice:** The major changes in the sea ice concentration are mostly located along the ice edge, except for the models that had too much sea ice in the central Labrador Sea (CanESM2 and IPSL, Figure 40 and 41). With MPI and HadGEM2 (that had the best representation of sea ice), the ice cover starts to form about one month later in fall and melts about one month sooner in spring in 50 years from now. At this time, the maximum ice thickness in winter reaches 150 and 120 cm for HadGEM2 and MPI, respectively. This corresponds to a thickness decrease of 5 cm and 6 cm per decade for RCP 4.5 and 15 cm and 8 cm per decade for RCP 8.5.

- **Mixed layer**: The three models from which the mixed layer depth was available show a decreasing trend, with MPI showing the greatest slope (Figure 42). The multi-model ensemble mean trends are -6.0±3.7 and -13.3±14.6 m per decade for RCPs 4.5 and 8.5, respectively. For the monthly maximum, the trends are -4.3±6.8 and -11.8±18.5 m per decade for RCP 4.5 and RCP 8.5, respectively.

- **Nitrate:** In the Labrador Sea, the models project a decrease in nitrate concentration in general, although the trends are variable with the RCP 4.5 scenario. ISPL shows a positive trend at the surface and at 50-100 m, while HadGEM2 shows a decrease in the deeper layers (Figure 43 to Figure 45). At the surface, the multi-model ensemble mean trends are -0.11±0.12 and -0.19±0.12 mmol m^{-3} per decade for RCPs 4.5 and 8.5, respectively. In the 50-100 m layer, the multi-model ensemble mean trends are -0.10±0.17 and -0.21±0.10 mmol m^{-3} per decade for RCPs 4.5 and 8.5, respectively. In the 100-400 m, the ensemble mean trends are -0.06±0.10 and -0.08±0.13 mmol m^{-3} per decade for RCPs 4.5 and 8.5, respectively.

- **Primary production:** The models show divergent trends for the vertically integrated primary production (Figure 46). The multi-model ensemble mean trends are +0.05±0.15 and -0.014±0.165 mol C m^{-3} per decade for RCPs 4.5 and 8.5, respectively. For RCP 8.5, IPSL and HadGEM2 trends cancel each other. Thus, no firm conclusion can be drawn on future primary production in the Labrador Sea from the model results. The increase in stratification might mean a greater light availability, but, on the other hand, nutrient availability is expected to decrease (see above).

- **Chlorophyll a:** All models show a weak decreasing trend for Chl a concentration at the surface except for IPSL, while in the 50-100 m layer, trends have different sign with the RCP 4.5 scenario, but are all positive for RCP 8.5 (Figure 47 and Figure 48). The multi-model ensemble mean for Chl a concentration at the surface basically shows no trends: -0.0002±0.0098 and -0.009±0.010 mg m^{-3} per decade for RCPs 4.5 and 8.5, respectively. In the 50-100 m layer, the ensemble mean trend for the RCP 8.5 scenario is +0.004±0.003 mg m^{-3} per decade.

- **Oxygen:** Oxygen concentration trends are variable in the surface layer but all negative in the 100-400 m layer (Figure 49 and Figure 50). The decreasing trend in the 100-400 m layer is present over most of the region in all four models (not shown). The multi-model ensemble mean trends at the surface are -0.6±1.3 and -0. 9±1.3 mmol m^{-3} per decade for RCP 4.5 and 8.5, respectively and -1.2±0.3 and -2.0±1.0 mmol m^{-3} per decade for the 100-400 m layer for RCP 4.5 and 8.5, respectively. As a comparison, the changes in oxygen solubility as a function of temperature and salinity (using Benson and Krause, 1984) in the 100-400 m layer have slightly smaller multi-model ensemble mean trends of -1.1±0.5 and -1.6±0.6 mmol m^{-3} per decade for RCP 4.5 and 8.5, respectively (not shown).

- **DIC:** All models show positive trends for DIC concentration both at the surface and in the 100-400 m layer, except for CanESM2 at the surface for RCP 8.5 (Figure 51 and Figure 52), likely due to the combination of larger warming and freshening in this model (Figure 37 and Figure 39). The multi-model ensemble mean trends at the surface are 0.005±0.004 and 0.006±0.006 mol m^{-3} per decade for RCPs 4.5 and 8.5, respectively. In the deeper layers, all the GCMs show positive DIC concentration trends for both scenarios. The multi-model ensemble mean trends at 50-100 m are +0.007±0.002 and +0.008±0.003 mol m^{-3} per decade for RCPs 4.5 and 8.5, respectively. For the 100-400m layer, the multi-model ensemble mean trends are +0.008±0.001 and +0.010±0.001 mol m^{-3} per decade for RCPs 4.5 and 8.5.

- **pH:** All models show negative trends for pH at the surface and in the 100-400 m layer (Figure 53 and 54). The multi-model ensemble mean trends at the surface are -0.026±0.002 and -0.042±0.003 unit per decade for RCPs 4.5 and 8.5, respectively and -0.024± 0.001 and -0.034±0.002 unit per decade for the 100-400 m layer for RCPs 4.5 and 8.5, respectively. Future pH would thus decrease by an additional 0.12 to 0.21 units in the next 50 years in the Labrador Sea.

- **Calcium carbonate saturation horizons**: In the Labrador Sea, calcite would remain oversaturated for the next 50 years. For aragonite, GFDL and CanESM2 show that aragonite saturation horizon depths would be more or less stable until 2035 when it would start to shallow. The mean decrease obtained with these two models is equal to -288±75 m and -444±81 m per decade for RCP 4.5 and RCP 8.5, respectively (Figure 55).

2.2 Atlantic Northwest

This area comprises part of the Labrador shelf, the Newfoundland shelf, the Grand Banks, the Scotian Shelf, the Gulf of St. Lawrence, the Gulf of Maine, Georges Bank, and part of the Gulf Stream. Sharp gradients in temperature and salinity are found in this region due to the confluence of the cold, southward-flowing Labrador Current, the outflow from the Gulf of St. Lawrence, and the poleward flowing Gulf Stream. Deeper layers are also a mixture of different water masses (e.g., Linder and Gawarkiewicz, 1998; Stramma et al., 2004). The bathymetry of the region is shown in Figure 56.

2.2.1 Historical trends

2.2.1.1 Sea surface salinity

MPI is the model that best represents the surface salinities in the AtlNW region, followed by HadGEM2 (see the comparison with observations, lower right panel in Figure 57). The other models show high salinities in the Gulf of Maine due to an incorrect positioning of the Gulf Stream separation from the coast. Two models (IPSL and HadGEM2) show an increasing sea surface salinity trend. The resulting multi-model ensemble mean displays no clear trend (-0.0008±0.037 per decade, Figure 58 and 59).

2.2.1.2 Sea surface temperature

MPI and HadGEM2 best represent the SST in the AtlNW region, with cold water flowing southward from the Labrador Sea, warm subtropical waters flowing northward with the Gulf Stream and intermediate SST in between, on the Scotian Shelf and in the Gulf of Maine (Figure 60). CanESM2 and IPSL are too warm in the Gulf of Maine region, and GFDL is in between. An important SST warming was observed in the region in the last three decades: 0.5°C per decade in the Gulf of St. Lawrence (Galbraith et al., 2012b), and 0.37 and 0.43°C per decade in the Newfoundland/Labrador Sea region and on the Scotian Shelf, respectively (Sherman et al., 2009). However, there is a strong component of decadal variability in these trends. The trends get smaller if the observation period used to calculate the trend is extended further into the past (Galbraith et al., 2012b). The multi-model ensemble mean trends are 0.18±0.06°C per decade for the 1960-2005 period (Figure 61) and 0.15±0.07°C per decade for the 1980-2005 period. This warming occurs over all or most of the region depending on the model (Figure 62).

2.2.1.3 Sea ice

There is no sea ice formation in the Gulf of Maine or on the Scotian Shelf. Sea ice is formed along the Labrador coast and advected south towards the Gulf of St. Lawrence (GSL) and the Newfoundland shelf (Yao et al., 2000). In the GSL, sea ice formation is initiated in the lower estuary in January and progresses towards Cabot Strait in February. Sea ice extent in the GSL reaches a maximum in March, and is usually advected towards the Scotian Shelf in February and March, pushed by northwesterly winds and ocean currents (Galbraith et al., 2012a; Petrie et al., 2008). Sea ice melts relatively rapidly in April, although some sea ice can still be advected down the Labrador coast in May (Yao et al., 2000). None of the models does a very good job at reproducing sea ice in that region. The sea ice concentration is either too low or extends too far (Figure 63). However, with few exceptions, all models simulated a decreasing sea ice concentration over the historical period (Figure 64), as was observed in the GSL (Galbraith et al., 2012a) and Labrador Sea (see section 2.1.1.3).

2.2.1.4 Mixed layer depth

The simulated annual mean mixed layer depth varies between 100 and 200 m in the Gulf Stream area, much deeper towards the Labrador Sea (upper right corner), while it is much shallower in the region influenced by freshwater outflow (around 40 m, Figure 65). Mixed layer depths in the Gulf of St. Lawrence, Scotian Shelf, and Gulf of Maine indeed vary between 10 and about 70 meters over the year (Christensen and Pringle, 2012; Doyon and Ingram, 2000; Zhai et al., 2011).

Although there are regional differences in the trends, there is an overall decreasing trend in MLD that reflects the general warming of the surface layer (Figure 66 and 67). The multi-model ensemble mean trend, using available data from three models, is -2.9±3.6 m per decade. This trend is high due to the large contribution of the shallowing/displacement of deep mixing zone in the Labrador Sea (northeast corner of the region) in MPI (see section 2.1.1.4).

2.2.1.5 Nitrate

Nitrate concentration in this region is spatially variable due to the different sources and variability in the mixture of these sources (Pepin et al., 2013; Petrie and Yeats, 2000; Townsend et al., 2010; Yeats et al., 2010). Mean surface nitrate concentration from WOA (Figure 68, lower right panel) are higher in the Southern Labrador Sea (~ 7 mmol N m^{-3}) area, and in the Gulf of St. Lawrence and Gulf of Maine (~ 5 mmol N m^{-3}). MPI is the model that best represents the average surface nitrate concentration. IPSL and HadGEM2 are too low, and GFDL is too high (Figure 68). On the other hand, in the 100-400 m layer, MPI values are too low (Figure 69). GFDL has a good spatial representation and range of values (although concentrations in the GSL are too low). CanESM2 also reproduces well the nitrate maximum around the Grand Banks and along the Scotian Shelf but the values are high.

The nitrate concentration trends over the whole region for the historical period are generally decreasing at all depths, except for HadGEM2 and for GFDL at 100-400 m, with multi-model ensemble means of -0.05 ± 0.07, -0.09 ± 0.11 and -0.05 ± 0.11 mmol N m^{-3} per decade for the surface, 50-100 m layer, and 100-400 m layer, respectively (Figure 70 and Figure 71). These trends are small and the standard deviations are large, due to the high spatial variability of the trends (Figure 72 to Figure 73). However, such a general decrease in nitrate concentration has been observed in the area since 1980, although spatial variability was present (Pepin et al., 2013).

2.2.1.6 Primary Production

The lower half of this region (40-45°N) represents the transition zone between subpolar and subtropical primary production regimes (Henson et al., 2009). This definition excludes the shelf regions. Platt and Sathyendranath (2008) show that this region is divided into multiple ecological provinces. Primary production in the Gulf of St. Lawrence ranges between 7-24 mol C m^{-2} yr^{-1} (Le Fouest et al., 2005 and references therein), on the Scotian Shelf, a moderately-high productive ecosystem, around 6-20 mol C m^{-2} yr^{-1} (Aquarone and Adams, 2008; Fournier et al., 1977; Mousseau et al., 1996), while on the Grand Banks it is of the order of 16 mol C m^{-2} yr^{-1} (Prasad and Haedrich, 1993). Figure 74 shows that integrated primary production with CanESM2 and GFDL are high and spatial patterns do not agree well with observations (e.g., high in Gulf Stream area), while values obtained with HadGEM2 are too low (about half, and less, of observed values). IPSL has the best range of values but also a poor spatial distribution (higher values in the Gulf Stream area).

There might have been a slight increase in primary production on the Scotian Shelf between 1998 and 2006 (Aquarone and Adams, 2008). The models show divergent trends for primary production over the historical period (1960-2005). CanESM2 and MPI show a decreasing trend while the others show an increasing trend (Figure 75 and Figure 76). No firm conclusion can be drawn about the past primary production trends.

2.2.1.7 Chl a

The comparison of surface Chl a from satellite images (Figure 77, bottom right panel) shows that all models display surface Chl a concentrations that are too low. However, higher Chl a values with GFDL are well distributed (GSL, Georges Bank, Grand Banks). Vantrepotte and Melin (2011) show regions with increasing trend and others with decreasing trend within the AtlNW region. However, when keeping only the statistically significant trends, only the decrease over the Grand Banks region stands out. Overall there should thus be a decreasing trend. As mentioned previously, the SeaWiFS record is too short to allow a comparison of trends with the GCMs. The models show variable trends over the historical period (Figure 78 and Figure 79) with a weak multi-model ensemble mean, and thus, as for primary production, no firm conclusion can be drawn about the trends.

2.2.1.8 Oxygen

Oxygen concentration values from the WOA in the AtlNW region range between 0.22 and 0.34 mol m^{-3} at the surface (Figure 80, bottom right panel) and between 0.15 and 0.35 in the 100-400 m layer (Figure 81, bottom right panel). In general, the models reproduce well the range of values and the latitudinal gradient. However, GFDL and IPSL have surface values that are too low in the Georges Bank/Gulf of Maine area (Figure 80) due to SSTs that are too warm (Figure 60). Nonetheless, in the deeper layers, GFDL has a good spatial representation of the observed values (except for the GSL). Yeats et al. (2010) observed decreasing O_2 concentrations from the early 1970s until 2008 in the 60–100 m depth range for the eastern, central, and western regions of the Scotian Shelf, and in waters >150 m depth in Emerald Basin (central Scotian Shelf). The trends varied between -0.012 and -0.285 mmol m^{-3} per year depending on the region. Similarly, Gilbert et al. (2005) observed an important decrease in oxygen concentration since the 1930s in the GSL, with a trend of -1.0±0.2 mmol m^{-3} per year (although concentrations did not change significantly after the mid-1980s). All models show a decreasing trend in the long term (1960-2005), both at the surface and in deeper layers, consistent with the observed trends (Figure 82 to Figure 85). The multi-model ensemble means are -0.0008±0.0006 mol m^{-3} per decade at the surface (with a similar trend in the 50-100 m layer), and -0.001±0.0008 mol m^{-3} per decade in the 100-400 m layer.

2.2.1.9 Ocean acidification

2.2.1.9.1 DIC

There are few observations with which to compare. However, in general, surface DIC concentrations in the AtlNW region are lower in fresher waters and increase towards saltier (oceanic) waters. Mucci et al. (2011) report low values of 1.3 mol m^{-3} for the St. Lawrence River, while on the Scotian Shelf, values would range between 1.9 and 2.1 mol m^{-3} (Shadwick et al., 2011). Among the GCMs, MPI and then HadGEM2 have the best spatial representation of DIC, with lower values in the GSL, Scotian Shelf and Gulf of Maine than offshore (Figure 86). All the models show an increasing DIC trend over the surface (Figure 87) that is consistent with the increase in atmospheric CO_2 partial pressure (Takahashi et al., 2009), although MPI shows a decreasing trend in the GSL and nearby areas (Figure 88). The multi-model ensemble mean trend is 6±2.6 mmol m^{-3} per decade.

2.2.1.9.2 pH

As for DIC, there are few surface pH measurements to compare with. Data from the GLODAP database (Figure 2 of Feely et al., 2009) show that pH values in the AtlNW decrease from the north towards the south. However, there are few spatial details and their interpolation most likely suffers from a lack of measurements on the Scotian Shelf. Measurements from the GSL and Scotian Shelf show a large range and high temporal spatial variation (K. Azetsu-Scott, personal communication; Mucci et al., 2011). However, in general, pH values on the Scotian Shelf (8.0-8.1) appear to be lower than offshore (8.05-8.15), while values in the GSL would vary between 8.0 and 8.15. MPI is the model that best represents the lower pH values on the shelf (Figure 89). All models show a decreasing surface pH trend over the historical period, consistent with the increase in surface DIC (Figure 90), with a multi-model ensemble mean trend of -0.015±0.0009 per decade. A decreasing trend, small at the surface but increasing with depth, was also observed in the GSL (Mucci et al., 2011) and on the Scotian Shelf (K. Azetsu-Scott, personal communication).

2.2.1.9.3 Calcium carbonate saturation horizons

In the AtlNW region, the aragonite saturation horizon is at about 2600 m while the calcite saturation horizon depth is much deeper, at about 4500 m (Chung et al., 2003). In the GSL, the aragonite saturation horizon is found at about 100 m (Mucci et al., 2011) while calcite is oversaturated. The aragonite saturation horizon has become shallower in the last decades. The aragonite saturation horizon in the Northwest Atlantic has migrated upward by approximately 100-150 m since the preindustrial era, while no changes were observed in the calcite saturation horizon (Chung et al., 2003). Out of the three models providing saturation horizon depths (CanESM2, GFDL, and HadGEM2), CanESM2 appears to reproduce the saturation horizon depth the best (Figure 91), while the multi-model ensemble mean trend over the historical period (-17.9±15.6 m per decade) is close to what Chung et al. (2003) observed.

2.2.2 Future trends

A summary table of future trends can be found in Appendix I.

- **Salinity:** Sea surface salinity trends for the AtlNW region are weak and/or inconsistent. Three models show an increasing trend with RCP 4.5 while four models show a decreasing trend for RCP 8.5 (Figure 92). Only IPSL shows an increasing trend under both scenarios. The multi-model ensemble mean trends are 0.008±0.032 and -0.02±0.03 unit per decade for RCPs 4.5 and 8.5, respectively. So we cannot conclude that sea surface salinity will change on average over the AtlNW region. However, four models show an increasing salinity trend in the Gulf Stream and a freshening trend around Newfoundland (Figure 93 and 94). Unlike the surface, the deeper waters have clear trends with all the GCMs displaying an increase in salinity. For the 50-100 m layer, the multi-model ensemble mean trends are 0.031±0.026 and 0.025±0.021 unit per decade and for the 100-400m layer the trends are 0.04±0.02 and 0.04±0.03 unit per decade for RCP 4.5 and RCP 8.5, respectively.

- **Temperature:** All models show an increasing trend for SST (Figure 95 and Figure 96) and an increase of potential temperature in deeper waters. The multi-model ensemble mean trends for the surface are 0.28±0.10 and 0.39±0.12°C per decade for RCP 4.5 and RCP 8.5, respectively. This corresponds approximately to an increase of 1.5-2.0°C over the next 50 years. For the 50-100 m and 100-400 m layers, the multi-model ensemble mean trends are 0.26±0.11 and 0.34±0.12°C per decade and 0.26±0.11 and 0.36±0.13°C per decade for RCP 4.5 and RCP 8.5, respectively.

- **Sea ice:** All models show decreasing sea ice concentration in the next 50 years (Figure 97 and Figure 98). In winter, the sea ice concentration in the GSL and on the Newfoundland Shelf decreases by 1 to 10 % per decade and by 1 and 17 % per decade for RCP 4.5 and RCP 8.5, respectively. The maximum ice thickness along the coast of Newfoundland ranges between 20 and 90 cm, depending on the model. In this region, the average sea ice thickness decreases by 5 and 7 cm for RCP 4.5 and RCP 8.5, respectively.

- **Mixed layer depth:** The three models from which the mixed layer depth was available show a decreasing trend with RCP 4.5 and RCP 8.5, except for CanESM2 which displays an increasing trend with RCP 4.5 (Figure 99). The resulting multi-model ensemble mean trends are -0.3±0.6 and -3.2±4.5 m per decade for RCPs 4.5 and 8.5, respectively. However, the decreasing trends are strongly influenced by changes in the deep Labrador Sea water (north east corner of the region) while deepening is observed in the slope waters/Gulf Stream area (Figure 100). It is thus difficult to reach a conclusion on the mean trend in the area.

- **NO_3:** In the Atlantic Northwest region, mean nitrate concentrations are decreasing at the surface, in the 50-100 m (Figure 101) and 100-400 m layers in all 5 models and for both RCPs, although spatial differences are observed (Figure 102 to Figure 104). The only case where there is a small mean increase is at the surface in RCP 4.5 with IPSL. At the surface, the multi-model ensemble mean trends are -0.05±0.04 and -0.08±0.06 mmol m^{-3} per decade for RCP 4.5 and 8.5, respectively. For the deeper layer, the multi-model ensemble mean trends are -0.08±0.05 and -0.19±0.12 mmol m^{-3} per decade for the 50-100 m layer, and -0.12±0.06 and -0.20±0.15 mmol m^{-3} per decade in the 100-400 m layer, for RCP 4.5 and 8.5, respectively.

- **Primary production:** The models show weak and variable trends for the vertically integrated primary production (Figure 105). The multi-model ensemble mean trends are 0.025±0.098 and -0.10±0.14 mol C m^{-2} per decade for RCPs 4.5 and 8.5, respectively.

- **Chlorophyll a:** All models show a weak decreasing trend for Chl a concentration at the surface (MPI's trend is a little higher), but varying trends for Chl a concentration in the 50-100 m layer (Figure 106 and Figure 107). The multi-model ensemble mean trends for Chl a concentration at the surface are -0.005±0.004 and -0.011±0.007 mg m^{-3} per decade for RCPs 4.5 and 8.5, respectively.

- **O_2:** All four models show decreasing oxygen concentrations at the surface and in the 100-400 m layer (Figure 108 and Figure 109). The multi-model ensemble mean trends are -1.4±0.5 and -2.0±0.7 mmol m^{-3} per decade at the surface, -1.3±0.5 and -1.5±0.7 mmol m^{-3} per decade for the 50-100 m layer and -1.2±0.4 and -1.5±0.7 mmol m^{-3} per decade for the 100-400 m layer for RCPs 4.5 and 8.5, respectively. As a comparison, the changes in oxygen solubility as a function of temperature and salinity (using Benson and Krause, 1984) in the 100-400 m layer have slightly larger multi-model ensemble mean trends of -1.5±0.7 and -2.0±0.7 mmol m^{-3} per decade for RCPs 4.5 and 8.5, respectively.

- **DIC:** All models show positive trends for DIC concentration both at the surface and in the 100-400 m layer (Figure 110 and Figure 111). The multi-model ensemble mean trends at the surface are 0.009±0.002 and 0.012±0.002 mol m^{-3} per decade for RCPs 4.5 and 8.5, respectively and 0.0095±0.0006 and 0.013±0.0004 mol m^{-3} per decade in the 100-400 m layer for RCPs 4.5 and 8.5, respectively.

- **pH:** All models show negative trends for pH at the surface and in the 100-400 m layer (Figure 112 and Figure 113). The multi-model ensemble mean trends at the surface are -0.021±0.0006 and -0.035±0.002 unit per decade for RCPs 4.5 and 8.5, respectively, representing a pH decrease of 0.11 and 0.18 over the next 50 years. In the 100-400 m layer, the decrease is lower than at the surface, with a multi-model ensemble mean trends of -0.019±0.0006 and -0.027±0.003 unit per decade for RCPs 4.5 and 8.5, respectively.

- **Calcium carbonate saturation horizons**: In the Atlantic Northwest, the calcite saturation horizon depths stay unchanged for CanESM2 and GFDL. In HadGEM2, the saturation horizon goes deeper with a trend of +120m and 136 m for RCP 4.5 and RCP 8.5, respectively. For the aragonite saturation horizon, there is little change with CanESM2 for 2012-2062, while stronger decreasing trends are simulated by GFDL and HadGEM2: -271 m and -10.2 m per decade for RCP 4.5 and -238 m and -108 m per decade for RCP 8.5 (Figure 114).

3 Discussion and Conclusion

We used the new generation of climate models with enhanced complexity from the CMIP5 intercomparison project. Increased complexity could increase uncertainty and not necessarily lead to better results, but recent studies using the output from these models tend to show similar or improved performance. The climate sensitivity (expected warming given a doubling of preindustrial atmospheric carbon dioxide levels) of this new generation of models is similar to the previous generation (Andrews et al., 2012). However, Sillmann et al. (2013) found that the CMIP5 models better represent climate extremes related to temperature and Knutti et al. (2013) found better agreement with observations in general. However, these results concerned only the physics of the models. This is the first generation that includes biogeochemistry, and the results are often quite different from one model to the other. MPI and GFDL appear to better represent the past environmental conditions in general in the Labrador Sea while MPI, GFDL, and HadGEM2 might give a better representation in the AtlNW region. However, it is not possible to predict which one better represents future trends. We can safely conclude that DIC concentration will increase and that oxygen concentration and pH will decrease (general model agreement on direction of change). There is a possible decrease of nitrate concentration (some models display a positive trend), while for Chl a and primary production, no firm conclusions can be drawn in the regions under study. This reflects the differences in the physical structure and circulation of the ocean engine but also reflects the large differences in the number of state variables and parameterization of the biogeochemical components in the different models (see section 1.1). Another aspect, much less understood and most likely not well reproduced by all or part of the GCMs, are the changes occurring in the delivery of nutrients from remote regions, usually in the subsurface layers (e.g., Levy, 2005; Palter et al., 2005; Torres-Valdés et al., 2013; Townsend et al., 2010; Yamamoto-Kawai et al., 2006), either through circulation changes or changes in nutrient inventory of advected water masses.

The three models that appear to perform better in this dynamically complex region seem to benefit from a better defined bathymetry and coastal contour (see Figure 2 [better definition of the shelf around Greenland] and Figure 56). Better performance of MPI for the AtlNW region shows the importance of model resolution in resolving the complex dynamics of the region. However, GCMs are built to represent climate change at a global scale. With the computing capacity we have at this time, regional downscaling systems need to be developed to project future changes at the regional scale (e.g., Guo et al., 2013). The biogeochemical components of the coupled models also need to be improved. This is necessary to better represent the complex dynamics of the regions under study in this document and the interactions between the physical environment and the biogeochemical variables (e.g. changes in seasonality of the spring bloom associated with sea ice retreat, changes in total primary production and in the contribution of small/large phytoplankton cells to primary production, expansion of low dissolved oxygen zones, expansion in low pH water, and shoaling of the calcium carbonate saturation horizon). With this more detailed knowledge, it will be possible to evaluate the impact on higher trophic levels (e.g. exploited stocks) to determine potential habitat changes, movements of marine organisms, and species' shifts.

4 Acknowledgements

We acknowledge the World Climate Research Programme's Working Group on Coupled Modelling, which is responsible for CMIP, and we thank the climate modelling groups (listed in Table 1 of this paper) for producing and making available their model output. For CMIP the U.S. Department of Energy's Program for Climate Model Diagnosis and Intercomparison provides coordinating support and led development of software infrastructure in partnership with the Global Organization for Earth System Science Portals.

We also thank Dave Brickman, Jim Christian, and Denis Gilbert for their careful review of the report.

5 References

Andrews, T., J. M. Gregory, M. J. Webb, and K. E. Taylor (2012), Forcing, feedbacks and climate sensitivity in CMIP5 coupled atmosphere-ocean climate models, *Geophys. Res. Lett., 39*(9), L09712, doi: 10.1029/2012gl051607.

Antonov, J. I., D. Seidov, T. P. Boyer, R. A. Locarnini, A. V. Mishonov, H. E. Garcia, O. K. Baranova, M. M. Zweng, and D. R. Johnson (2010), World Ocean Atlas 2009 Volume 2: Salinity, NOAA Atlas NESDIS 69, 2, 184 pp.

Aquarone, M. C., and S. Adams (2008), Scotian Shelf LME #8 in The UNEP Large Marine Ecosystem Report: A perspective on changing conditions in LMEs of the world's Regional Seas. , UNEP Regional Seas Report and Studies No. 182, 795-804 pp.

Arora, V. K., J. F. Scinocca, G. J. Boer, J. R. Christian, K. L. Denman, G. M. Flato, V. V. Kharin, W. G. Lee, and W. J. Merryfield (2011), Carbon emission limits required to satisfy future representative concentration pathways of greenhouse gases, *Geophys. Res. Lett., 38*, L05805, doi: 10.1029/2010gl046270.

Aumont, O., and L. Bopp (2006), Globalizing results from ocean in situ iron fertilization studies, *Global Biogeochem. Cycles, 20*, GB2017, doi: 10.1029/2005gb002591.

Azetsu-Scott, K., and P. Yeats (2007), Changing chemical environment in the Labrador Sea: consequences for climate and ecosystem studies., *AZMP Bulletin PMZA*, *6*, 16-19.

Azetsu-Scott, K., A. Clarke, K. Falkner, J. Hamilton, E. P. Jones, C. Lee, B. Petrie, S. Prinsenberg, M. Starr, and P. Yeats (2010), Calcium carbonate saturation states in the waters of the Canadian Arctic Archipelago and the Labrador Sea, *J. Geophys. Res., 115*(C11), C11021, doi: 10.1029/2009jc005917.

Benson, B. B., and D. Krause (1984), The Concentration and Isotopic Fractionation of Oxygen Dissolved in Fresh-Water and Seawater in Equilibrium with the Atmosphere, *Limnol. Oceanogr.*, *29*(3), 620-632.

Carmack, E., and F. McLaughlin (2011), Towards recognition of physical and geochemical change in Subarctic and Arctic Seas, *Prog. Oceanogr.*, *90*(1-4), 90-104.

Christensen, M. K., and J. M. Pringle (2012), The frequency and cause of shallow winter mixed layers in the Gulf of Maine, *J. Geophys. Res.*, *117*(C1), C01025, doi: 10.1029/2011jc007358.

Christian, J. R., V. K. Arora, G. J. Boer, C. L. Curry, K. Zahariev, K. L. Denman, G. M. Flato, W. G. Lee, W. J. Merryfield, N. T. Roulet, and J. F. Scinocca (2010), The global carbon cycle in the Canadian Earth system model (CanESM1): Preindustrial control simulation, *J. Geophys. Res.*, *115*(G3), G03014, doi: 10.1029/2008jg000920.

Chung, S. N., K. Lee, R. A. Feely, C. L. Sabine, F. J. Millero, R. Wanninkhof, J. L. Bullister, R. M. Key, and T. H. Peng (2003), Calcium carbonate budget in the Atlantic Ocean based on water column inorganic carbon chemistry, *Global Biogeochem. Cycles*, *17*(4), 1093, doi: 10.1029/2002gb002001.

Collins, W. J., et al. (2011), Development and evaluation of an Earth-System model-HadGEM2, *Geosci. Model. Dev.*, *4*(4), 1051-1075.

Danabasoglu, G., W. G. Large, J. J. Tribbia, P. R. Gent, B. P. Briegleb, and J. C. McWilliams (2006), Diurnal coupling in the tropical oceans of CCSM3, *J. Clim.*, *19*(11), 2347-2365.

Doyon, P., and R. G. Ingram (2000), Seasonal upper-layer T-S structure in the Gulf of St. Lawrence during the ice-free months, *Deep Sea Res. II*, *47*(3-4), 385-413.

Dufresne, J. L., et al. (2013), Climate change projections using the IPSL-CM5 Earth System Model: from CMIP3 to CMIP5, *Clim. Dyn.*, *40*(9-10), 2123-2165.

Dunne, J. P., et al. (2012), GFDL's ESM2 Global Coupled Climate-Carbon Earth System Models. Part I: Physical Formulation and Baseline Simulation Characteristics, *J. Clim.*, *25*(19), 6646-6665.

Dunne, J. P., et al. (2013), GFDL's ESM2 Global Coupled Climate-Carbon Earth System Models. Part II: Carbon System Formulation and Baseline Simulation Characteristics, *J. Clim.*, *26*(7), 2247-2267.

Feely, R. A., S. C. Doney, and S. R. Cooley (2009), Ocean Acidification: Present Conditions and Future Changes in a High-CO(2) World, *Oceanography*, *22*(4), 36-47.

Ferland, J., M. Gosselin, and M. Starr (2011), Environmental control of summer primary production in the Hudson Bay system: The role of stratification, *J. Mar. Syst.*, *88*(3), 385-400.

Fetterer, F., K. Knowles, W. Meier, and M. Savoie (2009), Sea Ice Index, edited by N. S. a. I. D. Center, National Snow and Ice Data Center, Boulder, Colorado USA.

Flato, G. M., G. J. Boer, W. G. Lee, N. A. McFarlane, D. Ramsden, M. C. Reader, and A. J. Weaver (2000), The Canadian centre for climate modelling and analysis global coupled model and its climate, *Clim. Dyn.*, *16*, 451-467.

Fournier, R. O., J. Marra, R. Bohrer, and M. Vandet (1977), Plankton Dynamics and Nutrient Enrichment of Scotian-Shelf, *J. Fish. Res. Board Can.*, *34*(7), 1004-1018.

Frajka-Williams, E., and P. B. Rhines (2010), Physical controls and interannual variability of the Labrador Sea spring phytoplankton bloom in distinct regions, *Deep Sea Research Part I: Oceanographic Research Papers*, *57*(4), 541-552.

Galbraith, P. S., J. Chassé, D. Gilbert, P. Larouche, D. Brickman, B. Pettigrew, L. Devine, A. Gosselin, R. Pettipas, and C. Lafleur (2012a), Physical Oceanographic Conditions in the Gulf of St. Lawrence in 2011, DFO Can. Sci. Advis. Sec. Res. Doc., 2012/023, iii + 85 pp.

Galbraith, P. S., P. Larouche, J. Chasse, and B. Petrie (2012b), Sea-surface temperature in relation to air temperature in the Gulf of St. Lawrence: Interdecadal variability and long term trends, *Deep-Sea Res. II*, *77-80*, 10-20.

Garcia, H. E., R. A. Locarnini, T. P. Boyer, J. I. Antonov, O. K. Baranova, M. M. Zweng, and D. R. Johnson (2010a), World Ocean Atlas 2009, Volume 3: Dissolved Oxygen, Apparent Oxygen Utilization, and Oxygen Saturation., World Ocean Atlas 2009, 3, 344 pp.

Garcia, H. E., R. A. Locarnini, T. P. Boyer, J. I. Antonov, M. M. Zweng, O. K. Baranova, and D. R. Johnson (2010b), World Ocean Atlas 2009, Volume 4: Nutrients (phosphate, nitrate, silicate), World Ocean Atlas 2009, 398 pp.

Gilbert, D., B. Sundby, C. Gobeil, A. Mucci, and G.-H. Tremblay (2005), A seventy-two-year record of diminishing deep-water oxygen in the St. Lawrence estuary: The northwest Atlantic connection, *Limnol. Oceanogr.*, *50*(5), 1654-1666.

Greenan, B., G. Harrison, I. Yashayaev, K. Azetsu-Scott, E. Head, W. Li, and J. Loder (2010), Physical, Chemical, and Biological Conditions in the Labrador Sea in 2009, AZMP Bulletin PMZA, 9, 11-19 pp.

Griffies, S. M., et al. (2005), Formulation of an ocean model for global climate simulations, *Ocean Science*, *1*(1), 45-79.

Guo, L., W. Perrie, Z. Long, J. Chassé, Y. Zhang, and A. Huang (2013), Dynamical downscaling over the Gulf of St. Lawrence using the Canadian Regional Climate Model., *Atmosphere-Ocean*, *51*(3), 265-283.

Harrison, W. G., and W. K. W. Li (2007), Phytoplankton Growth and Regulation in the Labrador Sea: Light and Nutrient Limitation, *J. Northwest Atl. Fish. Sci.*, *39*, 71-82.

Hendry, R., I. Yashayaev, A. Clarke, and J. Lazier (2003), Interannual Changes in the Hydrography of the Labrador Sea: 1990-2002, *AZMP Bulletin PMZA*, *3*, 33-37.

Hendry, R., and G. Harrison (2007), Status of the Labrador Sea, *AZMP Bulletin PMZA*, *6*, 11-15.

Henson, S. A., J. P. Dunne, and J. L. Sarmiento (2009), Decadal variability in North Atlantic phytoplankton blooms, *J. Geophys. Res.*, *114*, C04013, doi: 10.1029/2008JC005139.

Hofmann, A. F., E. T. Peltzer, P. M. Walz, and P. G. Brewer (2011), Hypoxia by degrees: Establishing definitions for a changing ocean, *Deep Sea Res. I*, *58*(12), 1212-1226.

Hunke, E., and W. H. Lipscomb (2004), CICE: The Los Alamos Sea Ice Model, documentation and software, Version 3.1., 56 pp.

Ilyina, T., K. D. Six, J. Segschneider, E. Maier-Reimer, H. Li, and I. Nunez-Riboni (2013), The global ocean biogeochemistry model HAMOCC: Model architecture and performance as component of the MPI-Earth System Model in different CMIP5 experimental realizations., *J. Adv. Model. Earth Syst.*, *accepted*.

Johns, T. C., et al. (2006), The new Hadley Centre Climate Model (HadGEM1): Evaluation of coupled simulations, *J. Clim.*, *19*(7), 1327-1353.

Jungclaus, J. H., N. Keenlyside, M. Botzet, H. Haak, J. J. Luo, M. Latif, J. Marotzke, U. Mikolajewicz, and E. Roeckner (2006), Ocean circulation and tropical variability in the coupled model ECHAM5/MPI-OM, *J. Clim.*, *19*(16), 3952-3972.

Knutti, R., D. Masson, and A. Gettelman (2013), Climate model genealogy: Generation CMIP5 and how we got there, *Geophys. Res. Lett.*, *40*(6), 1194-1199.

Large, W. G., J. C. McWilliams, and S. C. Doney (1994), Oceanic Vertical Mixing - a Review and a Model with a Nonlocal Boundary-Layer Parameterization, *Rev. Geophys.*, *32*(4), 363-403.

Large, W. G., G. Danabasoglu, J. C. McWilliams, P. R. Gent, and F. O. Bryan (2001), Equatorial circulation of a global ocean climate model with anisotropic horizontal viscosity, *J. Phys. Oceanogr.*, *31*(2), 518-536.

Le Fouest, V., B. Zakardjian, F. J. Saucier, and M. Starr (2005), Seasonal versus synoptic variability in planktonic production in a high-latitude marginal sea: The Gulf of St. Lawrence (Canada), *J. Geophys. Res.*, *110*, C09012, doi: 10.1029/2004JC002423.

Levy, M. (2005), Oceanography: Nutrients in remote mode, *Nature*, *437*(7059), 628-631.

Li, W. K. W., W. G. Harrison, and E. J. H. Head (2006), Coherent Sign Switching in Multiyear Trends of Microbial Plankton, *Science*, *311*(5764), 1157-1160.

Linder, C. A., and G. Gawarkiewicz (1998), A climatology of the shelfbreak front in the Middle Atlantic Bight, *J. Geophys. Res.*, *103*(C9), 18405-18423.

Locarnini, R. A., A. V. Mishonov, J. I. Antonov, T. P. Boyer, H. E. Garcia, O. K. Baranova, M. M. Zweng, and D. R. Johnson (2010), World Ocean Atlas 2009, Volume 1: Temperature, NOAA Atlas NESDIS 71, 184 pp.

Loder, J. W., and A. van der Baaren (2013), Climate change projections for the Northwest Atlantic from six CMIP5 Earth System Models., Can. Tech.. Rep. Hydrogr. Ocean. Sci., 286, xiv + 112 pp.

Louanchi, F., and R. G. Najjar (2001), Annual cycles of nutrients and oxygen in the upper layers of the North Atlantic Ocean, *Deep Sea Research Part II: Topical Studies in Oceanography*, *48*(10), 2155-2171.

Lu, Y. Y., D. G. Wright, and I. Yashayaev (2007), Modelling hydrographic changes in the Labrador Sea over the past five decades, *Prog. Oceanogr.*, *73*(3-4), 406-426.

Madec, G., and M. Imbard (1996), A global ocean mesh to overcome the North Pole singularity, *Clim. Dyn.*, *12*(6), 381-388.

Marsland, S. J., H. Haak, J. H. Jungclaus, M. Latif, and F. Roske (2003), The Max-Planck-Institute global ocean/sea ice model with orthogonal curvilinear coordinates, *Ocean Modelling*, *5*(2), 91-127.

Martin, G. M., et al. (2011), The HadGEM2 family of Met Office Unified Model climate configurations, *Geosci. Model. Dev.*, *4*(3), 723-757.

McGeehan, T., and W. Maslowski (2011), Impact of Shelf Basin Freshwater Transport on Deep Convection in the Western Labrador Sea, *J. Phys. Oceanogr.*, *41*(11), 2187-2210.

Mousseau, L., L. Legendre, and L. Fortier (1996), Dynamics of size-fractionated phytoplankton and trophic pathways on the Scotian Shelf and at the shelf break, northwest Atlantic, *Aquat. Microb. Ecol.*, *10*(2), 149-163.

Mucci, A., M. Starr, D. Gilbert, and B. Sundby (2011), Acidification of Lower St. Lawrence Estuary Bottom Waters, *Atmosphere-Ocean*, *49*(3), 206-218.

Palmer, J. R., and I. J. Totterdell (2001), Production and export in a global ocean ecosystem model, *Deep-Sea Res. II*, *48*(5), 1169-1198.

Palter, J. B., M. Lozier, and R. T. Barber (2005), The effect of advection on the nutrient reservoir in the North Atlantic subtropical gyre, *Nature*, *437*(7059), 687-692.

Parkinson, C. L., and D. J. Cavalieri (2008), Arctic sea ice variability and trends, 1979 - 2006, *J. Geophys. Res., 113*, C07003, doi: 10.1029/2007jc004558.

Pepin, P., G. L. Maillet, D. Lavoie, and C. Johnson (2013), Temporal trends in nutrient concentrations in the northwest Atlantic basin, in *Climate Trends and Projections Technical Summaries for the Atlantic Large Aquatic Basin. Can. Tech. Rep. Fish. Aquat. Sci., in press.*, edited by A. van der Baaren and others.

Petrie, B., and P. Yeats (2000), Annual and interannual variability of nutrients and their estimated fluxes in the Scotian Shelf, Gulf of Maine region, *Can. J. Fish. Aquat. Sci.*, *57*(12), 2536-2546.

Petrie, B., R. Pettipas, and W. M. Petrie (2008), An Overview of Meteorological, Sea Ice and Sea-Surface Temperature Conditions off Eastern Canada during 2007, DFO Can. Sci. Advis. Sec. Res. Doc., 2008/16, iv+38 pp.

Platt, T., and S. Sathyendranath (2008), Ecological indicators for the pelagic zone of the ocean from remote sensing, *Remote Sens. Environ., 112*(8), 3426–3436, doi: 10.1016/j.rse.2007.10.016.

Prasad, K. S., and R. L. Haedrich (1993), Primary Production Estimates on the Grand-Banks of Newfoundland, North-West Atlantic-Ocean, Derived from Remotely-Sensed Chlorophyll, *Int. J. Remote Sens.*, *14*(17), 3299-3304.

Shadwick, E. H., H. Thomas, K. Azetsu-Scott, B. J. W. Greenan, E. Head, and E. Horne (2011), Seasonal variability of dissolved inorganic carbon and surface water pCO_2 in the Scotian Shelf region of the Northwestern Atlantic, *Mar. Chem.*, *124*(1-4), 23-37.

Sherman, K., I. M. Belkin, K. D. Friedland, J. O'Reilly, and K. Hyde (2009), Accelerated Warming and Emergent Trends in Fisheries Biomass Yields of the World's Large Marine Ecosystems, *Ambio*, *38*(4), 215-224.

Sillmann, J., V. V. Kharin, X. Zhang, F. W. Zwiers, and D. Bronaugh (2013), Climate extremes indices in the CMIP5 multimodel ensemble: Part 1. Model evaluation in the present climate, *J. Geophys. Res.*, *118*(4), 1716-1733.

Stramma, L., D. Kieke, M. Rhein, F. Schott, I. Yashayaev, and K. P. Koltermann (2004), Deep water changes at the western boundary of the subpolar North Atlantic during 1996 to 2001, *Deep-Sea Res. II*, *51*(8), 1033-1056.

Strutton, P. G., T. R. Martz, M. D. DeGrandpre, W. R. McGillis, W. M. Drennan, and E. Boss (2011), Bio-optical observations of the 2004 Labrador Sea phytoplankton bloom, *J. Geophys. Res., 116*(C11), C11037, doi: 10.1029/2010jc006872.

Takahashi, T., et al. (2009), Climatological mean and decadal change in surface ocean pCO2, and net sea-air CO2 flux over the global oceans, *Deep Sea Res. II*, *56*(8-10), 554-577.

Taylor, K. E., R. J. Stouffer, and G. A. Meehl (2012), An Overview of CMIP5 and the Experiment Design, *Bull. Am. Meteorol. Soc.*, *93*(4), 485-498.

Tivy, A., S. E. L. Howell, B. Alt, S. McCourt, R. Chagnon, G. Crocker, T. Carrieres, and J. J. Yackel (2011a), Correction to :Trends and variability in summer sea ice cover in the Canadian Arctic based on the Canadian Ice Service Digital Archive, 1960-2008 and 1968-2008, *J. Geophys. Res.*, *116*(C6), C06027, doi: 10.1029/2011jc007248.

Tivy, A., S. E. L. Howell, B. Alt, S. McCourt, R. Chagnon, G. Crocker, T. Carrieres, and J. J. Yackel (2011b), Trends and variability in summer sea ice cover in the Canadian Arctic based on the Canadian Ice Service Digital Archive, 1960-2008 and 1968-2008, *J. Geophys. Res.*, *116*(C3), C03007, doi: 10.1029/2009jc005855.

Torres-Valdés, S., T. Tsubouchi, S. Bacon, A. C. Naveira-Garabato, R. Sanders, F. A. McLaughlin, B. Petrie, G. Kattner, K. Azetsu-Scott, and T. E. Whitledge (2013), Export of nutrients from the Arctic Ocean, *Journal of Geophysical Research: Oceans*, n/a-n/a.

Townsend, D. W., N. D. Rebuck, M. A. Thomas, L. Karp-Boss, and R. M. Gettings (2010), A changing nutrient regime in the Gulf of Maine, *Cont. Shelf Res.*, *30*(7), 820-832.

Vantrepotte, V., and F. Mélin (2011), Inter-annual variations in the SeaWiFS global chlorophyll a concentration (1997-2007), *Deep Sea Res. I*, *58*(4), 429-441.

Winton, M. (2000), A reformulated three-layer sea ice model, *J. Atmos. Ocean. Technol.*, *17*(4), 525-531.

Wu, Y. S., I. K. Peterson, C. C. L. Tang, T. Platt, S. Sathyendranath, and C. Fuentes-Yaco (2007), The impact of sea ice on the initiation of the spring bloom on the Newfoundland and Labrador Shelves, *J. Plankton Res.*, *29*(6), 509-514.

Yamamoto-Kawai, M., E. Carmack, and F. McLaughlin (2006), Nitrogen balance and Arctic throughflow, *Nature*, *443*(7107), 43.

Yao, T., C. L. Tang, and I. K. Peterson (2000), Modeling the seasonal variation of sea ice in the Labrador Sea with a coupled multicategory ice model and the Princeton ocean model, *J. Geophys. Res.*, *105*(C1), 1153-1165.

Yashayaev, I., and J. W. Loder (2009), Enhanced production of Labrador sea water in 2008, *Geophys. Res. Lett.*, *36*, L01606, doi: 10.1029/2008gl036162.

Yeats, P., S. Ryan, and G. Harrison (2010), Temporal Trends in Nutrient and Oxygen Concentrations in the Labrador Sea and on the Scotian Shelf, AZMP Bulletin PMZA, 9, 23-27 pp.

Zahariev, K., J. R. Christian, and K. L. Denman (2008), Preindustrial, historical, and fertilization simulations using a global ocean carbon model with new parameterizations of iron limitation, calcification, and N2 fixation, *Prog. Oceanogr.*, *77*(1), 56-82.

Zeebe, R. E., J. C. Zachos, K. Caldeira, and T. Tyrrell (2008), Oceans: Carbon Emissions and Acidification, *Science*, *321*(5885), 51-52.

Zhai, L., T. Platt, C. Tang, S. Sathyendranath, and R. Hernández Walls (2011), Phytoplankton phenology on the Scotian Shelf, *ICES J. Mar. Sci.*, *68*(4), 781-791.

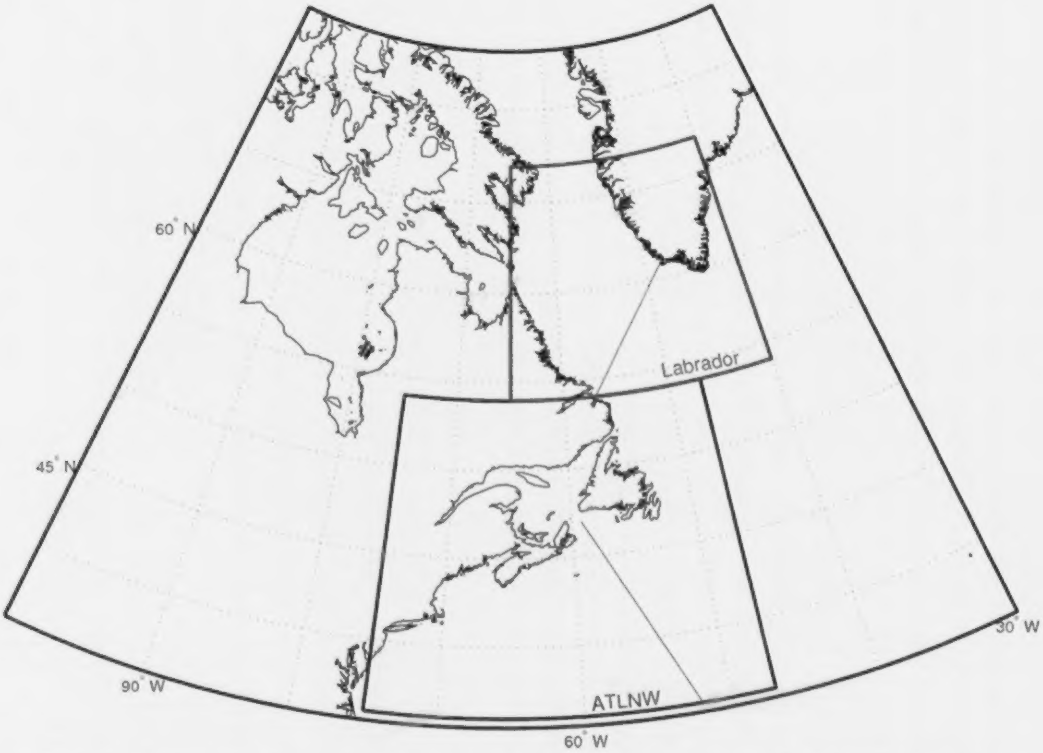
60° N
45° N
90° W
60° W
30° W
Labrador
ATLNW

Figure 1. Regions selected for trend analysis with position of transects. The Labrador Sea transect corresponds to the ARW7 line.

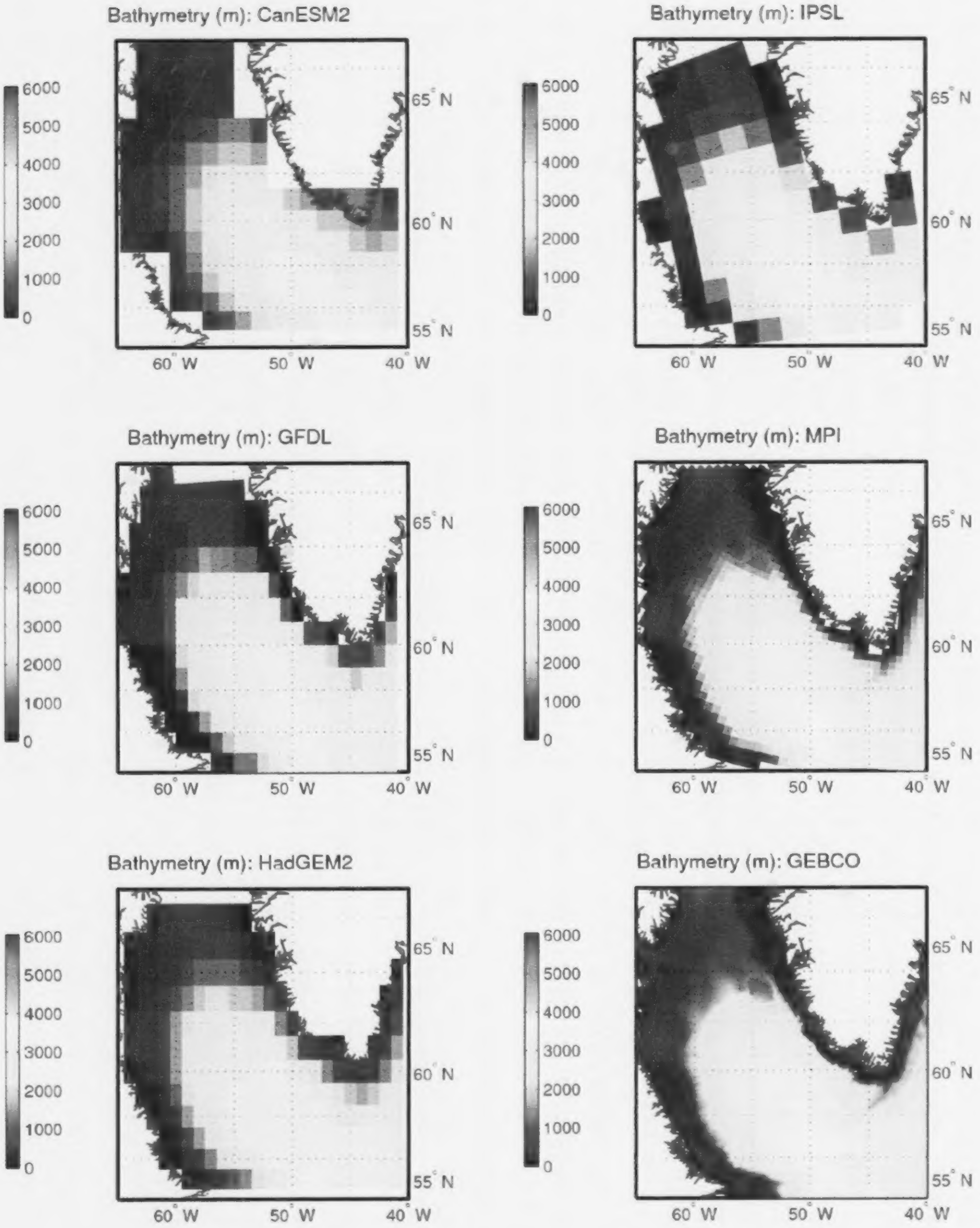

Bathymetry (m): CanESM2

Bathymetry (m): IPSL

Bathymetry (m): GFDL

Bathymetry (m): MPI

Bathymetry (m): HadGEM2

Bathymetry (m): GEBCO

6000
5000
4000
3000
2000
1000
0
65° N
60° N
55° N
60° W
50° W
40° W

Figure 2. Bathymetry of the Labrador Sea in the different models and bathymetry from the General Bathymetric Chart of the Oceans (GEBCO, www.gebco.net).

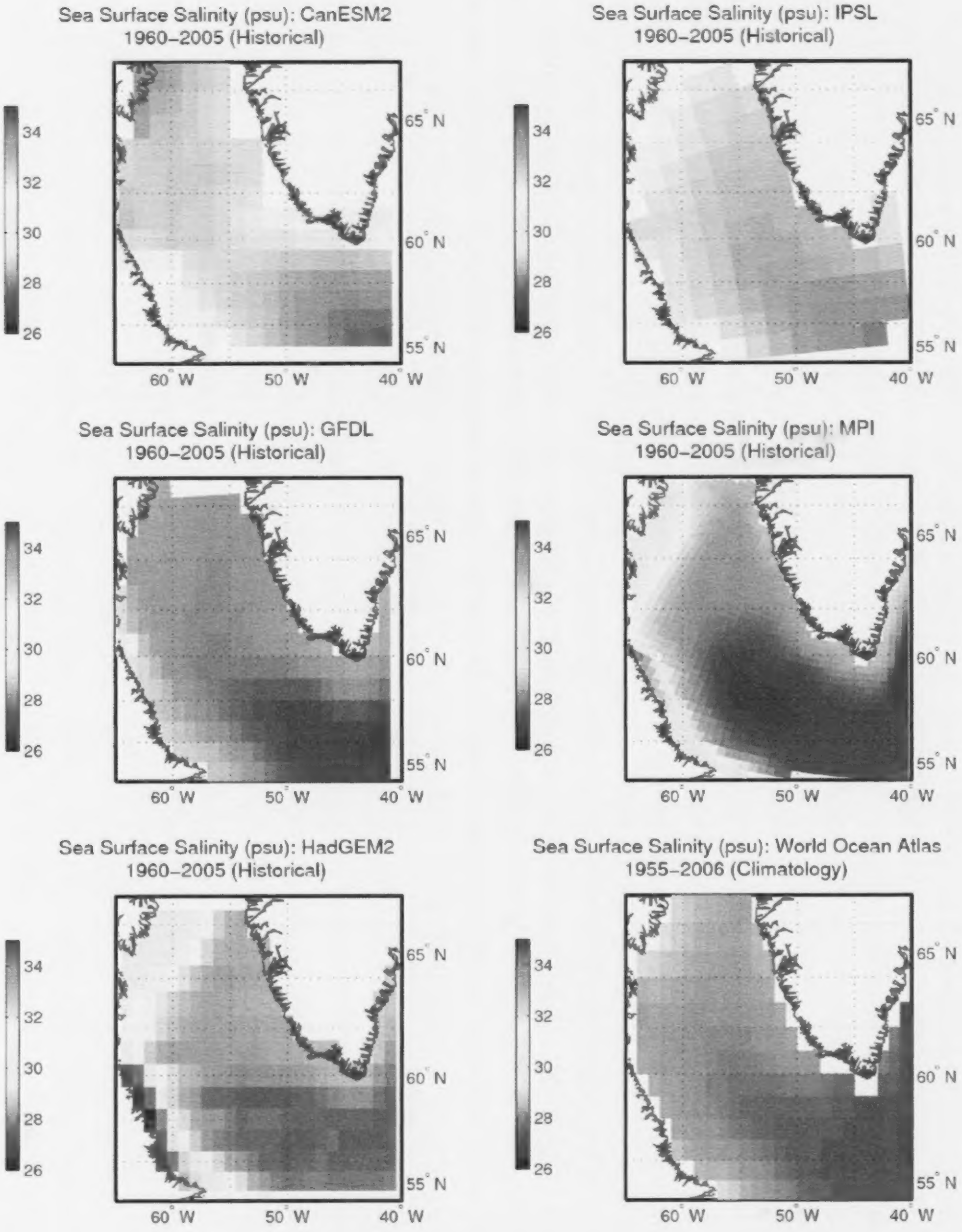
Sea Surface Salinity (psu): CanESM2
1960–2005 (Historical)
Sea Surface Salinity (psu): IPSL
1960–2005 (Historical)
Sea Surface Salinity (psu): GFDL
1960–2005 (Historical)
Sea Surface Salinity (psu): MPI
1960–2005 (Historical)
Sea Surface Salinity (psu): HadGEM2
1960–2005 (Historical)
Sea Surface Salinity (psu): World Ocean Atlas
1955–2006 (Climatology)
34
32
30
28
26
65° N
60° N
55° N
60° W
50° W
40° W

Figure 3. Mean simulated sea surface salinity in the Labrador Sea for the historical period (1960-2005) and annual sea surface salinity from the World Ocean Atlas (WOA; Antonov et al., 2010).

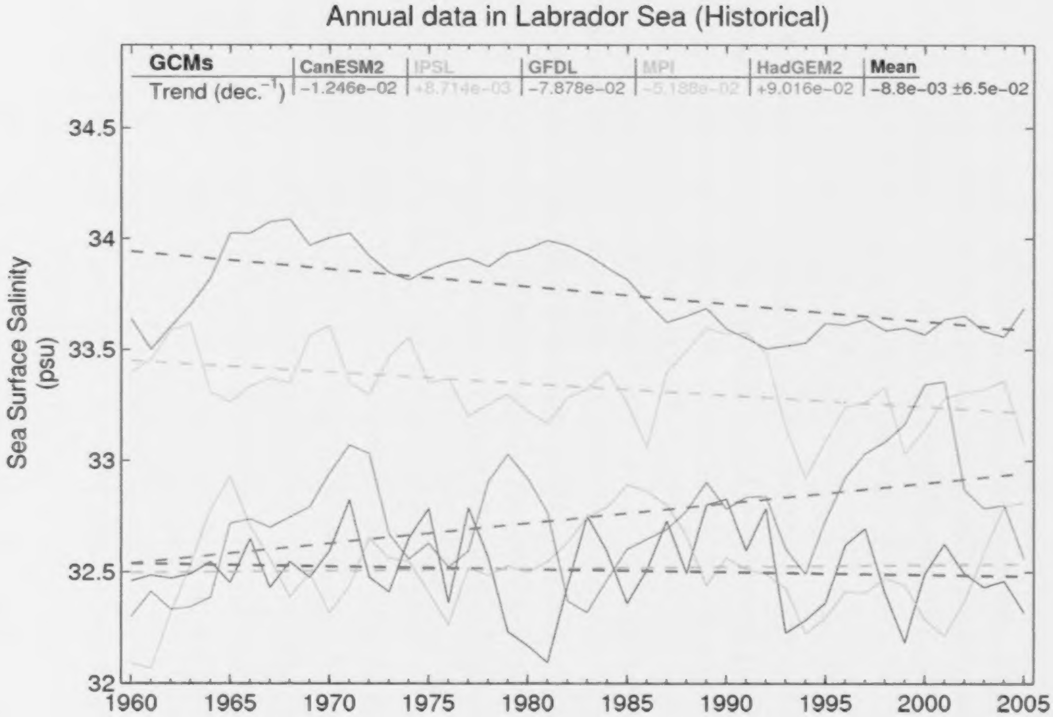

Figure 4. Average sea surface salinity trends (per decade) over the Labrador Sea (see box in Figure 1) for the historical period (1960-2005).

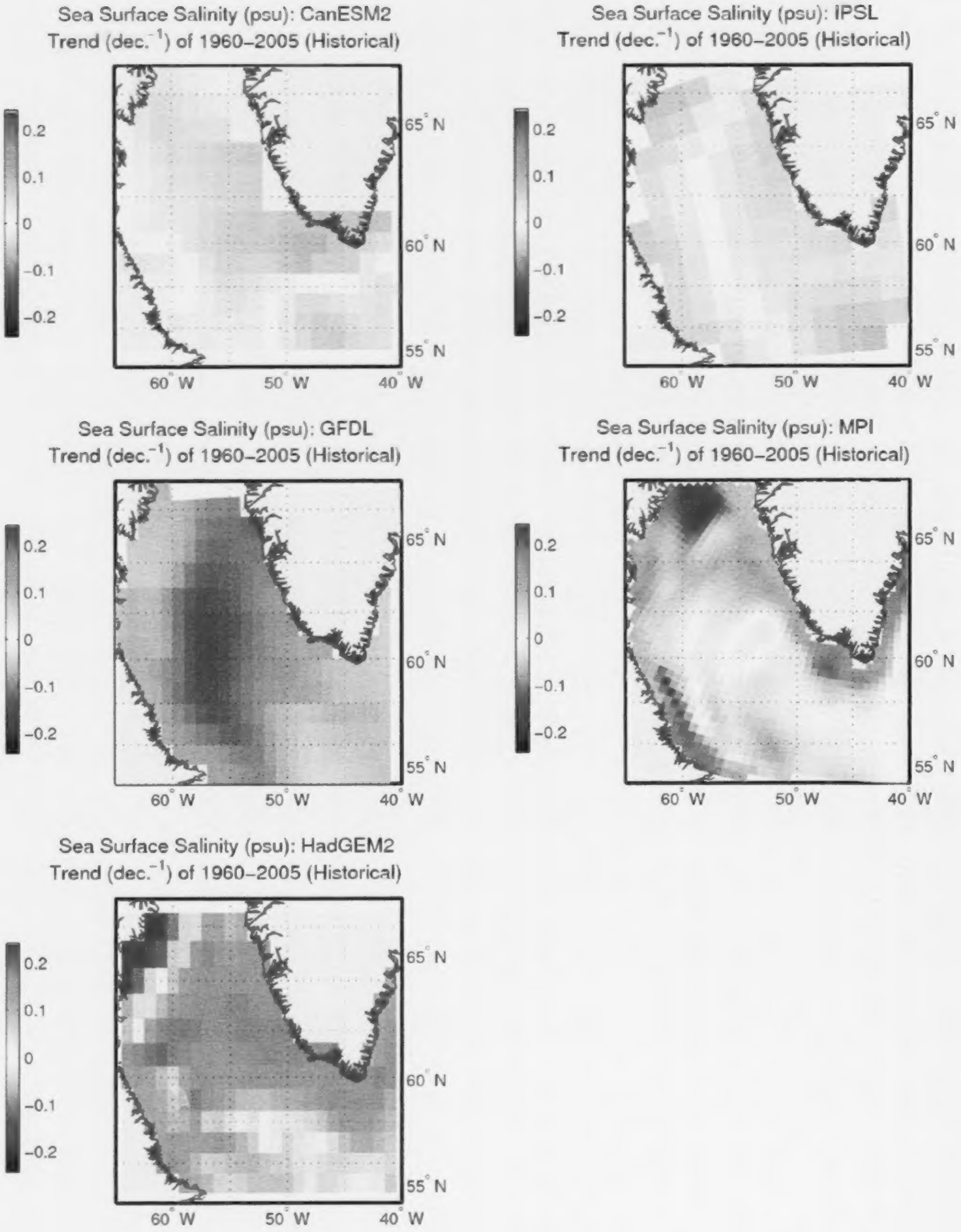
Sea Surface Salinity (psu): CanESM2 Trend (dec.$^{-1}$) of 1960–2005 (Historical)

Sea Surface Salinity (psu): IPSL Trend (dec.$^{-1}$) of 1960–2005 (Historical)

Sea Surface Salinity (psu): GFDL Trend (dec.$^{-1}$) of 1960–2005 (Historical)

Sea Surface Salinity (psu): MPI Trend (dec.$^{-1}$) of 1960–2005 (Historical)

Sea Surface Salinity (psu): HadGEM2 Trend (dec.$^{-1}$) of 1960–2005 (Historical)

Figure 5. Sea surface salinity trends (in decade^{-1}) at each grid cell in the Labrador Sea for the historical period (1960-2005).

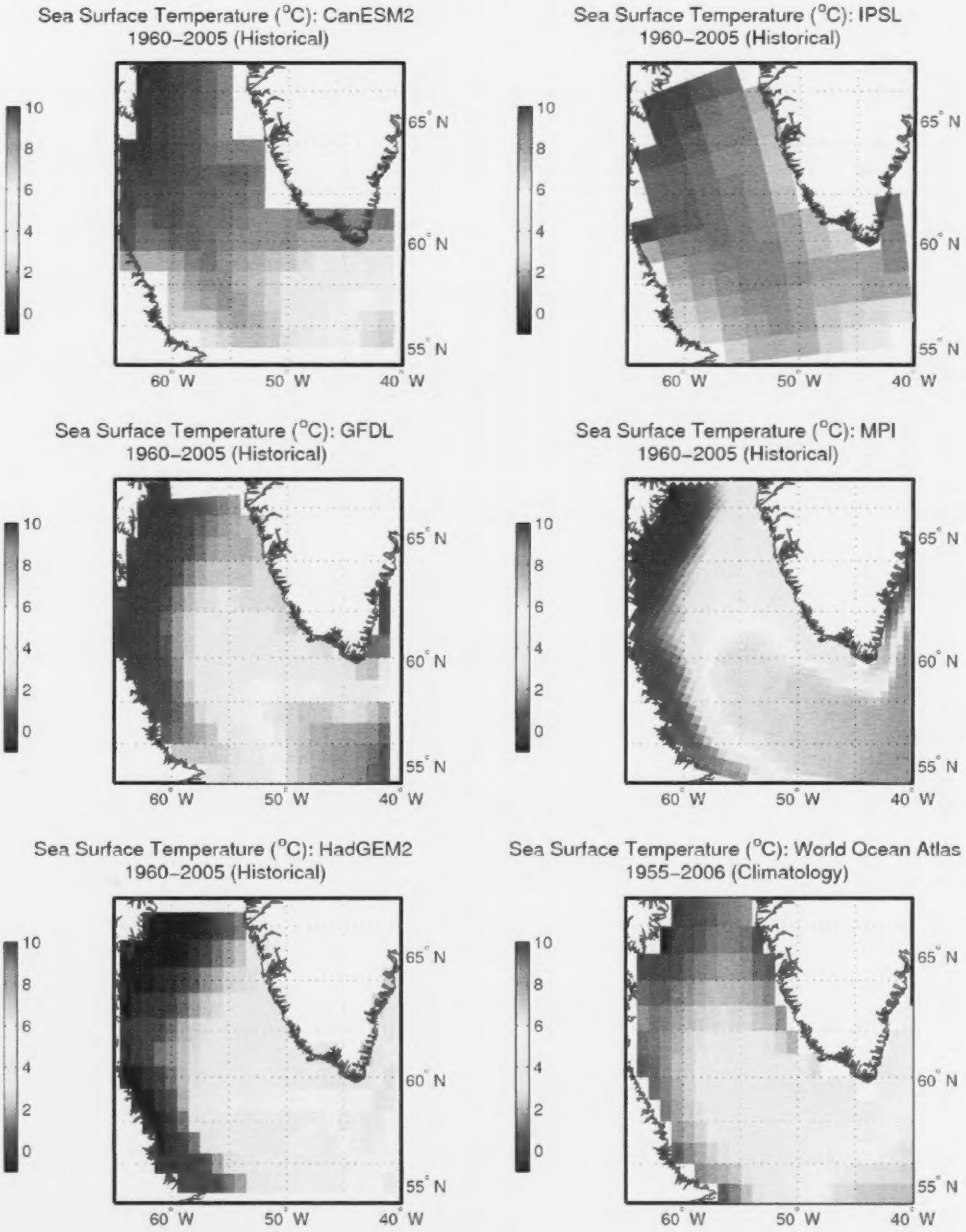

Sea Surface Temperature (°C): CanESM2
1960–2005 (Historical)

Sea Surface Temperature (°C): IPSL
1960–2005 (Historical)

Sea Surface Temperature (°C): GFDL
1960–2005 (Historical)

Sea Surface Temperature (°C): MPI
1960–2005 (Historical)

Sea Surface Temperature (°C): HadGEM2
1960–2005 (Historical)

Sea Surface Temperature (°C): World Ocean Atlas
1955–2006 (Climatology)

Figure 6. Mean simulated sea surface temperature in the Labrador Sea for the historical period (1960-2005) and annual sea surface temperature from the World Ocean Atlas (WOA; Locarnini et al., 2010).

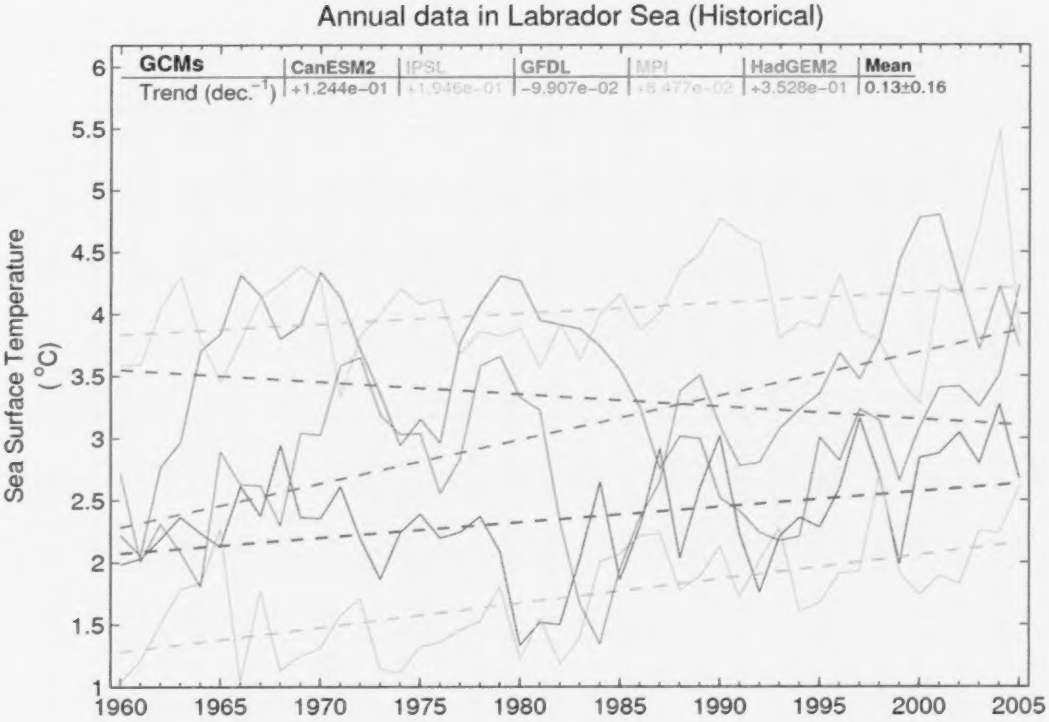

Figure 7. Average sea surface temperature trends (°C/decade) over the Labrador Sea for the historical period (1960-2005).

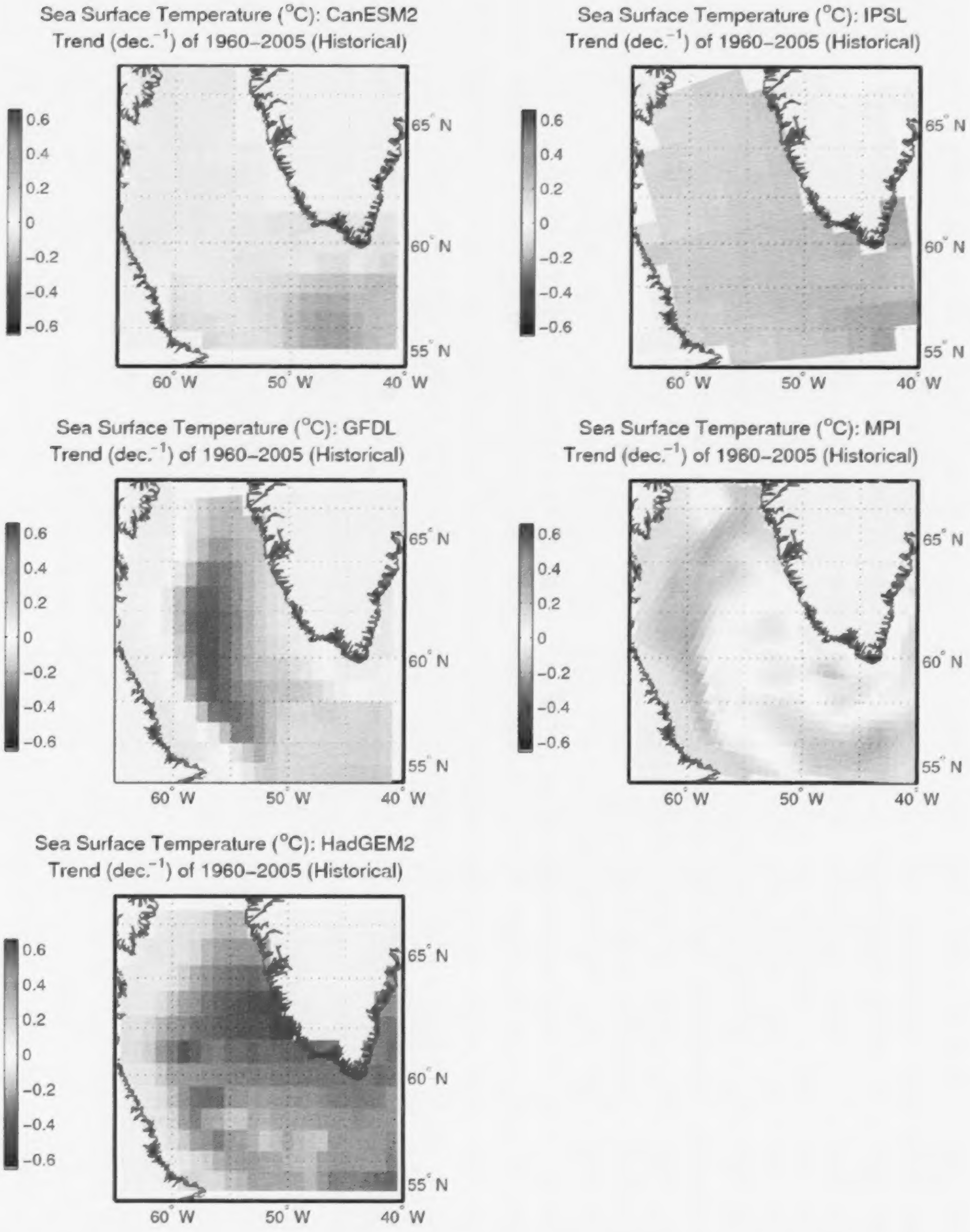
Sea Surface Temperature (°C): CanESM2
Trend (dec.⁻¹) of 1960–2005 (Historical)
Sea Surface Temperature (°C): IPSL
Trend (dec.⁻¹) of 1960–2005 (Historical)
Sea Surface Temperature (°C): GFDL
Trend (dec.⁻¹) of 1960–2005 (Historical)
Sea Surface Temperature (°C): MPI
Trend (dec.⁻¹) of 1960–2005 (Historical)
Sea Surface Temperature (°C): HadGEM2
Trend (dec.⁻¹) of 1960–2005 (Historical)
0.6
0.4
0.2
0
−0.2
−0.4
−0.6
65° N
60° N
55° N
60° W
50° W
40° W

Figure 8. Sea surface temperature trend (°C/decade) at each grid cell in the Labrador Sea for the historical period (1960-2005).

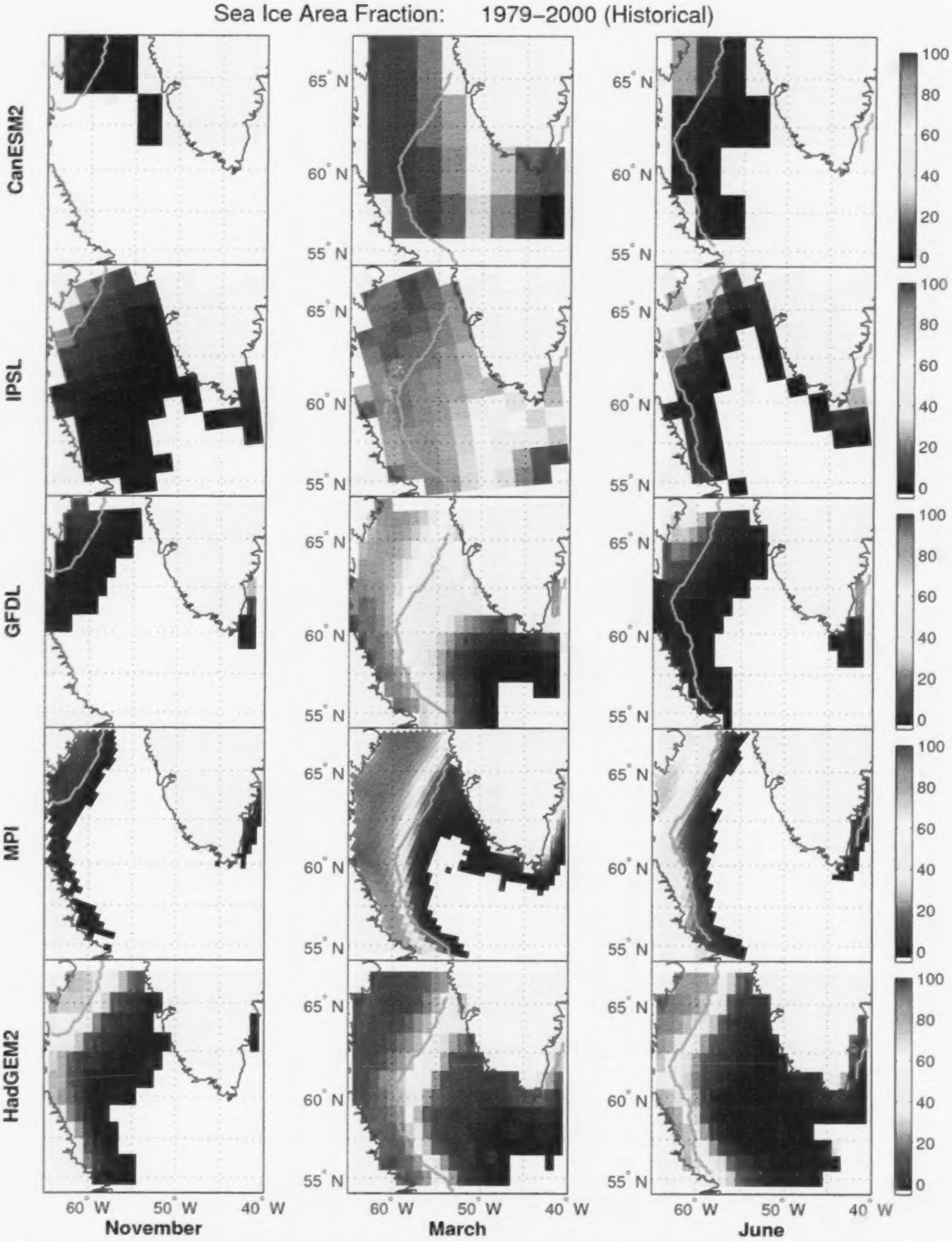
Sea Ice Area Fraction: 1979–2000 (Historical)
CanESM2
IPSL
GFDL
MPI
HadGEM2
65° N
60° N
55° N
60° W
50° W
40° W
November
March
June
100
80
60
40
20
0

Figure 9 : Average sea ice concentration in the Labrador Sea for the months of November, March and June for the historical period (1979-2000) and for the 5 GCMs. The magenta line represents the median extent (15% limit) measured by Fetterer et al. (2009) for the same period.

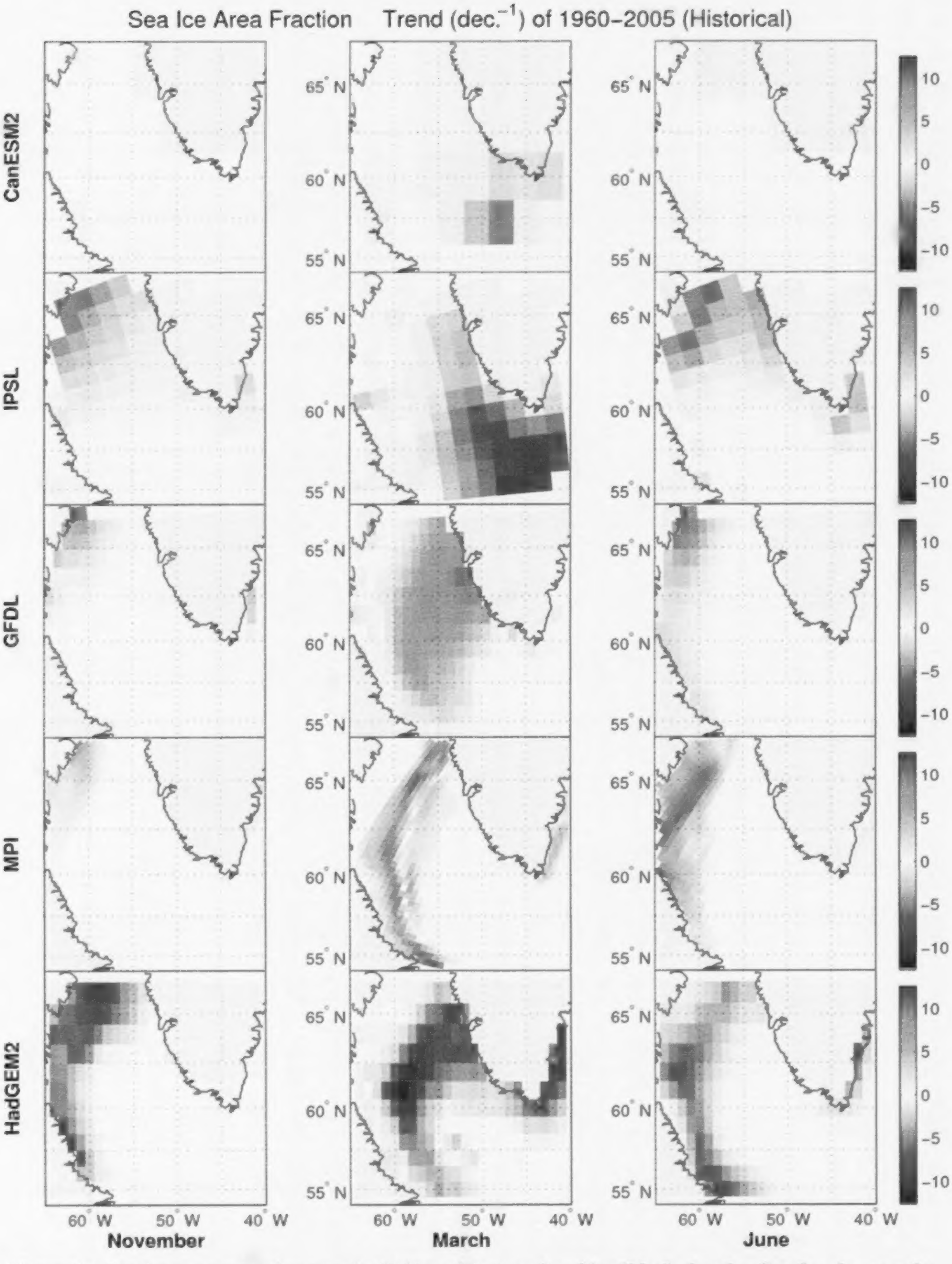
Sea Ice Area Fraction Trend (dec.$^{-1}$) of 1960-2005 (Historical)
CanESM2
IPSL
GFDL
MPI
HadGEM2
65° N
60° N
55° N
60° W
50° W
40° W
November
March
June
10
5
0
−5
−10

Figure 10. Sea ice concentration trends (%/decade) at each grid cell in Labrador Sea for the months of November, March, and June for the historical period (1960-2005) and for the 5 GCMs.

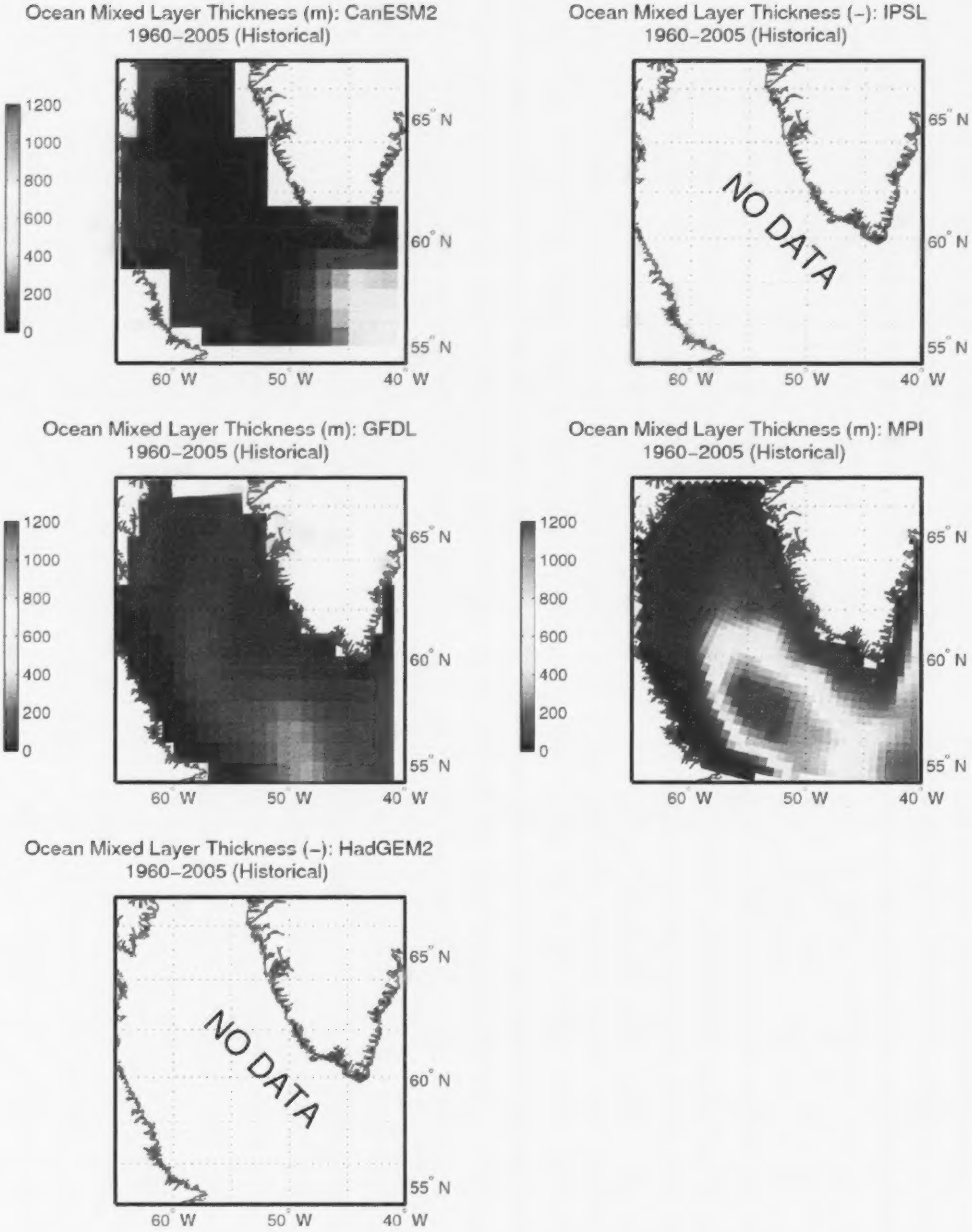
Ocean Mixed Layer Thickness (m): CanESM2
1960–2005 (Historical)
Ocean Mixed Layer Thickness (–): IPSL
1960–2005 (Historical)
NO DATA
Ocean Mixed Layer Thickness (m): GFDL
1960–2005 (Historical)
Ocean Mixed Layer Thickness (m): MPI
1960–2005 (Historical)
Ocean Mixed Layer Thickness (–): HadGEM2
1960–2005 (Historical)
NO DATA
1200
1000
800
600
400
200
0
65° N
60° N
55° N
60° W
50° W
40° W

Figure 11. Annual mean simulated mixed layer depth in the Labrador Sea for the historical period (1960-2005).

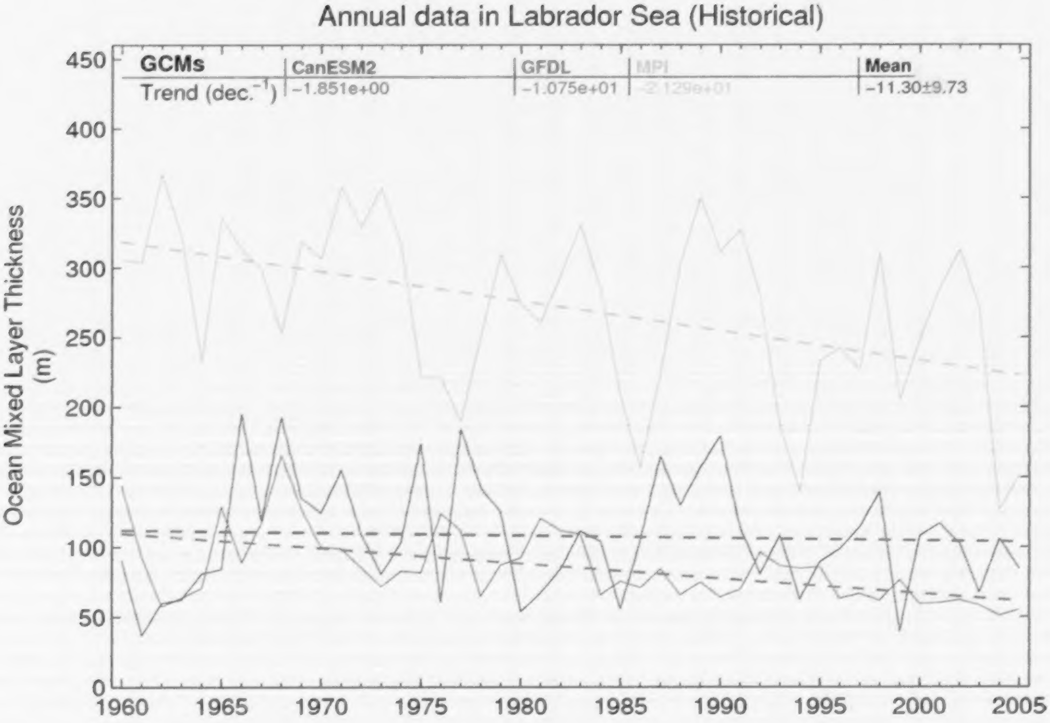

Figure 12. Annual mean mixed layer depth trends (m/decade) over the Labrador Sea for the historical period (1960-2005).

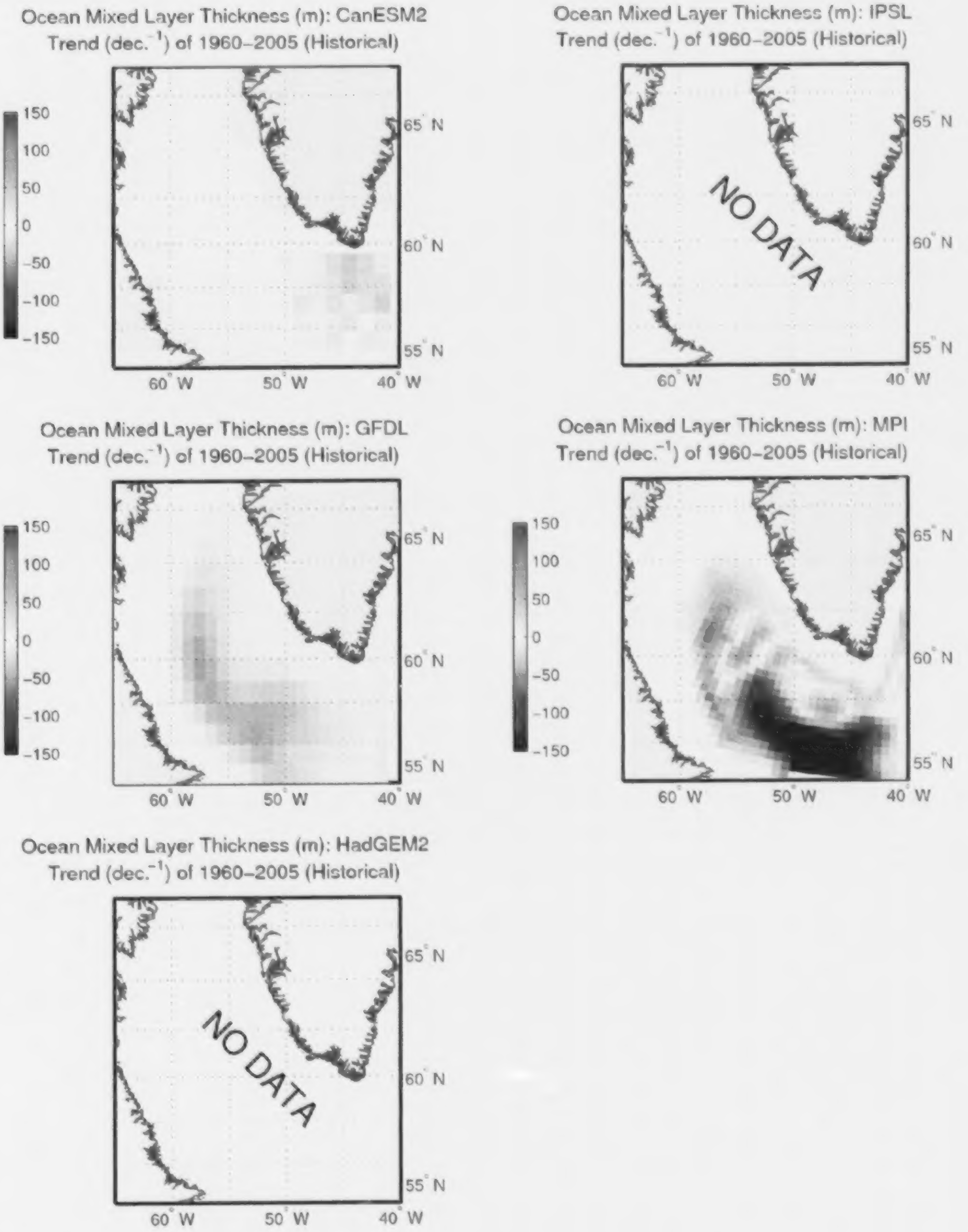
Ocean Mixed Layer Thickness (m): CanESM2 Trend (dec.$^{-1}$) of 1960–2005 (Historical)

Ocean Mixed Layer Thickness (m): IPSL Trend (dec.$^{-1}$) of 1960–2005 (Historical)

Ocean Mixed Layer Thickness (m): GFDL Trend (dec.$^{-1}$) of 1960–2005 (Historical)

Ocean Mixed Layer Thickness (m): MPI Trend (dec.$^{-1}$) of 1960–2005 (Historical)

Ocean Mixed Layer Thickness (m): HadGEM2 Trend (dec.$^{-1}$) of 1960–2005 (Historical)

Figure 13. Ocean mixed layer thickness trends (m/decade) in the Labrador Sea for the historical period (1960-2005).

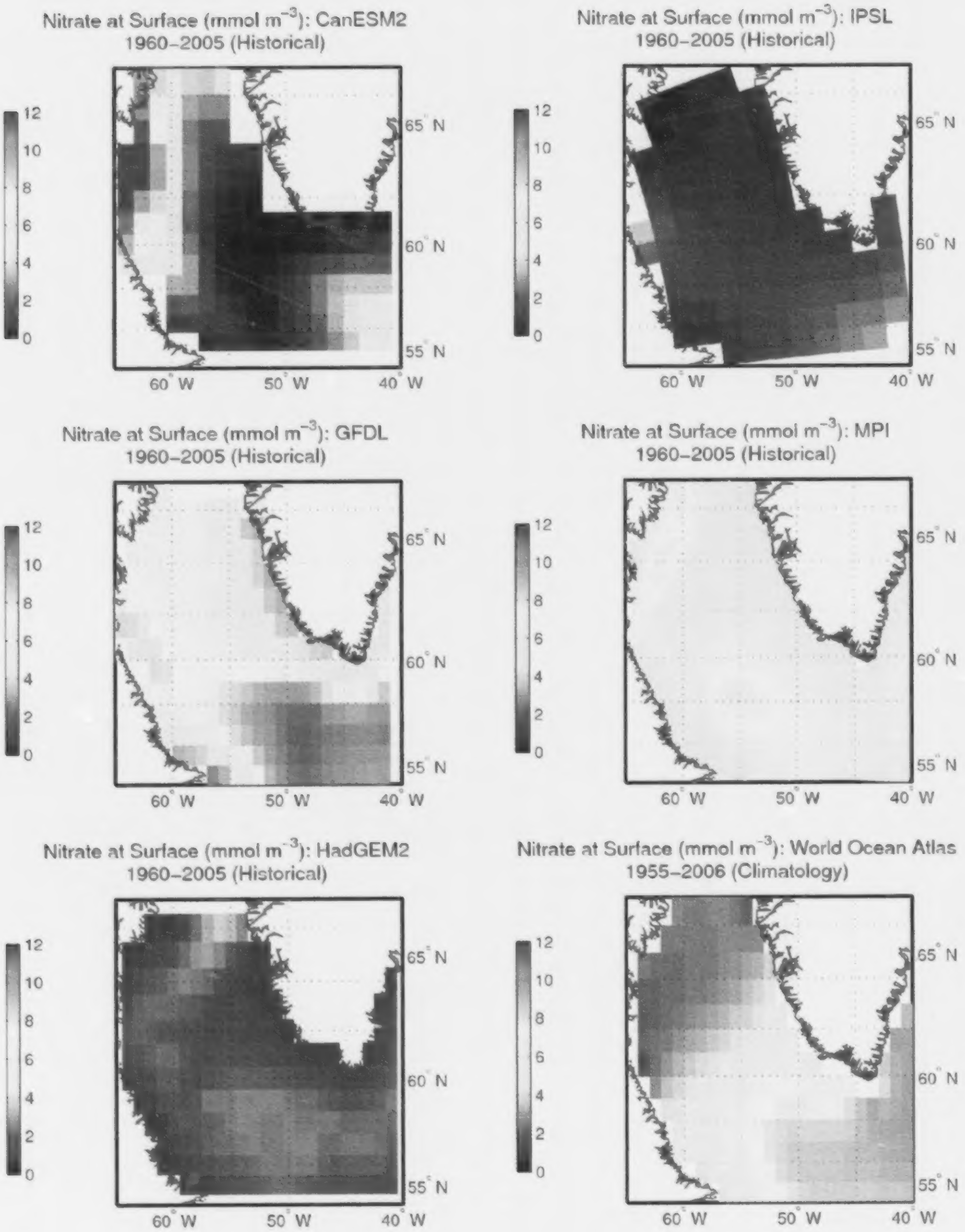
Nitrate at Surface (mmol m^{-3}): CanESM2
1960–2005 (Historical)
Nitrate at Surface (mmol m^{-3}): IPSL
1960–2005 (Historical)
Nitrate at Surface (mmol m^{-3}): GFDL
1960–2005 (Historical)
Nitrate at Surface (mmol m^{-3}): MPI
1960–2005 (Historical)
Nitrate at Surface (mmol m^{-3}): HadGEM2
1960–2005 (Historical)
Nitrate at Surface (mmol m^{-3}): World Ocean Atlas
1955–2006 (Climatology)
0
2
4
6
8
10
12
65° N
60° N
55° N
60° W
50° W
40° W

Figure 14. Annual mean simulated nitrate concentration at the surface of the Labrador Sea for the historical period (1960-2005) and nitrate concentration at the surface from the World Ocean Atlas (WOA; Garcia et al., 2010b).

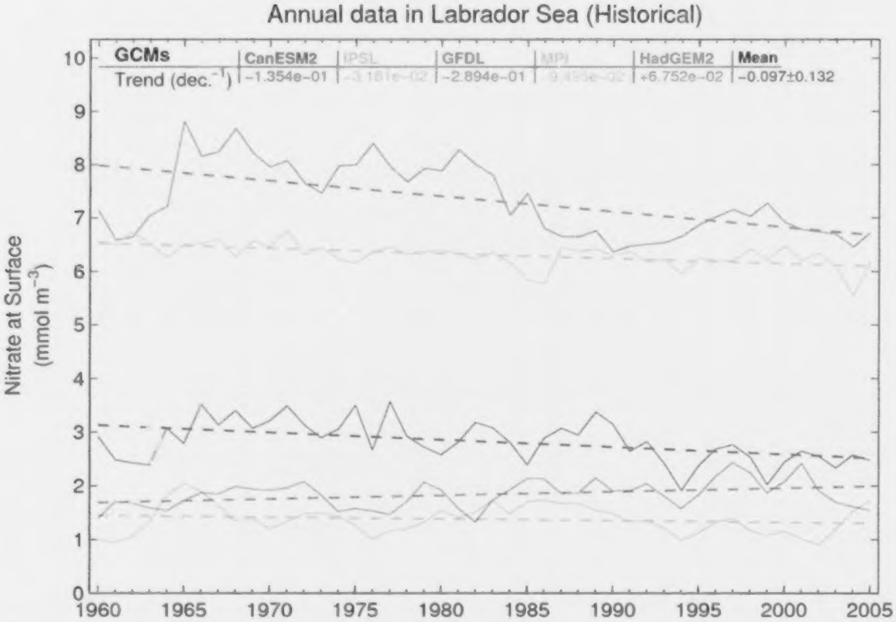

Figure 15. Average nitrate concentration trends (mmol m^{-3}/decade) at the surface over the Labrador Sea for the historical period (1960-2005).

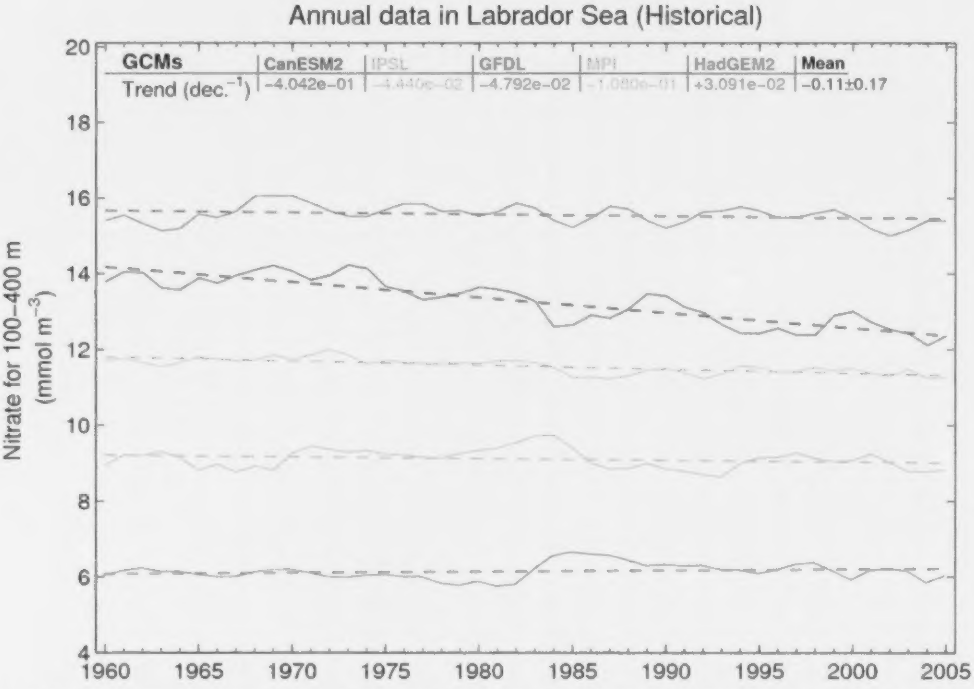

Figure 16. Average nitrate concentration trends (mmol m^{-3}/decade) at 100-400 m over the Labrador Sea for the historical period (1960-2005).

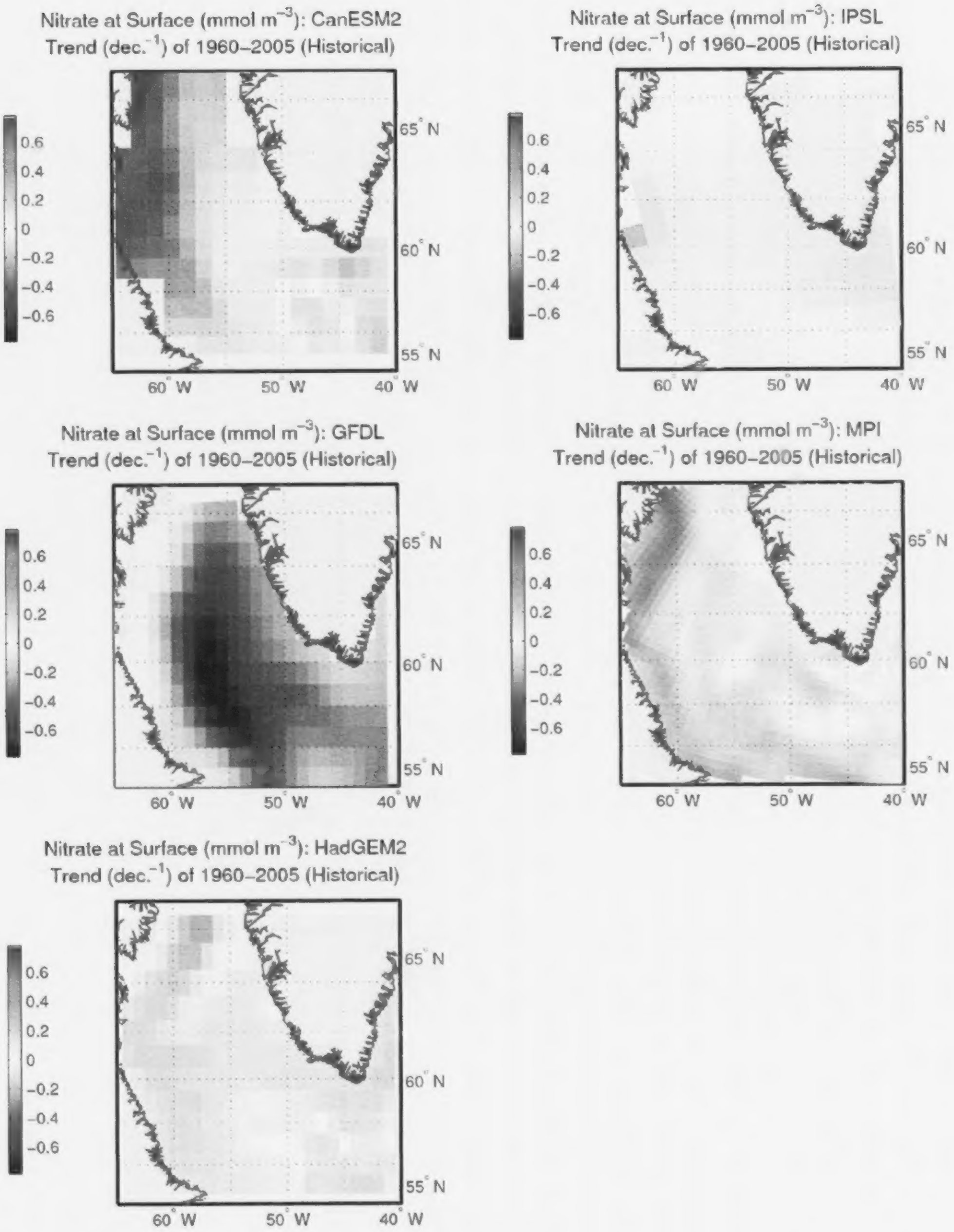
Nitrate at Surface (mmol m^{-3}): CanESM2
Trend (dec.$^{-1}$) of 1960–2005 (Historical)

Nitrate at Surface (mmol m^{-3}): IPSL
Trend (dec.$^{-1}$) of 1960–2005 (Historical)

Nitrate at Surface (mmol m^{-3}): GFDL
Trend (dec.$^{-1}$) of 1960–2005 (Historical)

Nitrate at Surface (mmol m^{-3}): MPI
Trend (dec.$^{-1}$) of 1960–2005 (Historical)

Nitrate at Surface (mmol m^{-3}): HadGEM2
Trend (dec.$^{-1}$) of 1960–2005 (Historical)

Figure 17. Nitrate concentration trends (mmol m^{-3}/decade) at the surface at each grid cell in the Labrador Sea for the historical period (1960-2005).

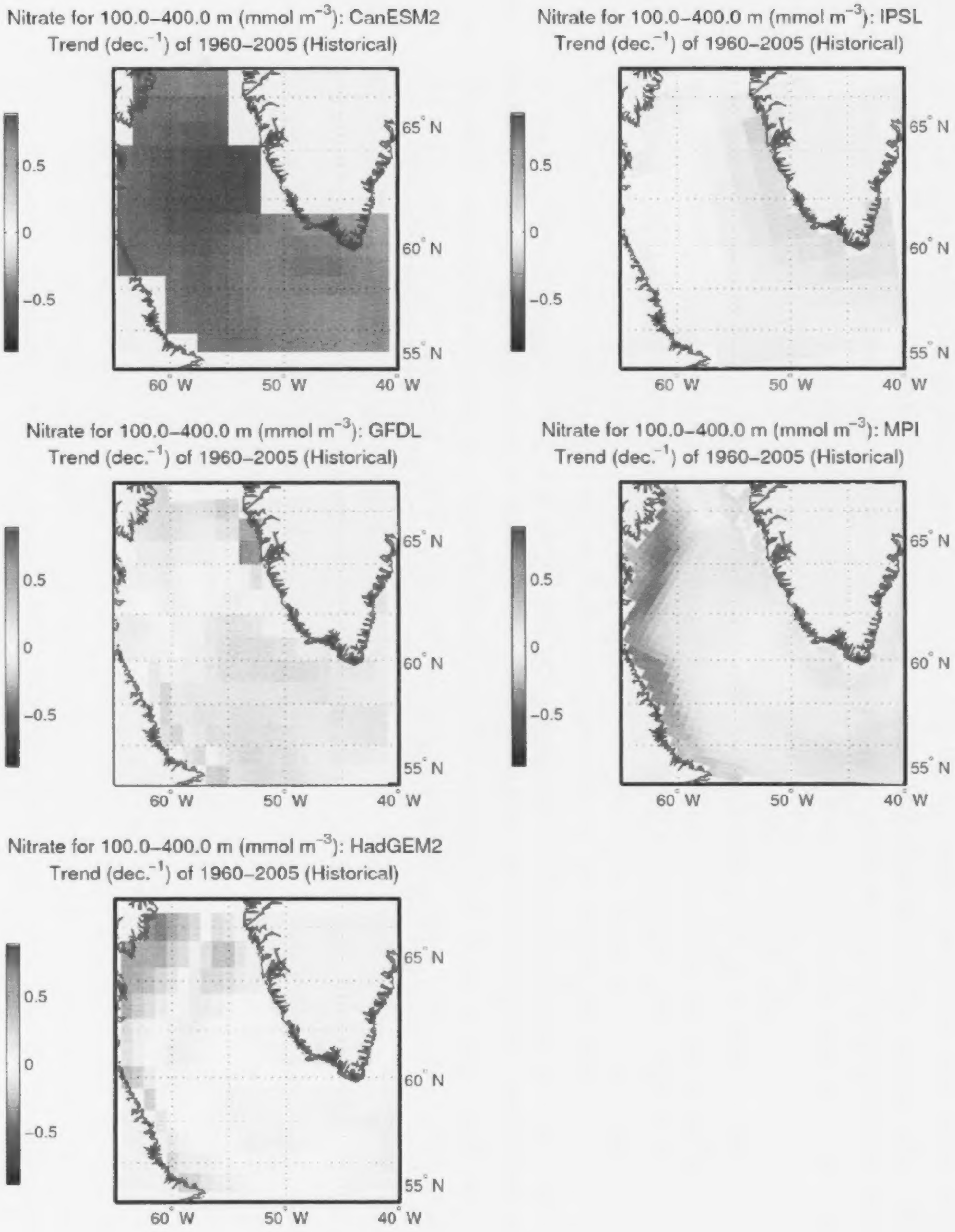

Nitrate for 100.0–400.0 m (mmol m^{-3}): CanESM2
Trend ($dec.^{-1}$) of 1960–2005 (Historical)

Nitrate for 100.0–400.0 m (mmol m^{-3}): IPSL
Trend ($dec.^{-1}$) of 1960–2005 (Historical)

Nitrate for 100.0–400.0 m (mmol m^{-3}): GFDL
Trend ($dec.^{-1}$) of 1960–2005 (Historical)

Nitrate for 100.0–400.0 m (mmol m^{-3}): MPI
Trend ($dec.^{-1}$) of 1960–2005 (Historical)

Nitrate for 100.0–400.0 m (mmol m^{-3}): HadGEM2
Trend ($dec.^{-1}$) of 1960–2005 (Historical)

Figure 18. Nitrate concentration trends (mmol m^{-3}/decade) at 100-400 m at each grid cell in the Labrador Sea for the historical period (1960-2005).

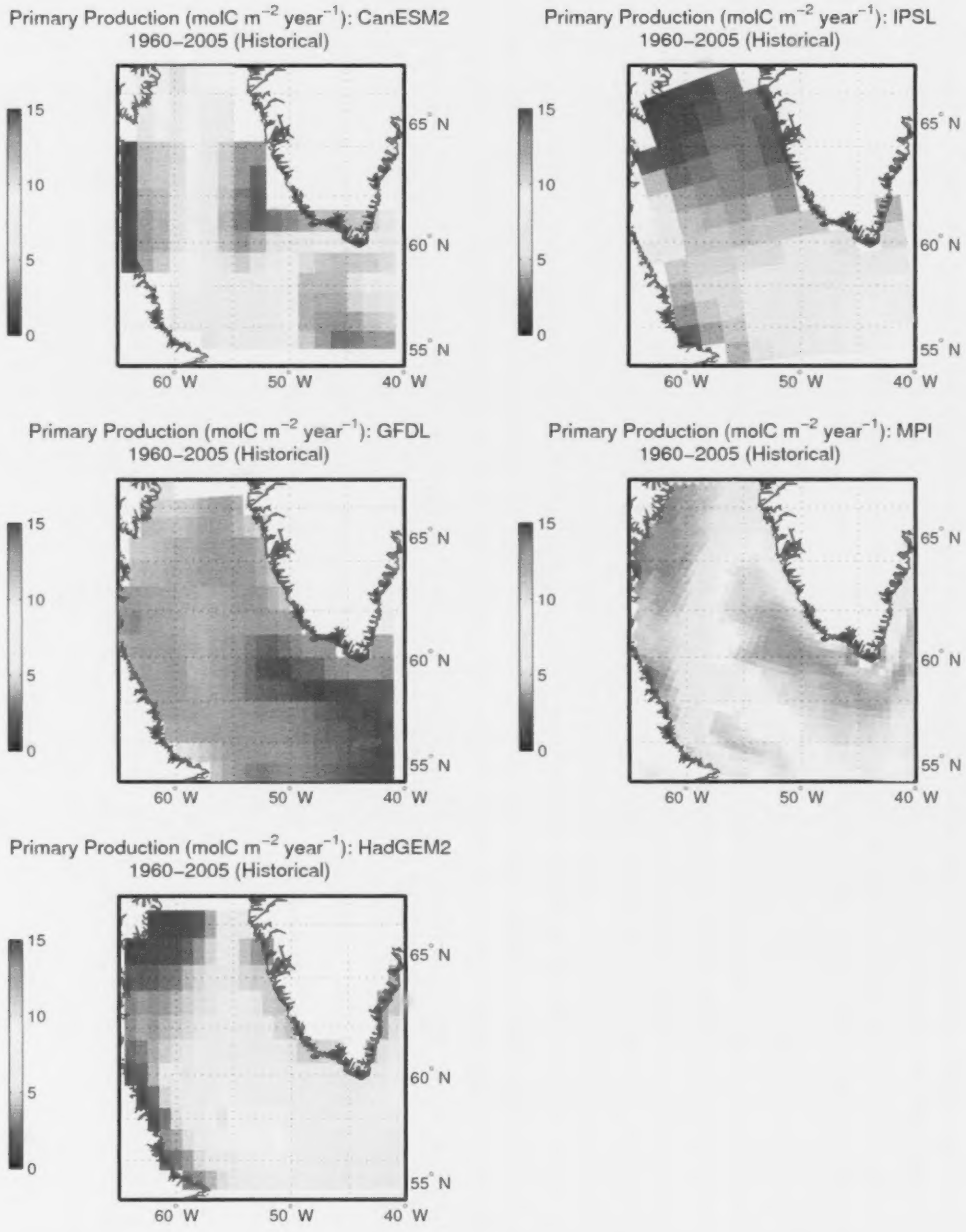
Primary Production (molC m^{-2} year^{-1}): CanESM2
1960–2005 (Historical)
Primary Production (molC m^{-2} year^{-1}): IPSL
1960–2005 (Historical)
Primary Production (molC m^{-2} year^{-1}): GFDL
1960–2005 (Historical)
Primary Production (molC m^{-2} year^{-1}): MPI
1960–2005 (Historical)
Primary Production (molC m^{-2} year^{-1}): HadGEM2
1960–2005 (Historical)
15
10
5
0
65° N
60° N
55° N
60° W
50° W
40° W

Figure 19. Mean vertically integrated primary production in the Labrador Sea for the historical period (1960-2005).

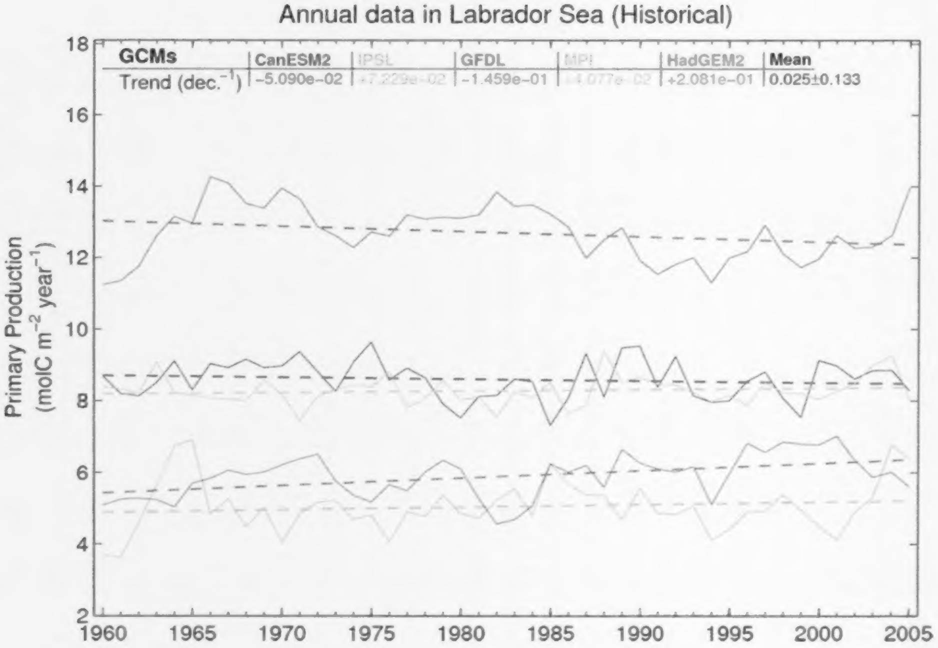

Figure 20. Average vertically integrated primary production trends (mol C m^{-2}/yr) over the Labrador Sea for the historical period (1960-2005).

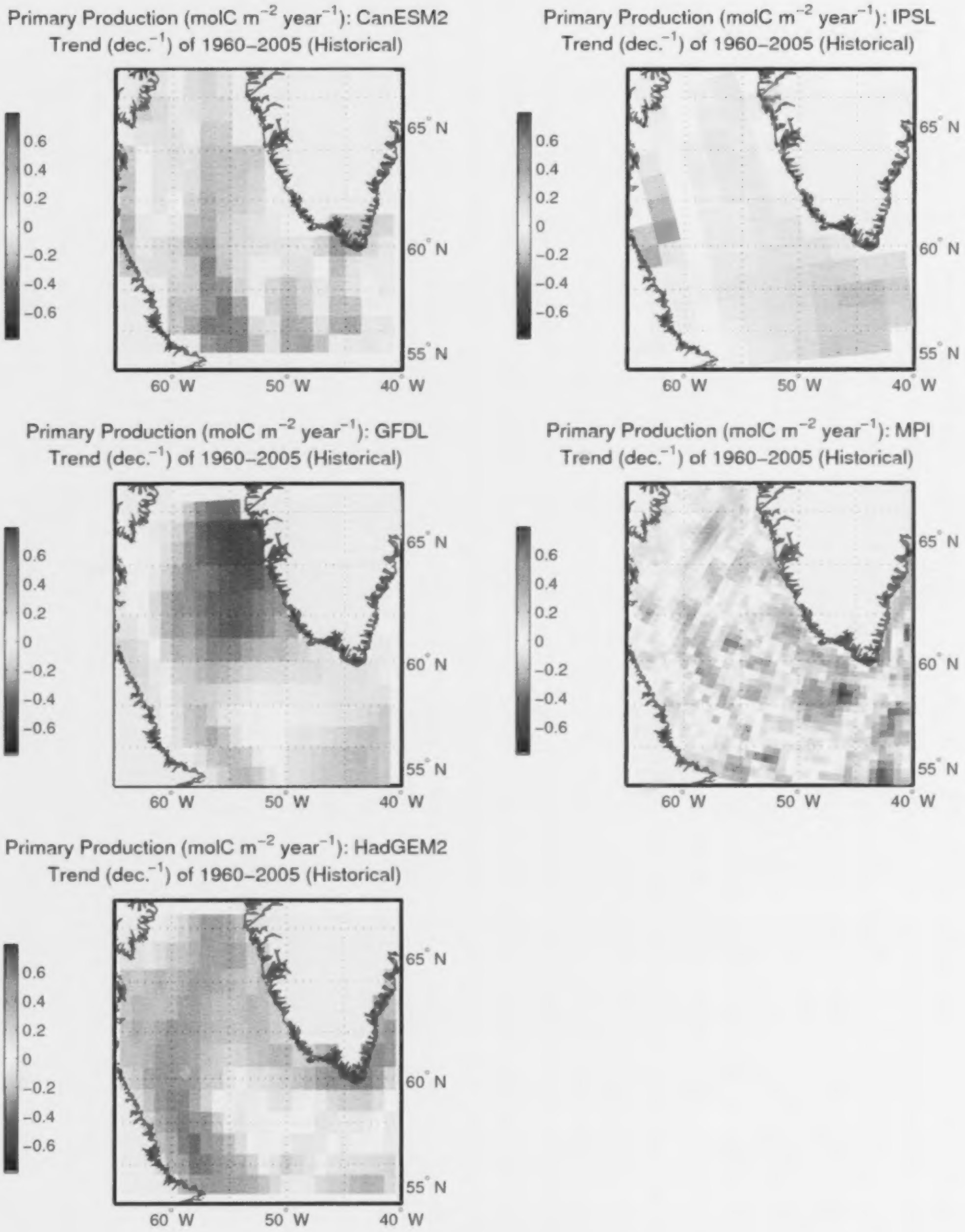

Primary Production (molC m^{-2} $year^{-1}$): CanESM2 Trend ($dec.^{-1}$) of 1960–2005 (Historical)

Primary Production (molC m^{-2} $year^{-1}$): IPSL Trend ($dec.^{-1}$) of 1960–2005 (Historical)

Primary Production (molC m^{-2} $year^{-1}$): GFDL Trend ($dec.^{-1}$) of 1960–2005 (Historical)

Primary Production (molC m^{-2} $year^{-1}$): MPI Trend ($dec.^{-1}$) of 1960–2005 (Historical)

Primary Production (molC m^{-2} $year^{-1}$): HadGEM2 Trend ($dec.^{-1}$) of 1960–2005 (Historical)

Figure 21. Vertically integrated primary production trend (mol C m^{-2}/decade) at each grid cell in the Labrador Sea for the historical period (1960-2005).

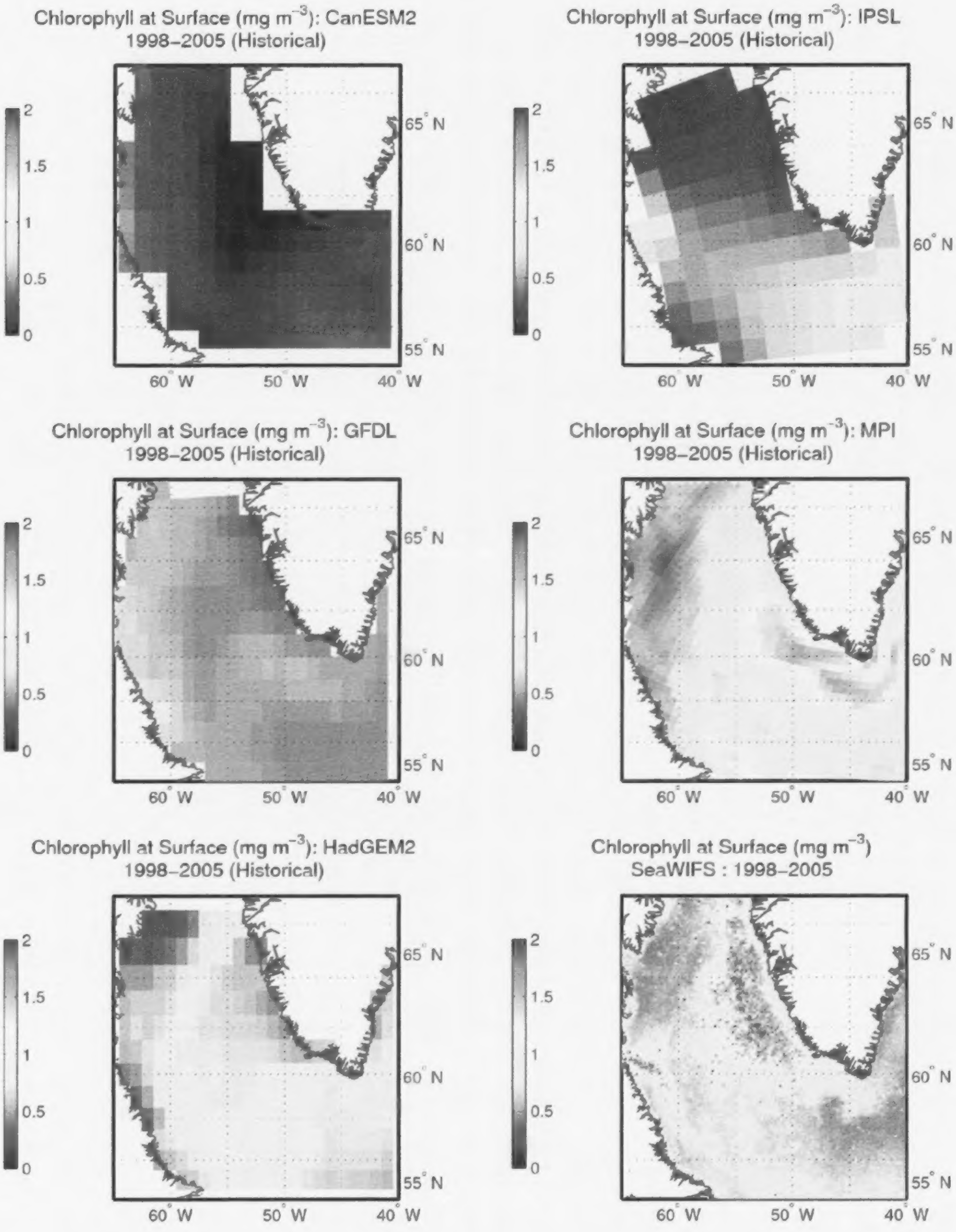
Chlorophyll at Surface (mg m^{-3}): CanESM2
1998–2005 (Historical)
Chlorophyll at Surface (mg m^{-3}): IPSL
1998–2005 (Historical)
Chlorophyll at Surface (mg m^{-3}): GFDL
1998–2005 (Historical)
Chlorophyll at Surface (mg m^{-3}): MPI
1998–2005 (Historical)
Chlorophyll at Surface (mg m^{-3}): HadGEM2
1998–2005 (Historical)
Chlorophyll at Surface (mg m^{-3})
SeaWIFS : 1998–2005
2
1.5
1
0.5
0
65° N
60° N
55° N
60° W
50° W
40° W

Figure 22. Mean simulated Chl a concentration from GCMs and Ch al data from SeaWiFS in the Labrador Sea for the 1998-2005 period.

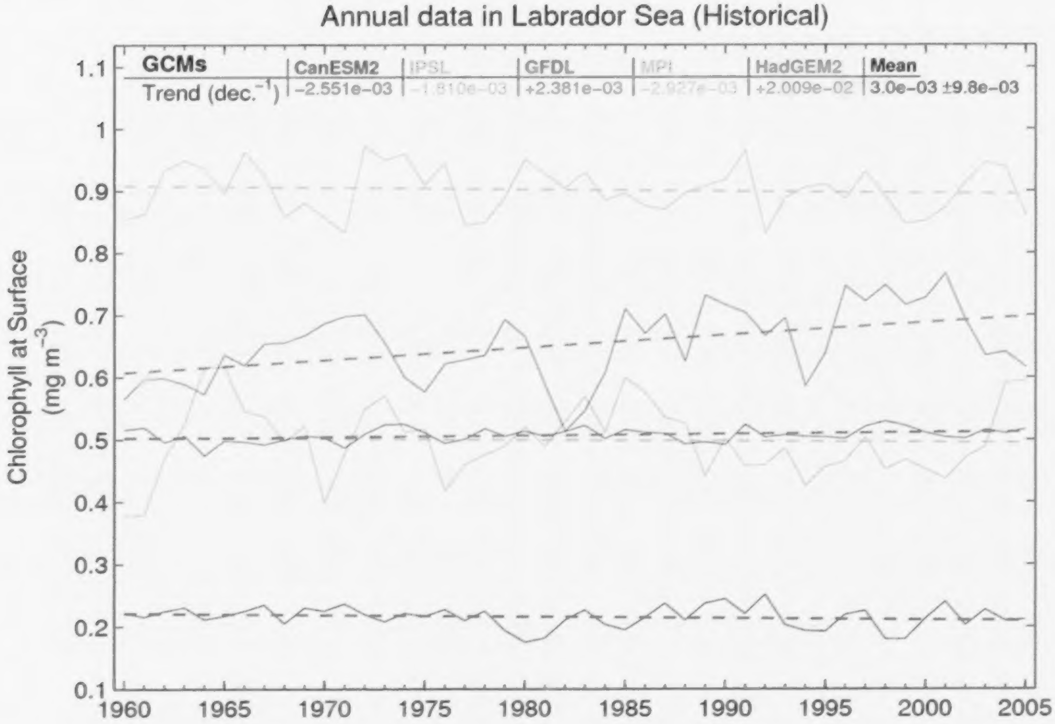

Figure 23. Average Chl a concentration trends (mg m^{-3}/decade) at the surface over the Labrador Sea for the historical period (1960-2005).

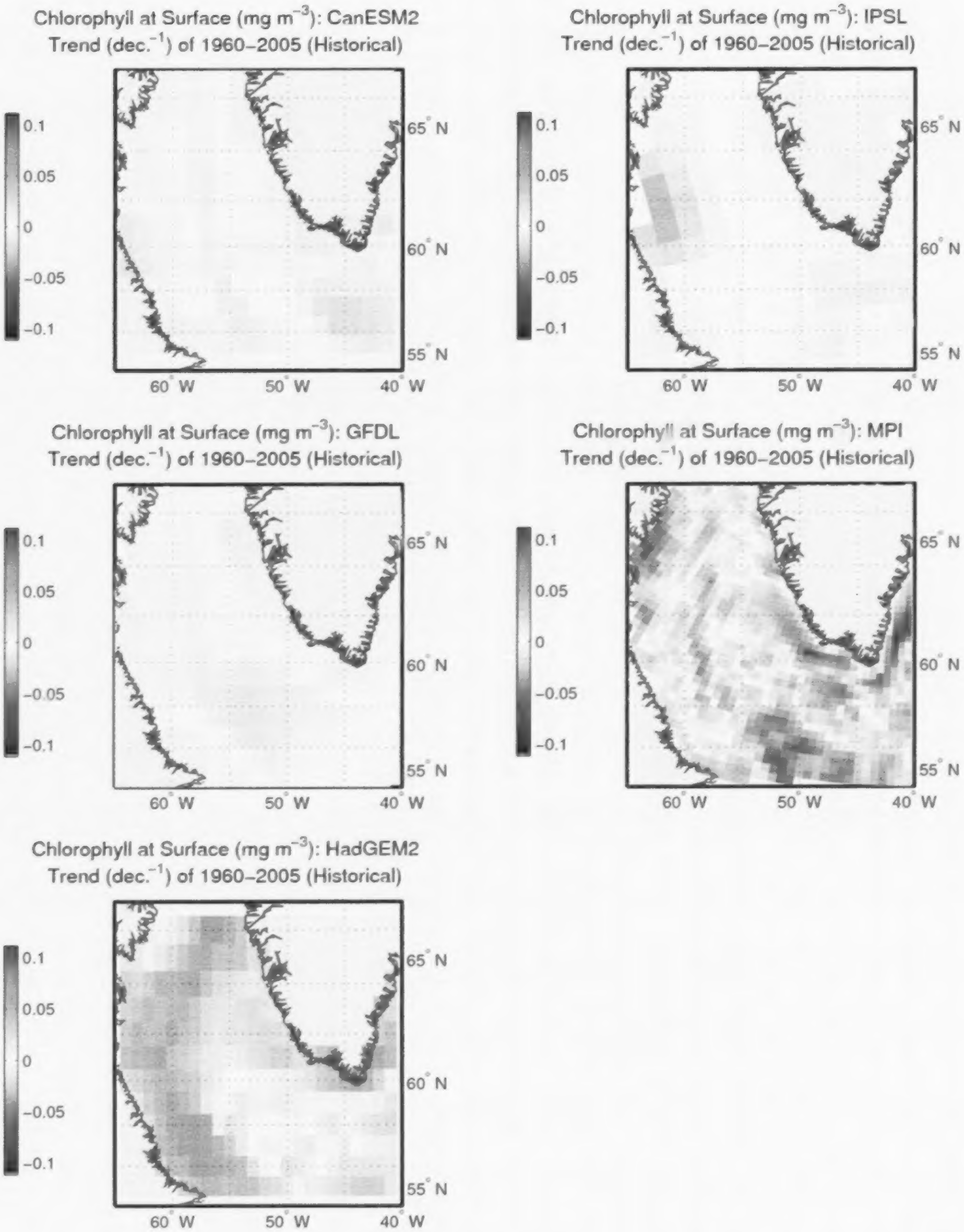

Chlorophyll at Surface (mg m^{-3}): CanESM2
Trend (dec.$^{-1}$) of 1960–2005 (Historical)
Chlorophyll at Surface (mg m^{-3}): IPSL
Trend (dec.$^{-1}$) of 1960–2005 (Historical)
Chlorophyll at Surface (mg m^{-3}): GFDL
Trend (dec.$^{-1}$) of 1960–2005 (Historical)
Chlorophyll at Surface (mg m^{-3}): MPI
Trend (dec.$^{-1}$) of 1960–2005 (Historical)
Chlorophyll at Surface (mg m^{-3}): HadGEM2
Trend (dec.$^{-1}$) of 1960–2005 (Historical)
0.1
0.05
0
−0.05
−0.1
65° N
60° N
55° N
60° W
50° W
40° W

Figure 24. Chl a concentration trends (mg m^{-3}/decade) at the surface at each grid cell in the Labrador Sea for the SeaWiFS period (1960-2005).

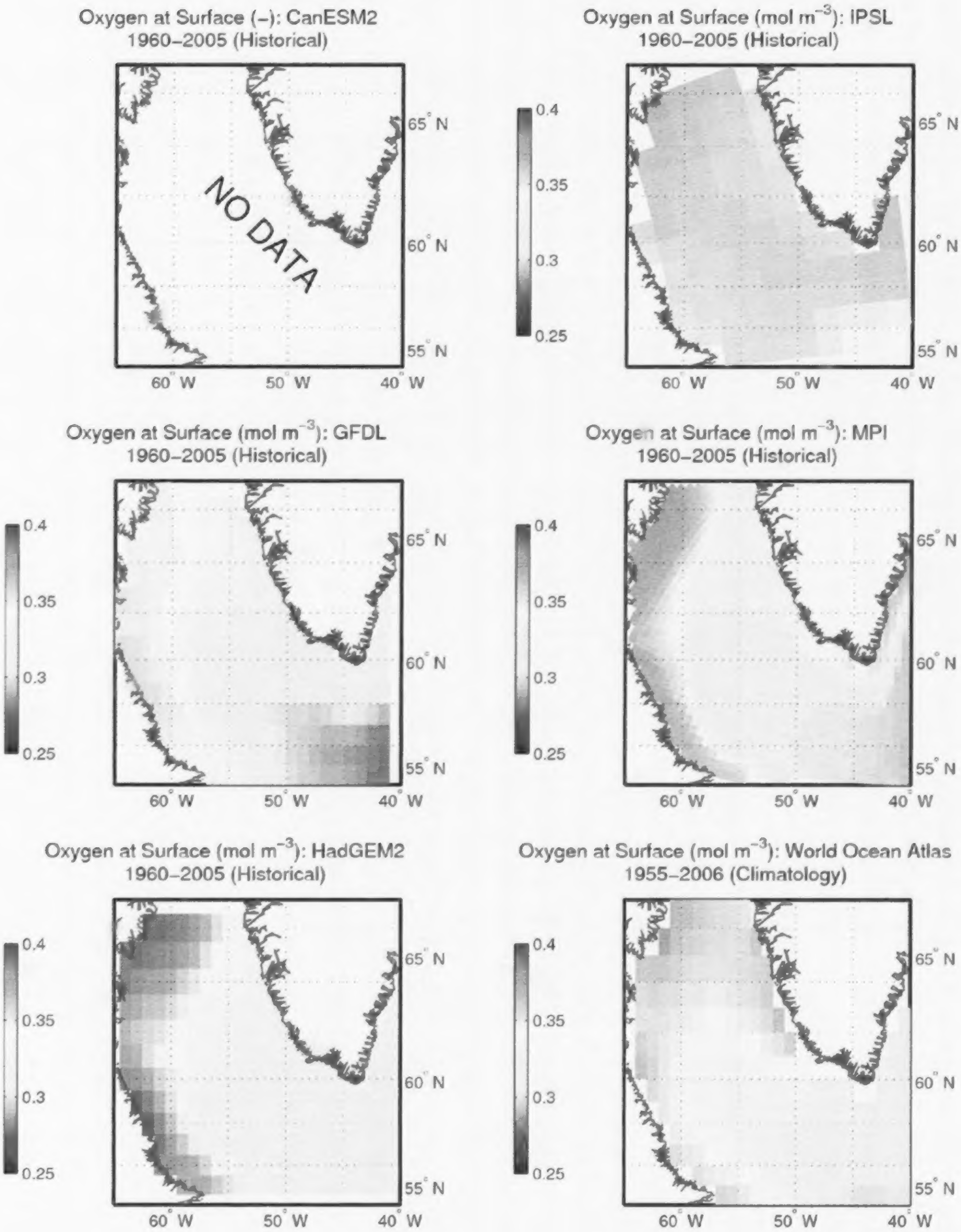
Oxygen at Surface (–): CanESM2
1960–2005 (Historical)
NO DATA
Oxygen at Surface (mol m^{-3}): IPSL
1960–2005 (Historical)
Oxygen at Surface (mol m^{-3}): GFDL
1960–2005 (Historical)
Oxygen at Surface (mol m^{-3}): MPI
1960–2005 (Historical)
Oxygen at Surface (mol m^{-3}): HadGEM2
1960–2005 (Historical)
Oxygen at Surface (mol m^{-3}): World Ocean Atlas
1955–2006 (Climatology)
0.4
0.35
0.3
0.25
65° N
60° N
55° N
60° W
50° W
40° W

Figure 25. Mean simulated dissolved oxygen concentration in the Labrador Sea for the historical period (1960-2005) and dissolved oxygen concentration at the surface from the World Ocean Atlas (WOA; Garcia et al., 2010a).

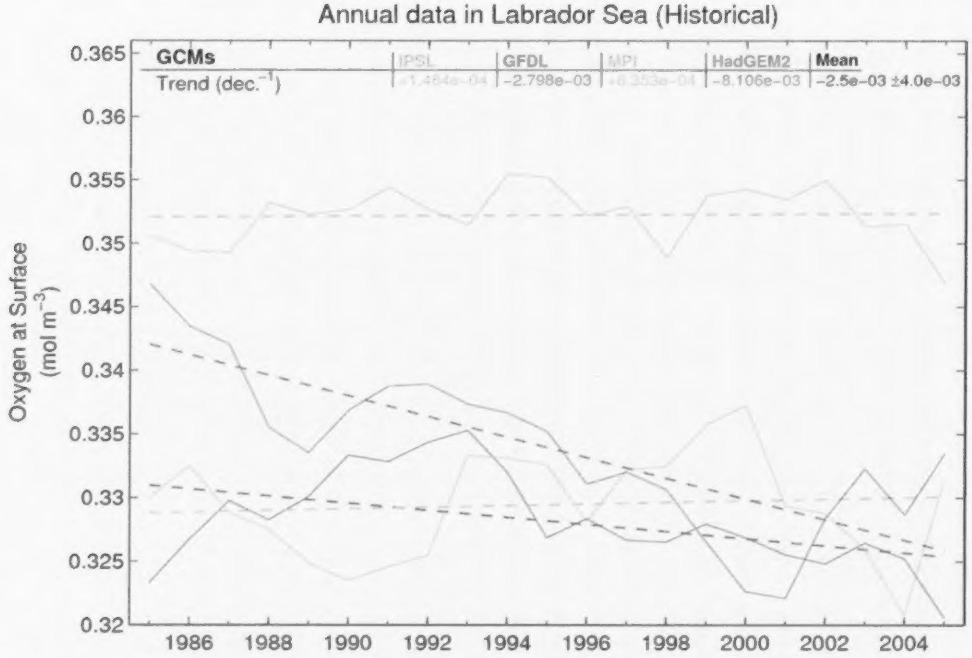

Figure 26. Average dissolved oxygen concentration trends (mol m^{-3}/decade) at the surface over the Labrador Sea for the 1985-2005 period.

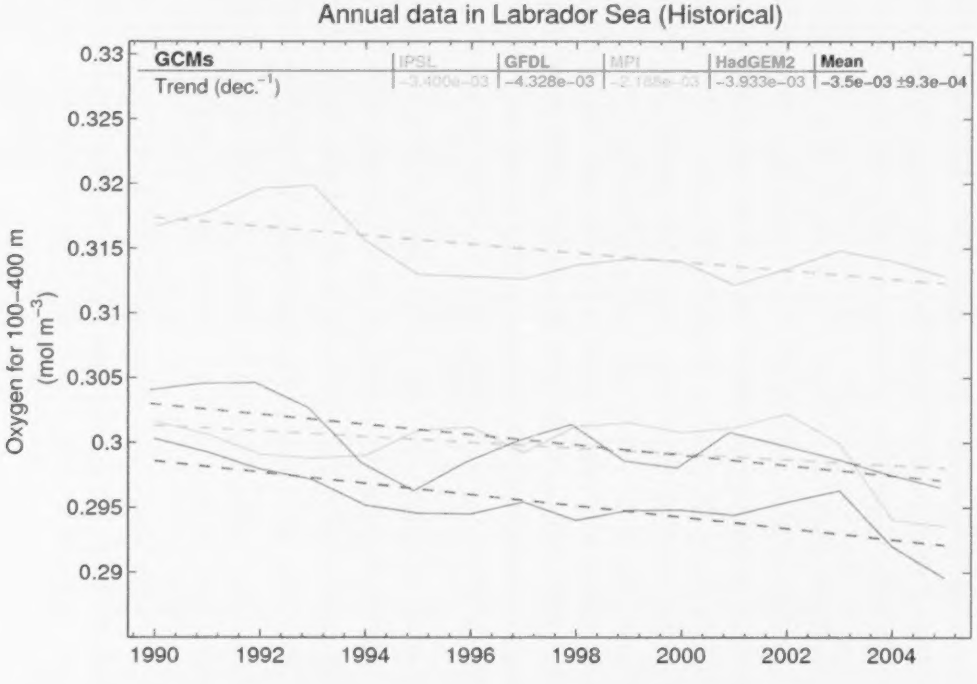

Figure 27. Average dissolved oxygen concentration trends (mol m^{-3}/decade) at 100-400 m over the Labrador Sea for the 1990-2005 period.

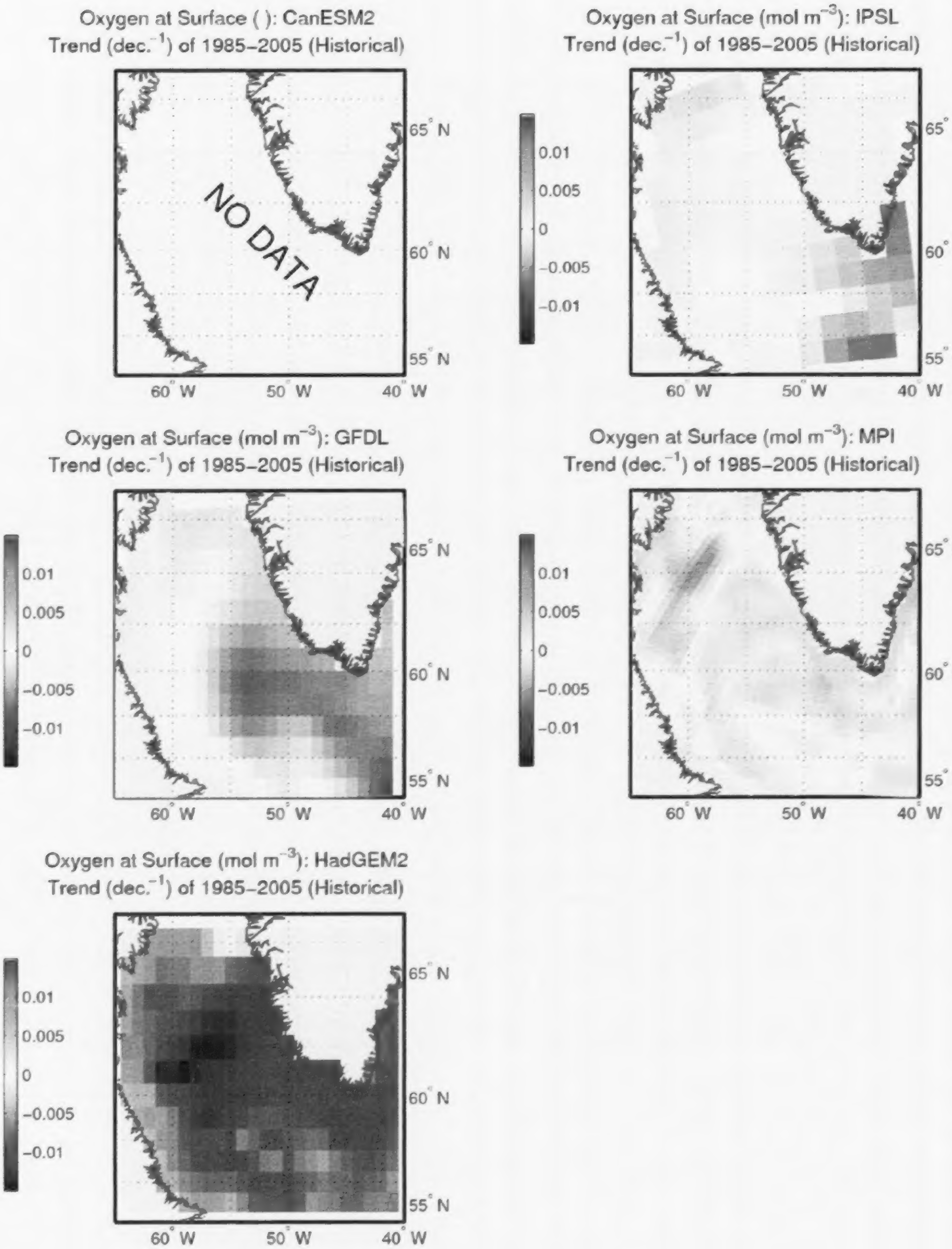
Oxygen at Surface ( ): CanESM2
Trend (dec.⁻¹) of 1985–2005 (Historical)
NO DATA
Oxygen at Surface (mol m⁻³): IPSL
Trend (dec.⁻¹) of 1985–2005 (Historical)
Oxygen at Surface (mol m⁻³): GFDL
Trend (dec.⁻¹) of 1985–2005 (Historical)
Oxygen at Surface (mol m⁻³): MPI
Trend (dec.⁻¹) of 1985–2005 (Historical)
Oxygen at Surface (mol m⁻³): HadGEM2
Trend (dec.⁻¹) of 1985–2005 (Historical)
0.01
0.005
0
−0.005
−0.01
65° N
60° N
55° N
60° W
50° W
40° W

Figure 28. Dissolved oxygen concentration trends (mol m^{-3}/decade) at the surface at each grid cell in the Labrador Sea for the 1985-2005 period.

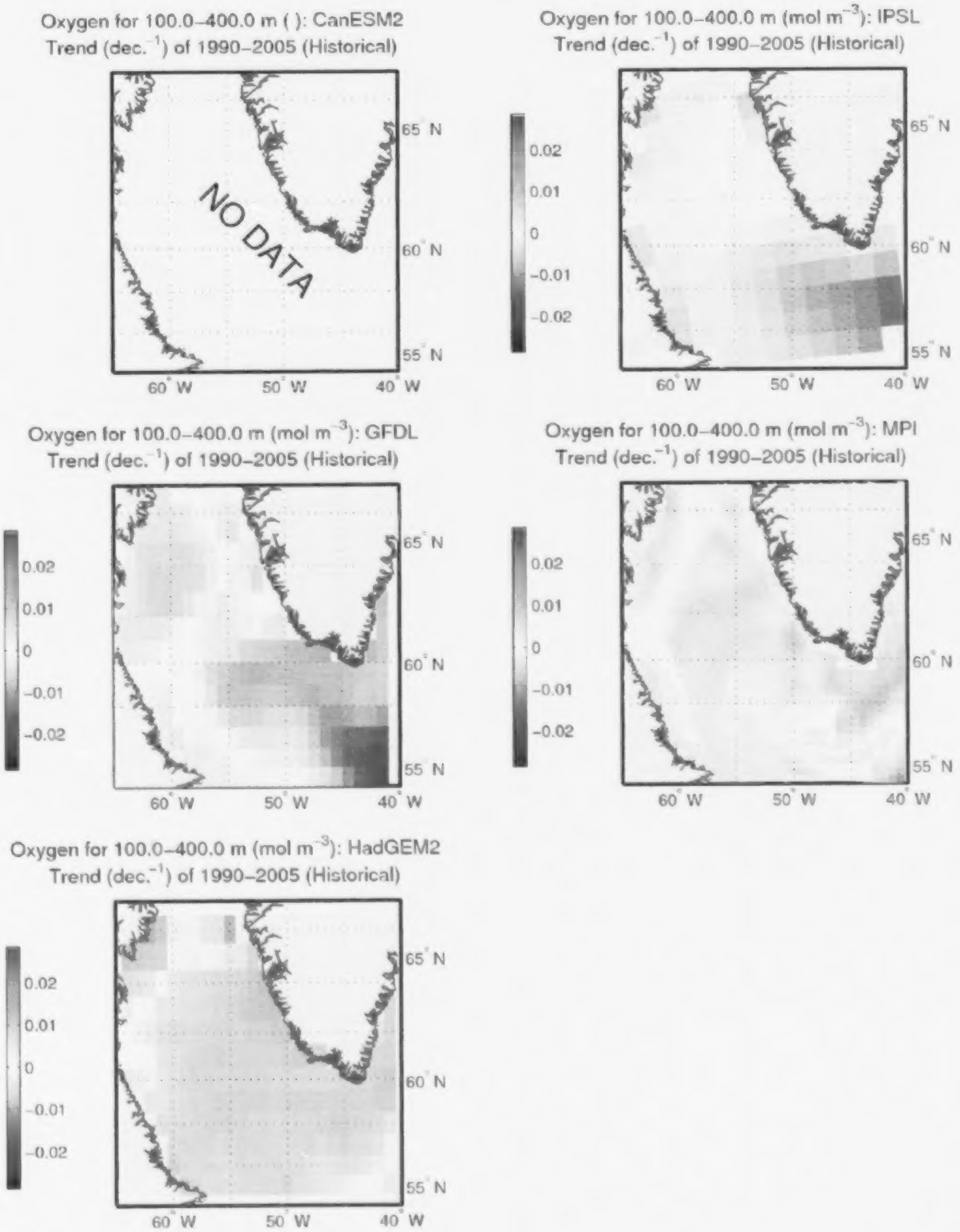

Oxygen for 100.0–400.0 m ( ): CanESM2
Trend (dec.$^{-1}$) of 1990–2005 (Historical)

Oxygen for 100.0–400.0 m (mol m^{-3}): IPSL
Trend (dec.$^{-1}$) of 1990–2005 (Historical)

Oxygen for 100.0–400.0 m (mol m^{-3}): GFDL
Trend (dec.$^{-1}$) of 1990–2005 (Historical)

Oxygen for 100.0–400.0 m (mol m^{-3}): MPI
Trend (dec.$^{-1}$) of 1990–2005 (Historical)

Oxygen for 100.0–400.0 m (mol m^{-3}): HadGEM2
Trend (dec.$^{-1}$) of 1990–2005 (Historical)

Figure 29. Dissolved oxygen concentration trends (mol m^{-3}/decade) at 100-400 at each grid cell in the Labrador Sea for the 1990-2005 period.

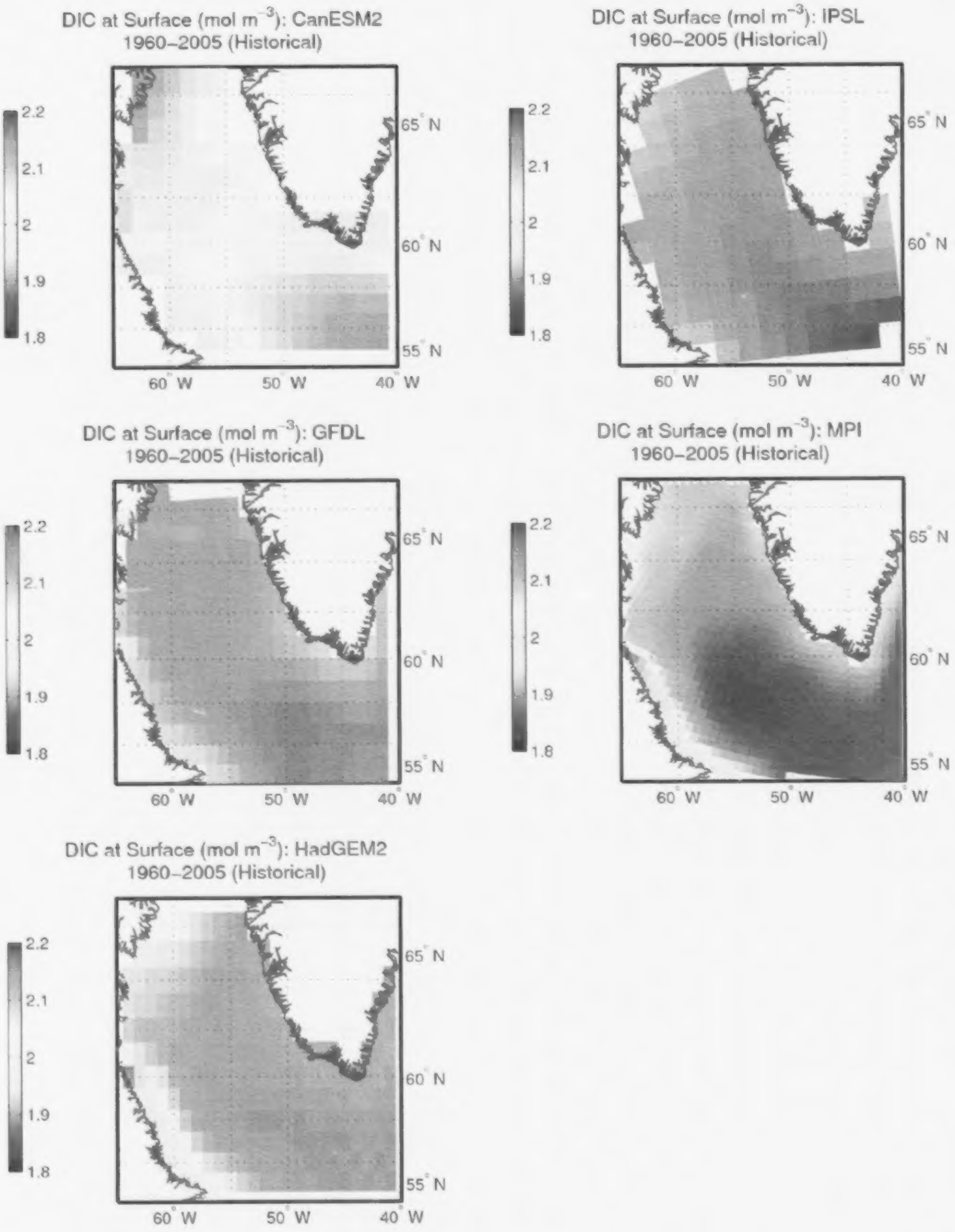

DIC at Surface (mol m^{-3}): CanESM2
1960–2005 (Historical)

DIC at Surface (mol m^{-3}): IPSL
1960–2005 (Historical)

DIC at Surface (mol m^{-3}): GFDL
1960–2005 (Historical)

DIC at Surface (mol m^{-3}): MPI
1960–2005 (Historical)

DIC at Surface (mol m^{-3}): HadGEM2
1960–2005 (Historical)

Figure 30. Mean simulated dissolved inorganic carbon concentration in the Labrador Sea for the historical period (1960-2005).

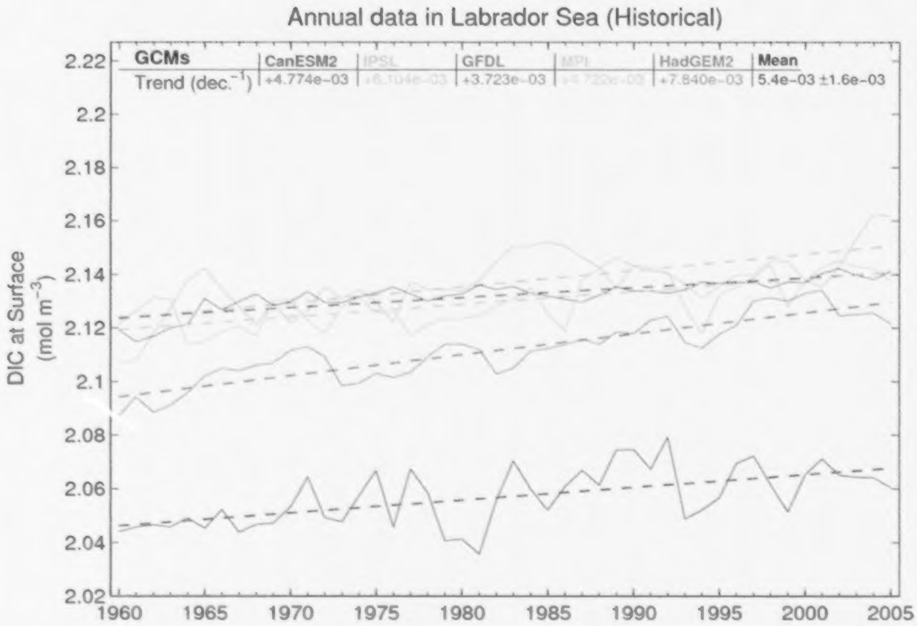

Figure 31. Average DIC concentration trends (mol m^{-3}/decade) at the surface over the Labrador Sea for the historical period (1960-2005).

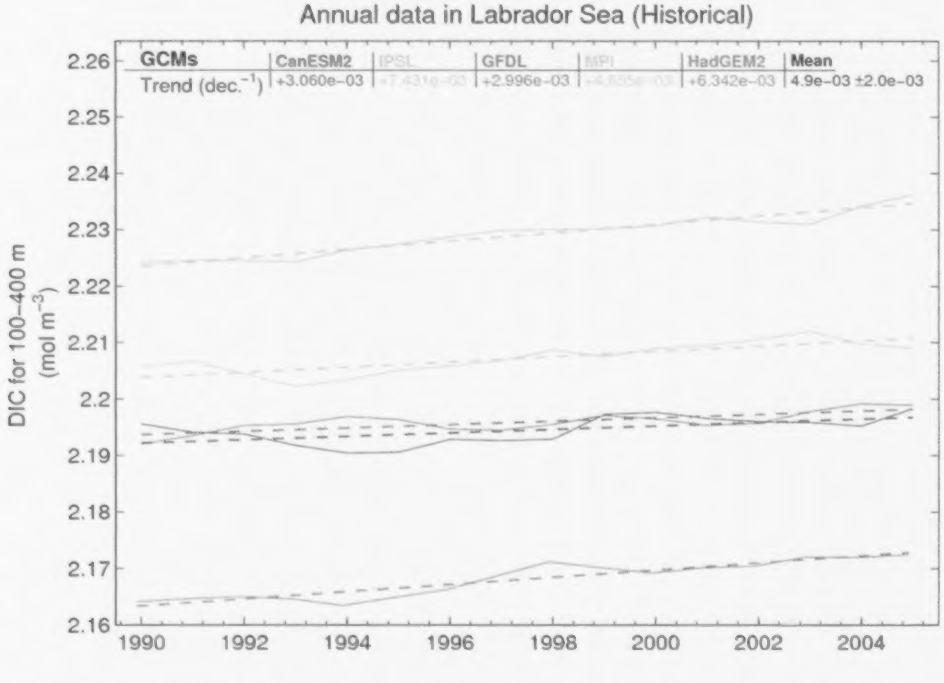

Figure 32. Average DIC concentration trends (mol m^{-3}/decade) at 100-400 m over the Labrador Sea for the 1990-2005 period.

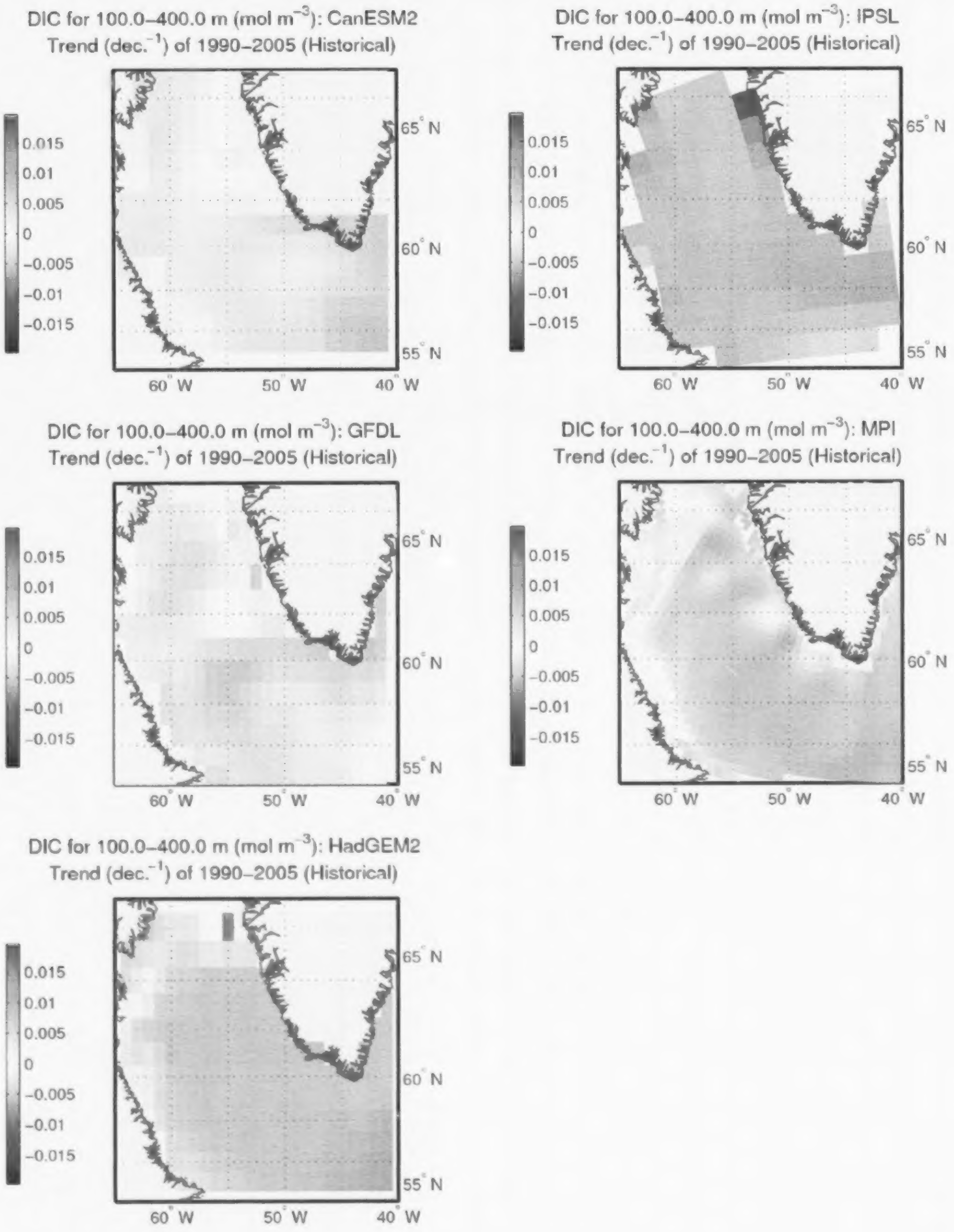
DIC for 100.0–400.0 m (mol m^-3): CanESM2
Trend (dec.^-1) of 1990–2005 (Historical)
DIC for 100.0–400.0 m (mol m^-3): IPSL
Trend (dec.^-1) of 1990–2005 (Historical)
DIC for 100.0–400.0 m (mol m^-3): GFDL
Trend (dec.^-1) of 1990–2005 (Historical)
DIC for 100.0–400.0 m (mol m^-3): MPI
Trend (dec.^-1) of 1990–2005 (Historical)
DIC for 100.0–400.0 m (mol m^-3): HadGEM2
Trend (dec.^-1) of 1990–2005 (Historical)
0.015
0.01
0.005
0
−0.005
−0.01
−0.015
65° N
60° N
55° N
60° W
50° W
40° W

Figure 33. DIC concentration trends (mol m^{-3}/decade) at 100-400 m at each grid cell in the Labrador Sea for the 1990-2005 period.

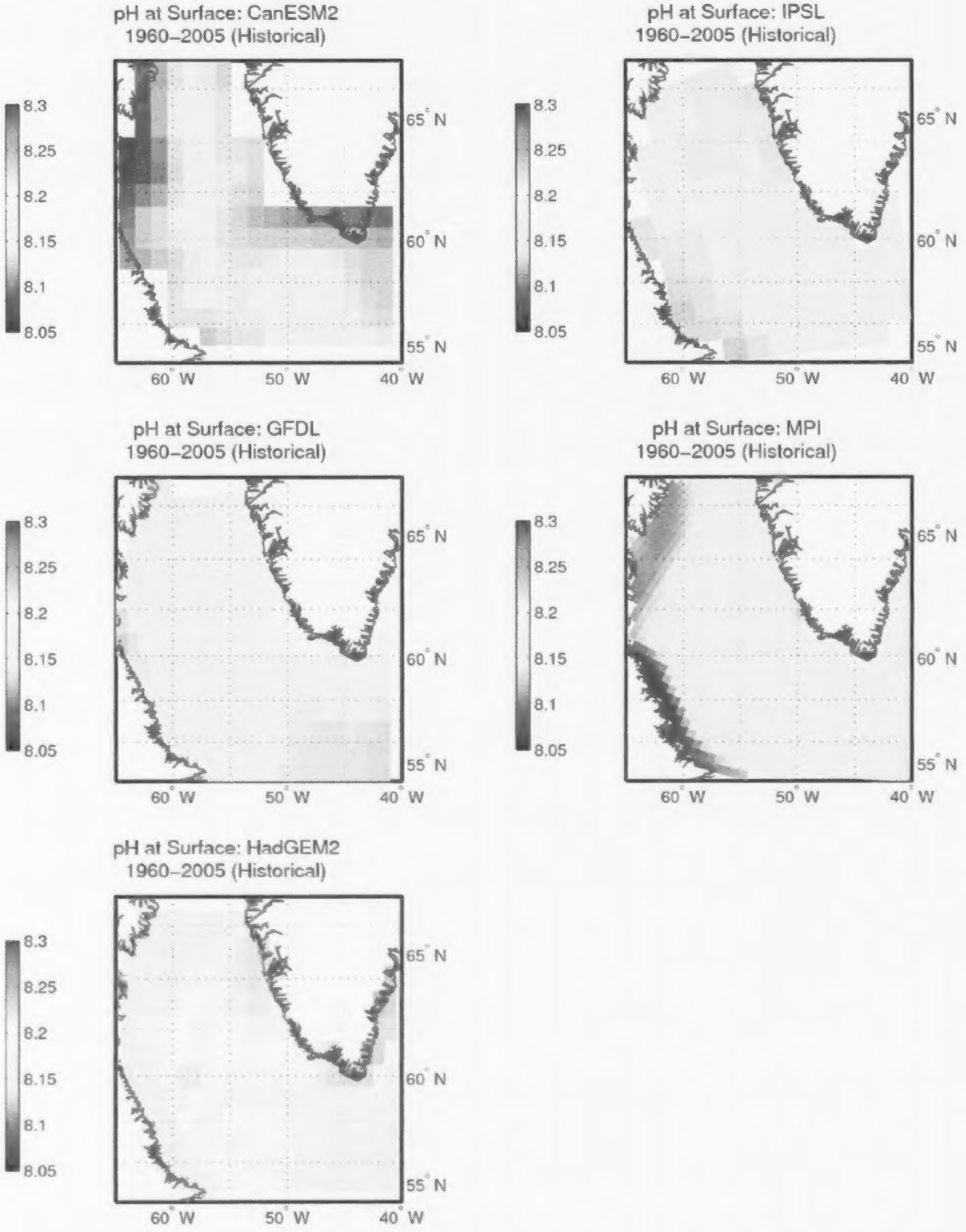
pH at Surface: CanESM2
1960–2005 (Historical)
pH at Surface: IPSL
1960–2005 (Historical)
pH at Surface: GFDL
1960–2005 (Historical)
pH at Surface: MPI
1960–2005 (Historical)
pH at Surface: HadGEM2
1960–2005 (Historical)
8.3
8.25
8.2
8.15
8.1
8.05
65° N
60° N
55° N
60° W
50° W
40° W

Figure 34. Mean simulated pH at the surface of the Labrador Sea for the historical period (1960-2005).

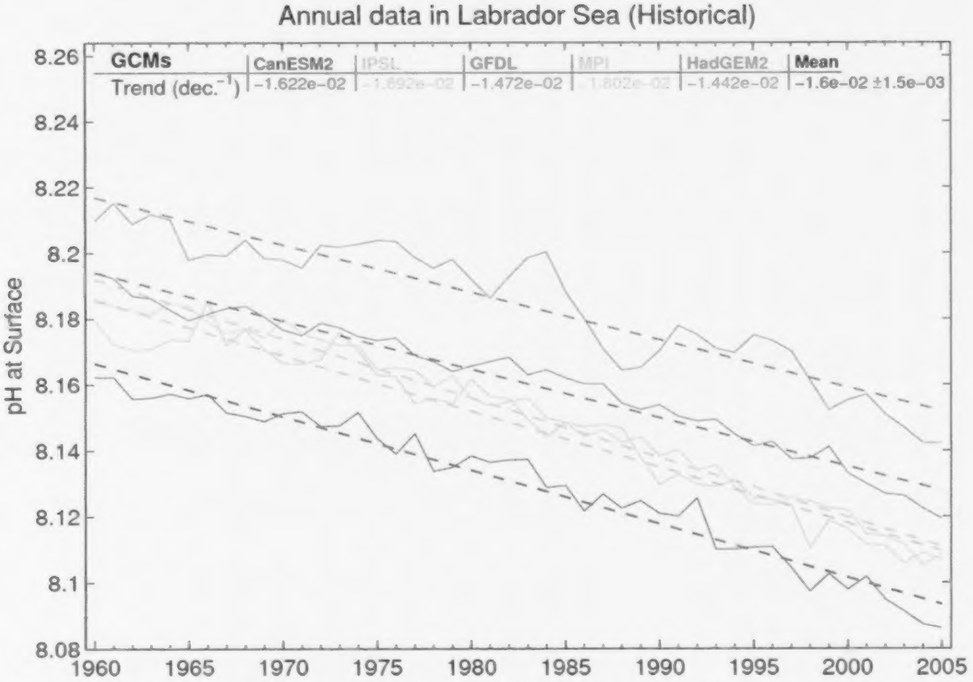

Figure 35. Average surface pH trends (per decade) over the Labrador Sea for the historical period (1960-2005).

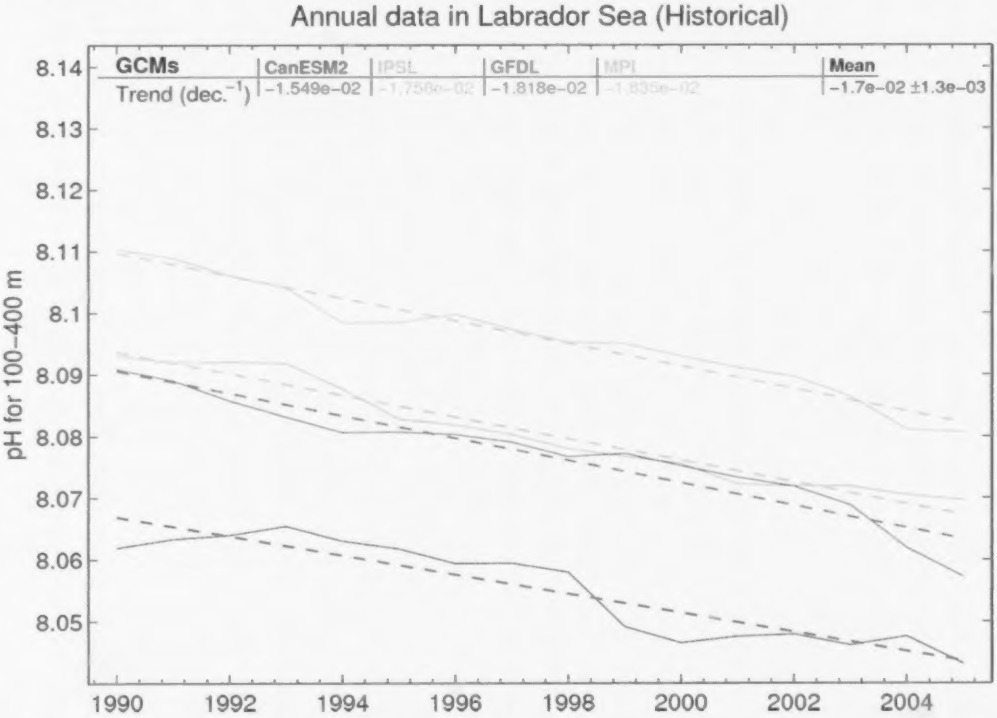

Figure 36. Average pH trends (per decade) at 100-400 m over the Labrador Sea for the 1990-2005 period.

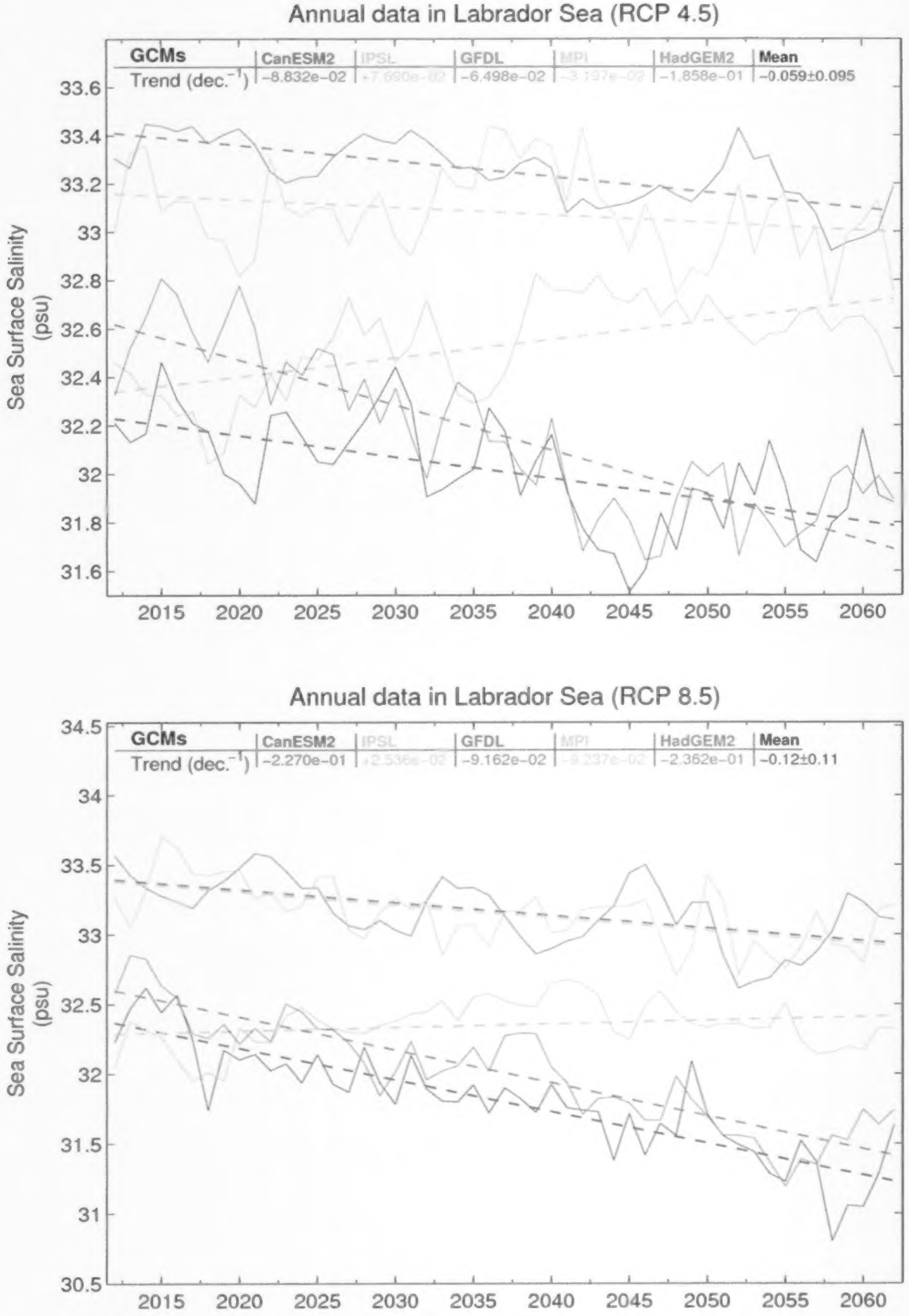

Figure 37. Future sea surface salinity trends (per decade) in the Labrador Sea for the 2012-2062 period for RCPs 4.5 and 8.5.

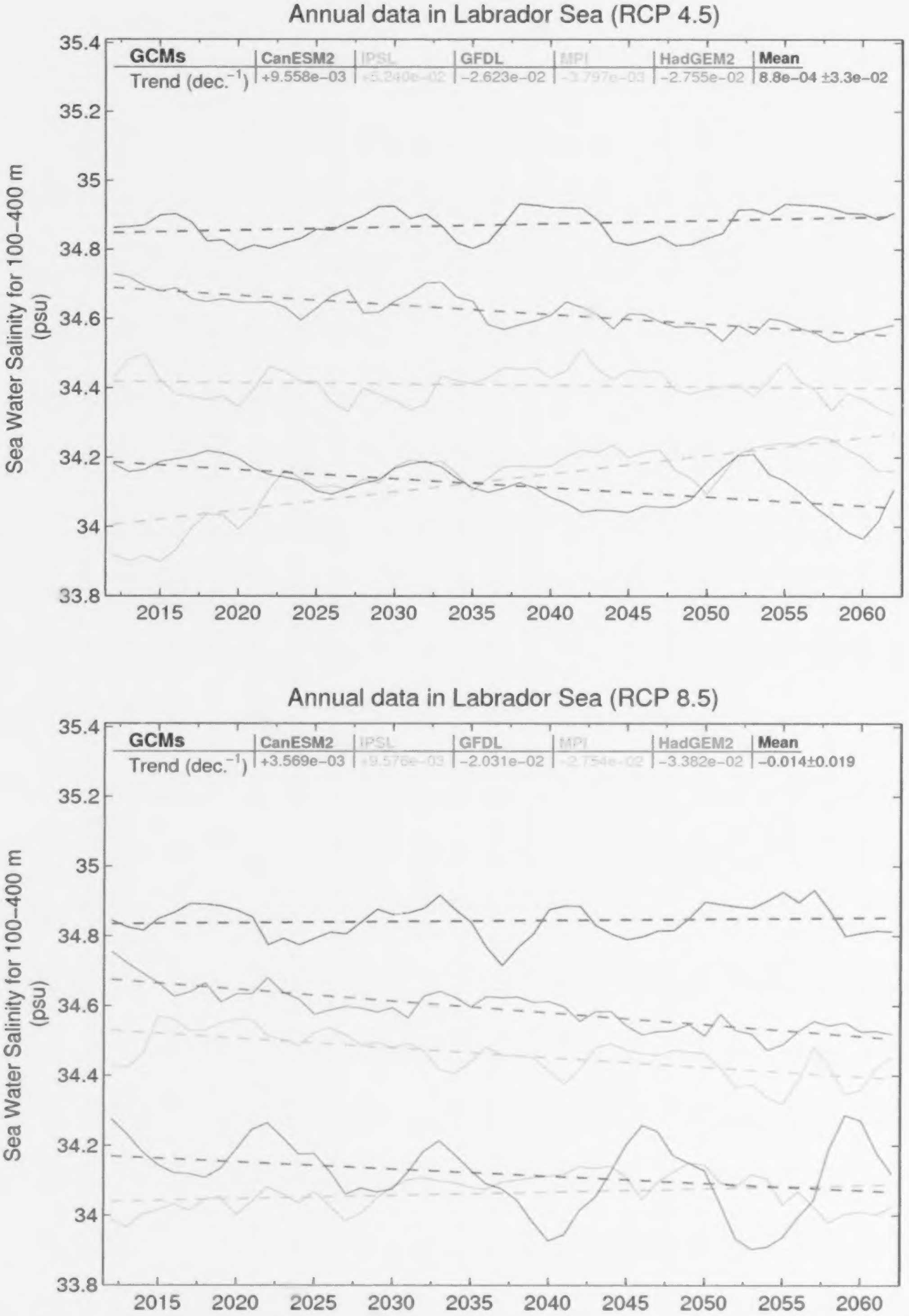

Figure 38. Future salinity trends (per decade) at 100-400 m in the Labrador Sea for the 2012-2062 period for RCPs 4.5 and 8.5.

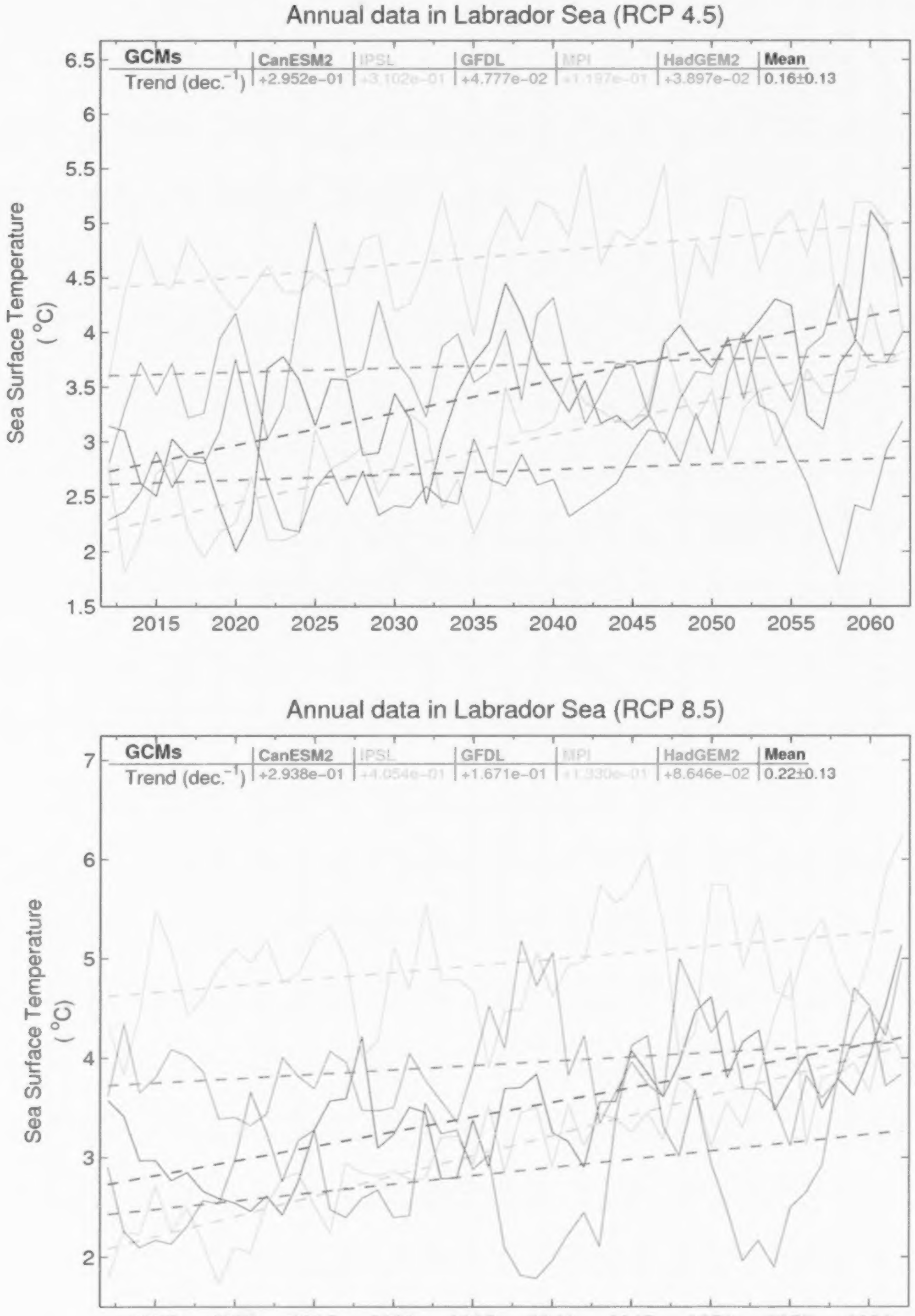

Figure 39. Future sea surface temperature trends (°C/decade) in the Labrador Sea for the 2012-2062 period for RCPs 4.5 and 8.5.

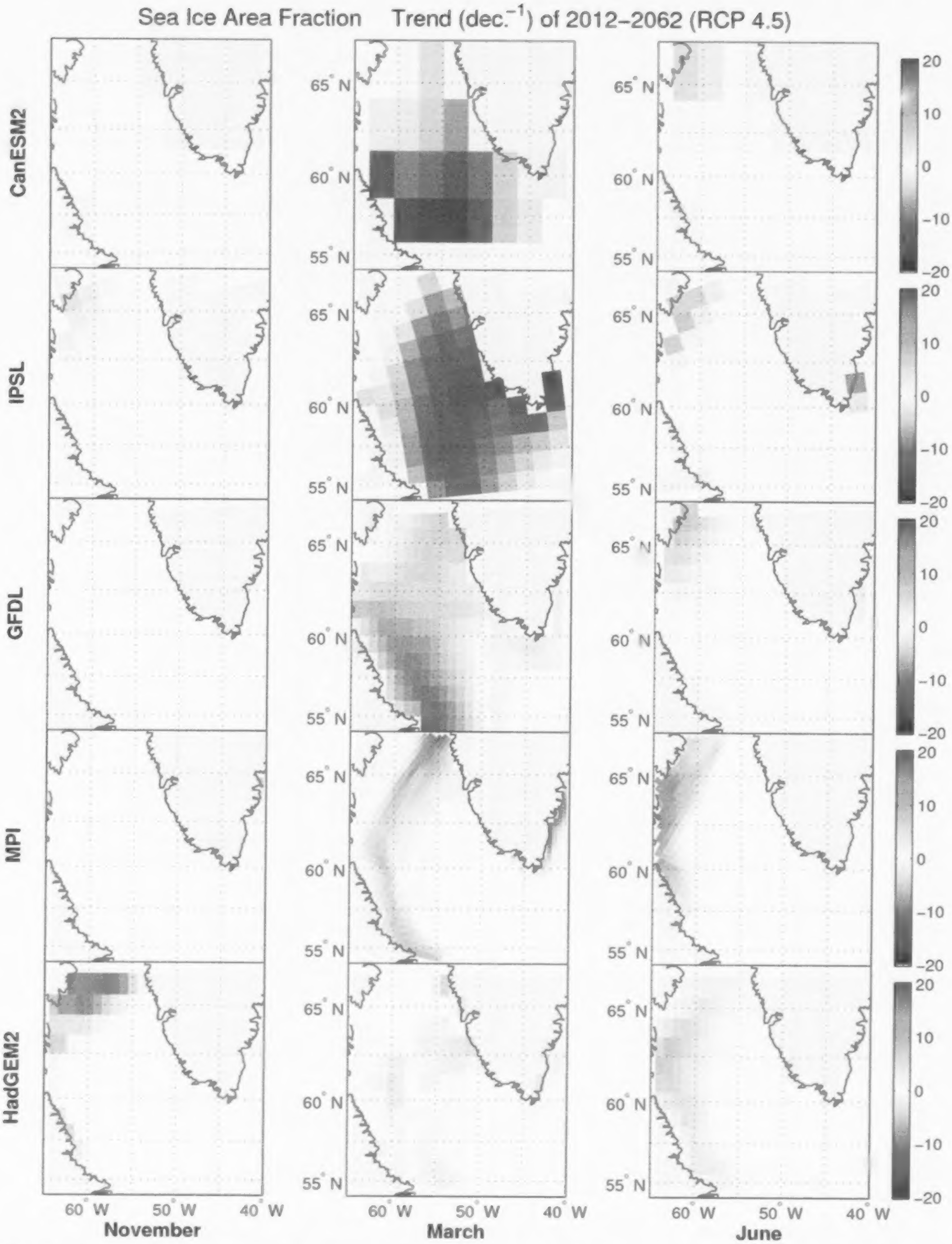
Sea Ice Area Fraction Trend (dec.$^{-1}$) of 2012-2062 (RCP 4.5)
CanESM2
IPSL
GFDL
MPI
HadGEM2
65° N
60° N
55° N
60° W
50° W
40° W
November
March
June
20
10
0
-10
-20

Figure 40. Future sea ice concentration trends (%/decade) in the Labrador Sea for the 2012-2062 period for RCP 4.5.

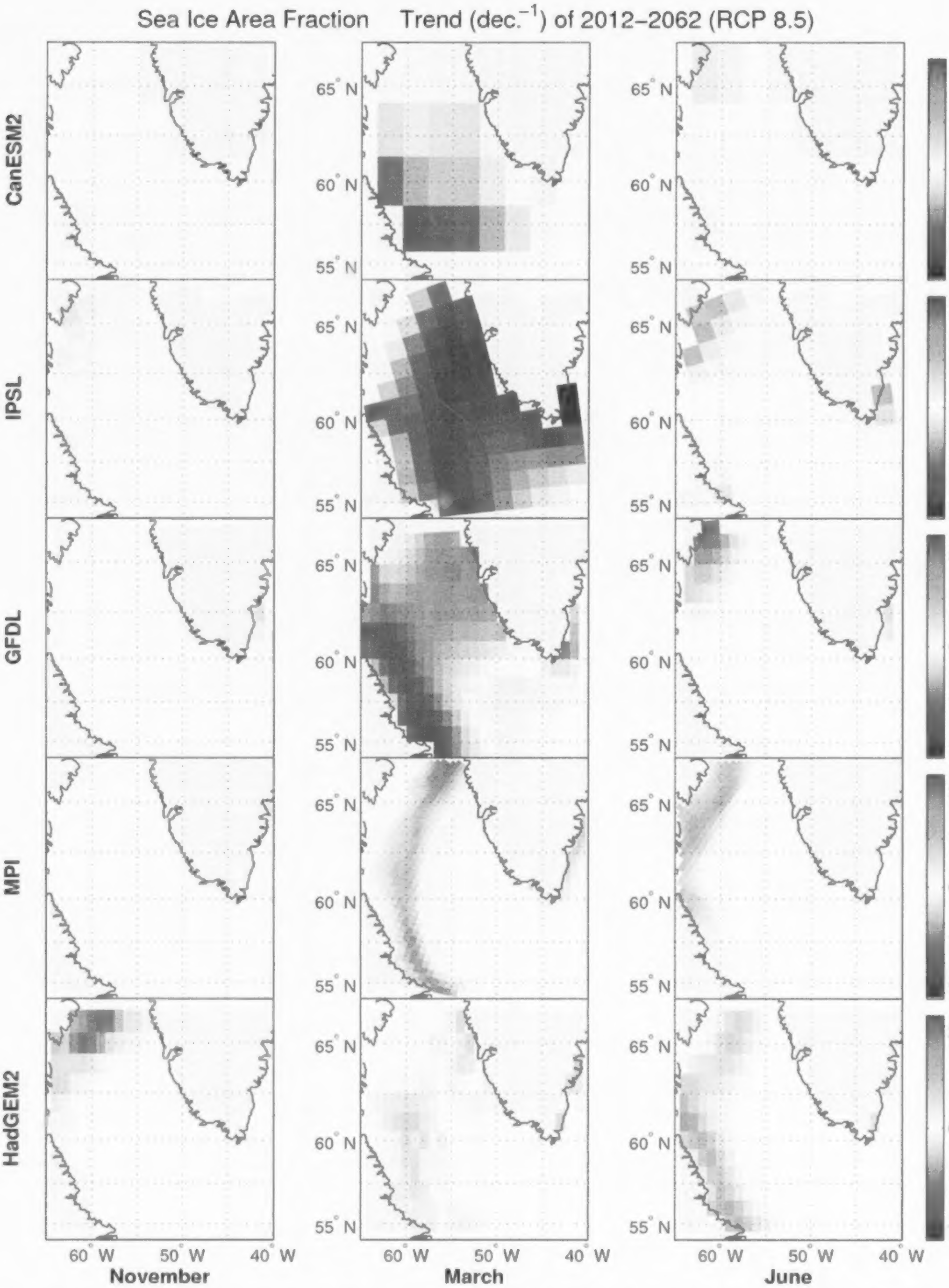
Sea Ice Area Fraction Trend (dec.$^{-1}$) of 2012–2062 (RCP 8.5)
CanESM2
IPSL
GFDL
MPI
HadGEM2
65° N
60° N
55° N
60° W
50° W
40° W
November
March
June
20
10
0
−10
−20

Figure 41. Future sea ice concentration trends (%/decade) in the Labrador Sea for the 2012-2062 period for RCP 8.5.

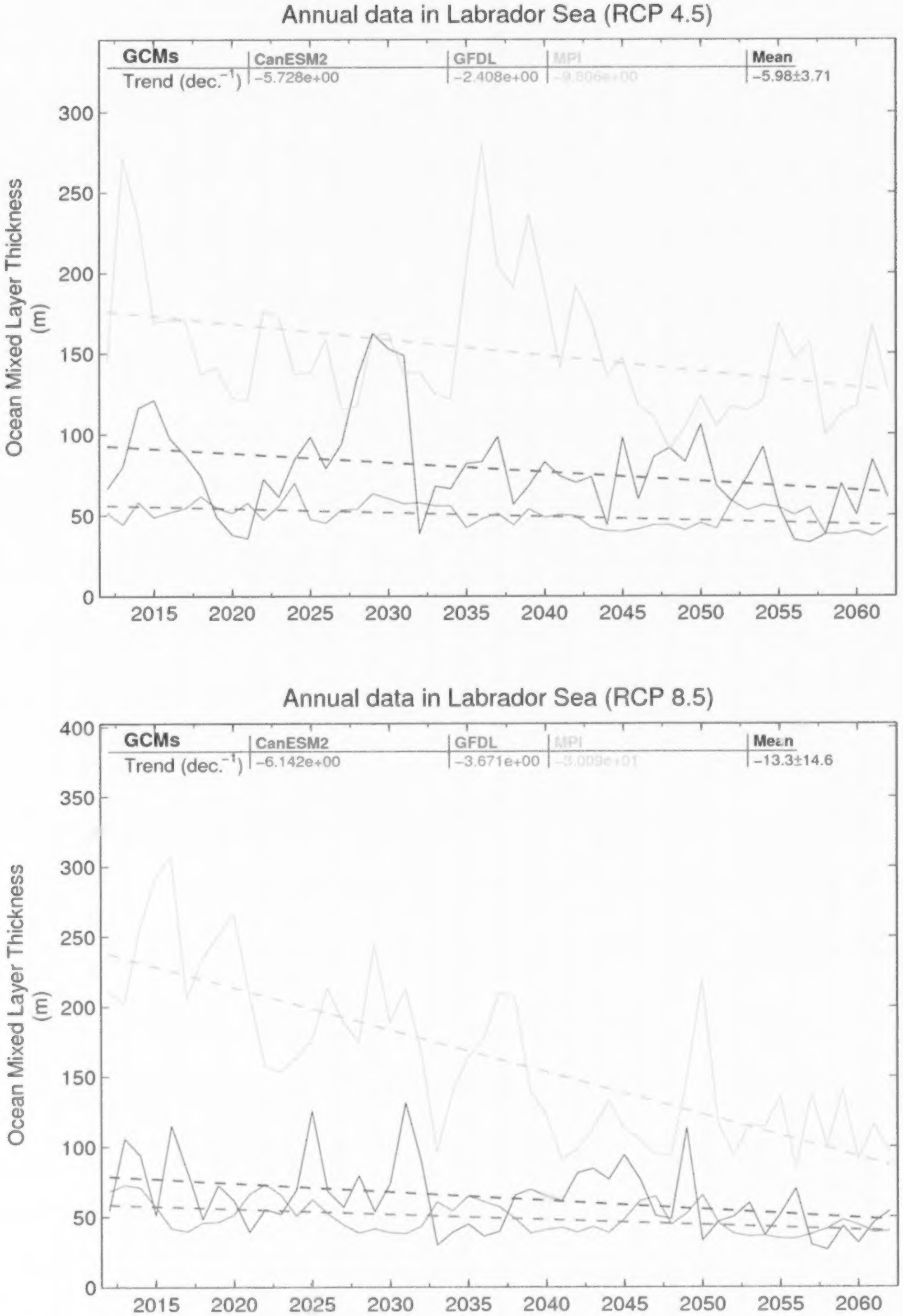

Figure 42. Future ocean mixed layer depth trends (m/decade) in the Labrador Sea for the 2012-2062 period for RCPs 4.5 and 8.5.

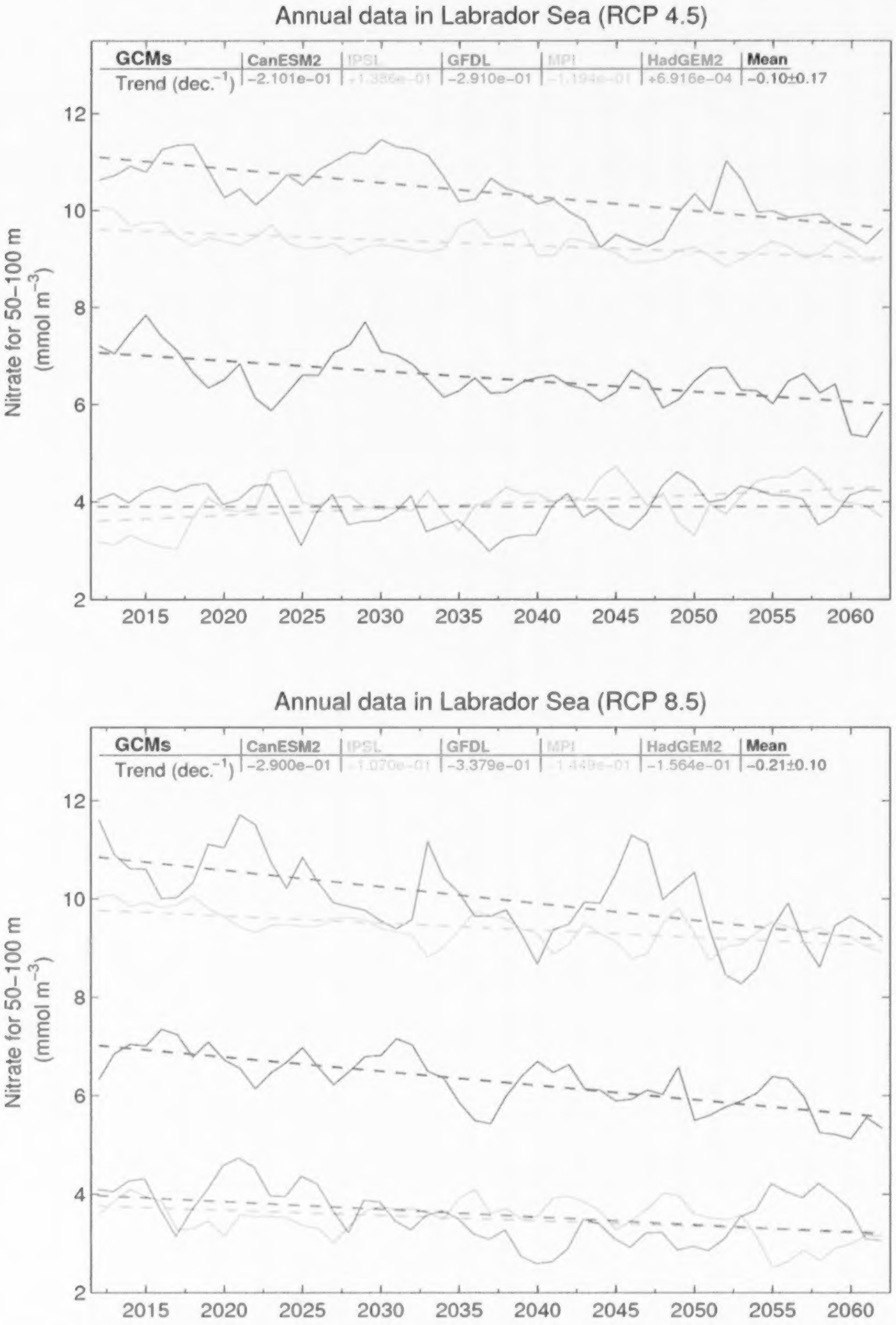

Figure 43. Future nitrate concentration trends (mmol m^{-3}/decade) at 50-100 m in the Labrador Sea for the 2012-2062 period for RCPs 4.5 and 8.5.

Annual data in Labrador Sea (RCP 4.5)

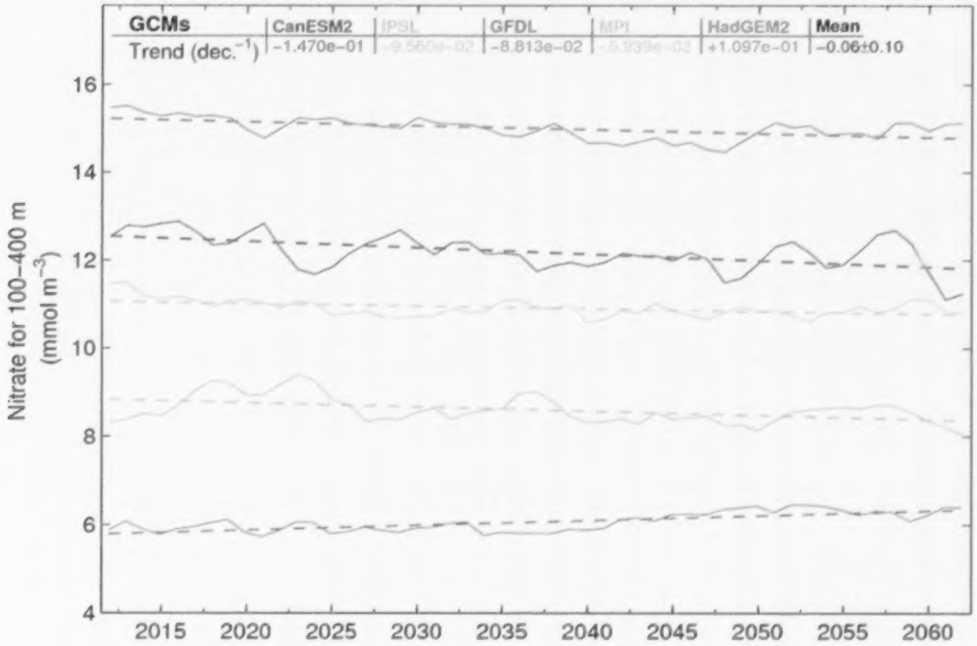

Annual data in Labrador Sea (RCP 8.5)

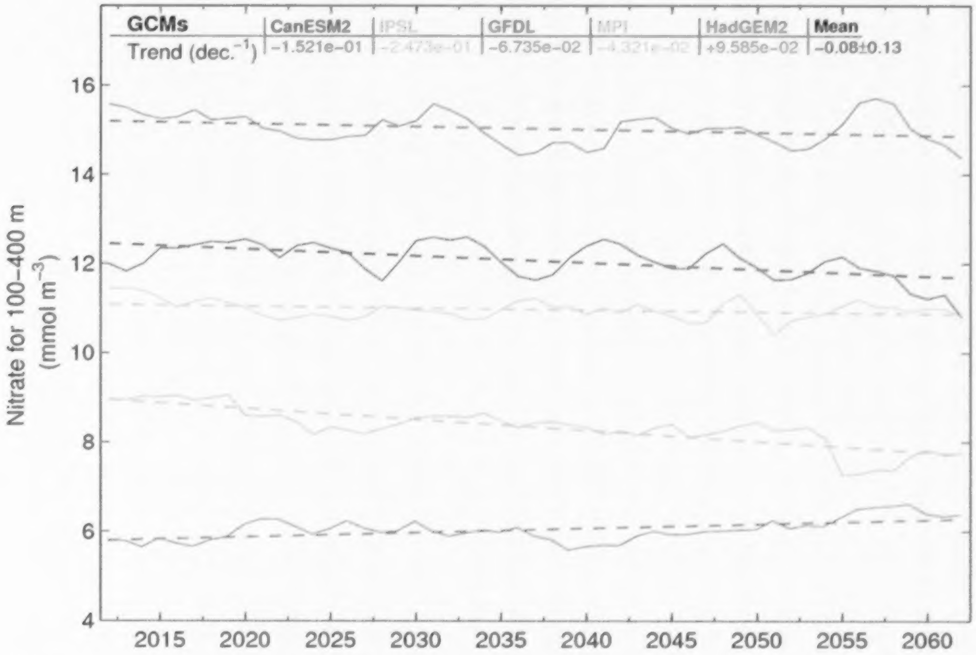

Figure 44. Future nitrate concentration trends (mmol m^{-3}/decade) at 100-400 m in the Labrador Sea for the 2012-2062 period for RCPs 4.5 and 8.5.

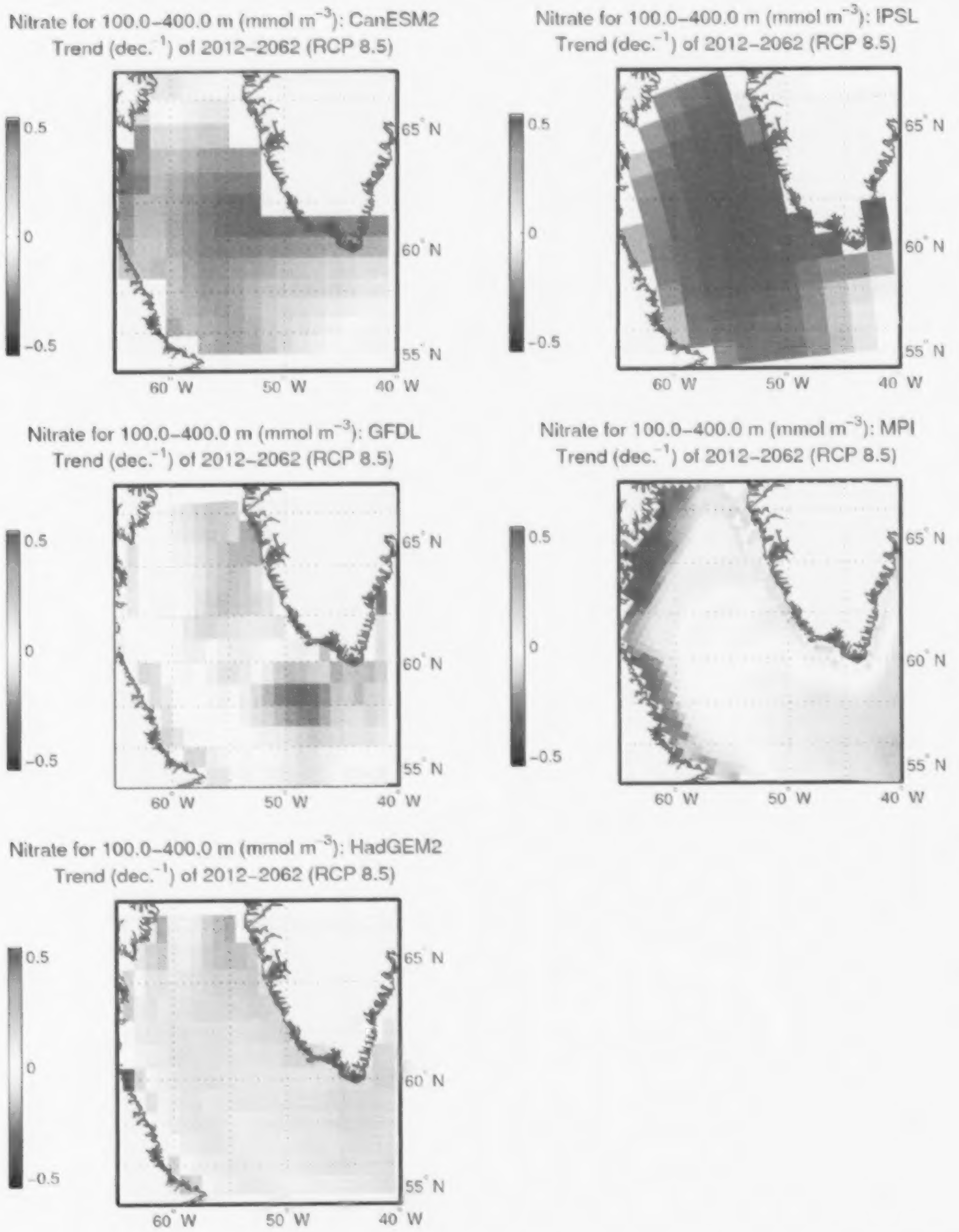

Nitrate for 100.0–400.0 m (mmol m^{-3}): CanESM2
Trend (dec.$^{-1}$) of 2012–2062 (RCP 8.5)

Nitrate for 100.0–400.0 m (mmol m^{-3}): IPSL
Trend (dec.$^{-1}$) of 2012–2062 (RCP 8.5)

Nitrate for 100.0–400.0 m (mmol m^{-3}): GFDL
Trend (dec.$^{-1}$) of 2012–2062 (RCP 8.5)

Nitrate for 100.0–400.0 m (mmol m^{-3}): MPI
Trend (dec.$^{-1}$) of 2012–2062 (RCP 8.5)

Nitrate for 100.0–400.0 m (mmol m^{-3}): HadGEM2
Trend (dec.$^{-1}$) of 2012–2062 (RCP 8.5)

Figure 45. Future nitrate concentration trends (mmol m^{-3}/decade) at each grid cell at 100-400 m in the Labrador Sea for the 2012-2062 period for RCP 8.5.

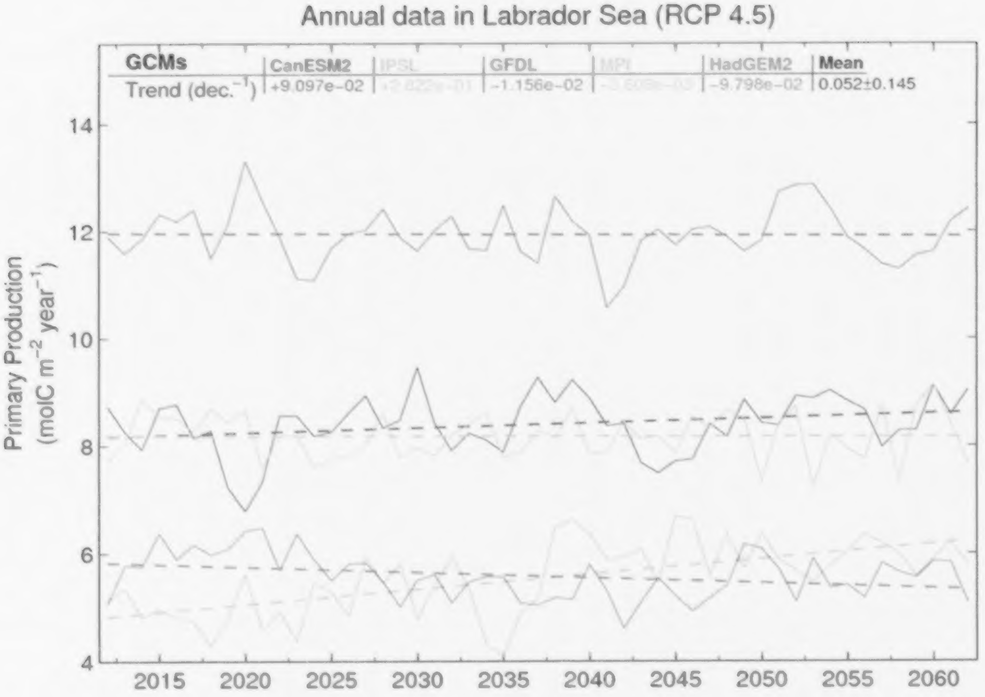

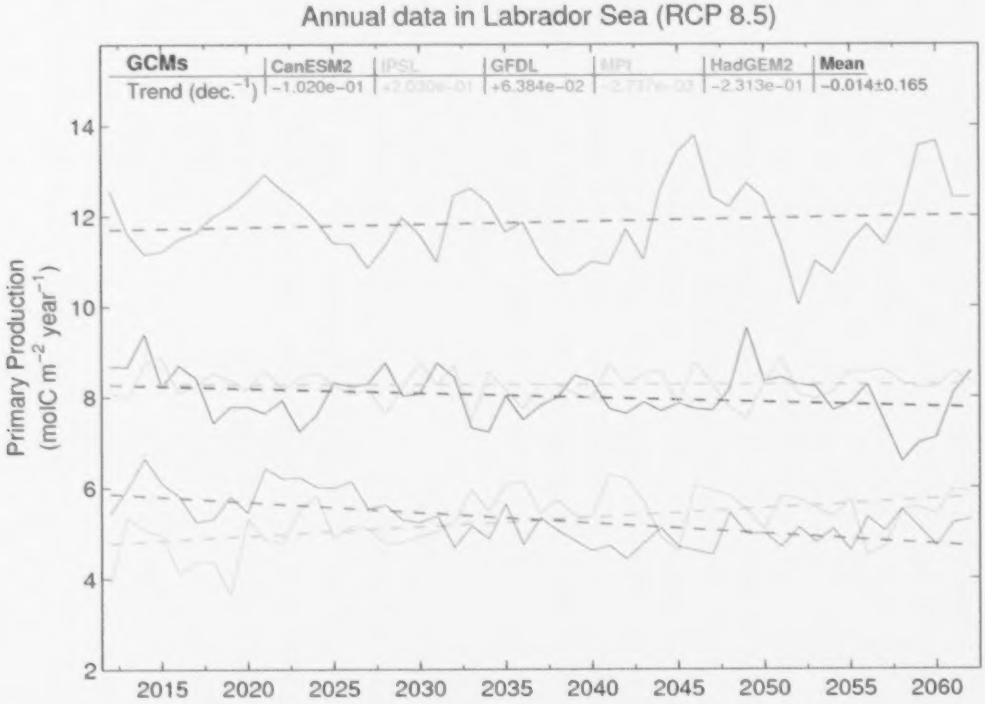

Figure 46. Future vertically integrated primary production trends (mol C m^{-2}/decade) in the Labrador Sea for the 2012-2062 period for RCPs 4.5 and 8.5.

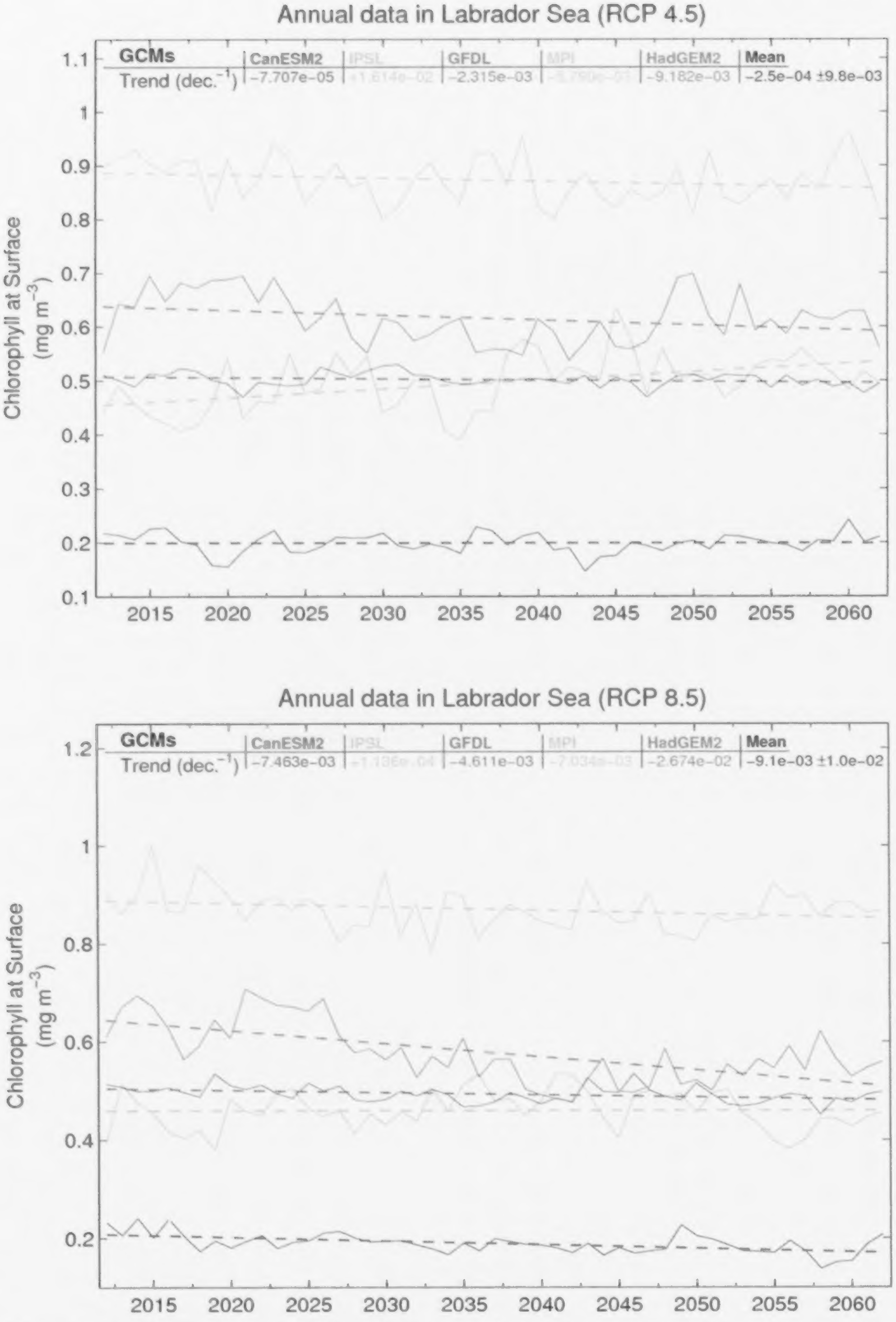

Figure 47. Future Chl a concentration trends (mg m^{-3}/decade) at the surface in the Labrador Sea for the 2012-2062 period for RCPs 4.5 and 8.5.

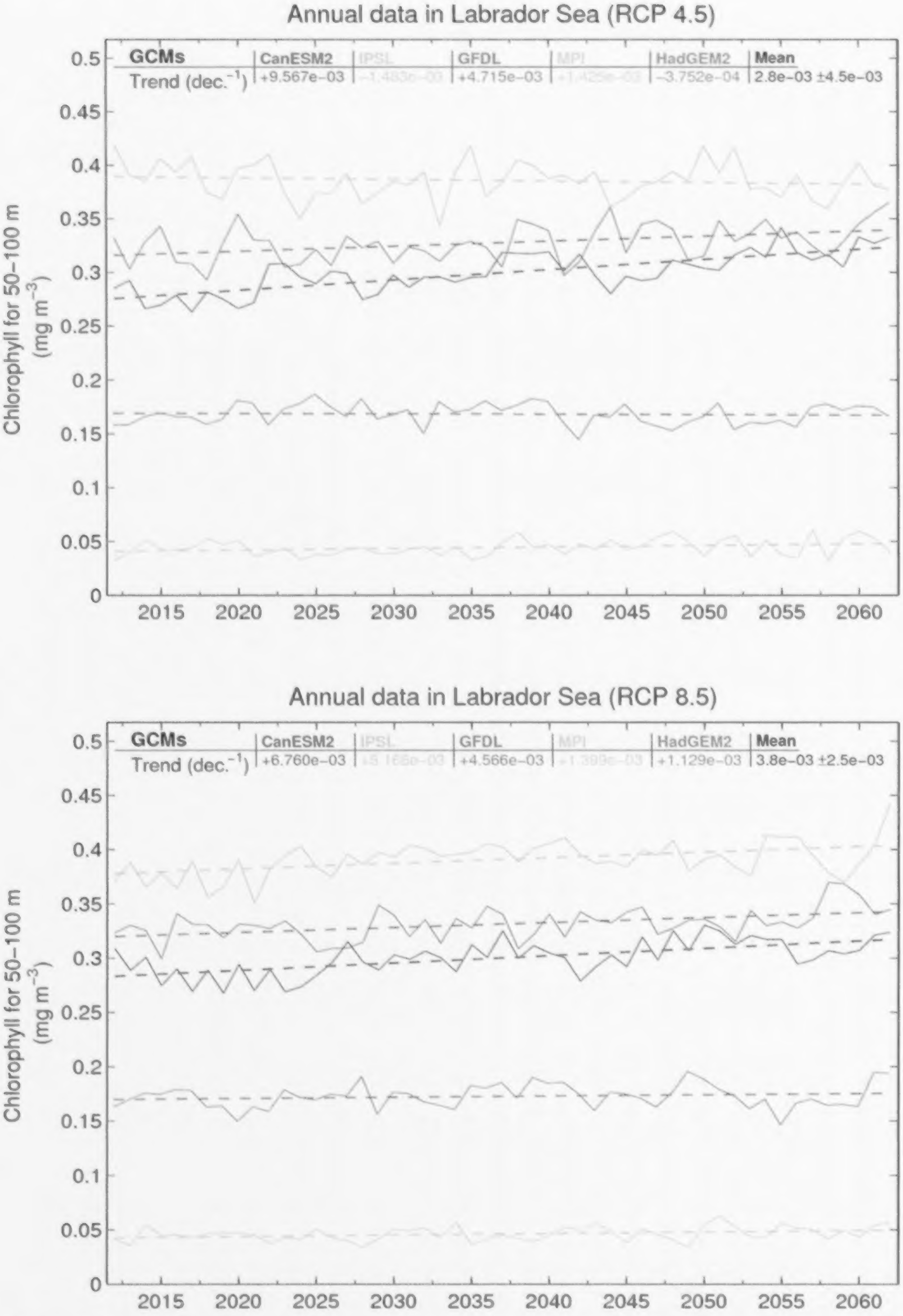

Figure 48. Future Chl a concentration trends (mg m^{-3}/decade) at 50-100 m in the Labrador Sea for the 2012-2062 period for RCPs 4.5 and 8.5.

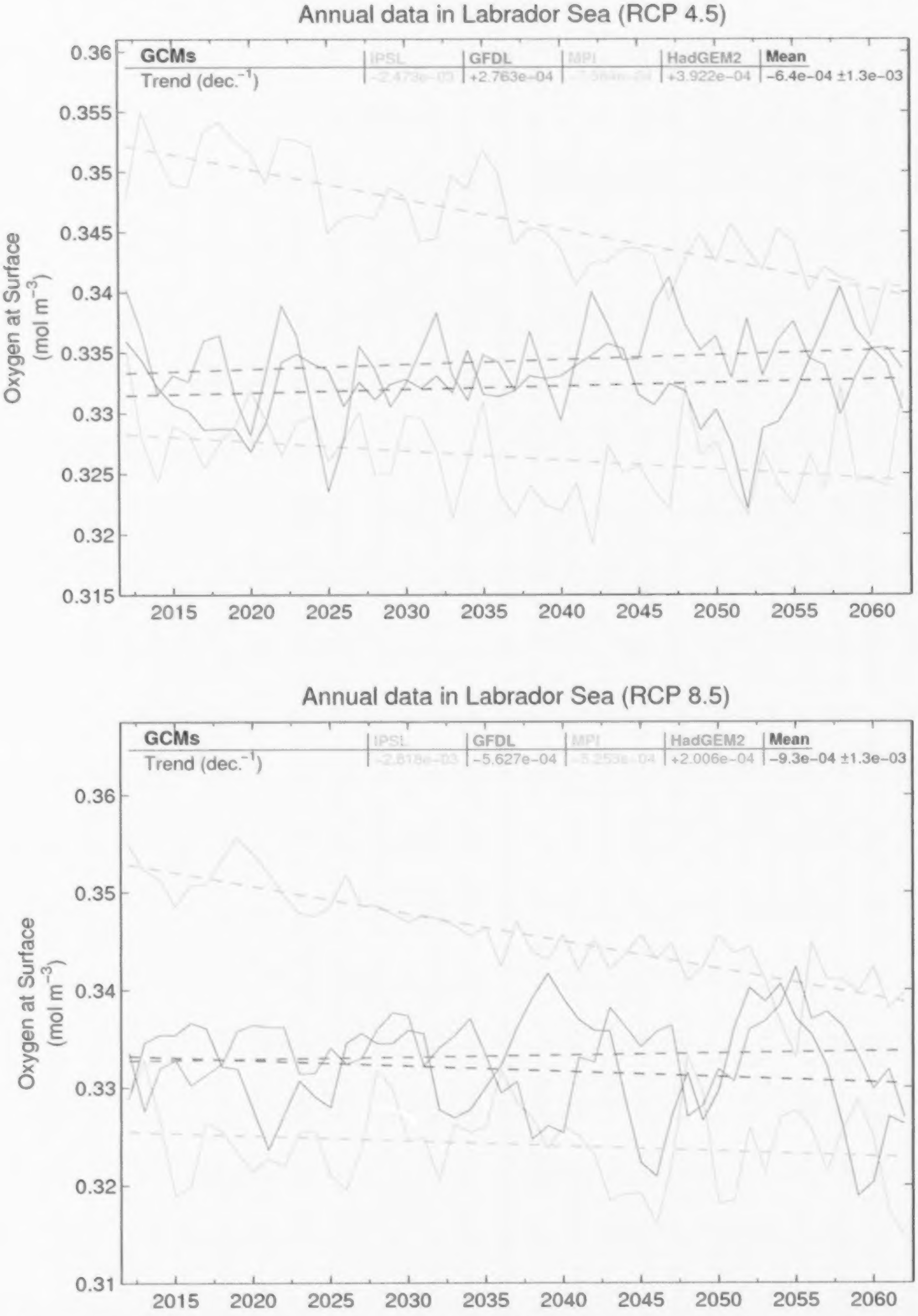

Figure 49. Future oxygen concentration trends (mol m^{-3}/decade) at the surface in the Labrador Sea for the 2012-2062 period for RCPs 4.5 and 8.5.

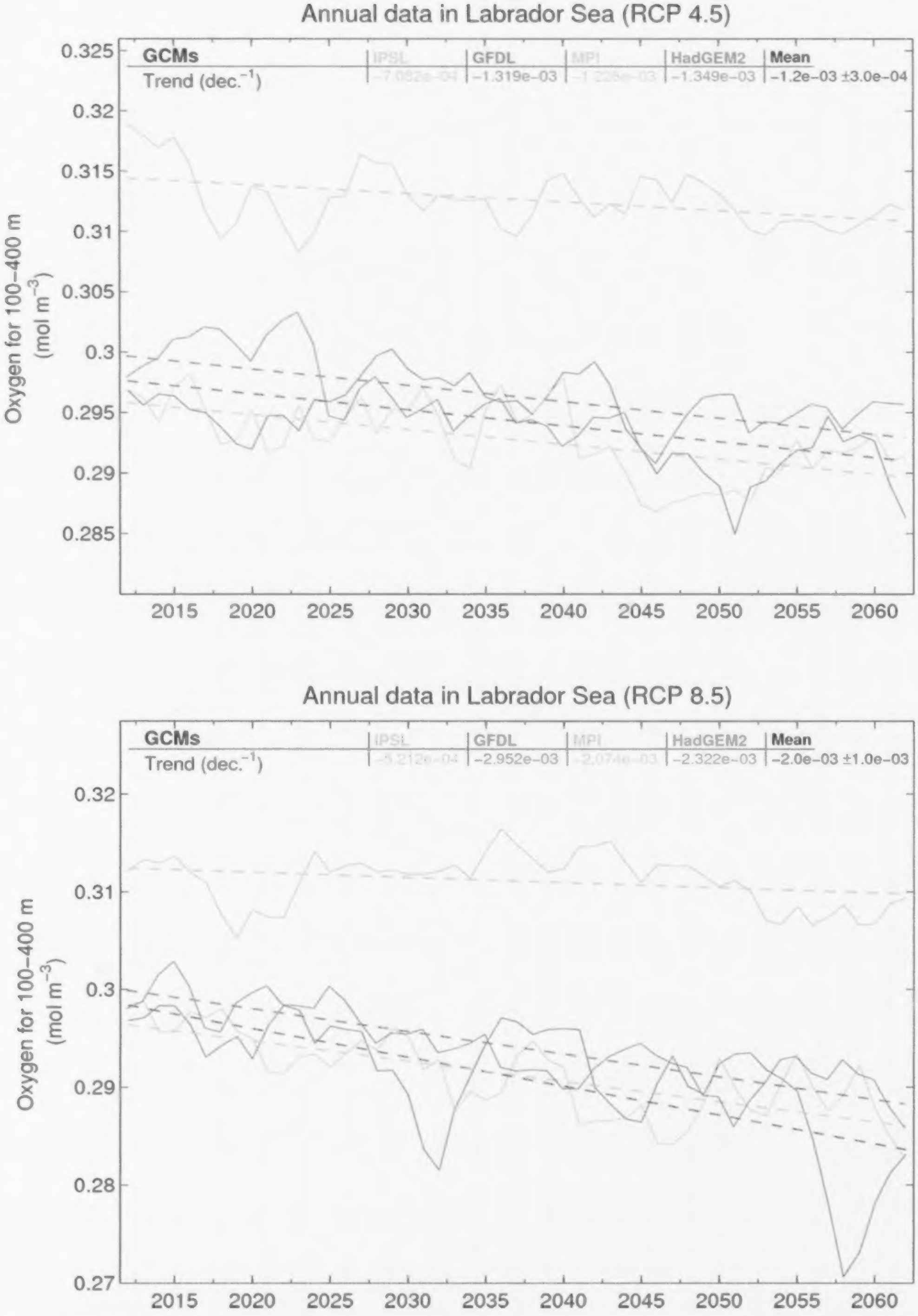

Figure 50. Future oxygen concentration trends (mol m^{-3}/decade) at 100-400 m in the Labrador Sea for the 2012-2062 period for RCPs 4.5 and 8.5.

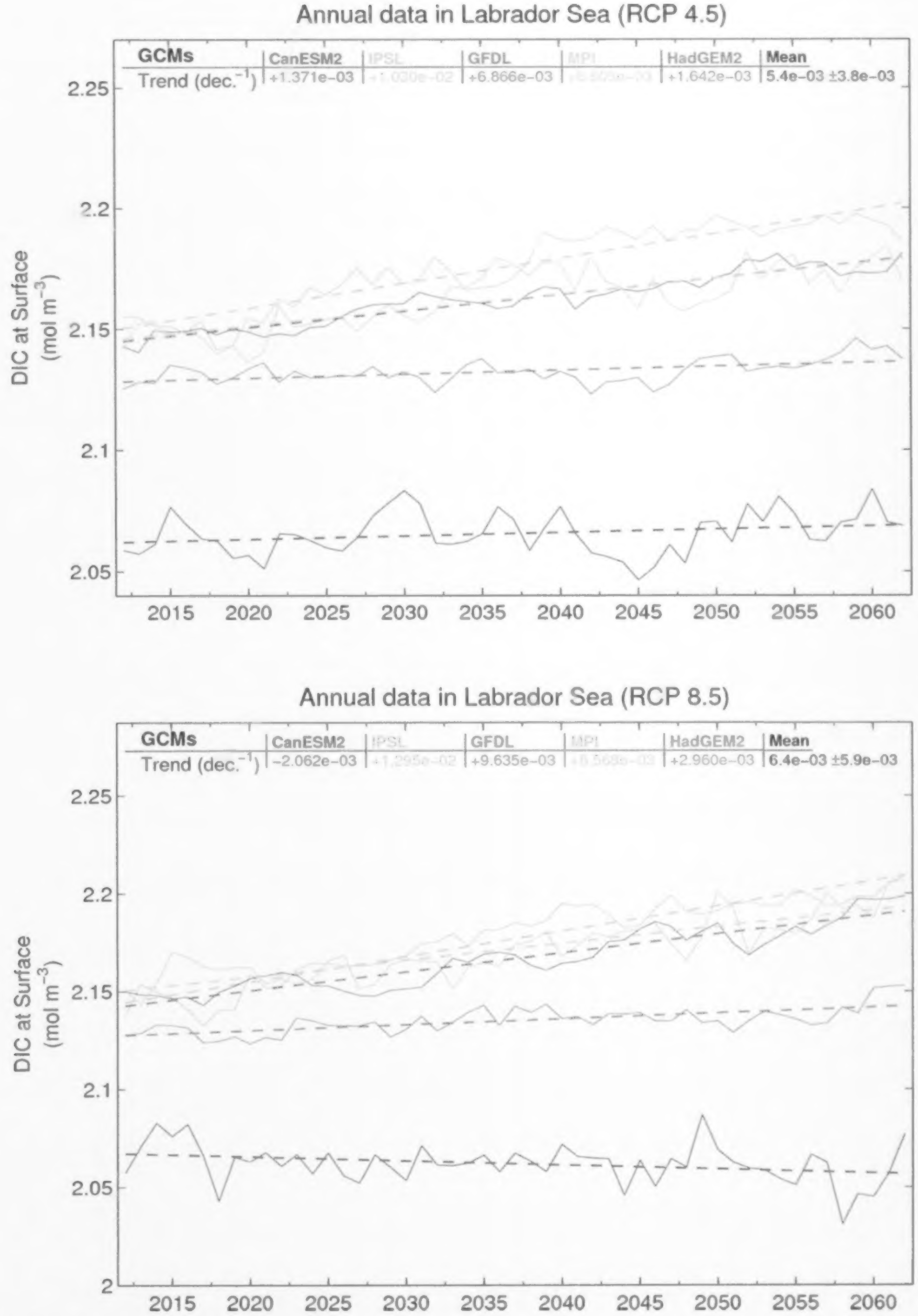

Figure 51. Future DIC concentration trends (mol m^{-3}/decade) at the surface in the Labrador Sea for the 2012-2062 period for RCPs 4.5 and 8.5.

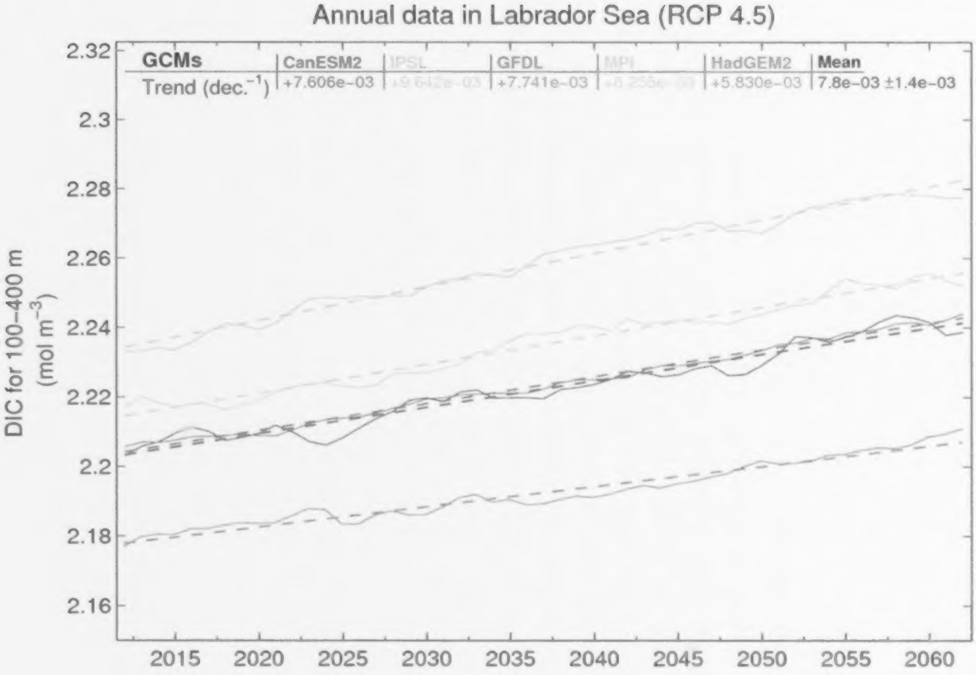

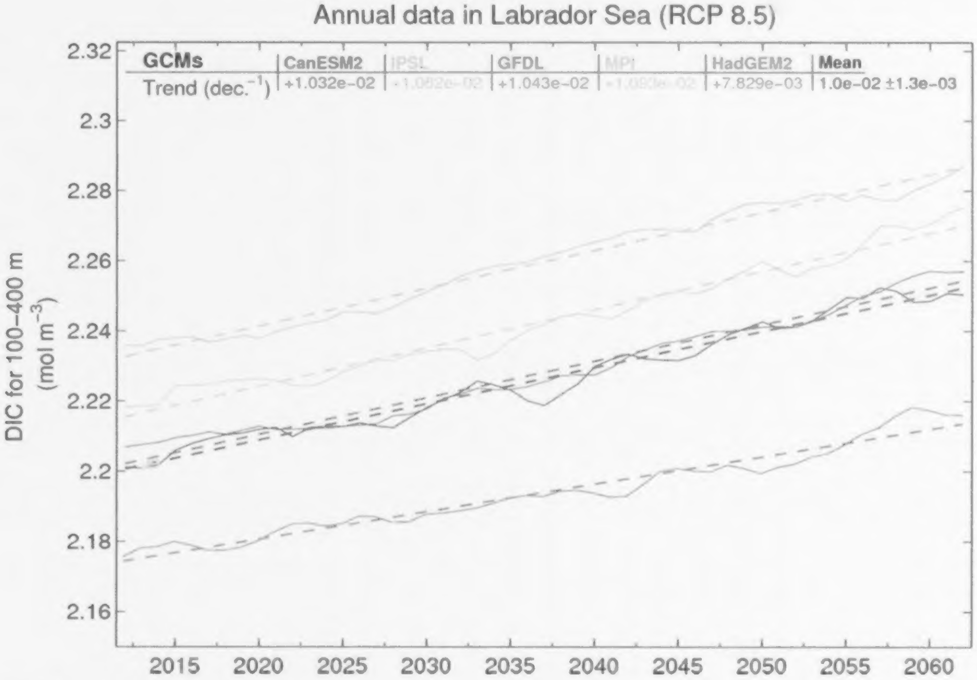

Figure 52. Future DIC concentration trends (mol m^{-3}/decade) at 100-400 m in the Labrador Sea for the 2012-2062 period for RCPs 4.5 and 8.5.

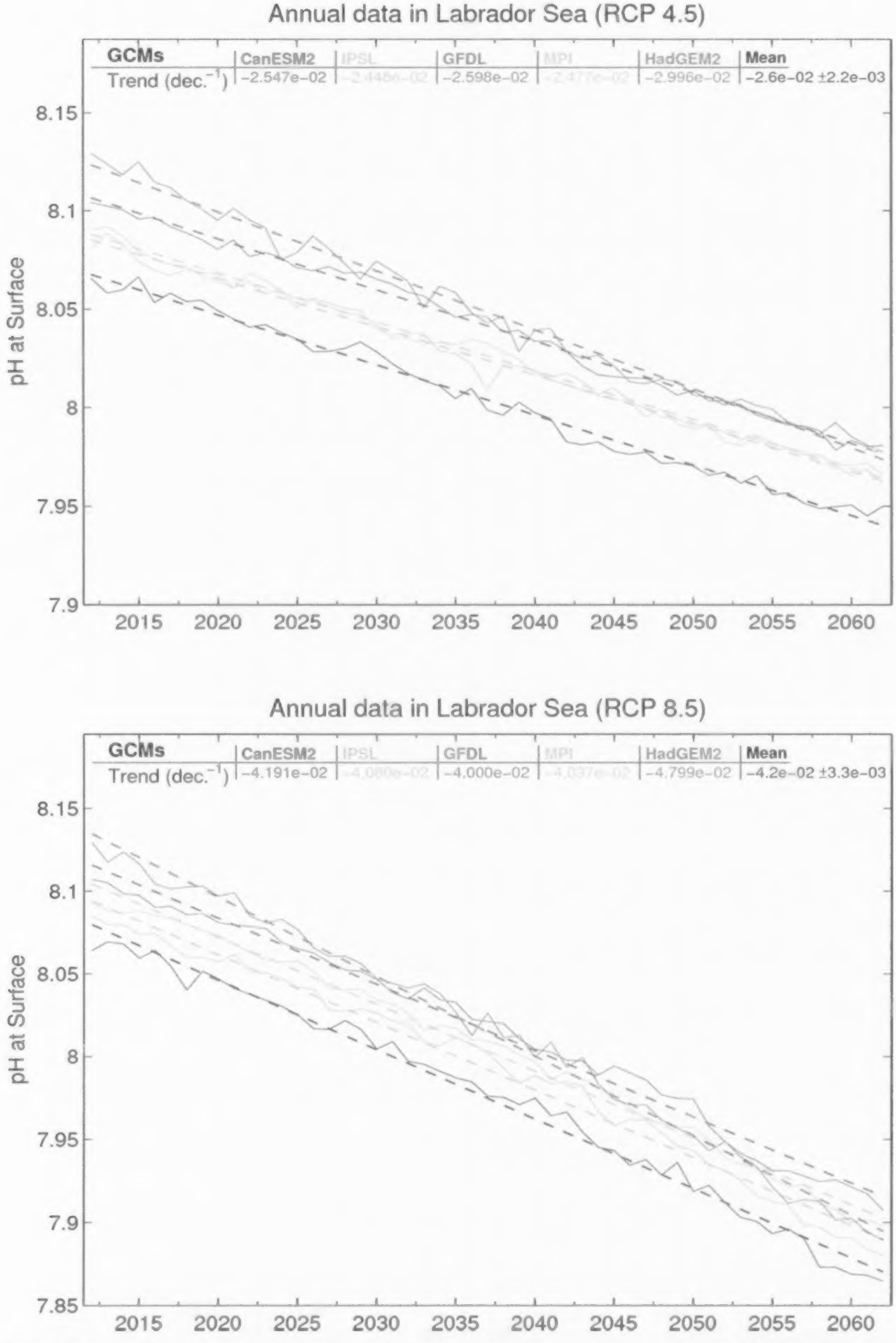

Figure 53. Future pH trends (per decade) at the surface m in the Labrador Sea for the 2012-2062 period for RCPs 4.5 and 8.5.

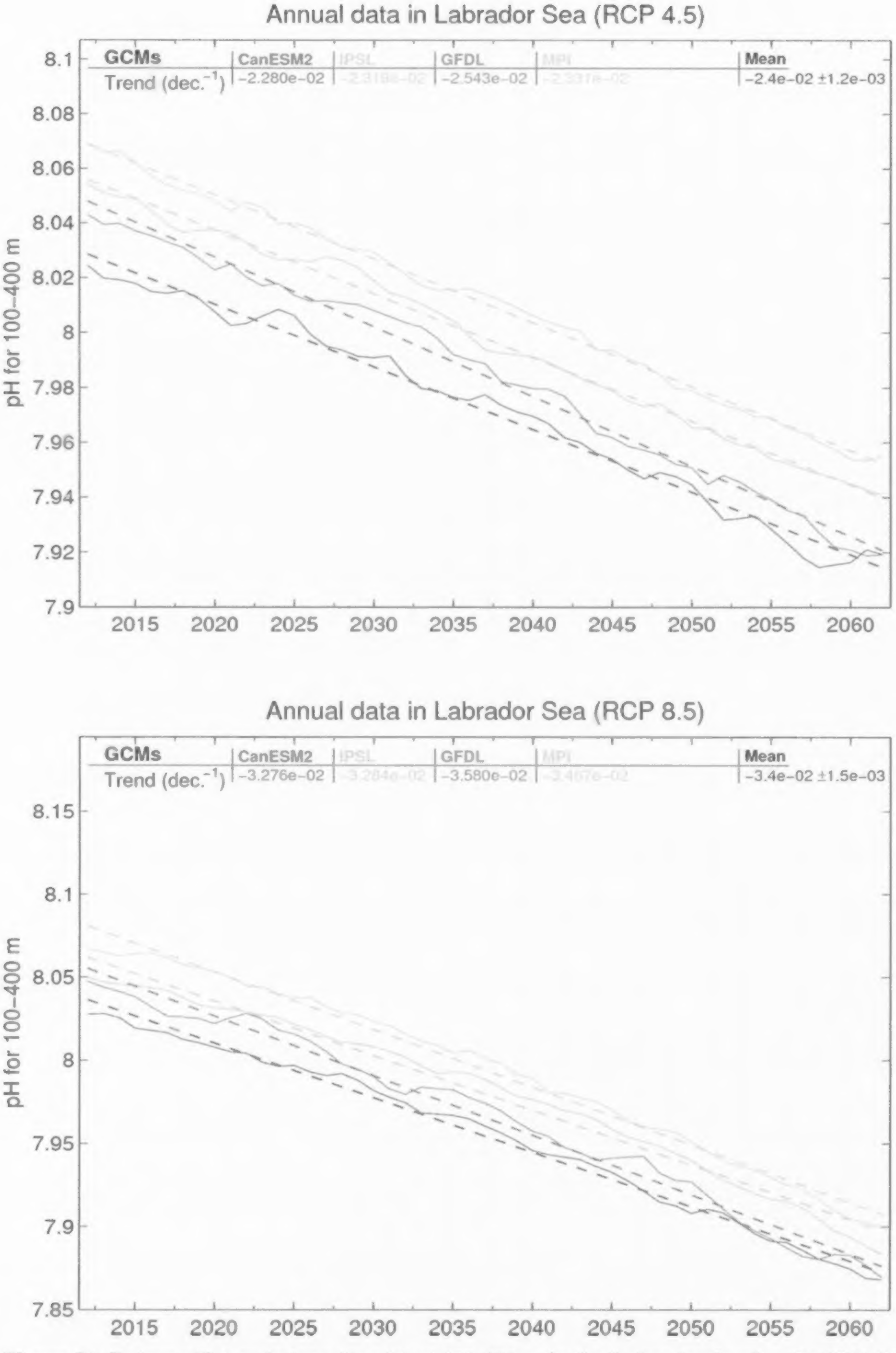

Figure 54. Future pH trends (per decade) at 100-400 m in the Labrador Sea for the 2012-2062 period for RCPs 4.5 and 8.5.

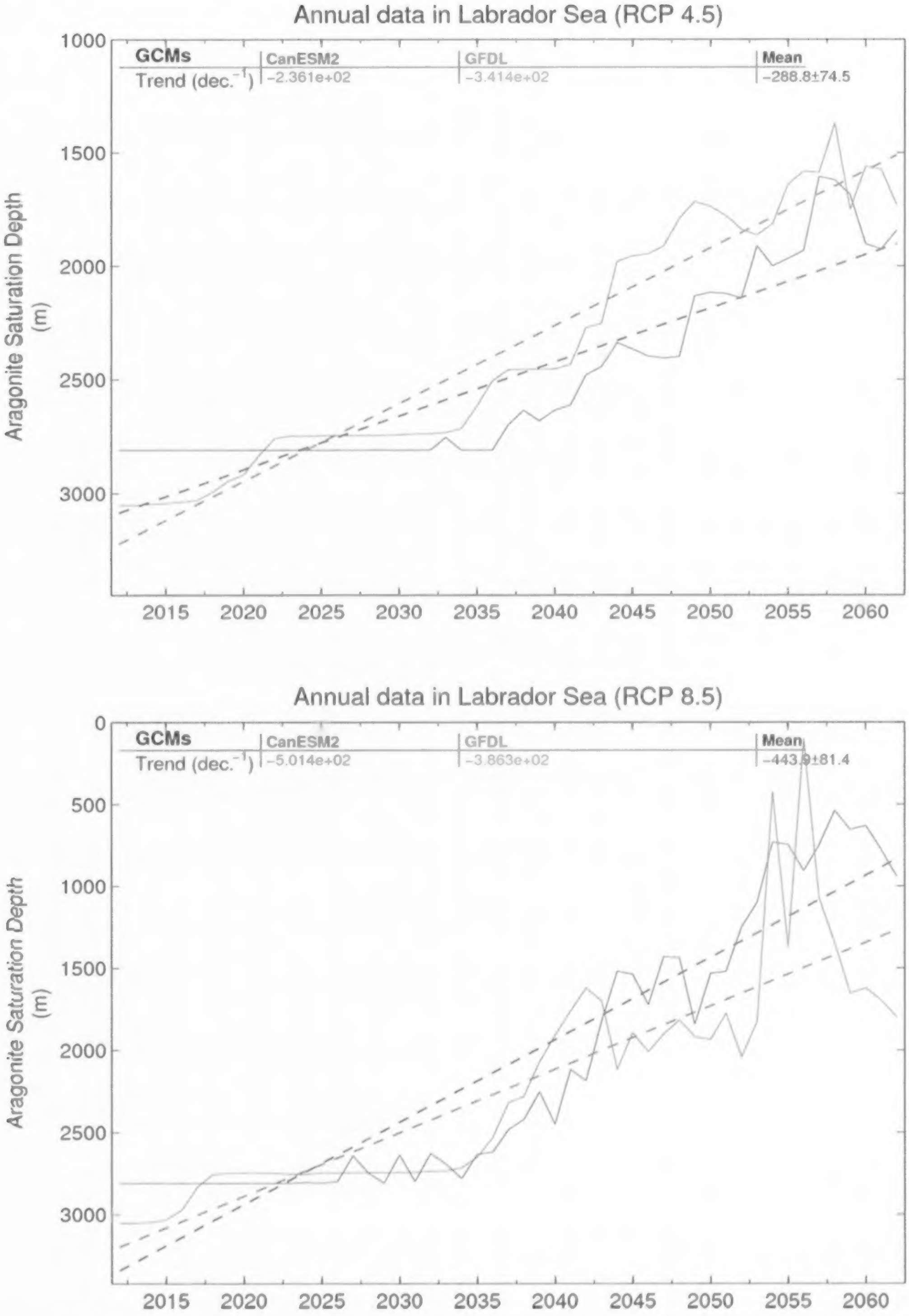

Figure 55. Future aragonite saturation horizon depth in the Labrador Sea for the 2012-2062 period for RCPs 4.5 and 8.5.

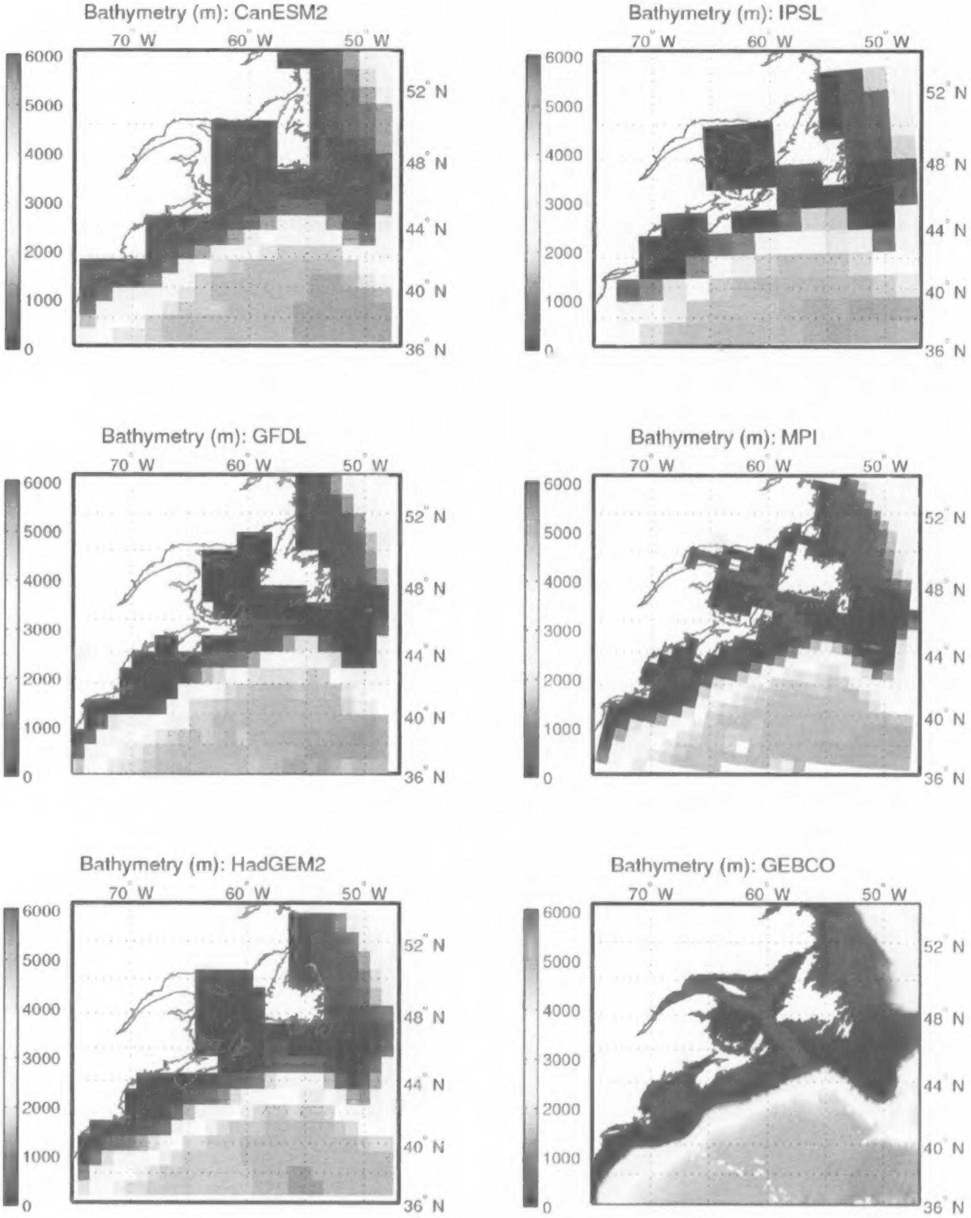
Bathymetry (m): CanESM2
Bathymetry (m): IPSL
Bathymetry (m): GFDL
Bathymetry (m): MPI
Bathymetry (m): HadGEM2
Bathymetry (m): GEBCO
70° W
60° W
50° W
52° N
48° N
44° N
40° N
36° N
6000
5000
4000
3000
2000
1000
0

Figure 56. Bathymetry of the AtlNW region (see Figure 1) in the different models and bathymetry from the General Bathymetric Chart of the Oceans (GEBCO).

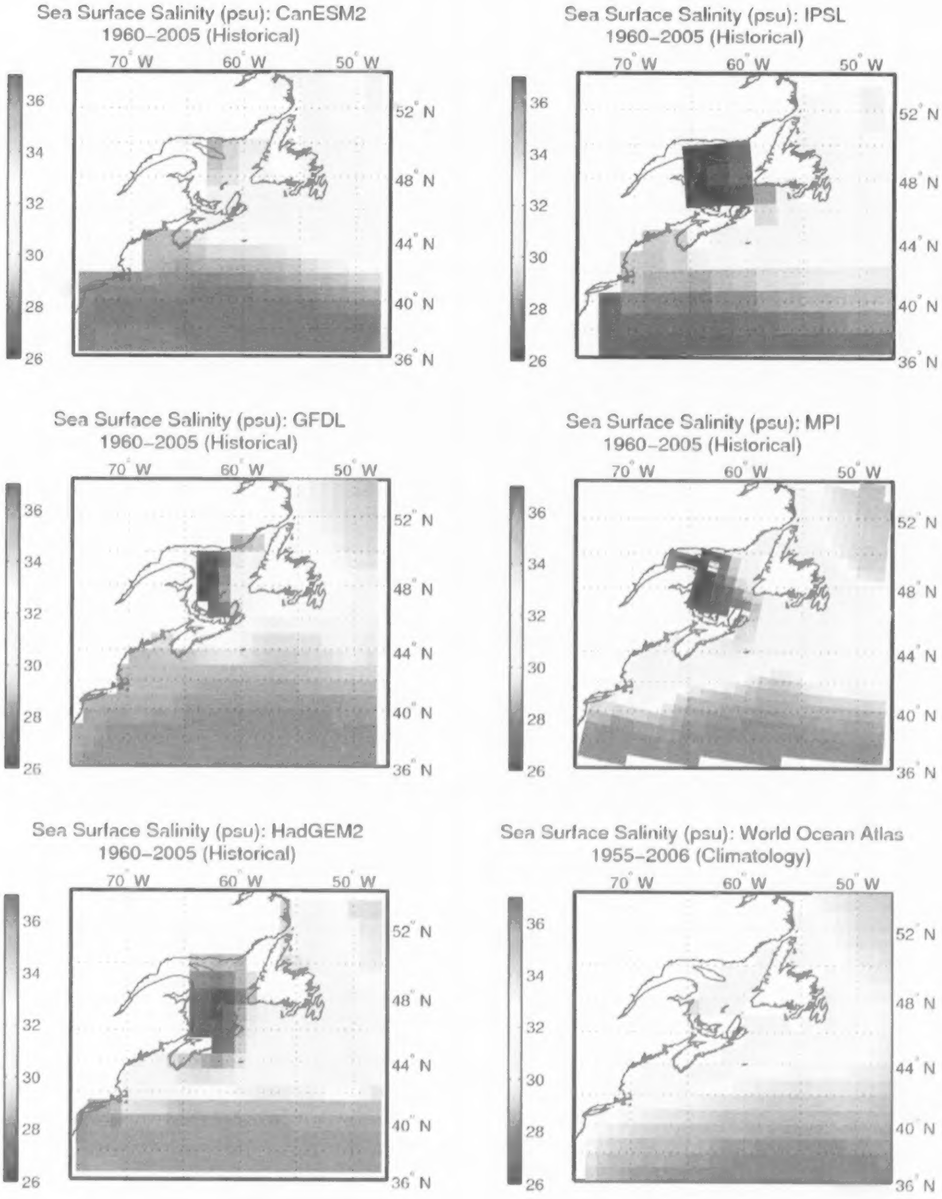

Sea Surface Salinity (psu): CanESM2
1960–2005 (Historical)

Sea Surface Salinity (psu): IPSL
1960–2005 (Historical)

Sea Surface Salinity (psu): GFDL
1960–2005 (Historical)

Sea Surface Salinity (psu): MPI
1960–2005 (Historical)

Sea Surface Salinity (psu): HadGEM2
1960–2005 (Historical)

Sea Surface Salinity (psu): World Ocean Atlas
1955–2006 (Climatology)

Figure 57. Mean simulated sea surface salinity in the AtlNW region for the historical period (1960-2005) compared with sea surface salinity from the World Ocean Atlas (WOA; Antonov et al., 2010).

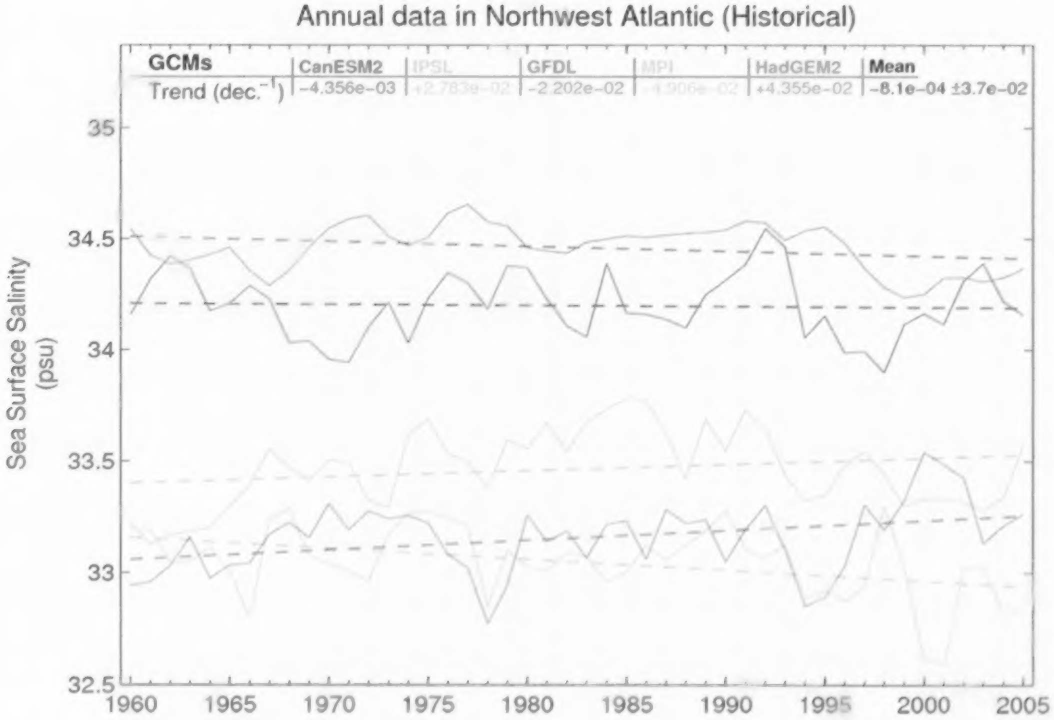

Figure 58. Average sea surface salinity trends (per decade) over the AtlNW region for the historical period (1960-2005).

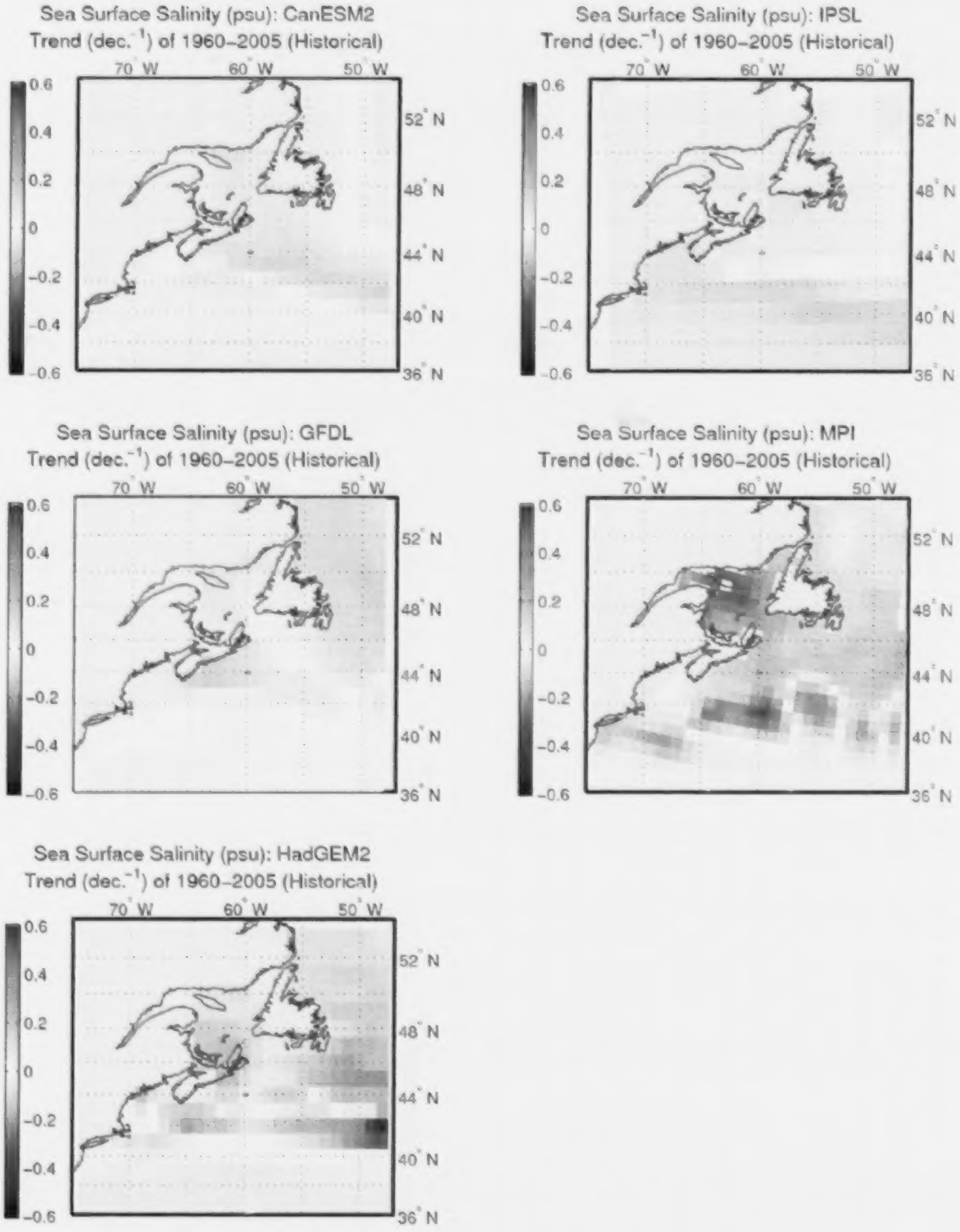
Sea Surface Salinity (psu): CanESM2
Trend (dec.$^{-1}$) of 1960–2005 (Historical)
Sea Surface Salinity (psu): IPSL
Trend (dec.$^{-1}$) of 1960–2005 (Historical)
Sea Surface Salinity (psu): GFDL
Trend (dec.$^{-1}$) of 1960–2005 (Historical)
Sea Surface Salinity (psu): MPI
Trend (dec.$^{-1}$) of 1960–2005 (Historical)
Sea Surface Salinity (psu): HadGEM2
Trend (dec.$^{-1}$) of 1960–2005 (Historical)
70° W
60° W
50° W
52° N
48° N
44° N
40° N
36° N
0.6
0.4
0.2
0
-0.2
-0.4
-0.6

Figure 59. Sea surface salinity trends (per decade) at each grid cell in the AtlNW region for the historical period (1960-2005).

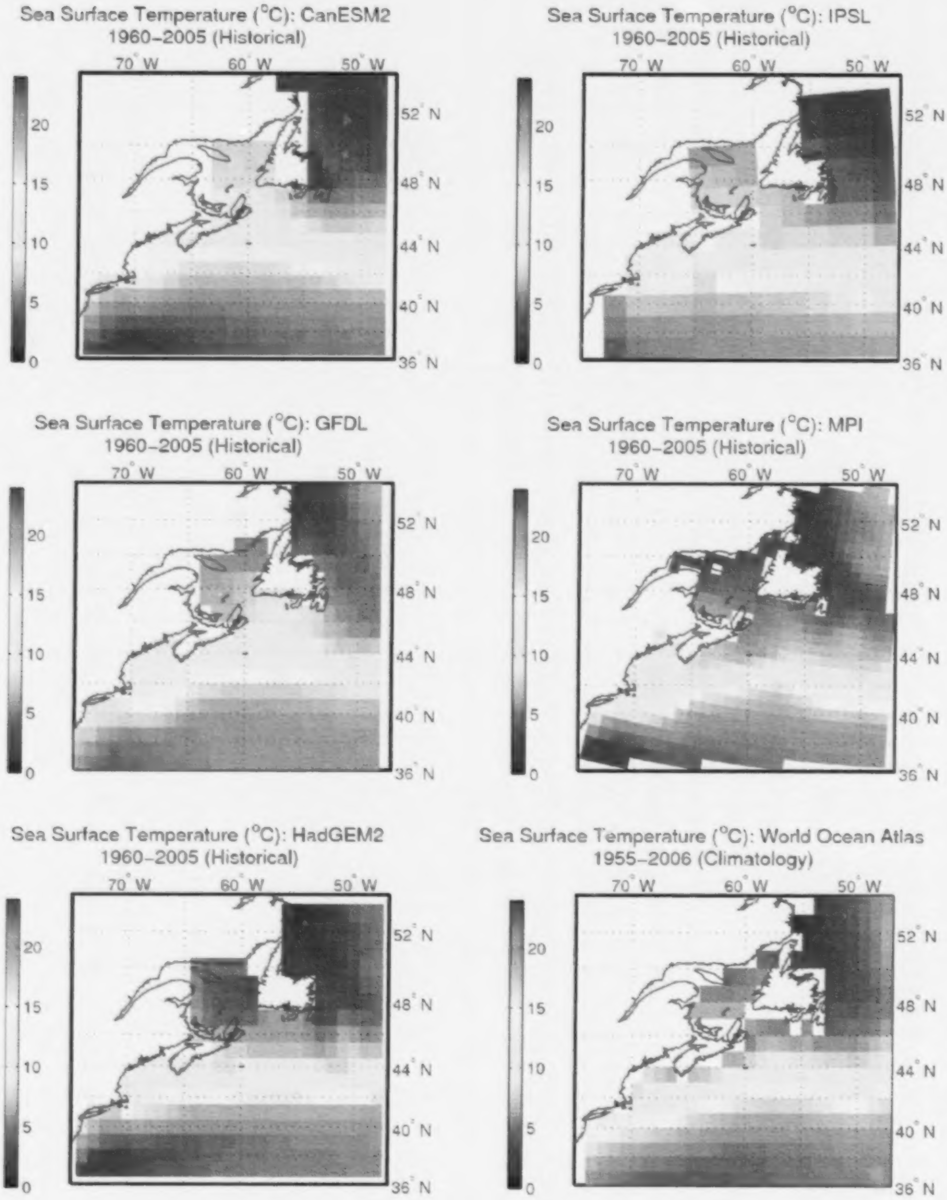
Sea Surface Temperature (°C): CanESM2
1960–2005 (Historical)
Sea Surface Temperature (°C): IPSL
1960–2005 (Historical)
Sea Surface Temperature (°C): GFDL
1960–2005 (Historical)
Sea Surface Temperature (°C): MPI
1960–2005 (Historical)
Sea Surface Temperature (°C): HadGEM2
1960–2005 (Historical)
Sea Surface Temperature (°C): World Ocean Atlas
1955–2006 (Climatology)
70° W
60° W
50° W
52° N
48° N
44° N
40° N
36° N
0
5
10
15
20

Figure 60. Mean simulated sea surface temperature in the AtlNW region for the historical period (1960-2005) compared with sea surface temperature from the World Ocean Atlas (WOA; Locarnini et al., 2010).

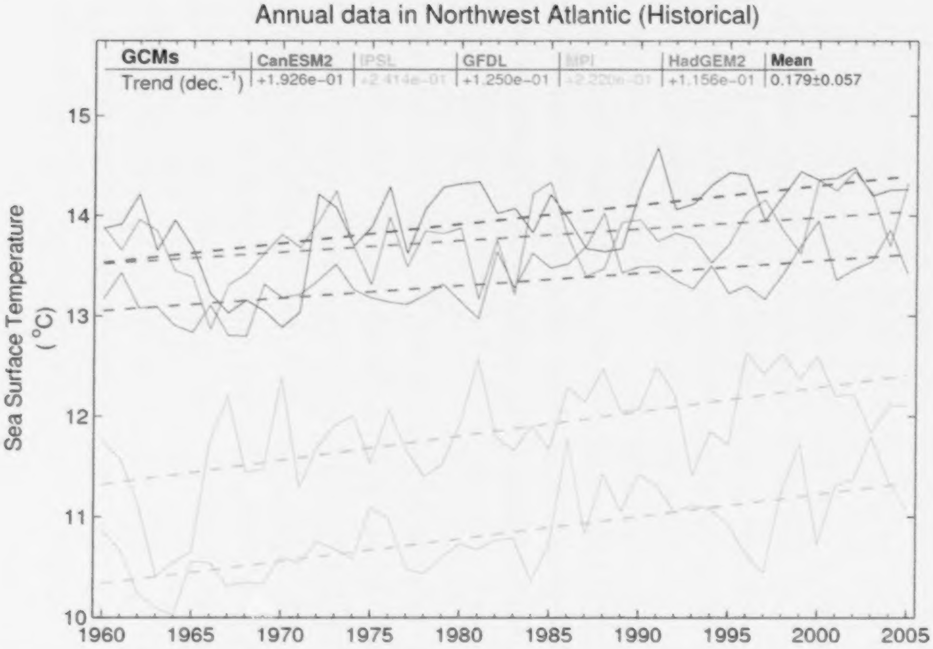

Figure 61. Average sea surface temperature trends (°C/decade) over the AtlNW region for the historical period (1960-2005).

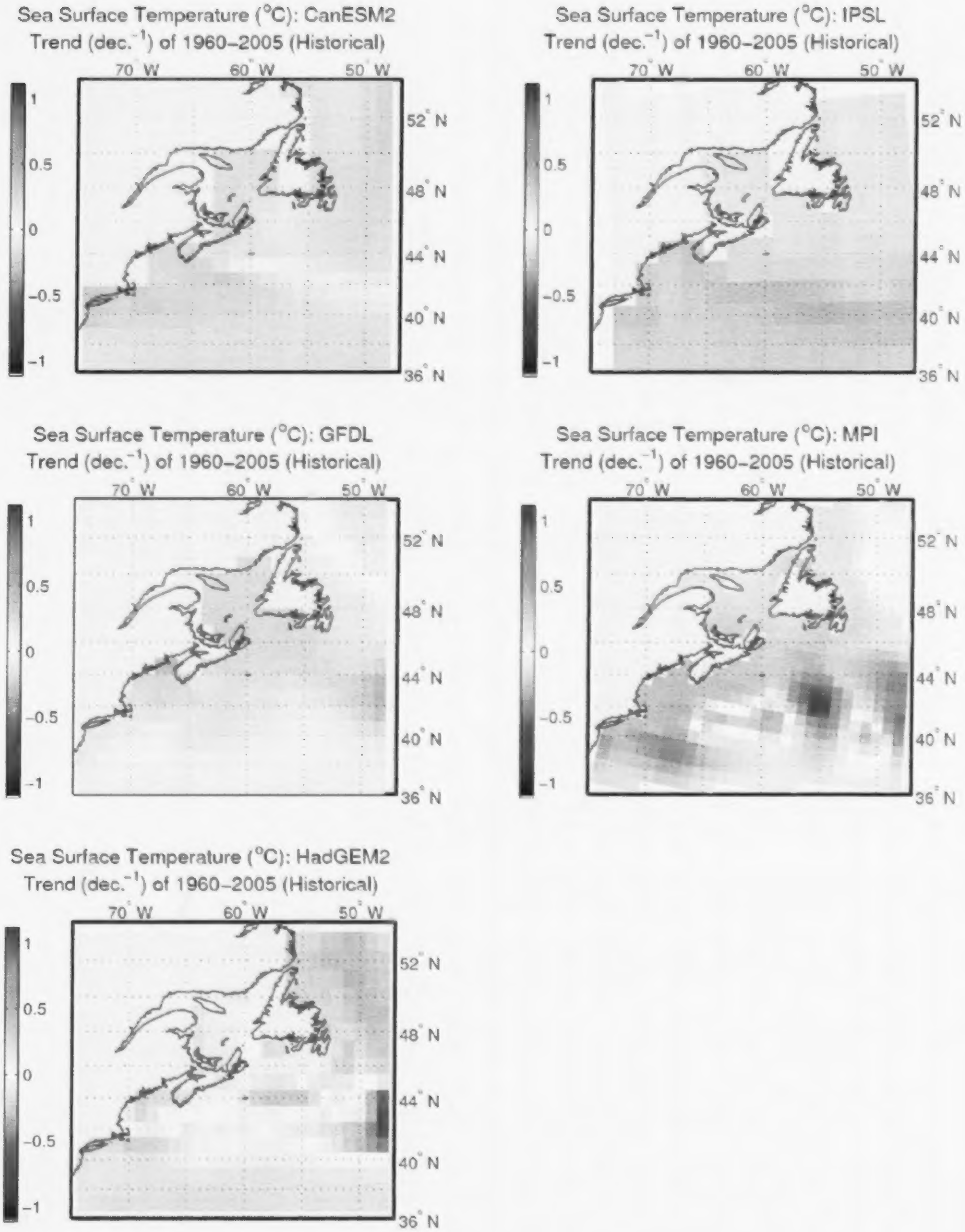
Sea Surface Temperature (°C): CanESM2
Trend (dec.⁻¹) of 1960–2005 (Historical)
Sea Surface Temperature (°C): IPSL
Trend (dec.⁻¹) of 1960–2005 (Historical)
Sea Surface Temperature (°C): GFDL
Trend (dec.⁻¹) of 1960–2005 (Historical)
Sea Surface Temperature (°C): MPI
Trend (dec.⁻¹) of 1960–2005 (Historical)
Sea Surface Temperature (°C): HadGEM2
Trend (dec.⁻¹) of 1960–2005 (Historical)
70° W
60° W
50° W
52° N
48° N
44° N
40° N
36° N
1
0.5
0
−0.5
−1

Figure 62. Sea surface temperature trends (°C/decade) at each grid cell in the AtlNW region for the historical period (1960-2005).

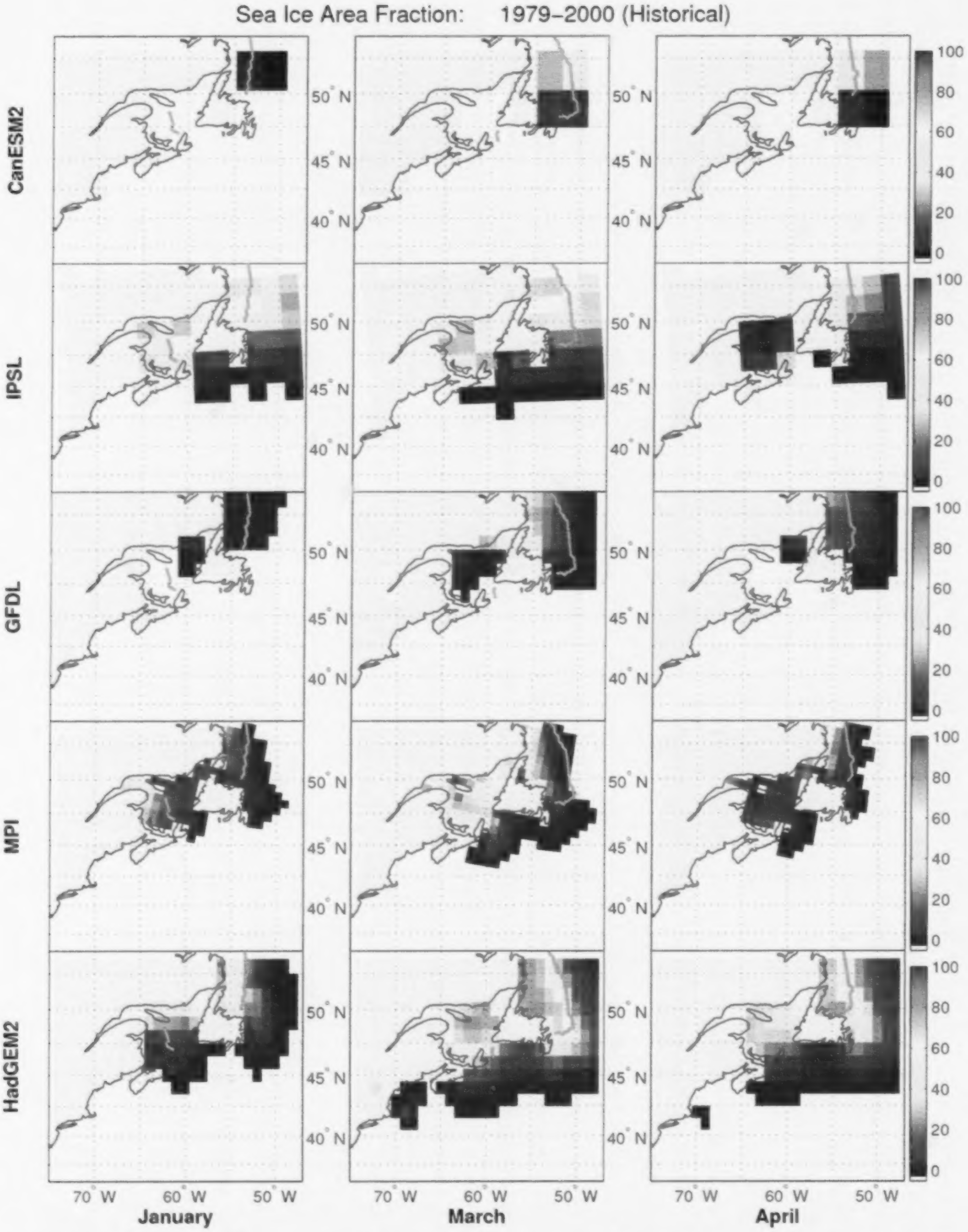

Sea Ice Area Fraction: 1979-2000 (Historical)
CanESM2
IPSL
GFDL
MPI
HadGEM2
50° N
45° N
40° N
100
80
60
40
20
0
70° W
60° W
50° W
January
March
April

Figure 63. Average sea ice concentration in the Atlantic Northwest for the months of January, March and April for the historical period (1971-2000) and for the 5 GCMs. The purple line represents the median extent (15% limit) measured by Fetterer et al. (2009) for the same period.

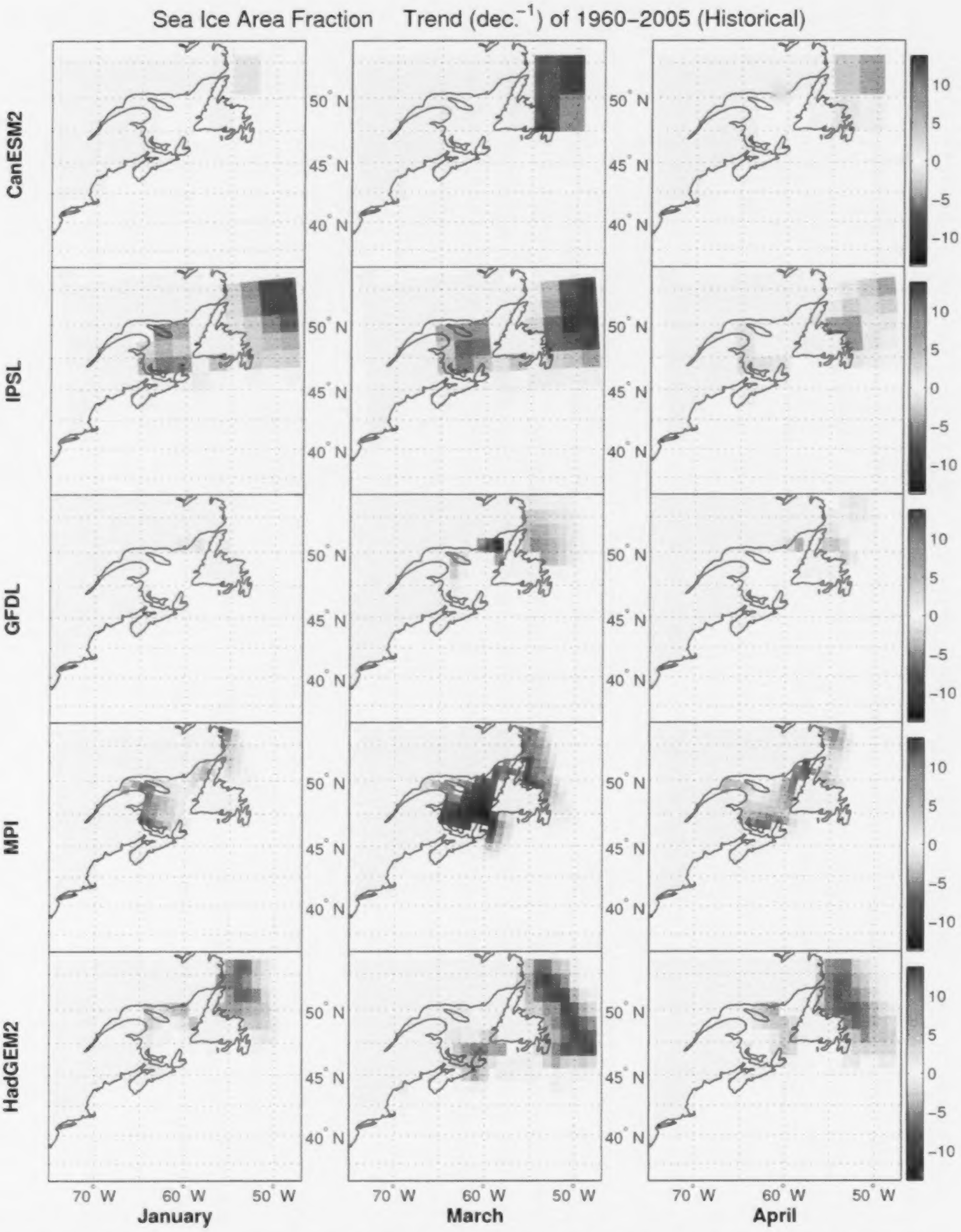
Sea Ice Area Fraction Trend (dec.$^{-1}$) of 1960-2005 (Historical)
CanESM2
IPSL
GFDL
MPI
HadGEM2
50° N
45° N
40° N
70° W
60° W
50° W
January
March
April
10
5
0
−5
−10

Figure 64. Sea ice concentration trends (%/decade) at each grid cell in Labrador Sea for the months of January, March, and April for the historical period (1960-2005) and for the 5 GCMs.

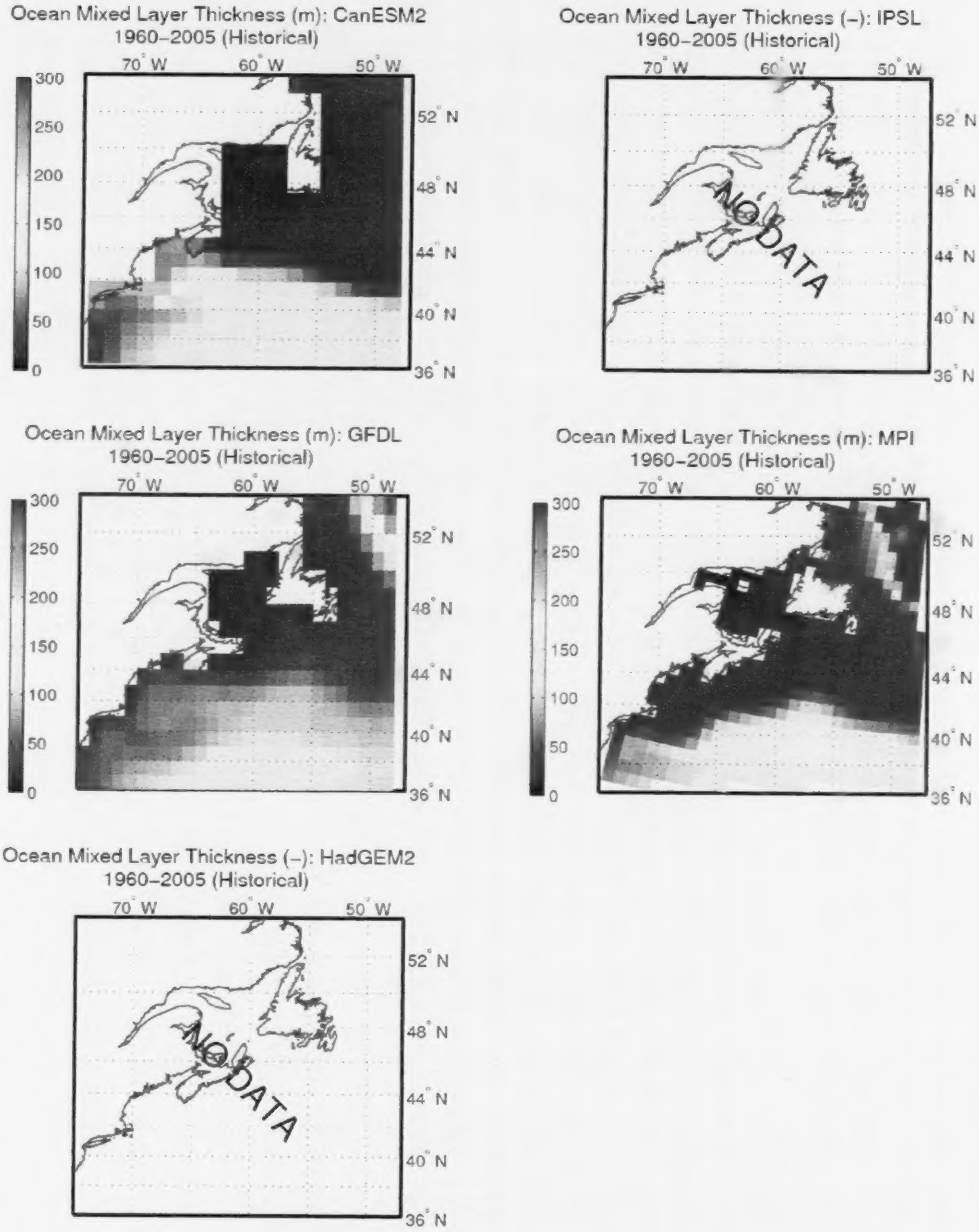
Ocean Mixed Layer Thickness (m): CanESM2
1960–2005 (Historical)

Ocean Mixed Layer Thickness (–): IPSL
1960–2005 (Historical)

Ocean Mixed Layer Thickness (m): GFDL
1960–2005 (Historical)

Ocean Mixed Layer Thickness (m): MPI
1960–2005 (Historical)

Ocean Mixed Layer Thickness (–): HadGEM2
1960–2005 (Historical)

70° W
60° W
50° W
52° N
48° N
44° N
40° N
36° N
300
250
200
150
100
50
0
NO DATA

Figure 65. Annual mean mixed layer depths in the AtlNW region for the historical period (1960-2005). Upper right corner around 800 m for MPI and 400 m for GFDL.

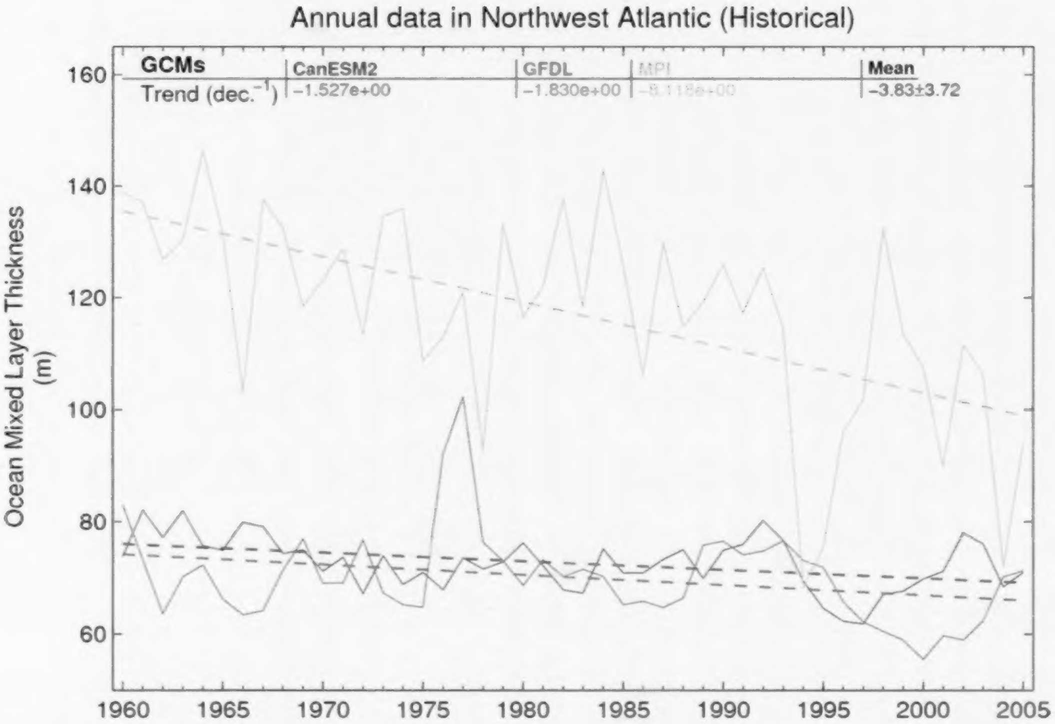

Figure 66. Annual mean mixed layer depth trends (m/decade) over the AtlNW region for the historical period (1960-2005).

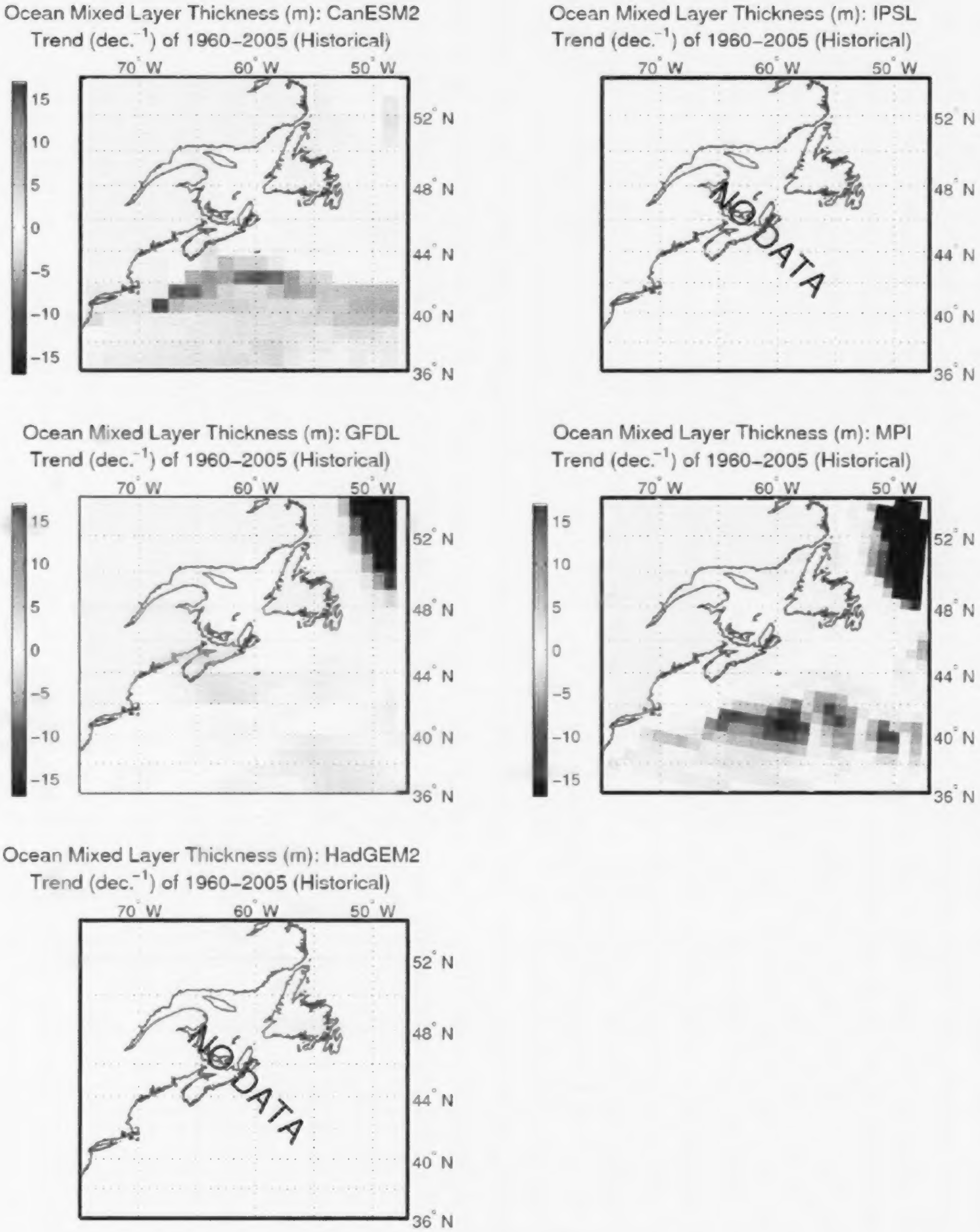
Ocean Mixed Layer Thickness (m): CanESM2
Trend (dec.$^{-1}$) of 1960–2005 (Historical)

Ocean Mixed Layer Thickness (m): IPSL
Trend (dec.$^{-1}$) of 1960–2005 (Historical)

Ocean Mixed Layer Thickness (m): GFDL
Trend (dec.$^{-1}$) of 1960–2005 (Historical)

Ocean Mixed Layer Thickness (m): MPI
Trend (dec.$^{-1}$) of 1960–2005 (Historical)

Ocean Mixed Layer Thickness (m): HadGEM2
Trend (dec.$^{-1}$) of 1960–2005 (Historical)

Figure 67. Annual mean mixed layer depth trends (m/decade) at each grid cell in the AtlNW region for the historical period (1990-2005).

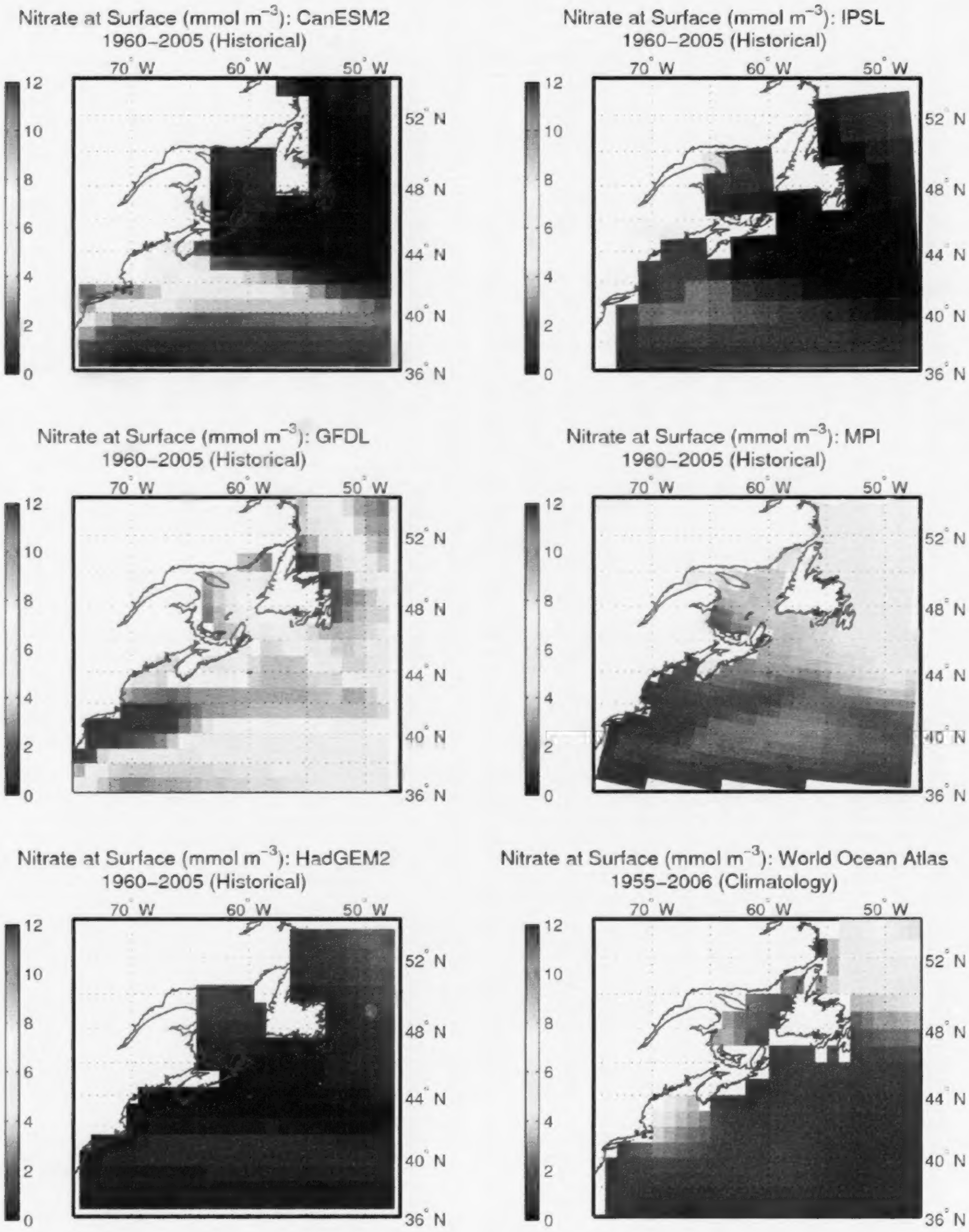
Nitrate at Surface (mmol m^{-3}): CanESM2
1960–2005 (Historical)
Nitrate at Surface (mmol m^{-3}): IPSL
1960–2005 (Historical)
Nitrate at Surface (mmol m^{-3}): GFDL
1960–2005 (Historical)
Nitrate at Surface (mmol m^{-3}): MPI
1960–2005 (Historical)
Nitrate at Surface (mmol m^{-3}): HadGEM2
1960–2005 (Historical)
Nitrate at Surface (mmol m^{-3}): World Ocean Atlas
1955–2006 (Climatology)
70° W
60° W
50° W
52° N
48° N
44° N
40° N
36° N
0
2
4
6
8
10
12

Figure 68. Mean simulated nitrate concentration at the surface in the AtlNW region for the historical period (1960-2005) compared with nitrate concentration at the surface from the World Ocean Atlas (Garcia et al., 2010b).

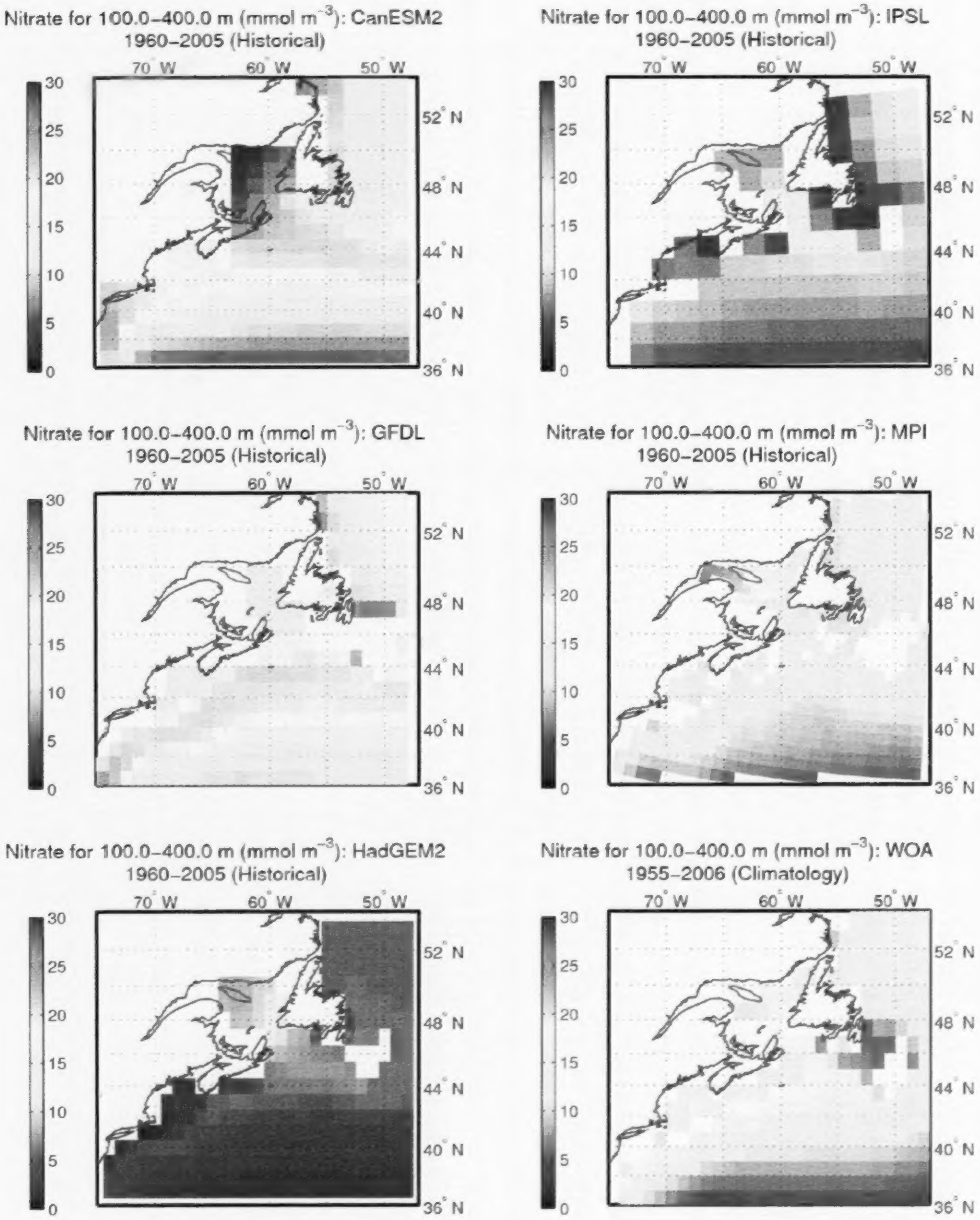
Nitrate for 100.0–400.0 m (mmol m^{-3}): CanESM2
1960–2005 (Historical)
Nitrate for 100.0–400.0 m (mmol m^{-3}): IPSL
1960–2005 (Historical)
Nitrate for 100.0–400.0 m (mmol m^{-3}): GFDL
1960–2005 (Historical)
Nitrate for 100.0–400.0 m (mmol m^{-3}): MPI
1960–2005 (Historical)
Nitrate for 100.0–400.0 m (mmol m^{-3}): HadGEM2
1960–2005 (Historical)
Nitrate for 100.0–400.0 m (mmol m^{-3}): WOA
1955–2006 (Climatology)
70° W
60° W
50° W
52° N
48° N
44° N
40° N
36° N
30
25
20
15
10
5
0

Figure 69. Mean simulated nitrate concentration at 100-400 m in the AtlNW region for the historical period (1960-2005) compared with nitrate concentration at 100-400 m from the World Ocean Atlas (Garcia et al., 2010b).

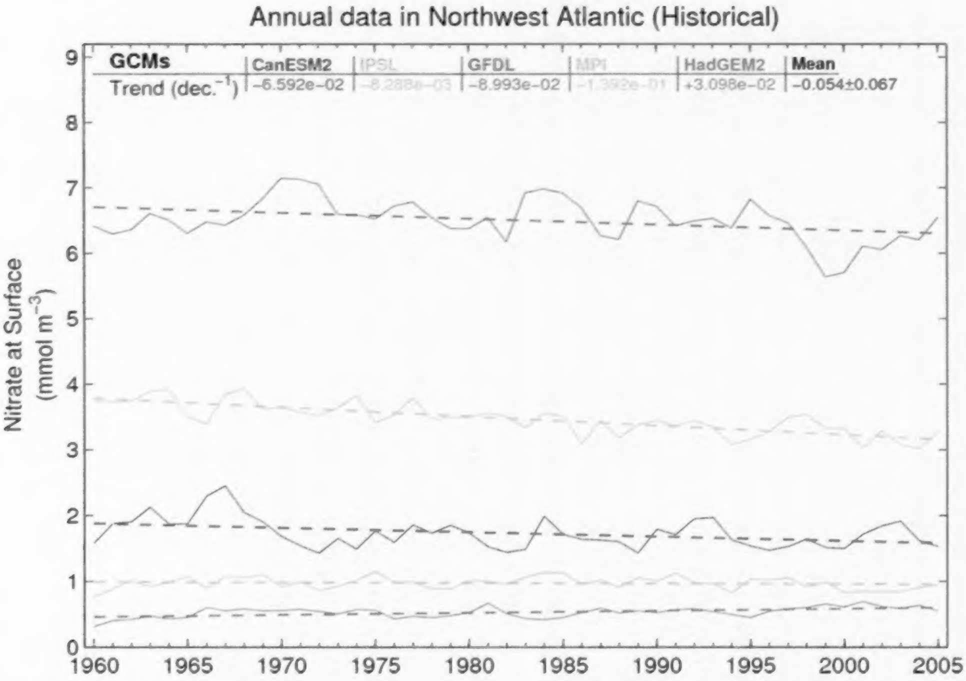

Figure 70. Average nitrate concentration trends (mmol m^{-3}/decade) at the surface over the AtlNW region for the historical period (1960-2005).

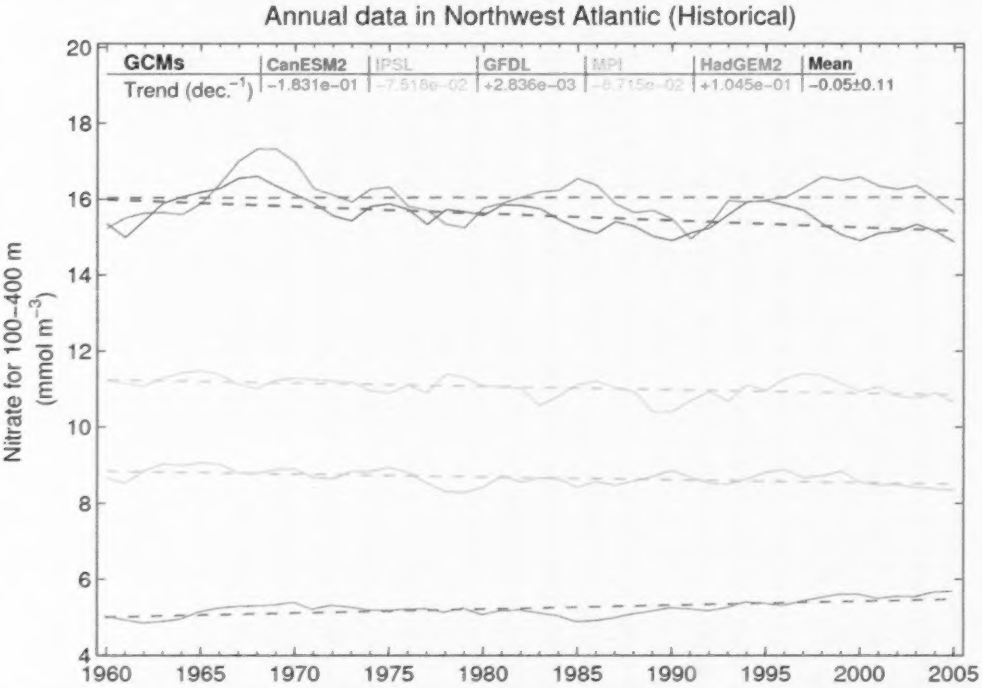

Figure 71. Average nitrate concentration trends (mmol m^{-3}/decade) at 100-400 m over the AtlNW region for the historical period (1960-2005).

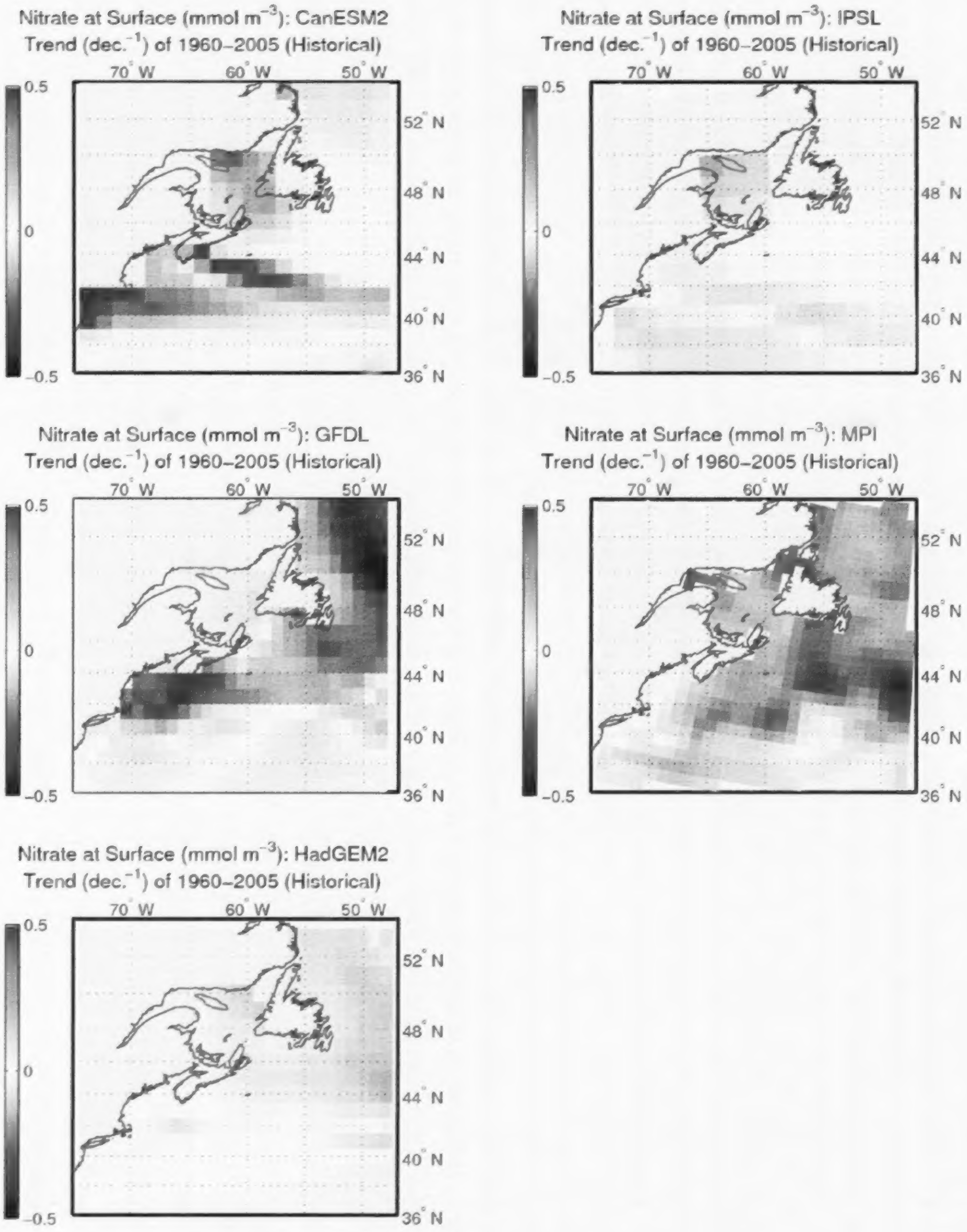
Nitrate at Surface (mmol m^{-3}): CanESM2 Trend (dec.$^{-1}$) of 1960–2005 (Historical)

Nitrate at Surface (mmol m^{-3}): IPSL Trend (dec.$^{-1}$) of 1960–2005 (Historical)

Nitrate at Surface (mmol m^{-3}): GFDL Trend (dec.$^{-1}$) of 1960–2005 (Historical)

Nitrate at Surface (mmol m^{-3}): MPI Trend (dec.$^{-1}$) of 1960–2005 (Historical)

Nitrate at Surface (mmol m^{-3}): HadGEM2 Trend (dec.$^{-1}$) of 1960–2005 (Historical)

Figure 72. Nitrate concentration trends (mmol m^{-3}/decade) at the surface at each grid cell in the AtlNW region for the historical period (1960-2005).

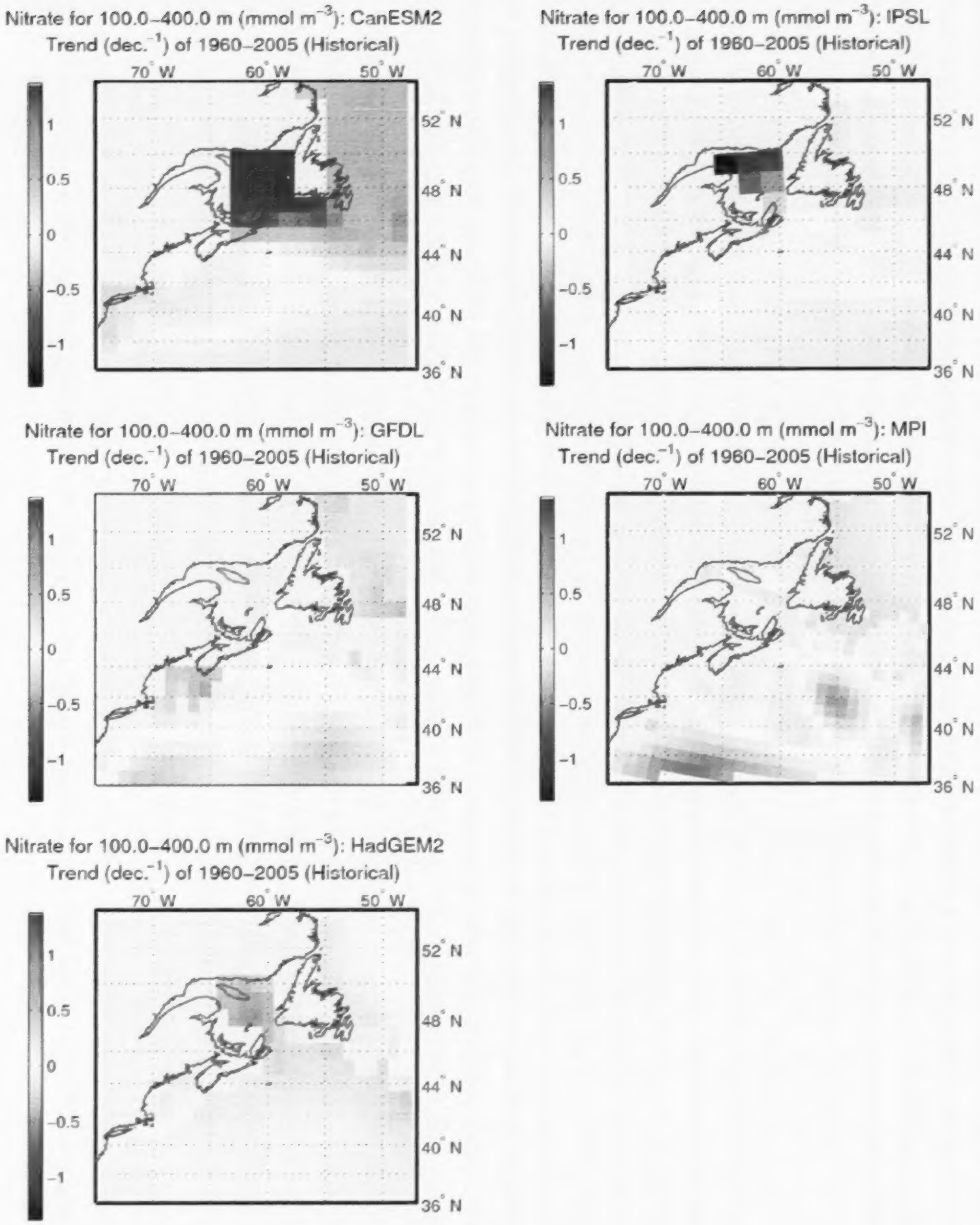

Nitrate for 100.0–400.0 m (mmol m^{-3}): CanESM2
Trend (dec.$^{-1}$) of 1960–2005 (Historical)

Nitrate for 100.0–400.0 m (mmol m^{-3}): IPSL
Trend (dec.$^{-1}$) of 1960–2005 (Historical)

Nitrate for 100.0–400.0 m (mmol m^{-3}): GFDL
Trend (dec.$^{-1}$) of 1960–2005 (Historical)

Nitrate for 100.0–400.0 m (mmol m^{-3}): MPI
Trend (dec.$^{-1}$) of 1960–2005 (Historical)

Nitrate for 100.0–400.0 m (mmol m^{-3}): HadGEM2
Trend (dec.$^{-1}$) of 1960–2005 (Historical)

Figure 73. Nitrate concentration trends (mmol m^{-3}/decade) at 100-400 at each grid cell in the AtlNW region for the historical period (1960-2005).

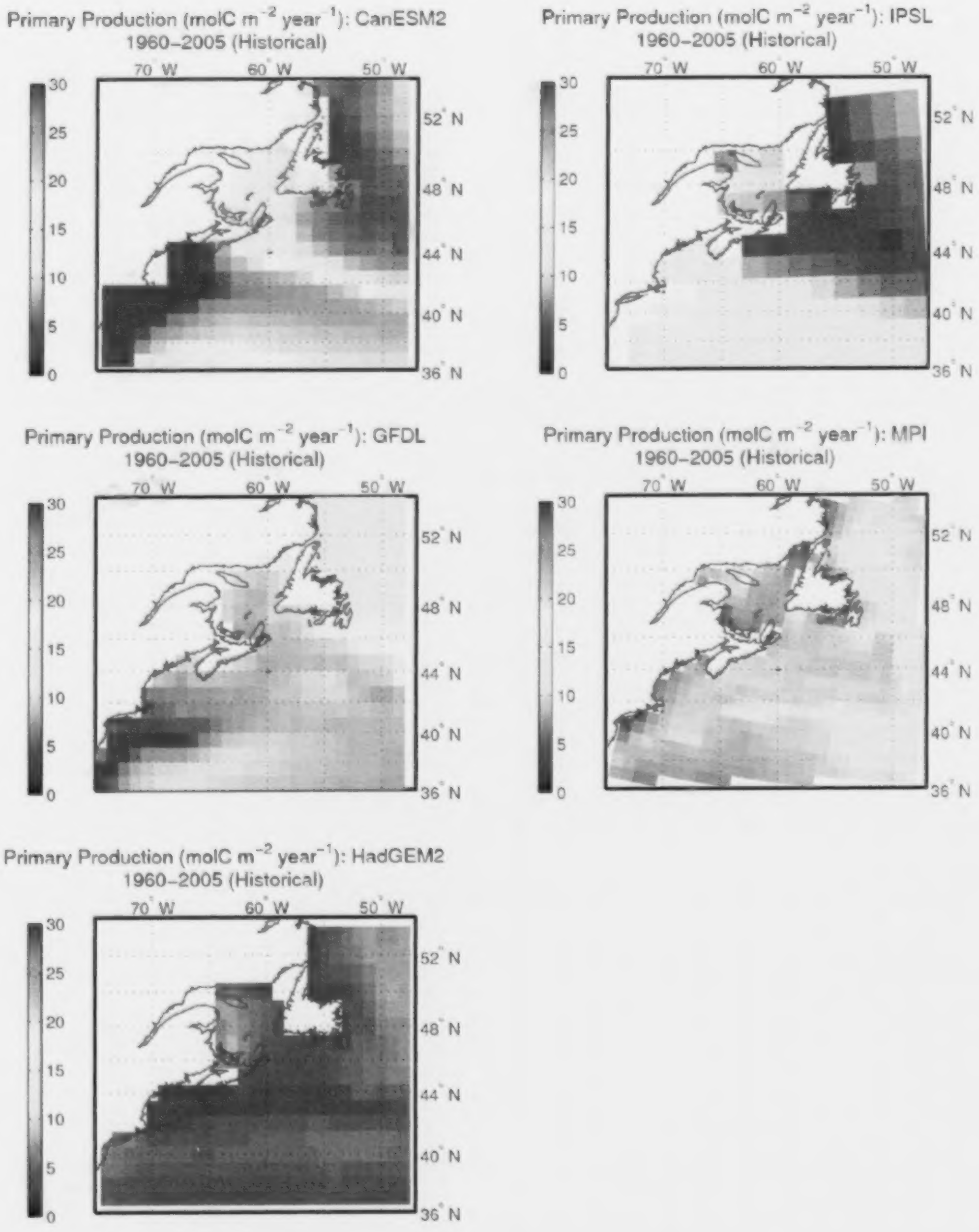
Primary Production (molC m^{-2} $year^{-1}$): CanESM2
1960–2005 (Historical)

Primary Production (molC m^{-2} $year^{-1}$): IPSL
1960–2005 (Historical)

Primary Production (molC m^{-2} $year^{-1}$): GFDL
1960–2005 (Historical)

Primary Production (molC m^{-2} $year^{-1}$): MPI
1960–2005 (Historical)

Primary Production (molC m^{-2} $year^{-1}$): HadGEM2
1960–2005 (Historical)

Figure 74. Mean vertically integrated primary production in the AtlNW region for the historical period (1960-2005). Saturated value with CanESM2 range between 35-40 molC m^{-2} $year^{-1}$.

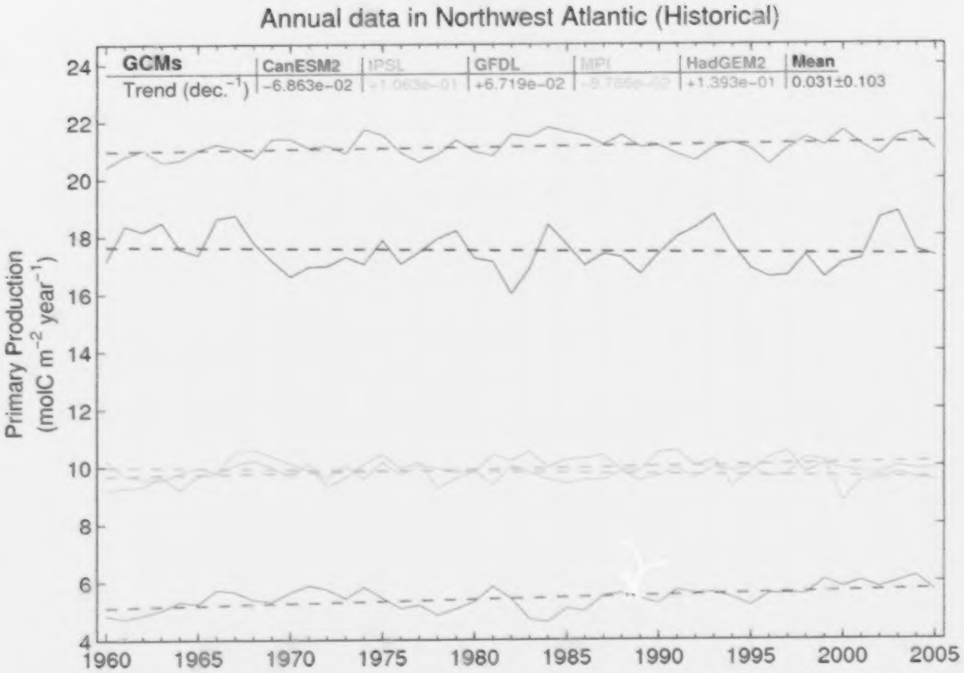

Figure 75. Average vertically integrated primary production trends (mol C m^{-2}/decade) at the surface in the AtlNW region for the historical period (1960-2005).

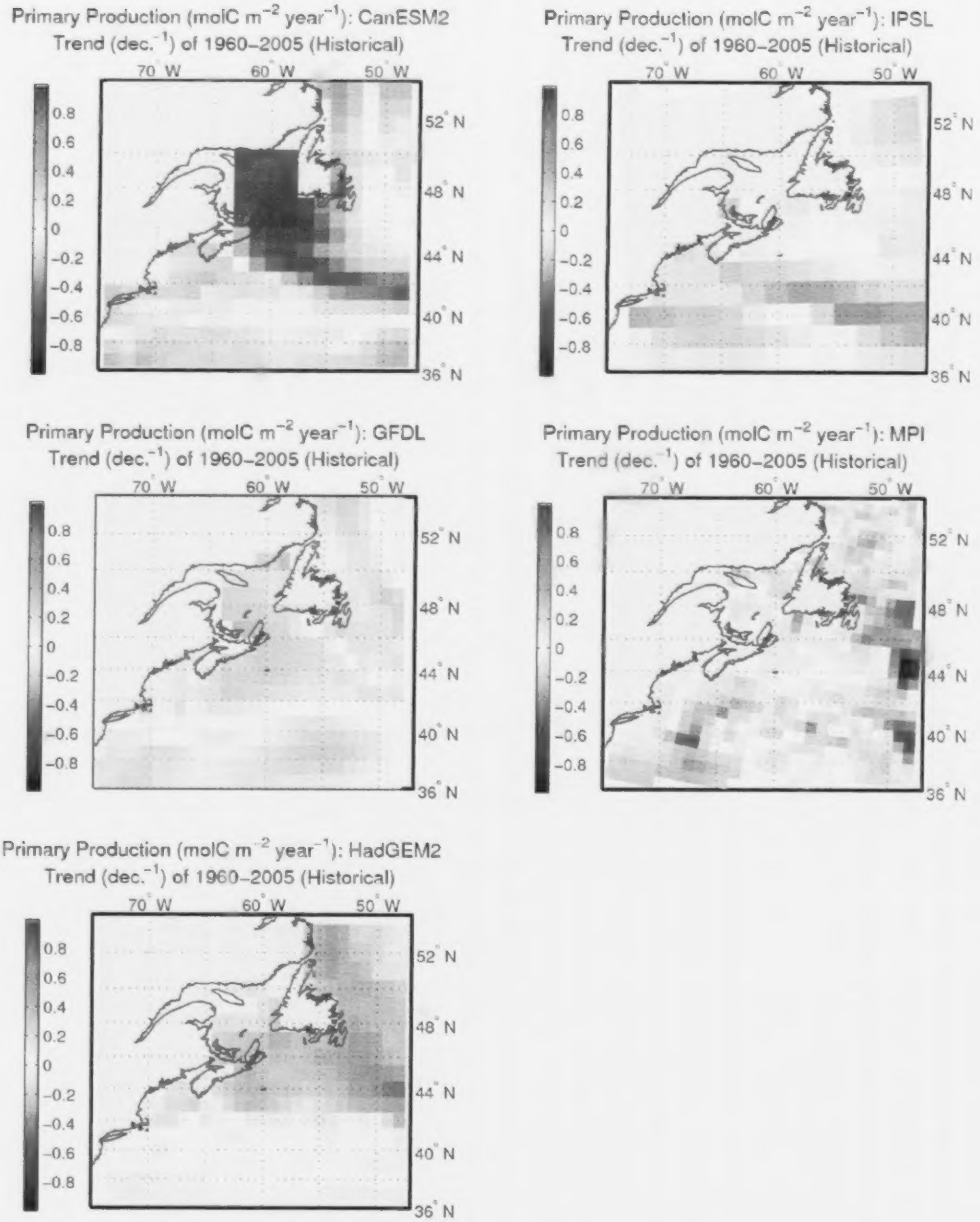
Primary Production (molC m⁻² year⁻¹): CanESM2
Trend (dec.⁻¹) of 1960–2005 (Historical)
Primary Production (molC m⁻² year⁻¹): IPSL
Trend (dec.⁻¹) of 1960–2005 (Historical)
Primary Production (molC m⁻² year⁻¹): GFDL
Trend (dec.⁻¹) of 1960–2005 (Historical)
Primary Production (molC m⁻² year⁻¹): MPI
Trend (dec.⁻¹) of 1960–2005 (Historical)
Primary Production (molC m⁻² year⁻¹): HadGEM2
Trend (dec.⁻¹) of 1960–2005 (Historical)
70° W
60° W
50° W
52° N
48° N
44° N
40° N
36° N
0.8
0.6
0.4
0.2
0
-0.2
-0.4
-0.6
-0.8

Figure 76. Vertically integrated primary production trends (mol C m^{-2}/decade) at each grid cell in the AtlNW region for the historical period (1960-2005).

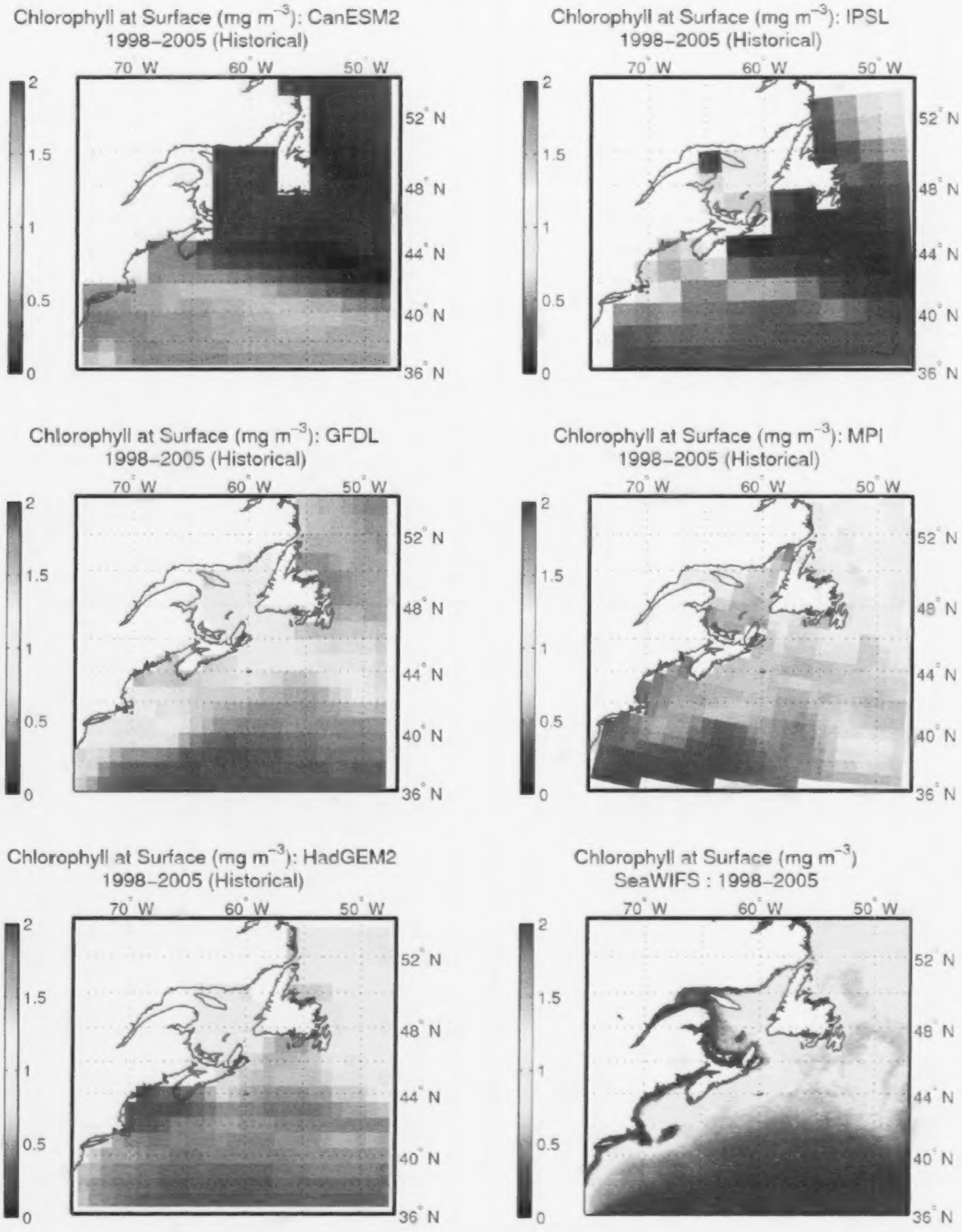
Chlorophyll at Surface (mg m^{-3}): CanESM2
1998–2005 (Historical)
Chlorophyll at Surface (mg m^{-3}): IPSL
1998–2005 (Historical)
Chlorophyll at Surface (mg m^{-3}): GFDL
1998–2005 (Historical)
Chlorophyll at Surface (mg m^{-3}): MPI
1998–2005 (Historical)
Chlorophyll at Surface (mg m^{-3}): HadGEM2
1998–2005 (Historical)
Chlorophyll at Surface (mg m^{-3})
SeaWIFS : 1998–2005
70° W
60° W
50° W
52° N
48° N
44° N
40° N
36° N
2
1.5
1
0.5
0

Figure 77. Mean simulated Chl a concentrations and Chlorophyll data from SeaWiFS in the AtlNW region for the historical period (1998-2005).

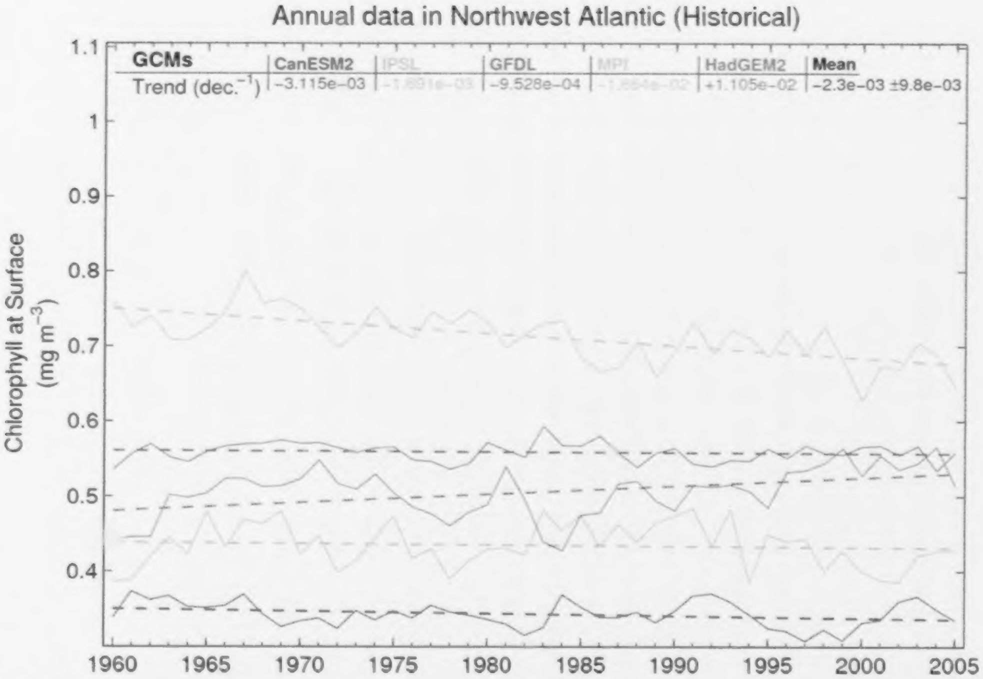

Figure 78. Average Chl a concentration trends (mg m^{-3}/decade) at the surface in the AtlNW region for the historical period (1960-2005).

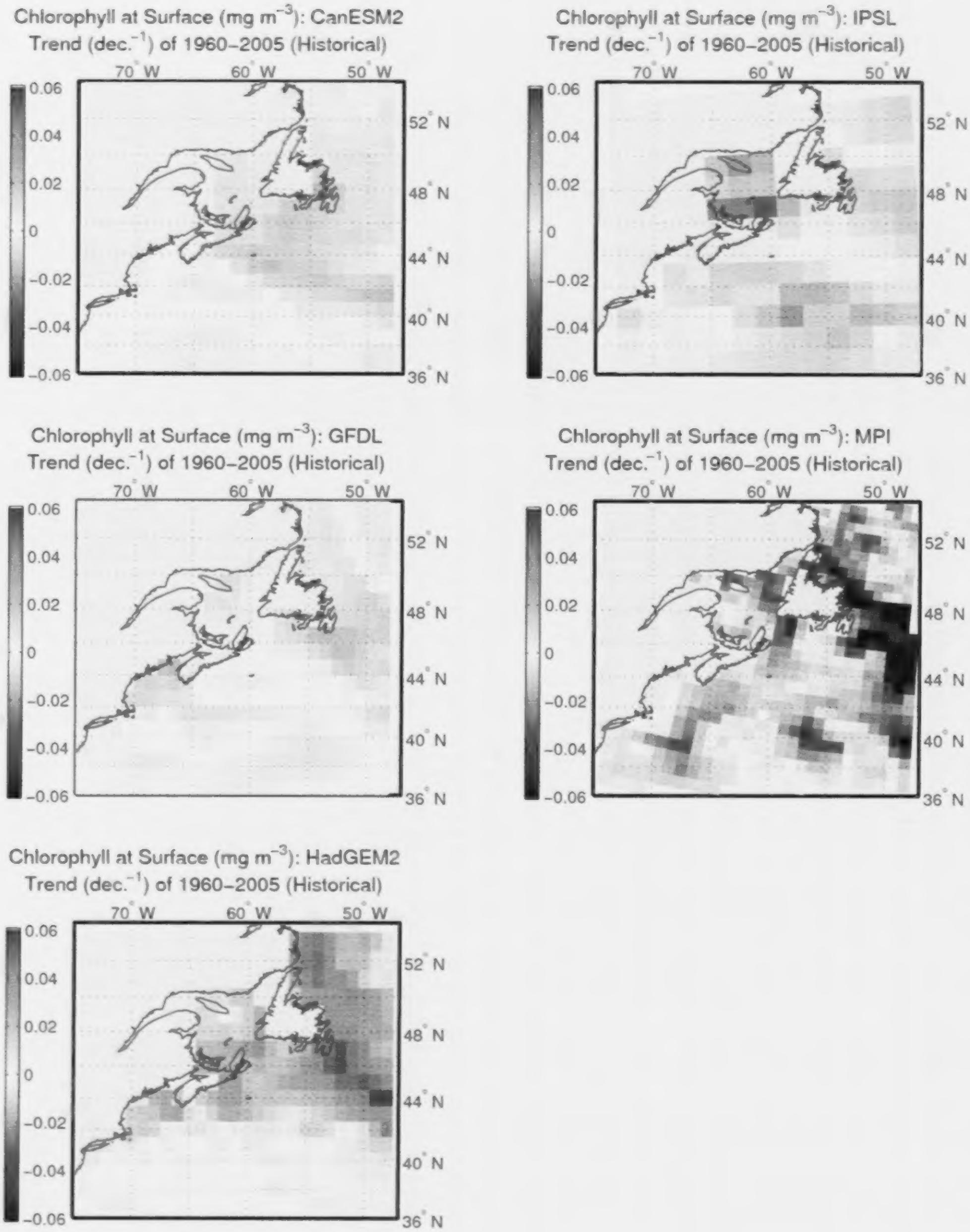

Chlorophyll at Surface (mg m^{-3}): CanESM2 Trend (dec.$^{-1}$) of 1960–2005 (Historical)

Chlorophyll at Surface (mg m^{-3}): IPSL Trend (dec.$^{-1}$) of 1960–2005 (Historical)

Chlorophyll at Surface (mg m^{-3}): GFDL Trend (dec.$^{-1}$) of 1960–2005 (Historical)

Chlorophyll at Surface (mg m^{-3}): MPI Trend (dec.$^{-1}$) of 1960–2005 (Historical)

Chlorophyll at Surface (mg m^{-3}): HadGEM2 Trend (dec.$^{-1}$) of 1960–2005 (Historical)

Figure 79. Surface Chl a concentration trends (mg m^{-3}/decade) at each grid cell in the AtlNW region for the SeaWiFS period (1960-2005).

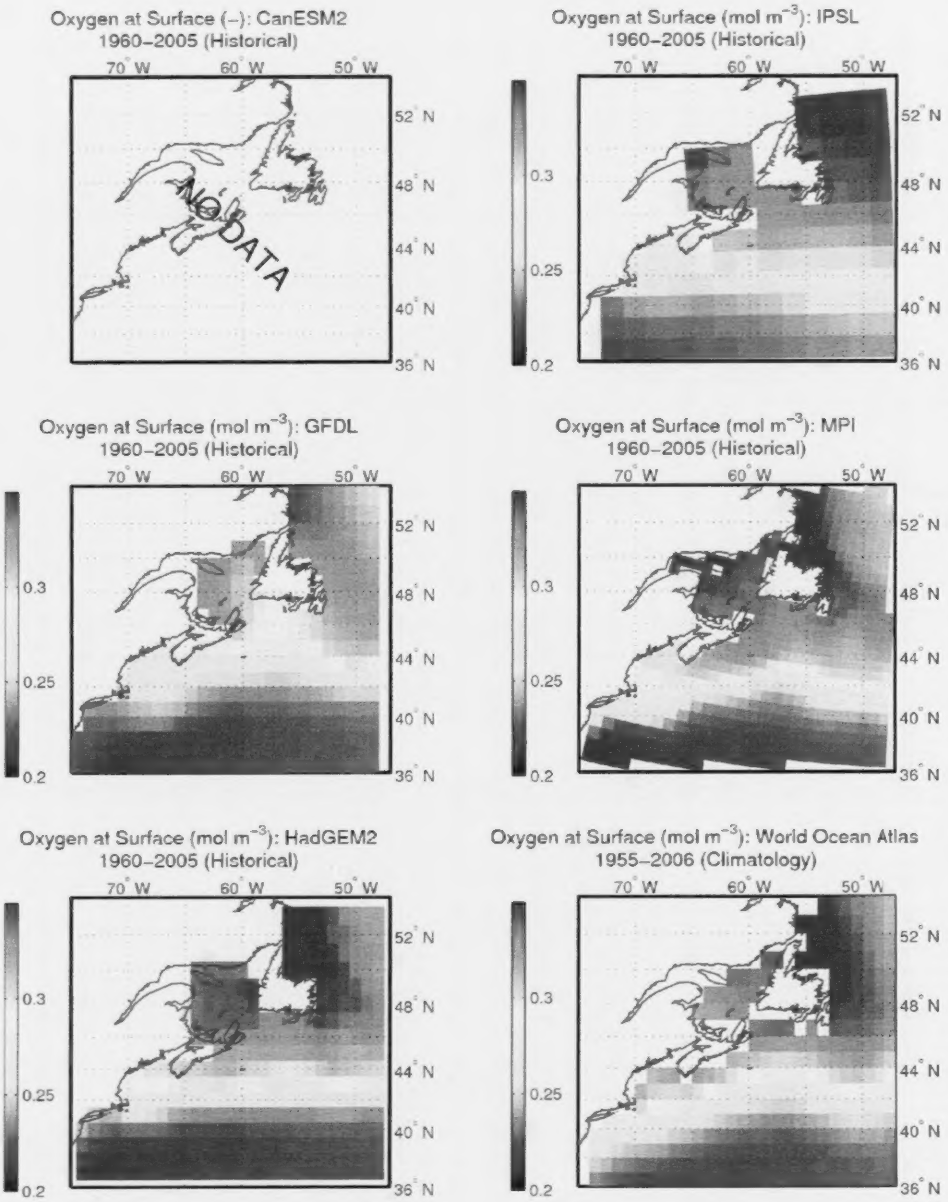
Oxygen at Surface (–): CanESM2
1960–2005 (Historical)
NO DATA
Oxygen at Surface (mol m−3): IPSL
1960–2005 (Historical)
Oxygen at Surface (mol m−3): GFDL
1960–2005 (Historical)
Oxygen at Surface (mol m−3): MPI
1960–2005 (Historical)
Oxygen at Surface (mol m−3): HadGEM2
1960–2005 (Historical)
Oxygen at Surface (mol m−3): World Ocean Atlas
1955–2006 (Climatology)
70° W
60° W
50° W
52° N
48° N
44° N
40° N
36° N
0.3
0.25
0.2

Figure 80. Mean simulated dissolved oxygen concentration at the surface in the AtlNW region for the historical period (1960-2005) and dissolved oxygen concentration at the surface from the World Ocean Atlas (Garcia et al., 2010a).

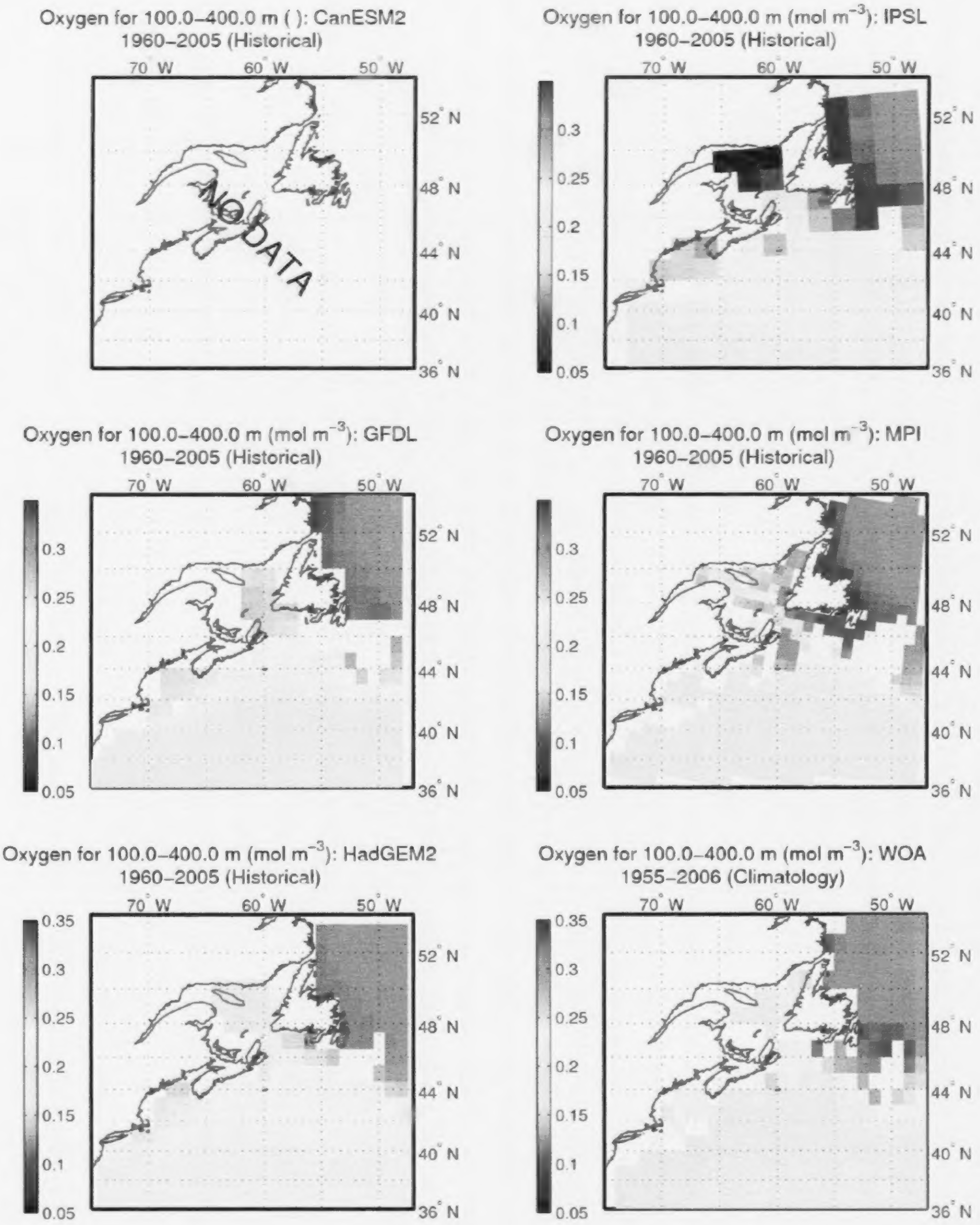
Oxygen for 100.0–400.0 m ( ): CanESM2
1960–2005 (Historical)

Oxygen for 100.0–400.0 m (mol m^{-3}): IPSL
1960–2005 (Historical)

Oxygen for 100.0–400.0 m (mol m^{-3}): GFDL
1960–2005 (Historical)

Oxygen for 100.0–400.0 m (mol m^{-3}): MPI
1960–2005 (Historical)

Oxygen for 100.0–400.0 m (mol m^{-3}): HadGEM2
1960–2005 (Historical)

Oxygen for 100.0–400.0 m (mol m^{-3}): WOA
1955–2006 (Climatology)

Figure 81. Mean simulated dissolved oxygen concentration at 100-400 m in the AtlNW region for the historical period (1960-2005) and dissolved oxygen concentration at 100-400 m from the World Ocean Atlas (Garcia et al., 2010a).

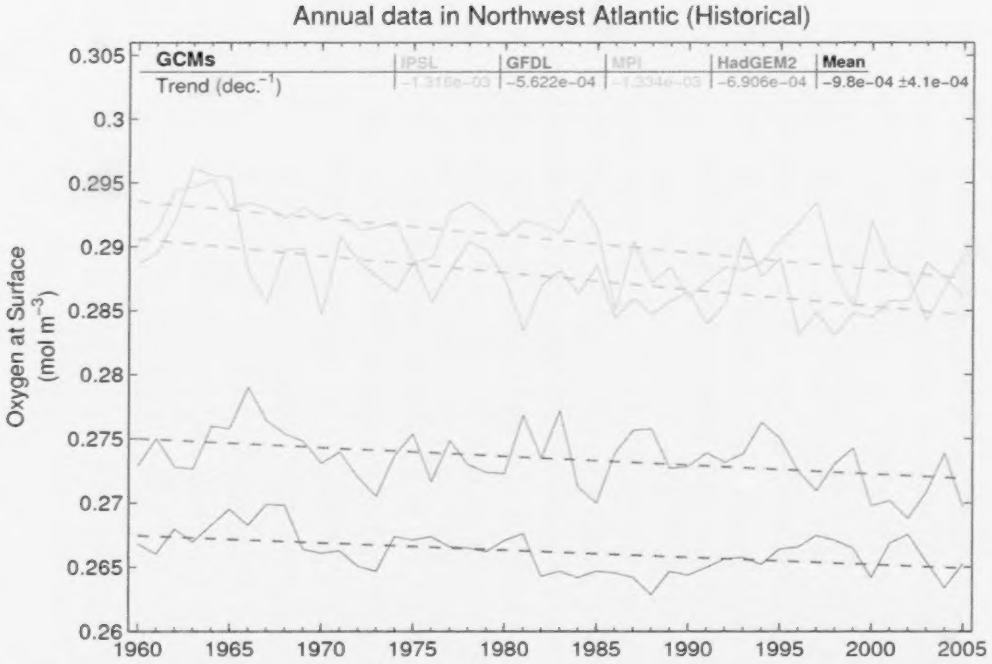

Figure 82. Average oxygen concentration trends (mol m^{-3}/decade) at the surface in the AtlNW region for the historical period (1960-2005).

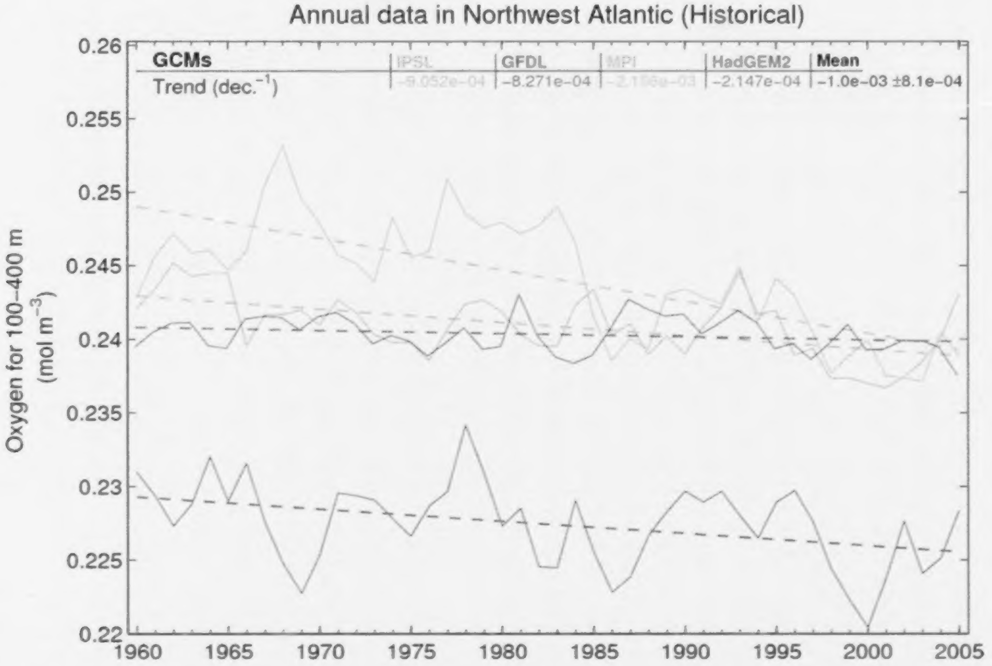

Figure 83. Average oxygen concentration trends (mol m^{-3}/decade) at 100-400 m in the AtlNW region for the historical period (1960-2005).

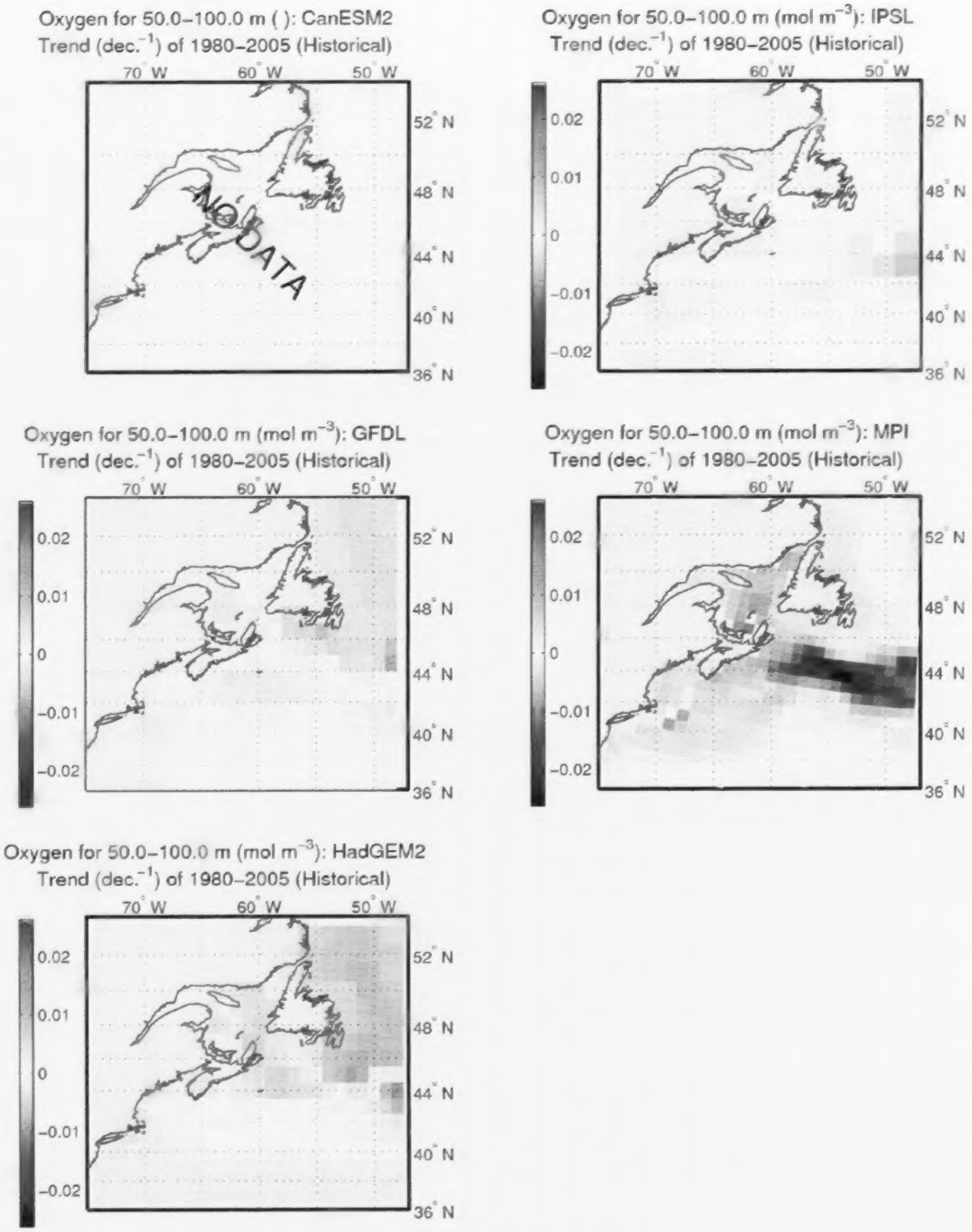
Oxygen for 50.0–100.0 m ( ): CanESM2 Trend (dec.$^{-1}$) of 1980–2005 (Historical)

Oxygen for 50.0–100.0 m (mol m^{-3}): IPSL Trend (dec.$^{-1}$) of 1980–2005 (Historical)

Oxygen for 50.0–100.0 m (mol m^{-3}): GFDL Trend (dec.$^{-1}$) of 1980–2005 (Historical)

Oxygen for 50.0–100.0 m (mol m^{-3}): MPI Trend (dec.$^{-1}$) of 1980–2005 (Historical)

Oxygen for 50.0–100.0 m (mol m^{-3}): HadGEM2 Trend (dec.$^{-1}$) of 1980–2005 (Historical)

70° W
60° W
50° W
52° N
48° N
44° N
40° N
36° N
NO DATA
0.02
0.01
0
−0.01
−0.02

Figure 84. Surface oxygen concentration trends (mol m^{-3}/decade) at each grid cell in the AtlNW region for the 1980-2005 period.

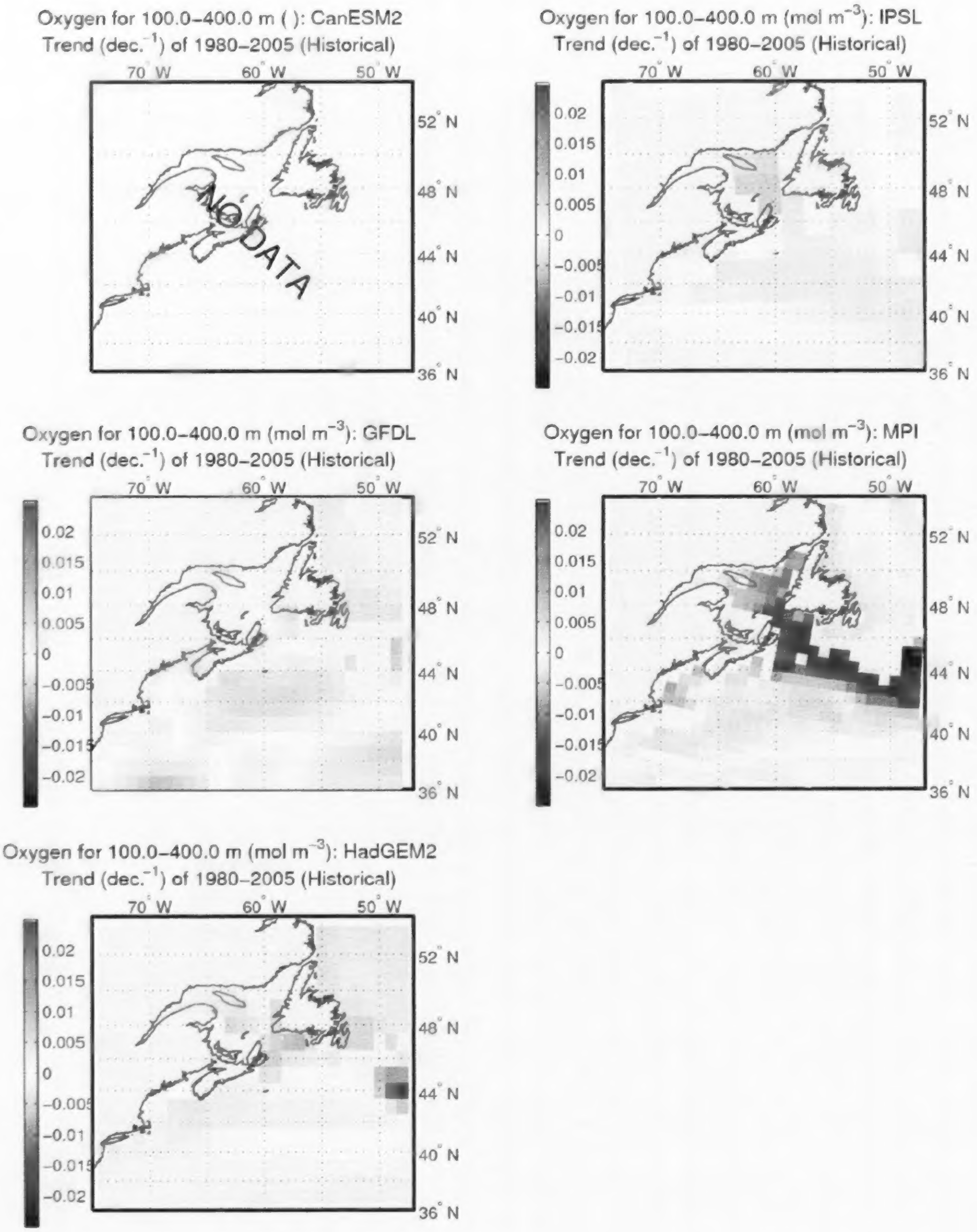
Oxygen for 100.0–400.0 m ( ): CanESM2
Trend (dec.$^{-1}$) of 1980–2005 (Historical)
NO DATA
Oxygen for 100.0–400.0 m (mol m^{-3}): IPSL
Trend (dec.$^{-1}$) of 1980–2005 (Historical)
Oxygen for 100.0–400.0 m (mol m^{-3}): GFDL
Trend (dec.$^{-1}$) of 1980–2005 (Historical)
Oxygen for 100.0–400.0 m (mol m^{-3}): MPI
Trend (dec.$^{-1}$) of 1980–2005 (Historical)
Oxygen for 100.0–400.0 m (mol m^{-3}): HadGEM2
Trend (dec.$^{-1}$) of 1980–2005 (Historical)
70° W
60° W
50° W
52° N
48° N
44° N
40° N
36° N
0.02
0.015
0.01
0.005
0
-0.005
-0.01
-0.015
-0.02

Figure 85. Oxygen concentration trends (mol m^{-3}/decade) at 100-400 m at each grid cell in the AtlNW region for the 1980-2005 period.

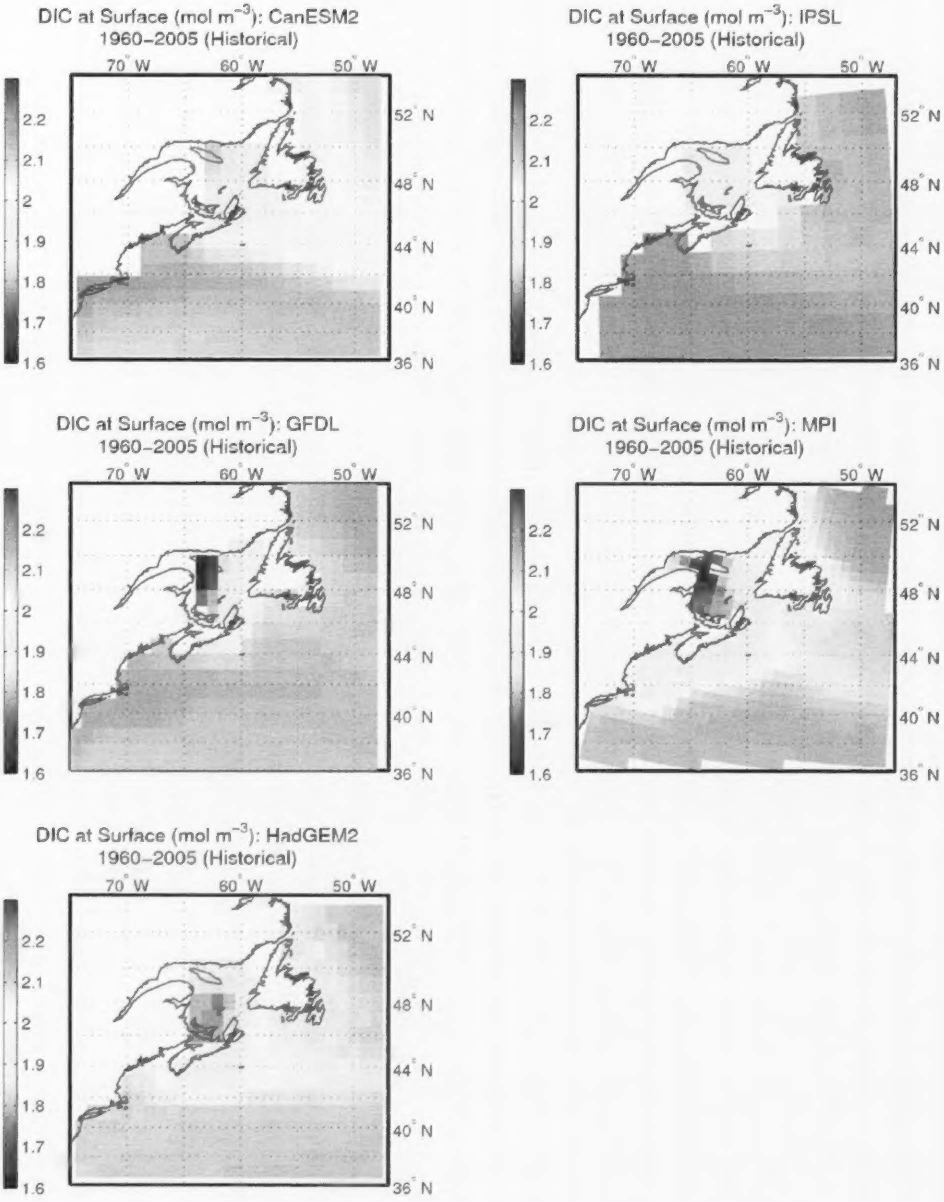
DIC at Surface (mol m^{-3}): CanESM2
1960–2005 (Historical)
DIC at Surface (mol m^{-3}): IPSL
1960–2005 (Historical)
DIC at Surface (mol m^{-3}): GFDL
1960–2005 (Historical)
DIC at Surface (mol m^{-3}): MPI
1960–2005 (Historical)
DIC at Surface (mol m^{-3}): HadGEM2
1960–2005 (Historical)
70° W
60° W
50° W
52° N
48° N
44° N
40° N
36° N
2.2
2.1
2
1.9
1.8
1.7
1.6

Figure 86. Mean simulated dissolved inorganic carbon concentration in the AtlNW region for the historical period (1960-2005).

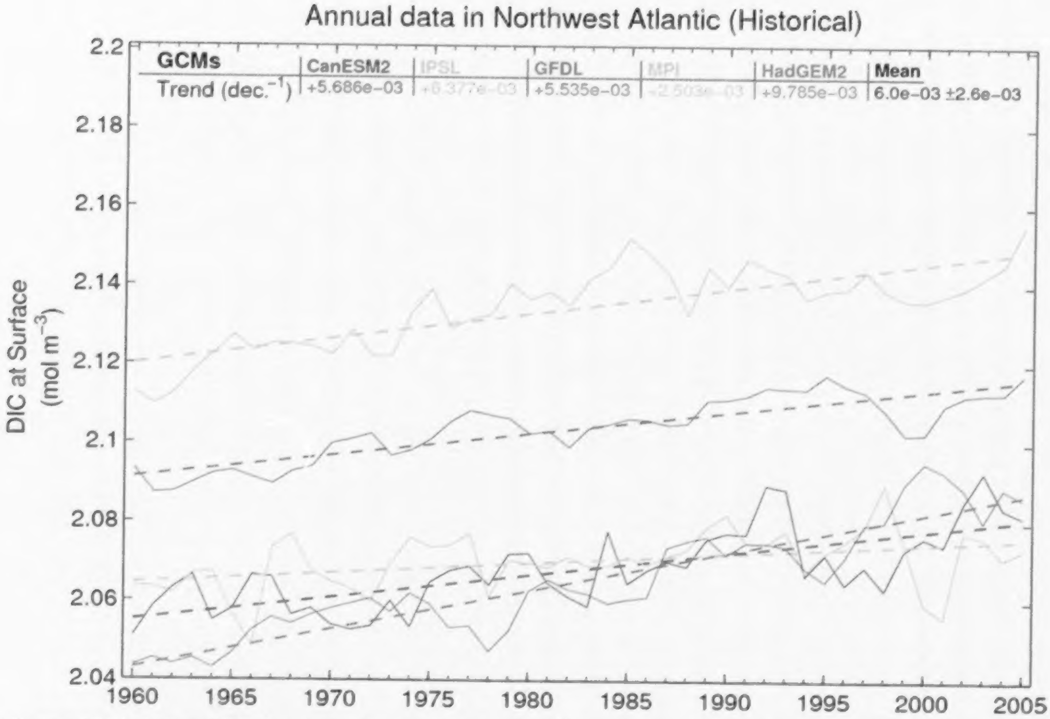

Figure 87. Average DIC concentration trends (mol m^{-3}/decade) at the surface in the AtlNW region for the historical period (1960-2005).

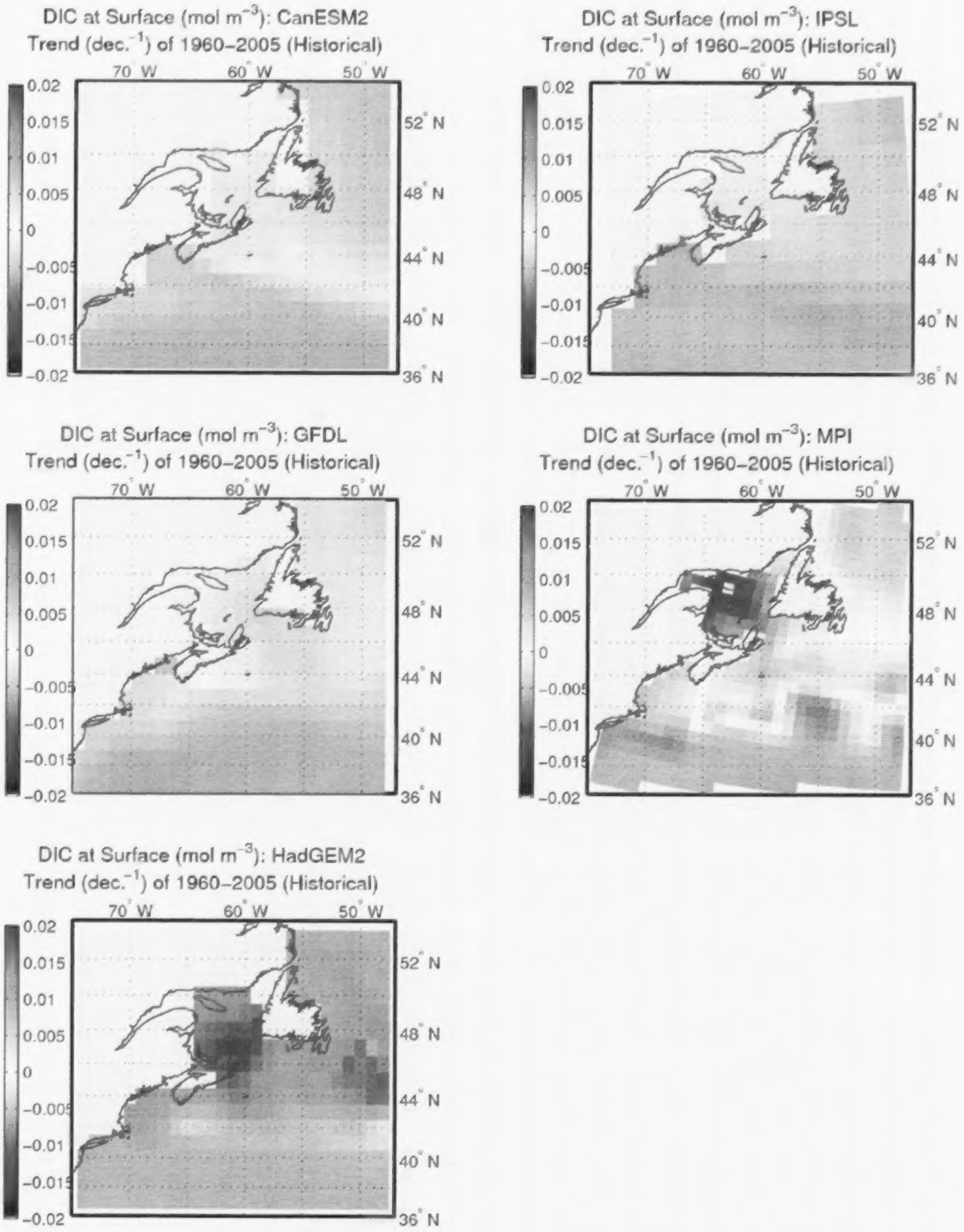
DIC at Surface (mol m^{-3}): CanESM2
Trend (dec.$^{-1}$) of 1960–2005 (Historical)
DIC at Surface (mol m^{-3}): IPSL
Trend (dec.$^{-1}$) of 1960–2005 (Historical)
DIC at Surface (mol m^{-3}): GFDL
Trend (dec.$^{-1}$) of 1960–2005 (Historical)
DIC at Surface (mol m^{-3}): MPI
Trend (dec.$^{-1}$) of 1960–2005 (Historical)
DIC at Surface (mol m^{-3}): HadGEM2
Trend (dec.$^{-1}$) of 1960–2005 (Historical)
70° W
60° W
50° W
52° N
48° N
44° N
40° N
36° N
0.02
0.015
0.01
0.005
0
−0.005
−0.01
−0.015
−0.02

Figure 88. Dissolved inorganic carbon concentration trends (mol m^{-3}/decade) at the surface at each grid cell in the AtlNW region for the historical period (1960-2005).

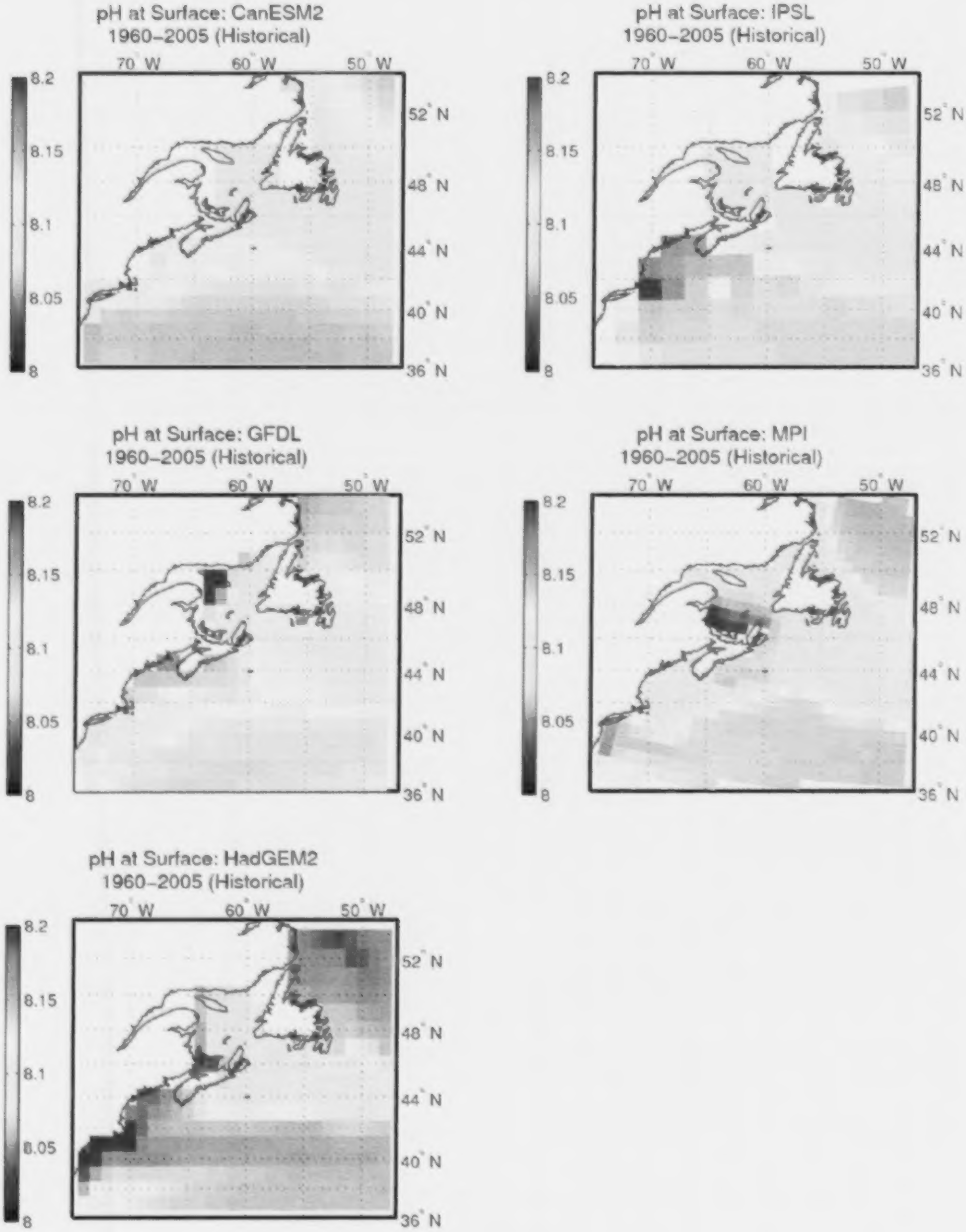
pH at Surface: CanESM2
1960–2005 (Historical)
pH at Surface: IPSL
1960–2005 (Historical)
pH at Surface: GFDL
1960–2005 (Historical)
pH at Surface: MPI
1960–2005 (Historical)
pH at Surface: HadGEM2
1960–2005 (Historical)
70° W
60° W
50° W
52° N
48° N
44° N
40° N
36° N
8.2
8.15
8.1
8.05
8

Figure 89. Mean simulated surface pH in the AtlNW region for the historical period (1960-2005).

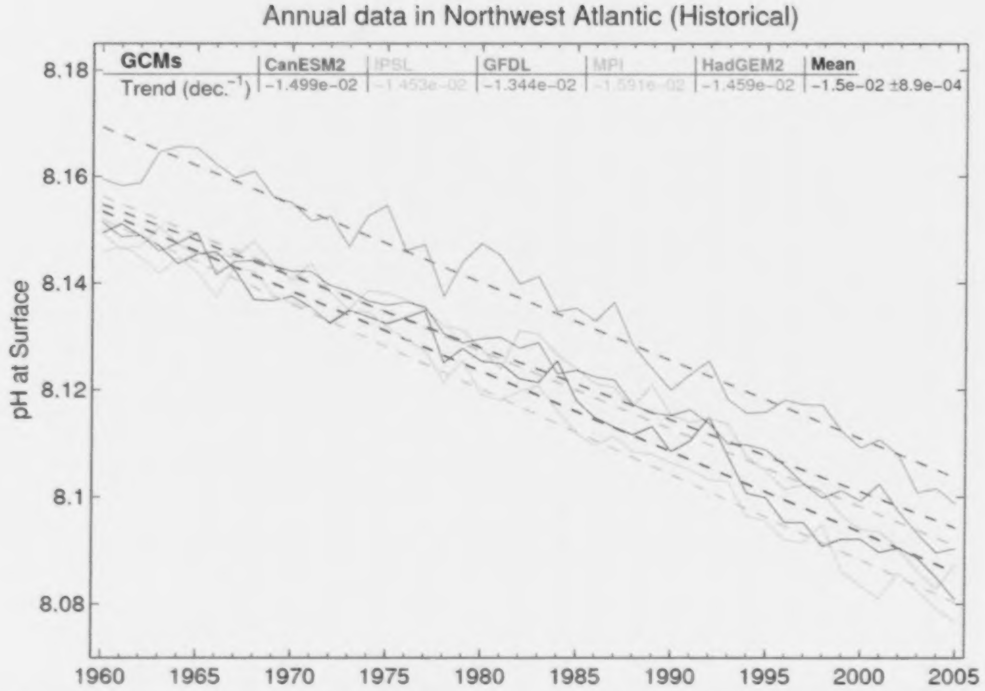

Figure 90. Average pH trends (mol m^{-3}/decade) at the surface in the AtlNW region for the historical period (1960-2005).

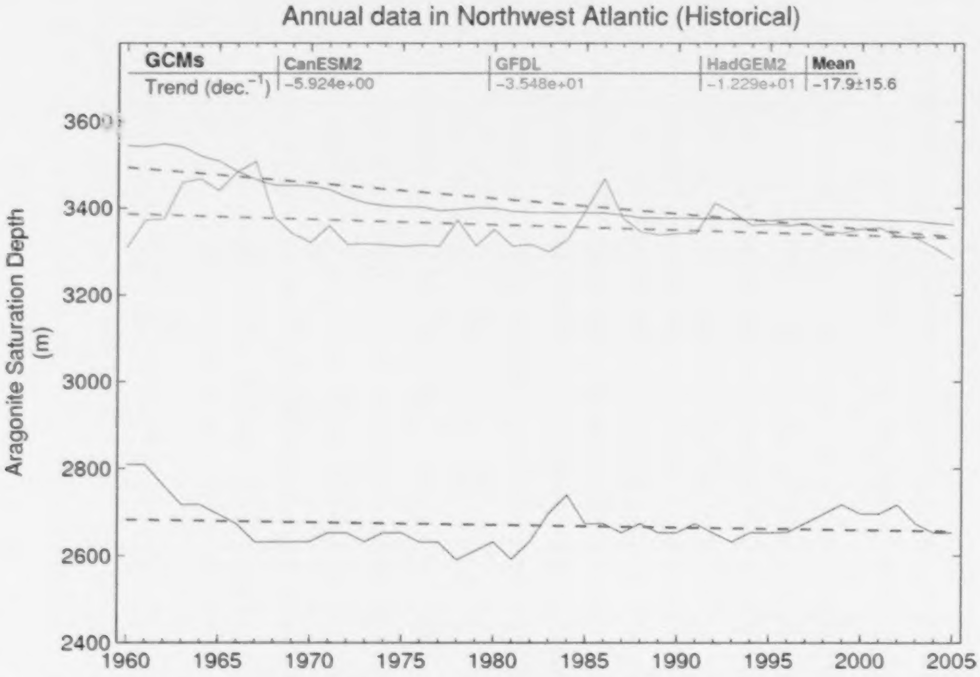

Figure 91. Average aragonite saturation horizon depth trends (m/decade) in the AtlNW region for the historical period (1960-2005).

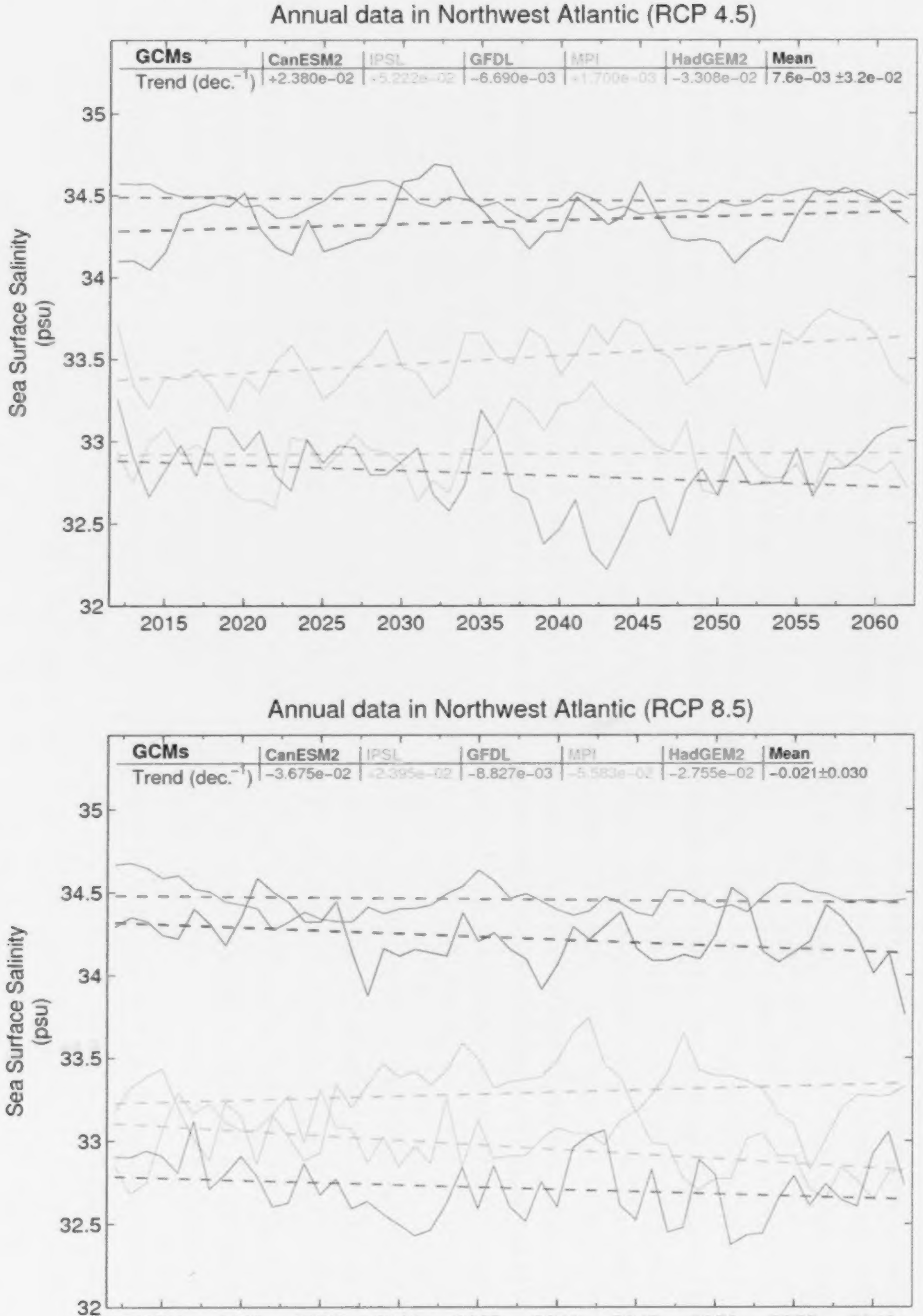

Figure 92. Future sea surface salinity trends (per decade) in the AtlNW region for the 2012-2062 period for RCPs 4.5 and 8.5.

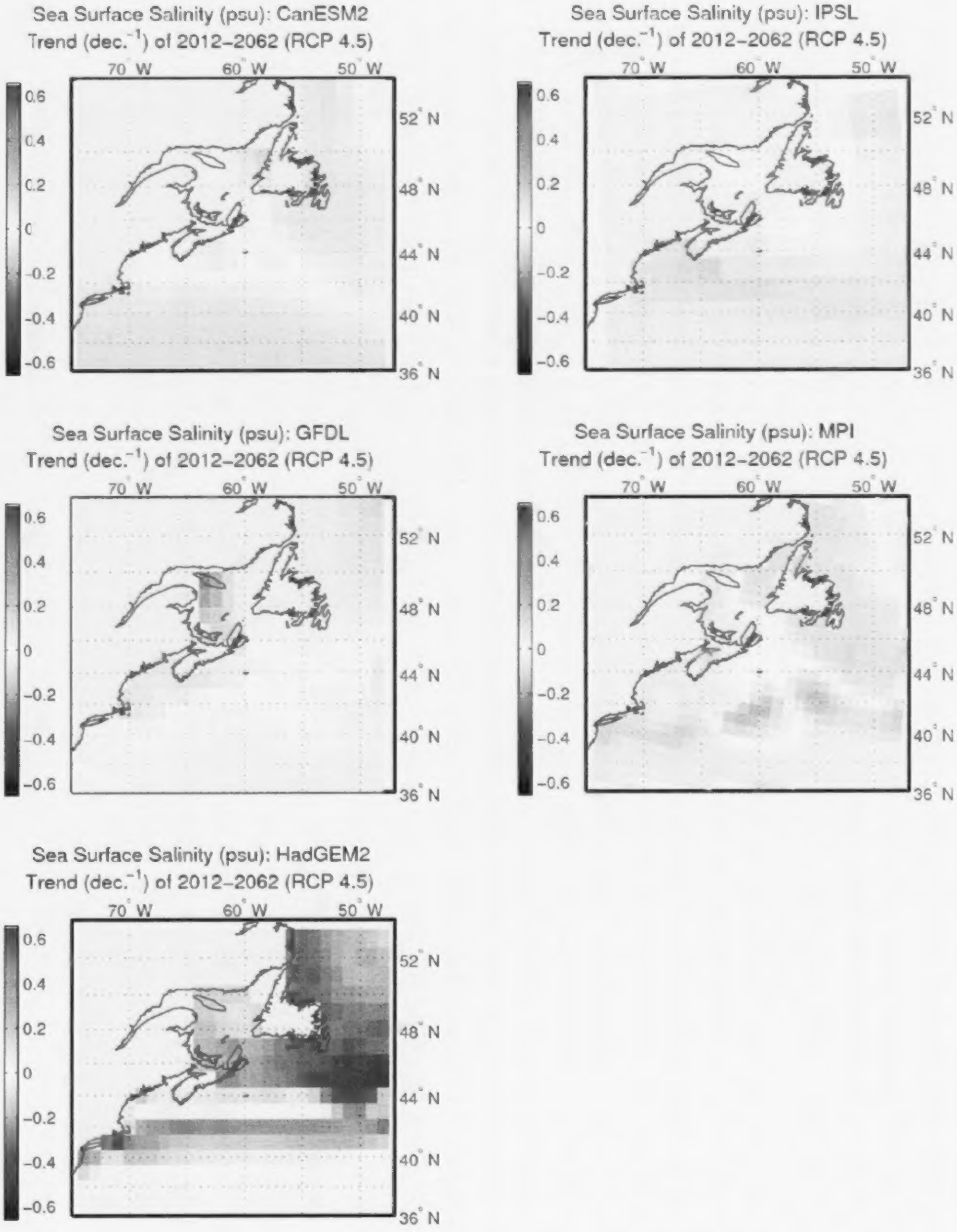
Sea Surface Salinity (psu): CanESM2
Trend (dec.$^{-1}$) of 2012-2062 (RCP 4.5)
Sea Surface Salinity (psu): IPSL
Trend (dec.$^{-1}$) of 2012-2062 (RCP 4.5)
Sea Surface Salinity (psu): GFDL
Trend (dec.$^{-1}$) of 2012-2062 (RCP 4.5)
Sea Surface Salinity (psu): MPI
Trend (dec.$^{-1}$) of 2012-2062 (RCP 4.5)
Sea Surface Salinity (psu): HadGEM2
Trend (dec.$^{-1}$) of 2012-2062 (RCP 4.5)
70° W
60° W
50° W
52° N
48° N
44° N
40° N
36° N
0.6
0.4
0.2
0
-0.2
-0.4
-0.6

Figure 93. Future sea surface salinity trends (per decade) at each grid cell in the AtlNW region for the 2012-2062 period for RCP 4.5.

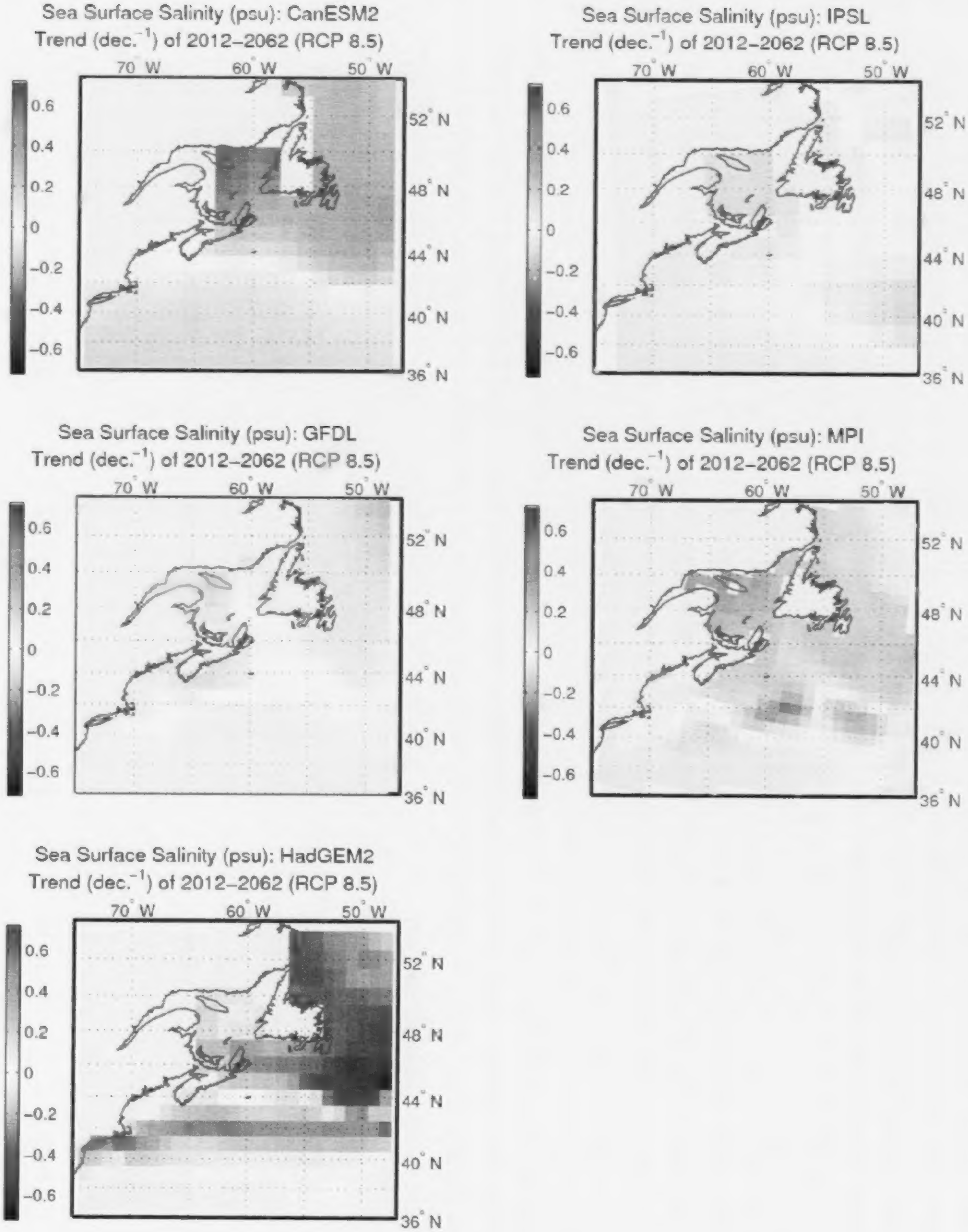
Sea Surface Salinity (psu): CanESM2
Trend (dec.$^{-1}$) of 2012–2062 (RCP 8.5)

Sea Surface Salinity (psu): IPSL
Trend (dec.$^{-1}$) of 2012–2062 (RCP 8.5)

Sea Surface Salinity (psu): GFDL
Trend (dec.$^{-1}$) of 2012–2062 (RCP 8.5)

Sea Surface Salinity (psu): MPI
Trend (dec.$^{-1}$) of 2012–2062 (RCP 8.5)

Sea Surface Salinity (psu): HadGEM2
Trend (dec.$^{-1}$) of 2012–2062 (RCP 8.5)

Figure 94. Future sea surface salinity trends (per decade) at each grid cell in the AtlNW region for the 2012-2062 period for RCP 8.5.

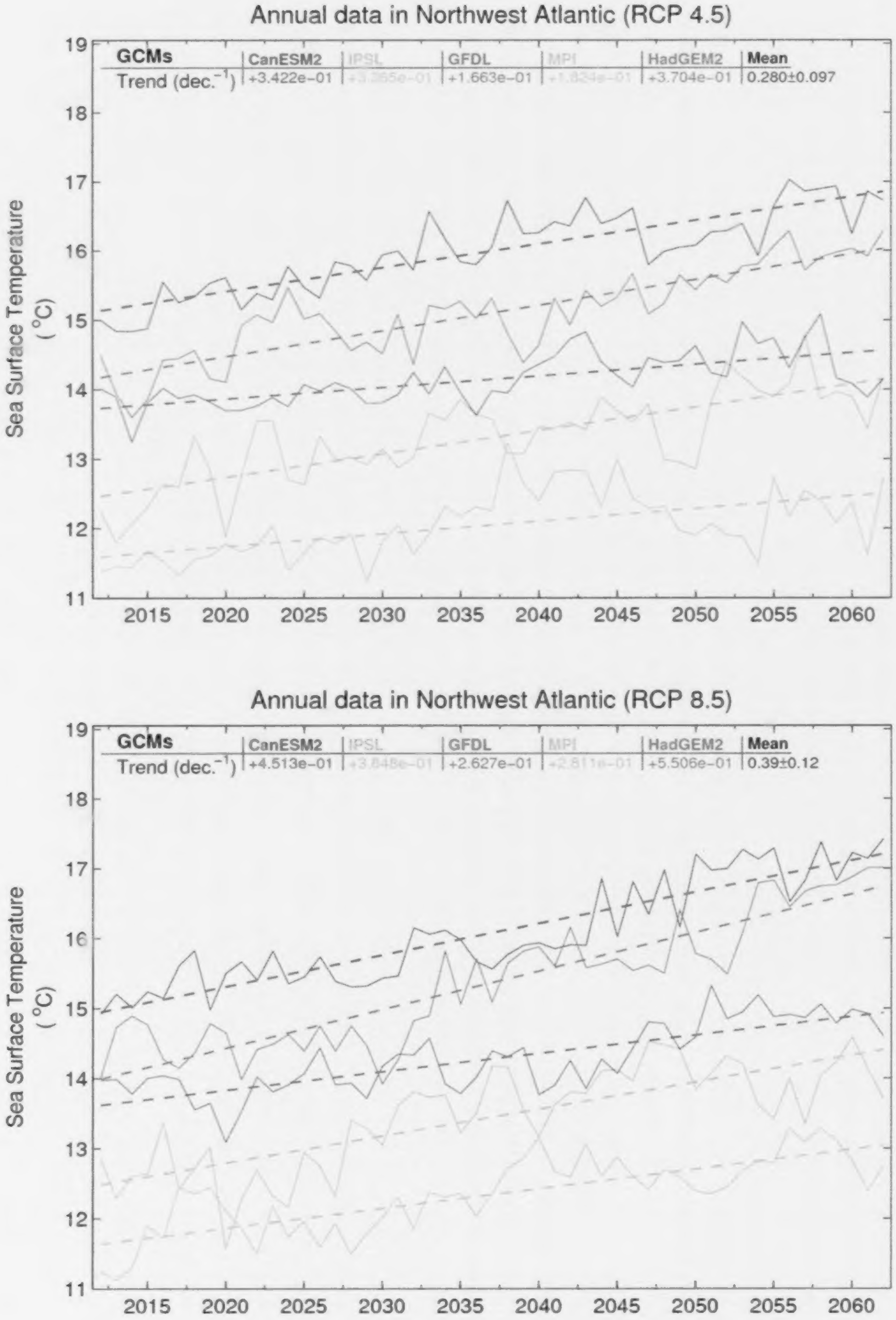

Figure 95. Future sea surface temperature trends (°C/decade) in the AtlNW region for the 2012-2062 period for RCPs 4.5 and 8.5.

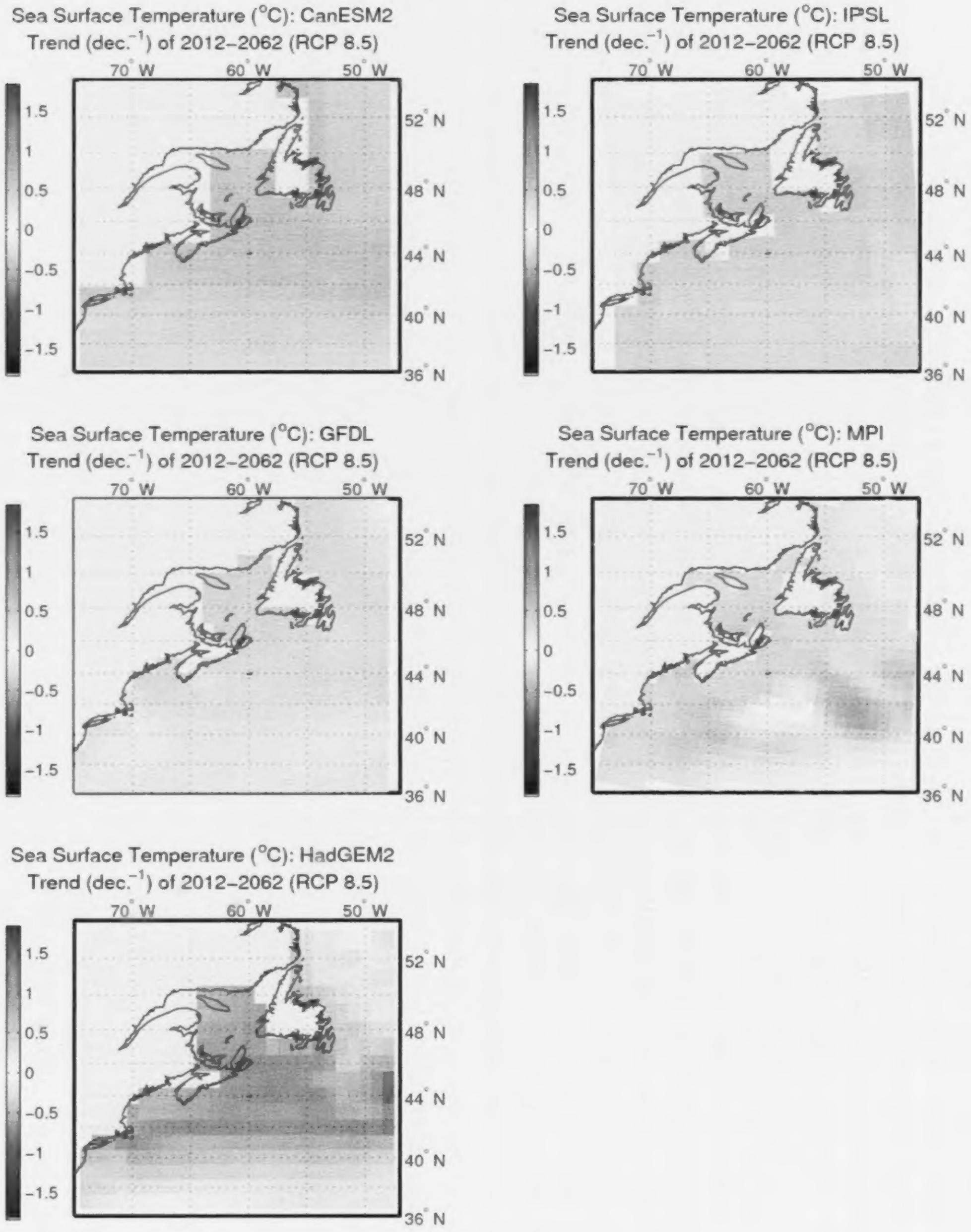

Sea Surface Temperature (°C): CanESM2
Trend ($dec.^{-1}$) of 2012–2062 (RCP 8.5)

Sea Surface Temperature (°C): IPSL
Trend ($dec.^{-1}$) of 2012–2062 (RCP 8.5)

Sea Surface Temperature (°C): GFDL
Trend ($dec.^{-1}$) of 2012–2062 (RCP 8.5)

Sea Surface Temperature (°C): MPI
Trend ($dec.^{-1}$) of 2012–2062 (RCP 8.5)

Sea Surface Temperature (°C): HadGEM2
Trend ($dec.^{-1}$) of 2012–2062 (RCP 8.5)

Figure 96. Future sea surface temperature trends (°C/decade) at each grid cell in the AtlNW region for the 2012-2062 period for RCP 8.5.

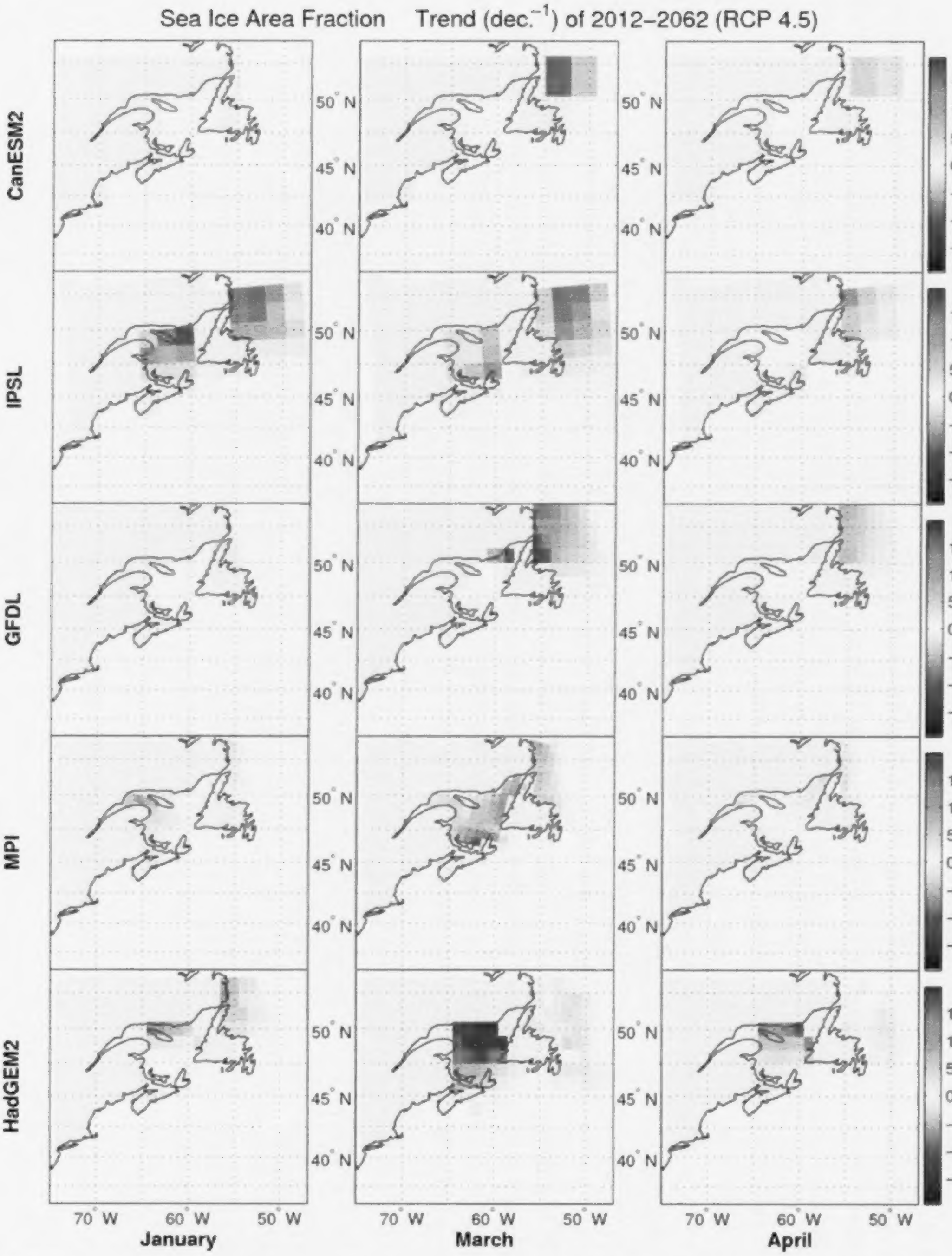
Sea Ice Area Fraction Trend (dec.$^{-1}$) of 2012–2062 (RCP 4.5)
CanESM2
IPSL
GFDL
MPI
HadGEM2
50° N
45° N
40° N
15
10
5
0
−5
−10
−15
70° W
60° W
50° W
January
March
April

Figure 97. Future sea ice concentration trends (%/decade) in the Labrador Sea for the 2012-2062 period for RCP 4.5.

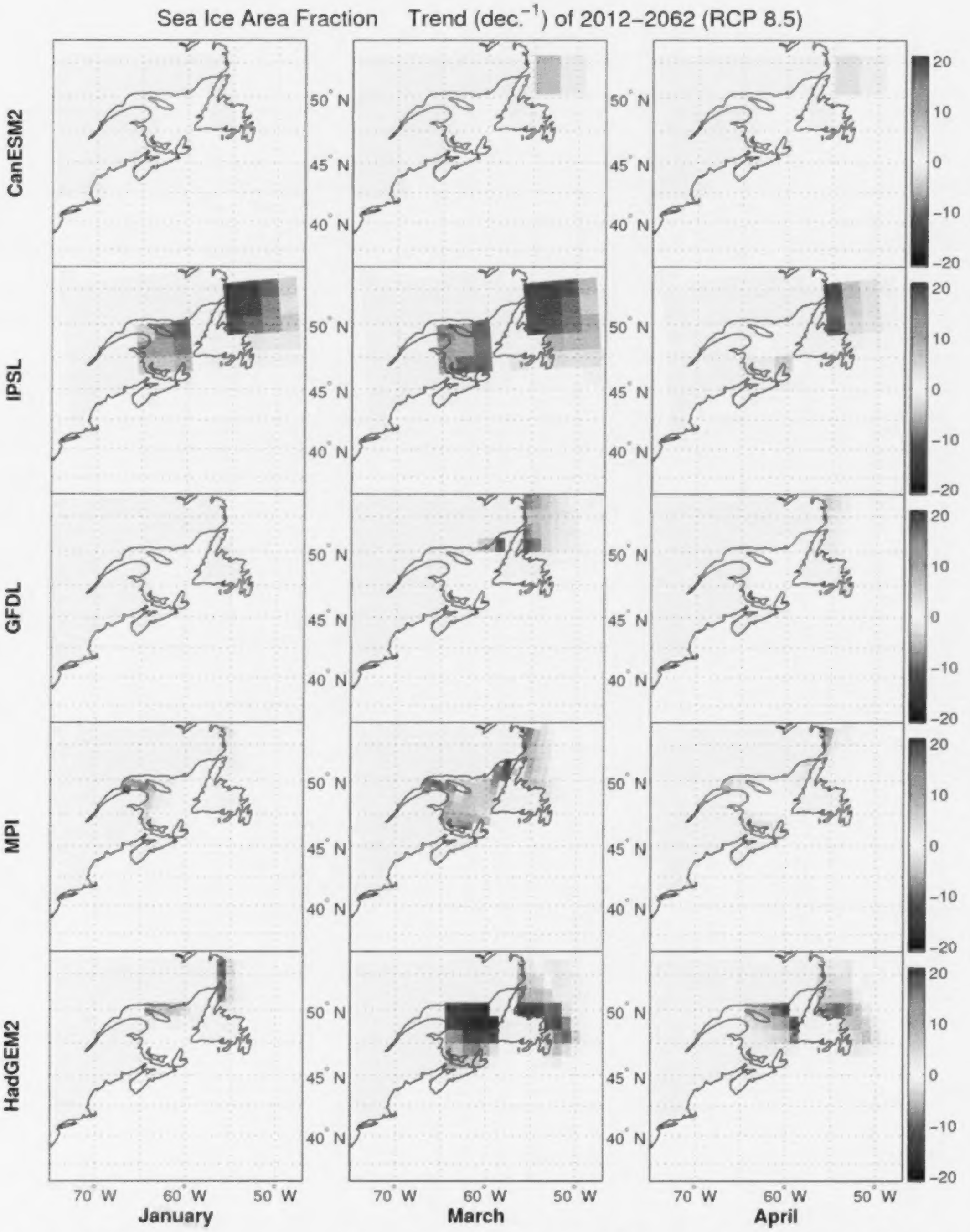
Sea Ice Area Fraction Trend (dec.$^{-1}$) of 2012–2062 (RCP 8.5)
CanESM2
IPSL
GFDL
MPI
HadGEM2
50° N
45° N
40° N
70° W
60° W
50° W
January
March
April
20
10
0
−10
−20

Figure 98. Future sea ice concentration trends (%/decade) in the Labrador Sea for the 2012-2062 period for RCP 8.5.

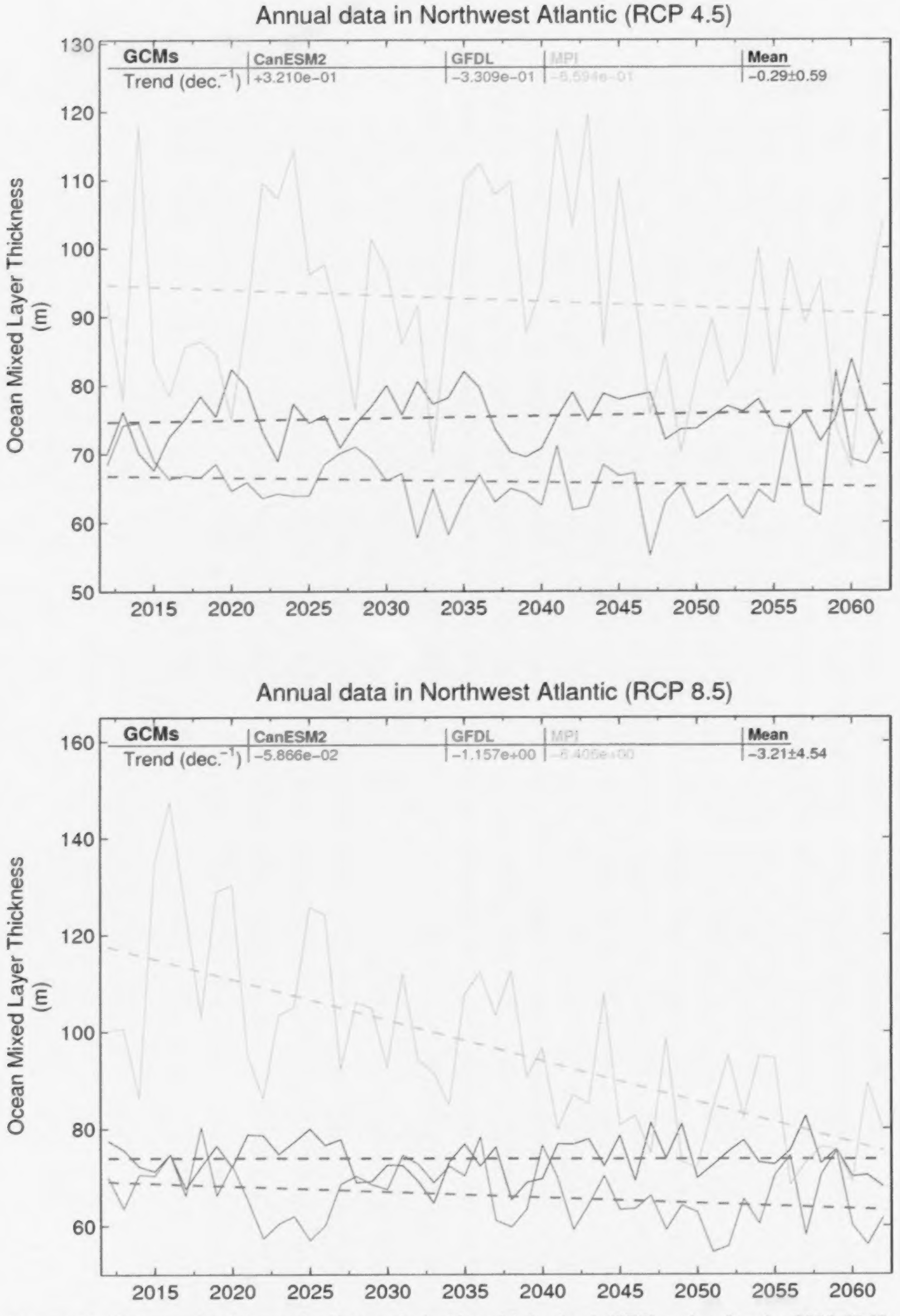

Figure 99. Future mixed layer depth trends (m/decade) in the AtlNW region for the 2012-2062 period for RCPs 4.5 and 8.5.

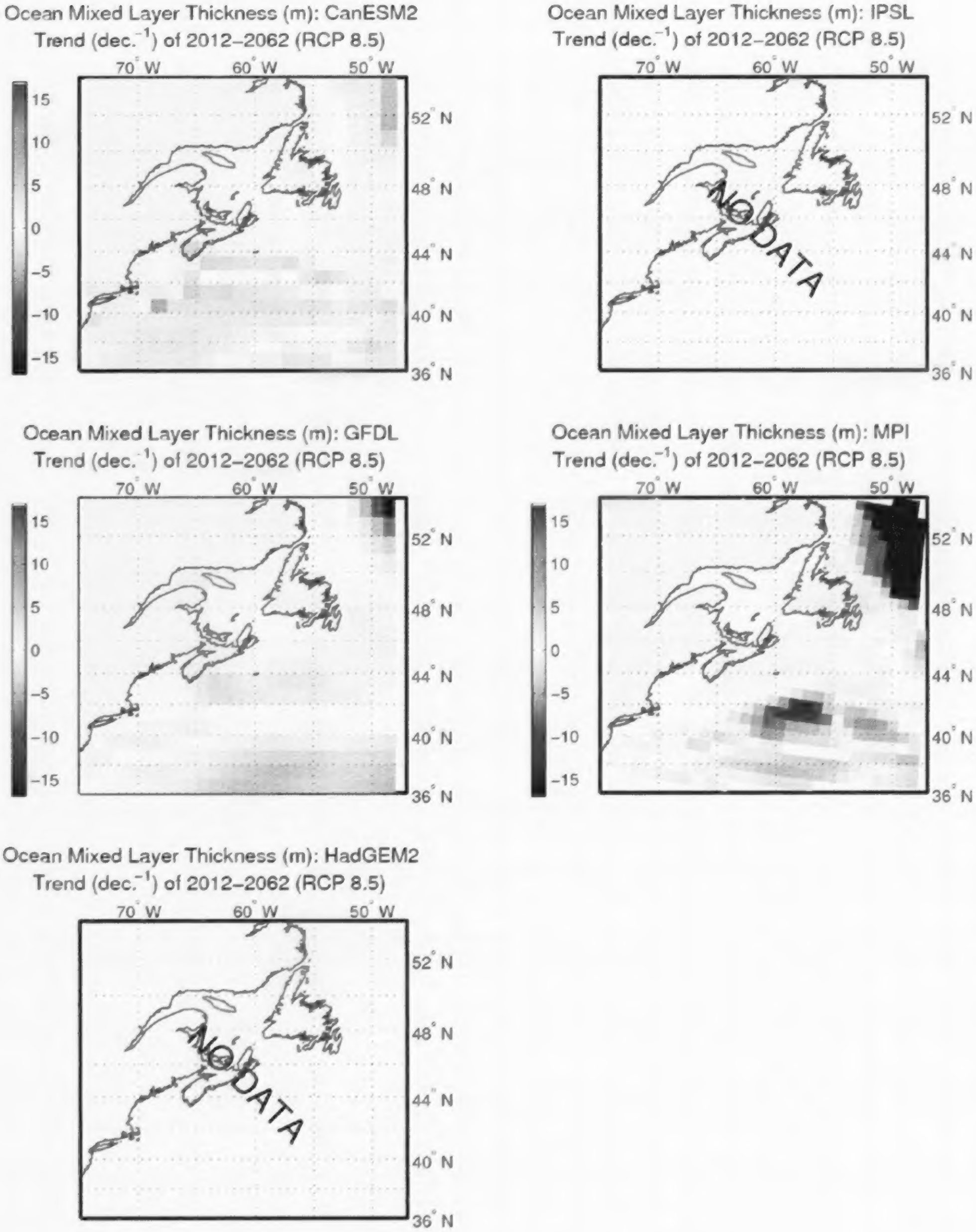

Ocean Mixed Layer Thickness (m): CanESM2 Trend ($dec.^{-1}$) of 2012–2062 (RCP 8.5)

Ocean Mixed Layer Thickness (m): IPSL Trend ($dec.^{-1}$) of 2012–2062 (RCP 8.5)

Ocean Mixed Layer Thickness (m): GFDL Trend ($dec.^{-1}$) of 2012–2062 (RCP 8.5)

Ocean Mixed Layer Thickness (m): MPI Trend ($dec.^{-1}$) of 2012–2062 (RCP 8.5)

Ocean Mixed Layer Thickness (m): HadGEM2 Trend ($dec.^{-1}$) of 2012–2062 (RCP 8.5)

Figure 100. Future mixed layer depth trends (m/decade) per grid cell in the AtlNW region for the 2012-2062 period for RCP 8.5.

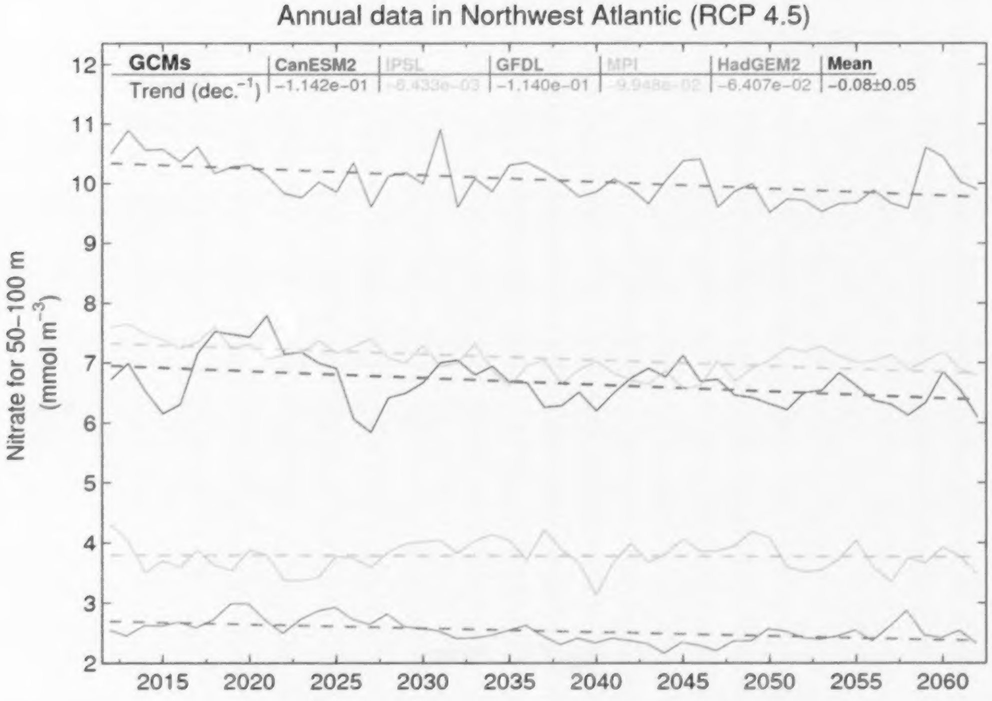

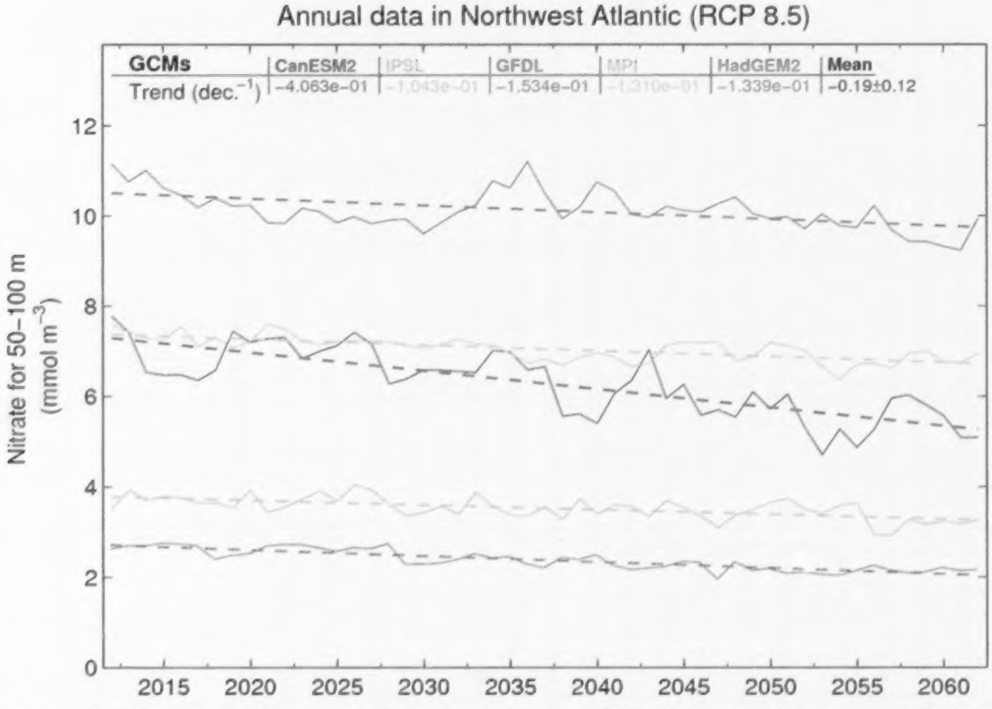

Figure 101. Future nitrate concentration trends (mmol m^{-3}/decade) at 50-100 m in the AltNW region for the 2012-2062 period for RCPs 4.5 and 8.5.

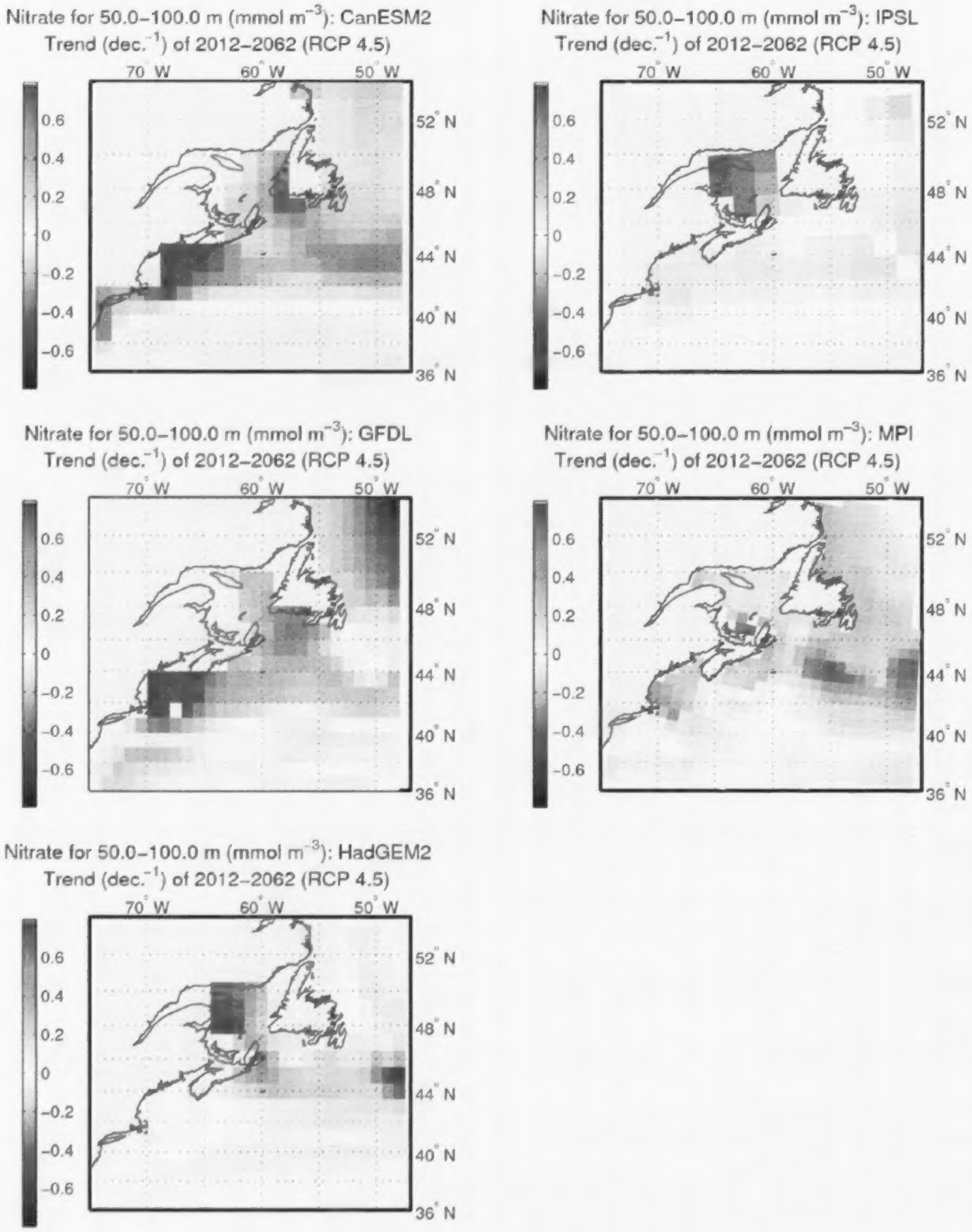

Nitrate for 50.0–100.0 m (mmol m^{-3}): CanESM2 Trend ($dec.^{-1}$) of 2012–2062 (RCP 4.5)

Nitrate for 50.0–100.0 m (mmol m^{-3}): IPSL Trend ($dec.^{-1}$) of 2012–2062 (RCP 4.5)

Nitrate for 50.0–100.0 m (mmol m^{-3}): GFDL Trend ($dec.^{-1}$) of 2012–2062 (RCP 4.5)

Nitrate for 50.0–100.0 m (mmol m^{-3}): MPI Trend ($dec.^{-1}$) of 2012–2062 (RCP 4.5)

Nitrate for 50.0–100.0 m (mmol m^{-3}): HadGEM2 Trend ($dec.^{-1}$) of 2012–2062 (RCP 4.5)

Figure 102. Future nitrate concentration trends (mmol m^{-3}/decade) at 50-100 m at each grid cell in the AtlNW for the 2012-2062 period for RCP 4.5.

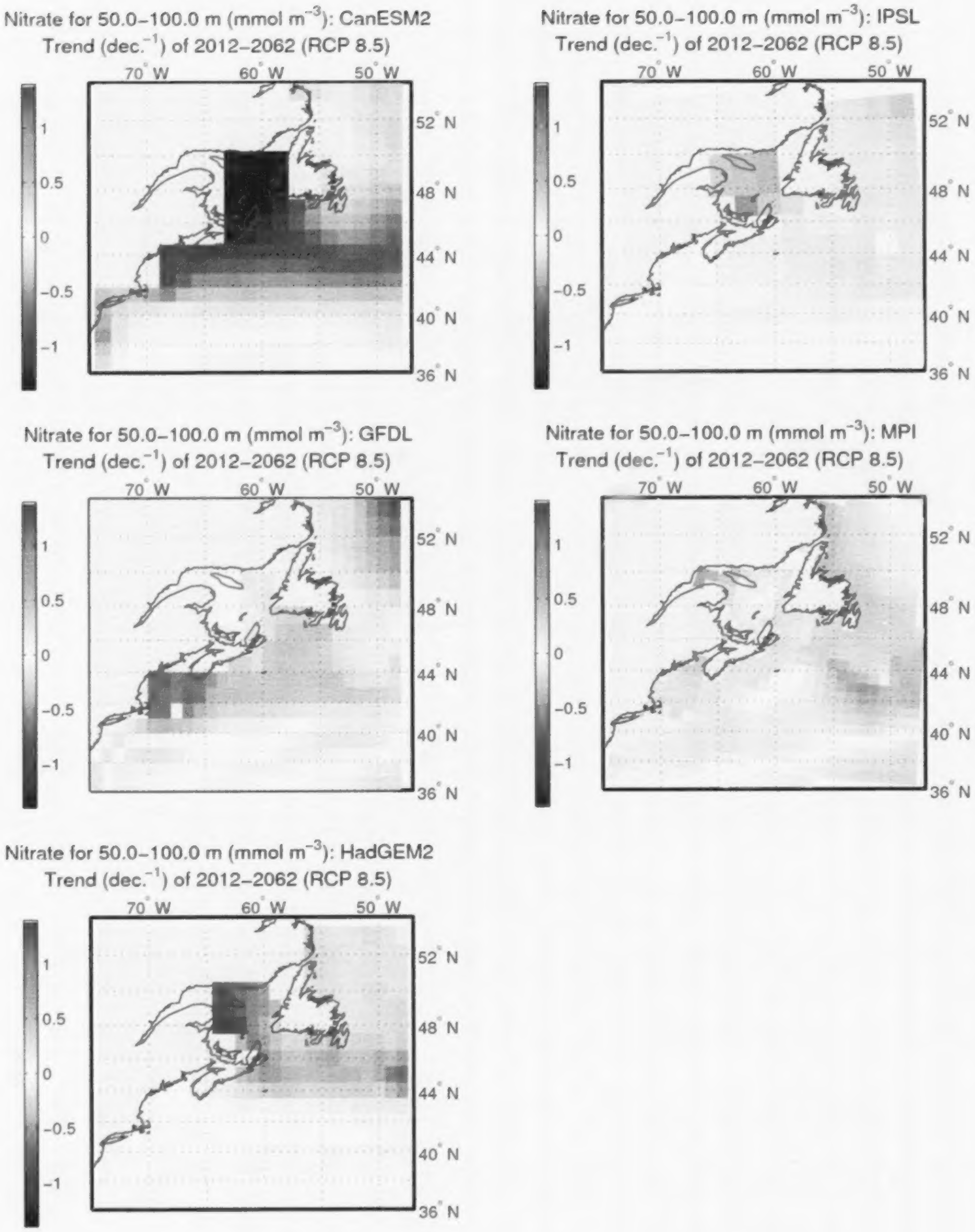

Nitrate for 50.0–100.0 m (mmol m^{-3}): CanESM2
Trend (dec.$^{-1}$) of 2012–2062 (RCP 8.5)

Nitrate for 50.0–100.0 m (mmol m^{-3}): IPSL
Trend (dec.$^{-1}$) of 2012–2062 (RCP 8.5)

Nitrate for 50.0–100.0 m (mmol m^{-3}): GFDL
Trend (dec.$^{-1}$) of 2012–2062 (RCP 8.5)

Nitrate for 50.0–100.0 m (mmol m^{-3}): MPI
Trend (dec.$^{-1}$) of 2012–2062 (RCP 8.5)

Nitrate for 50.0–100.0 m (mmol m^{-3}): HadGEM2
Trend (dec.$^{-1}$) of 2012–2062 (RCP 8.5)

Figure 103. Future nitrate concentration trends (mmol m^{-3}/decade) at 50-100 m at each grid cell in the AtlNW for the 2012-2062 period for RCP 8.5.

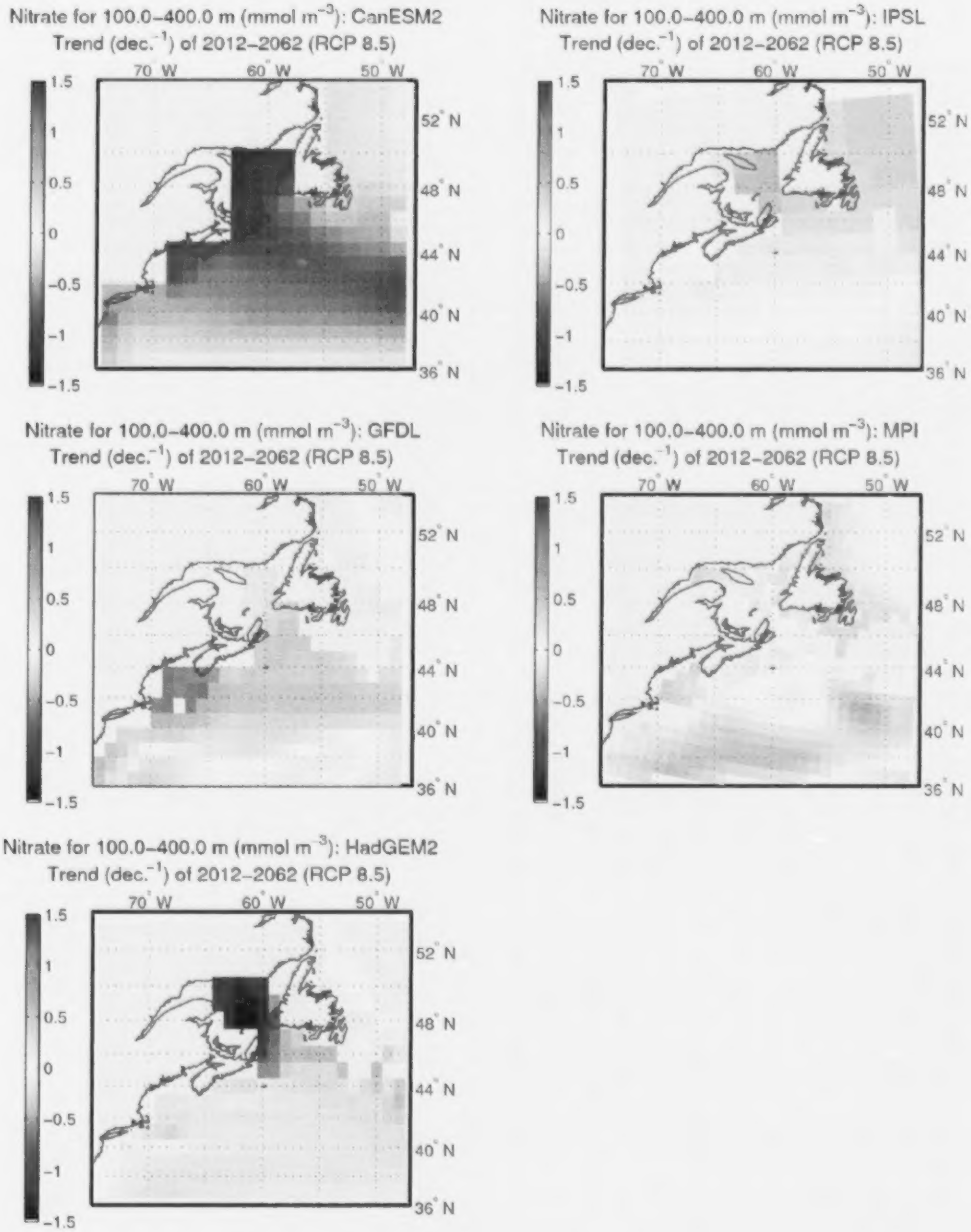
Nitrate for 100.0–400.0 m (mmol m^{-3}): CanESM2
Trend (dec.$^{-1}$) of 2012–2062 (RCP 8.5)

Nitrate for 100.0–400.0 m (mmol m^{-3}): IPSL
Trend (dec.$^{-1}$) of 2012–2062 (RCP 8.5)

Nitrate for 100.0–400.0 m (mmol m^{-3}): GFDL
Trend (dec.$^{-1}$) of 2012–2062 (RCP 8.5)

Nitrate for 100.0–400.0 m (mmol m^{-3}): MPI
Trend (dec.$^{-1}$) of 2012–2062 (RCP 8.5)

Nitrate for 100.0–400.0 m (mmol m^{-3}): HadGEM2
Trend (dec.$^{-1}$) of 2012–2062 (RCP 8.5)

Figure 104. Future nitrate concentration trends (mmol m^{-3}/decade) at 100-400 m at each grid cell in the AtlNW for the 2012-2062 period for RCP 8.5.

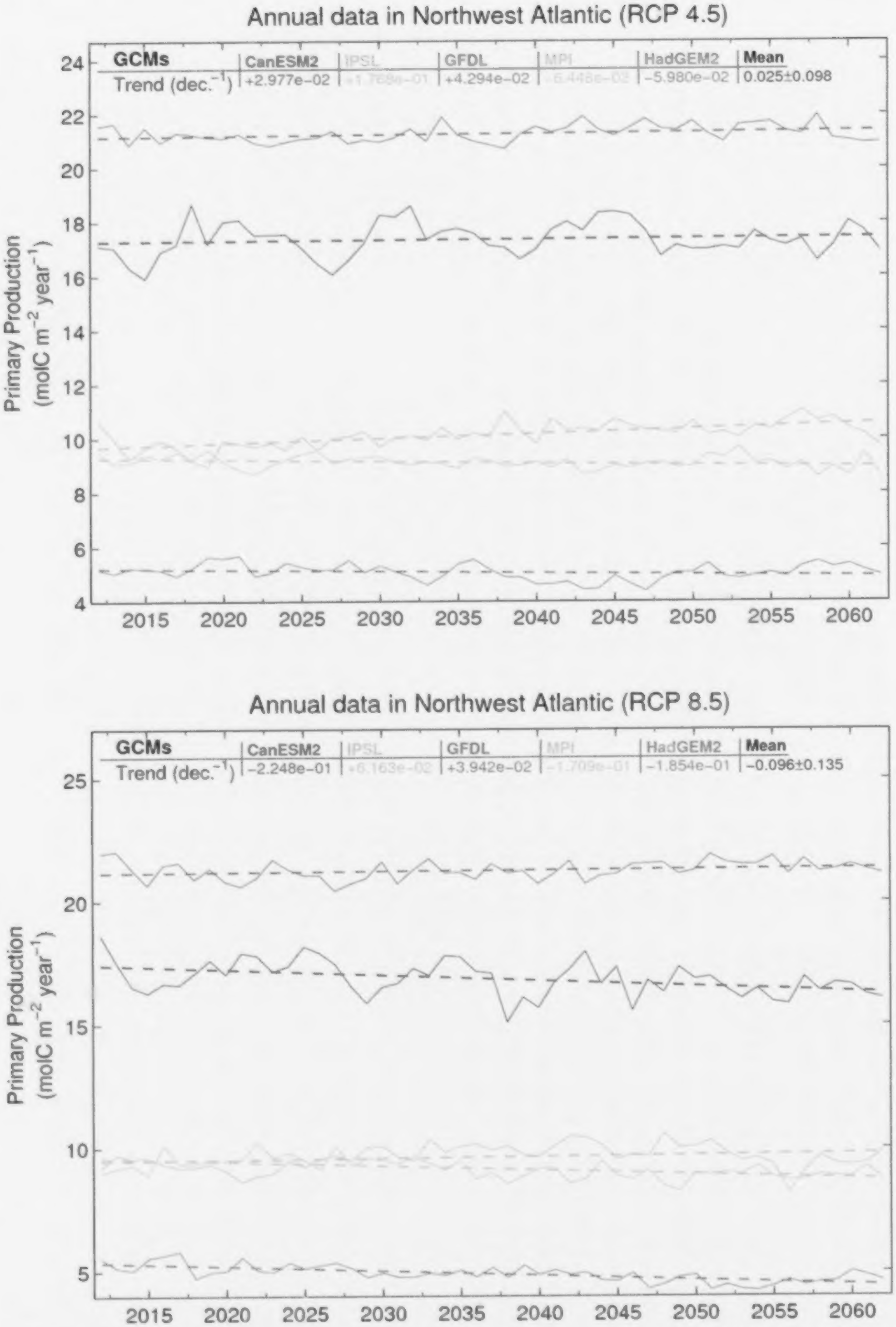

Figure 105. Future vertically integrated primary production trends (mol C m^{-2}/decade) in the AltNW region for the 2012-2062 period for RCPs 4.5 and 8.5.

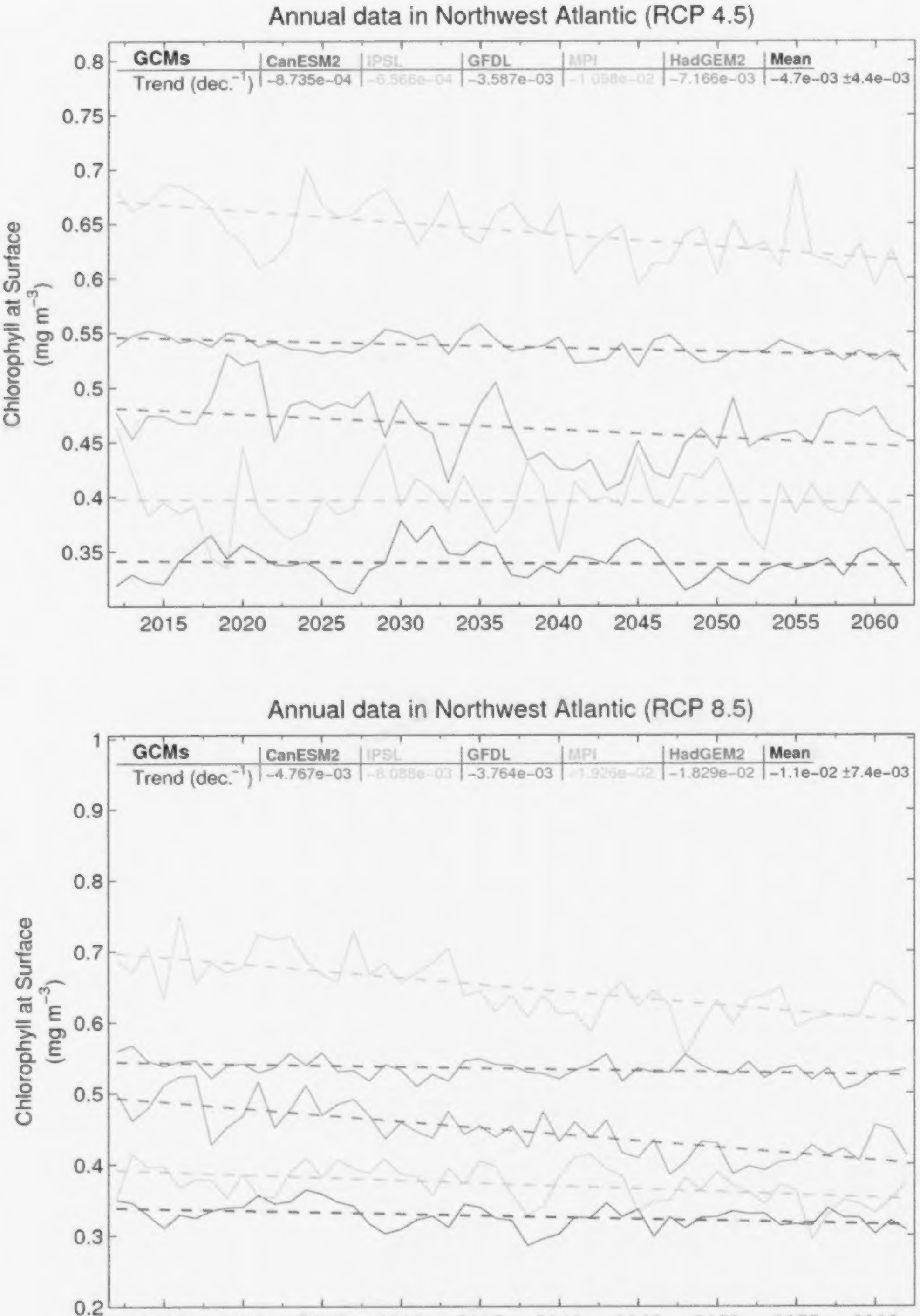

Figure 106. Future Chl a concentration trends (mg m^{-3}/decade) at the surface in the AtlNW region for the 2012-2062 period for RCPs 4.5 and 8.5.

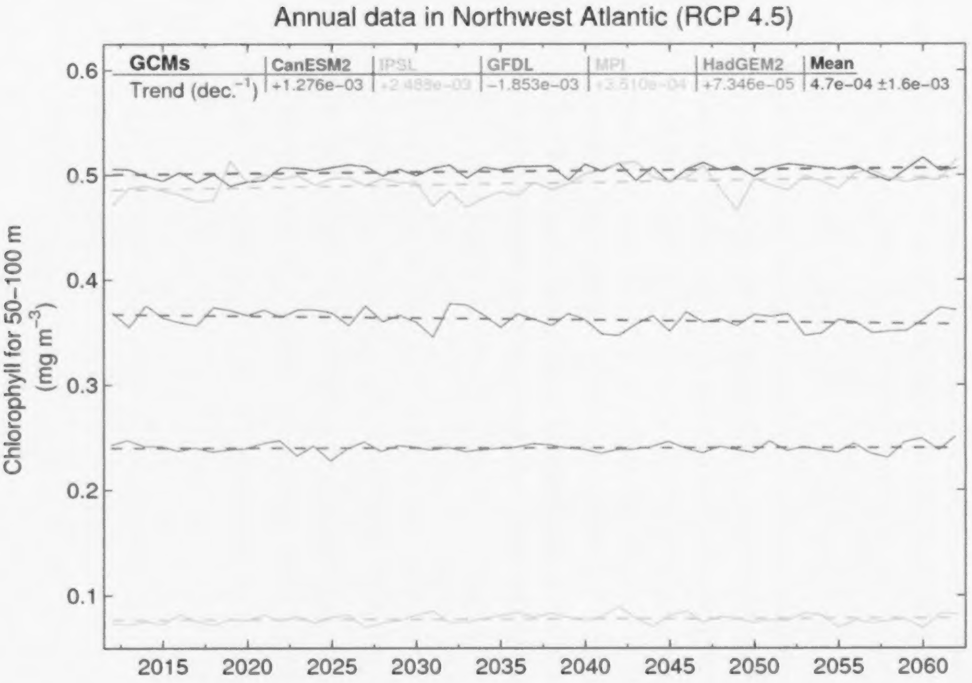

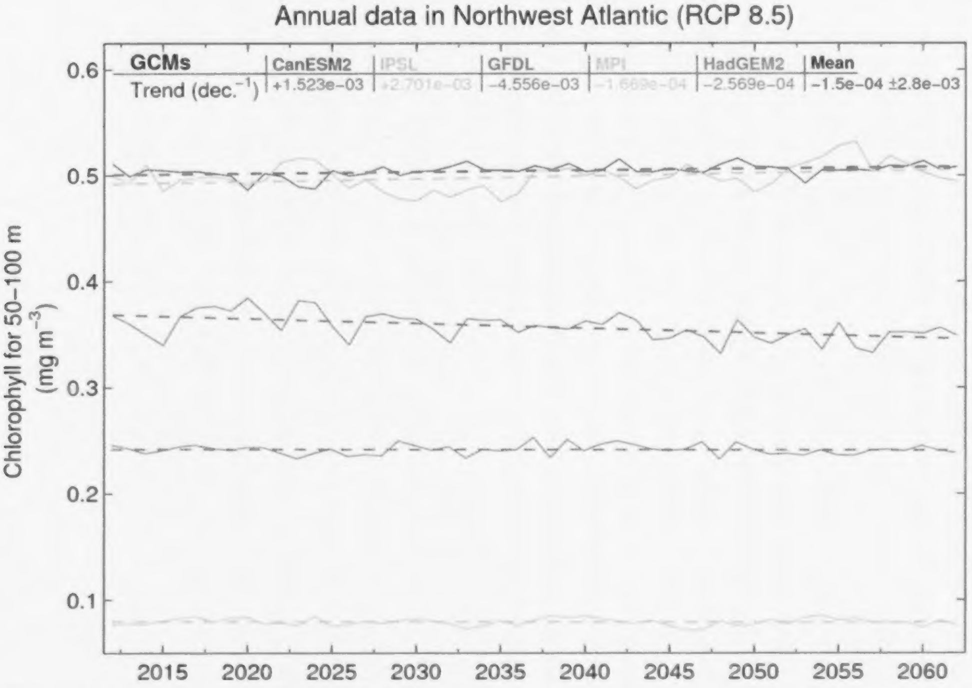

Figure 107. Future Chl a concentration trends (mg m^{-3}/decade) at 50-100 m in the AtlNW region for the 2012-2062 period for RCPs 4.5 and 8.5.

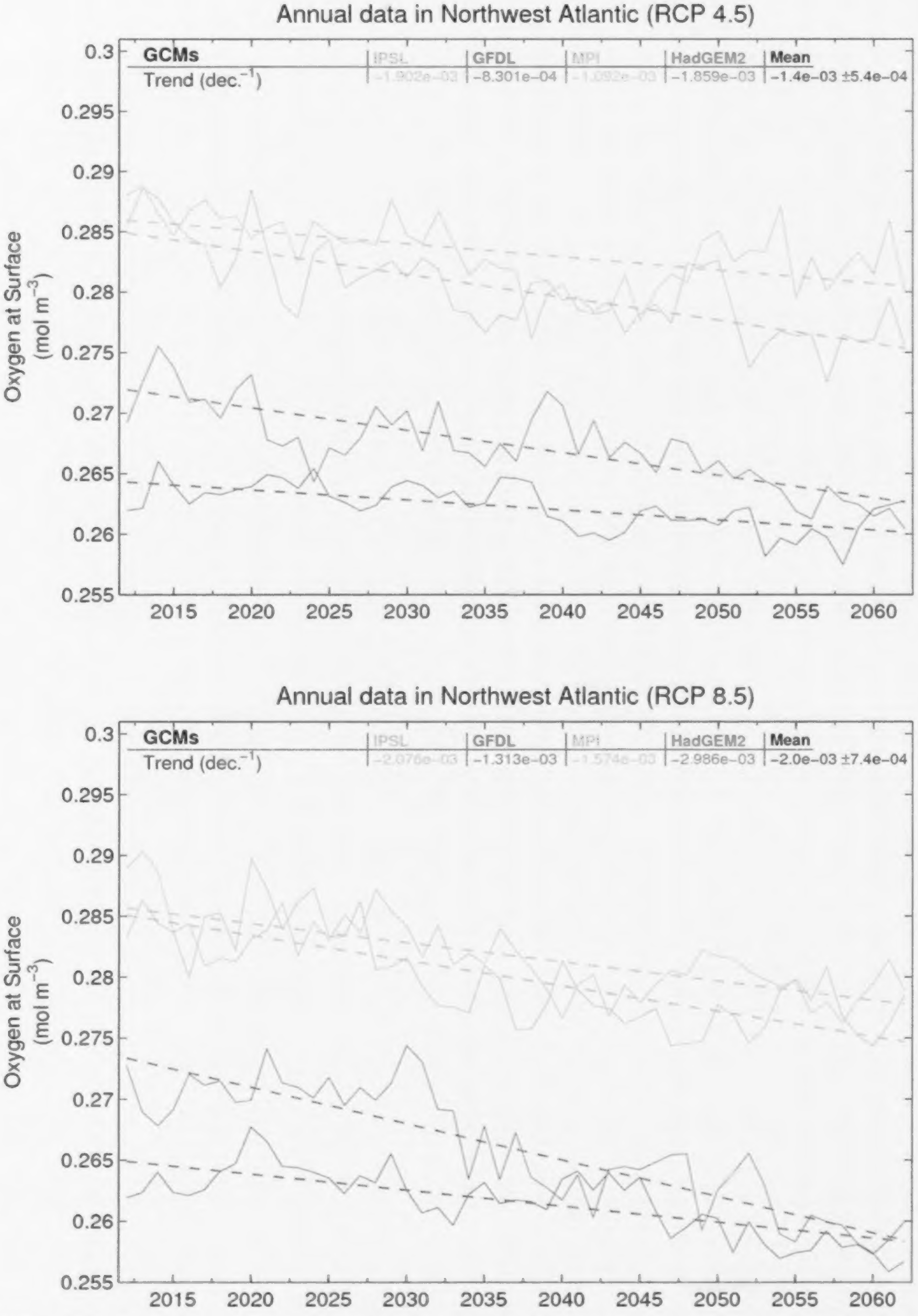
Annual data in Northwest Atlantic (RCP 4.5)

Annual data in Northwest Atlantic (RCP 8.5)

Figure 108. Future oxygen concentration trends (mol m^{-3}/decade) at the surface in the AtlNW region for the 2012-2062 period for RCPs 4.5 and 8.5.

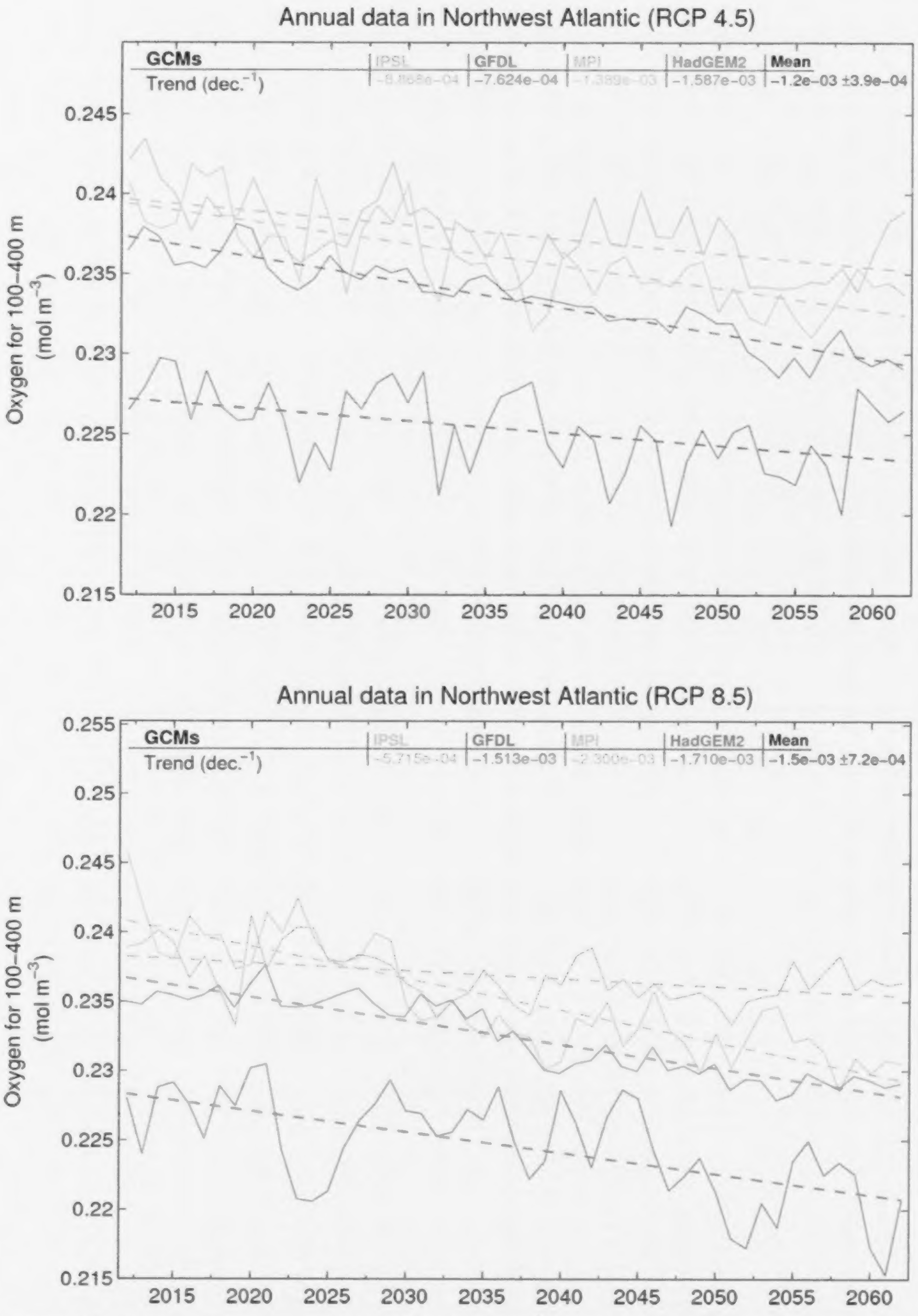

Figure 109. Future oxygen concentration trends (mol m^{-3}/decade) at 100-400 m in the AtlNW region for the 2012-2062 period for RCPs 4.5 and 8.5.

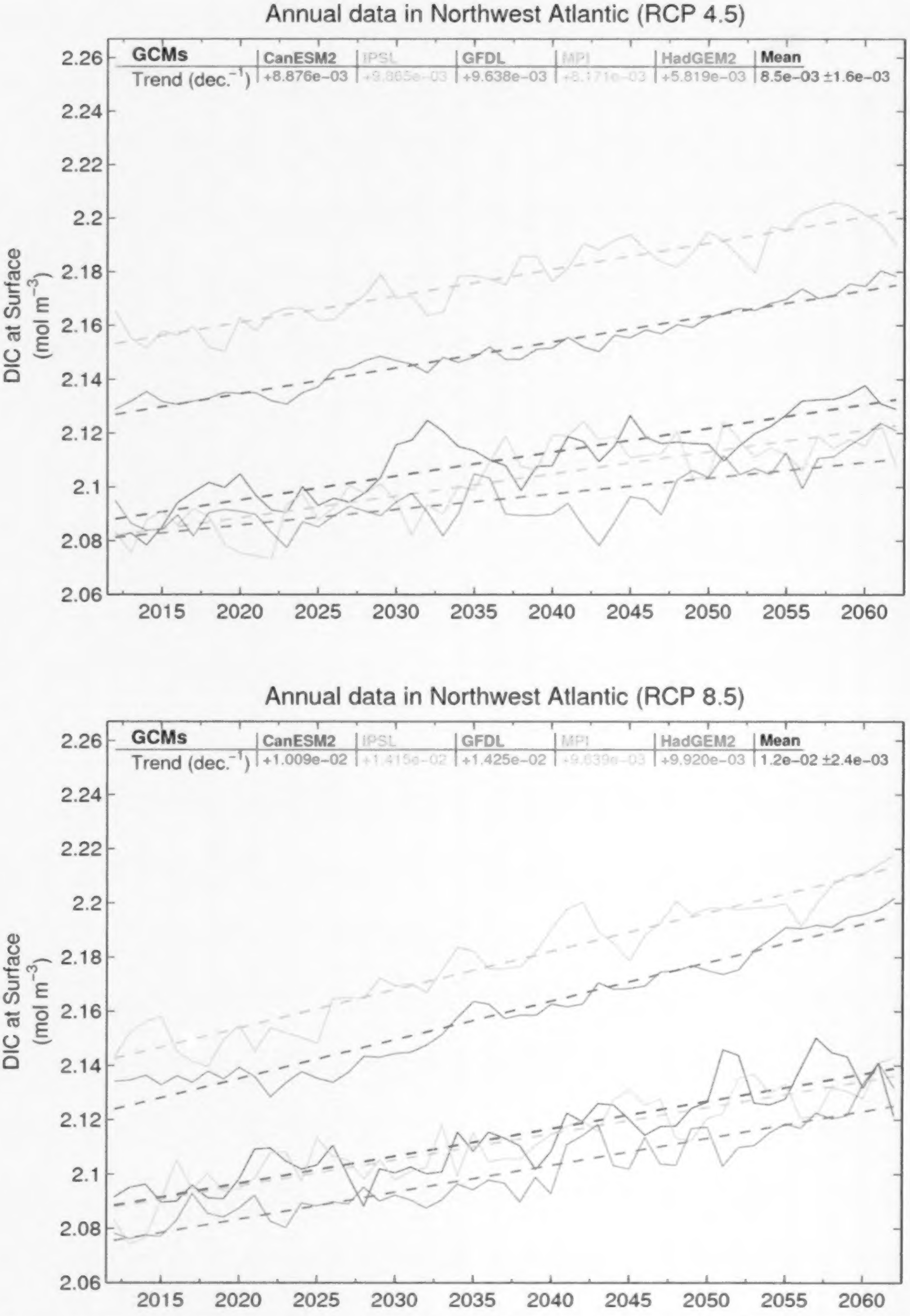

Figure 110. Future DIC concentration trends (mol m^{-3}/decade) at the surface in the AtlNW region for the 2012-2062 period for RCPs 4.5 and 8.5.

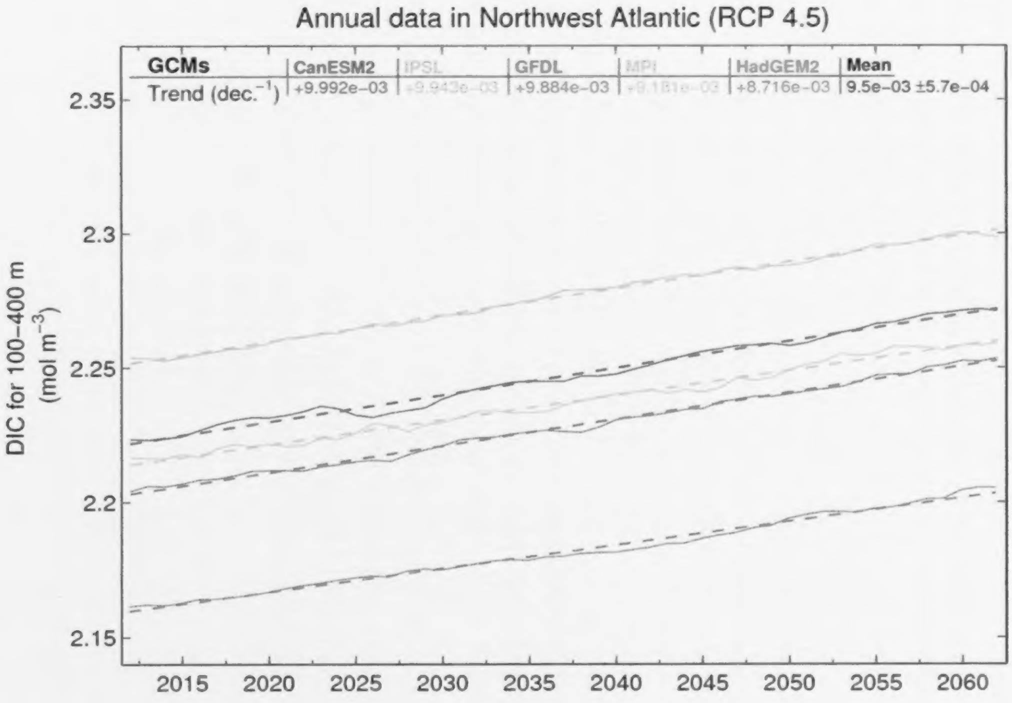
Annual data in Northwest Atlantic (RCP 4.5)

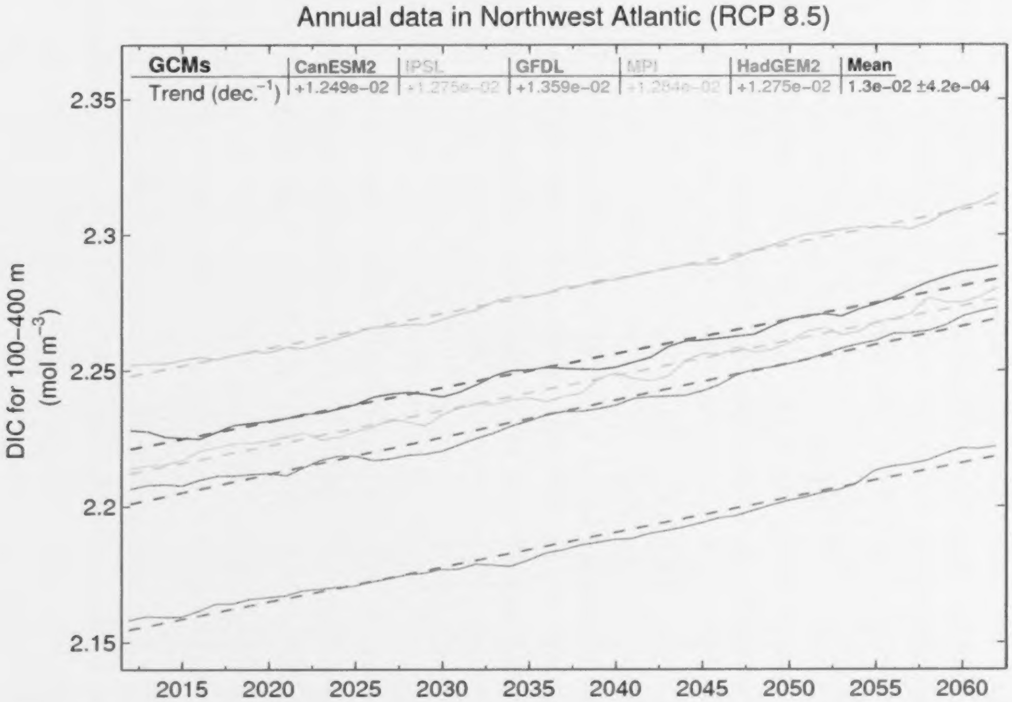
Annual data in Northwest Atlantic (RCP 8.5)

Figure 111. Future DIC concentration trends (mol m^{-3}/decade) at 100-400 m in the AtlNW region for the 2012-2062 period for RCPs 4.5 and 8.5.

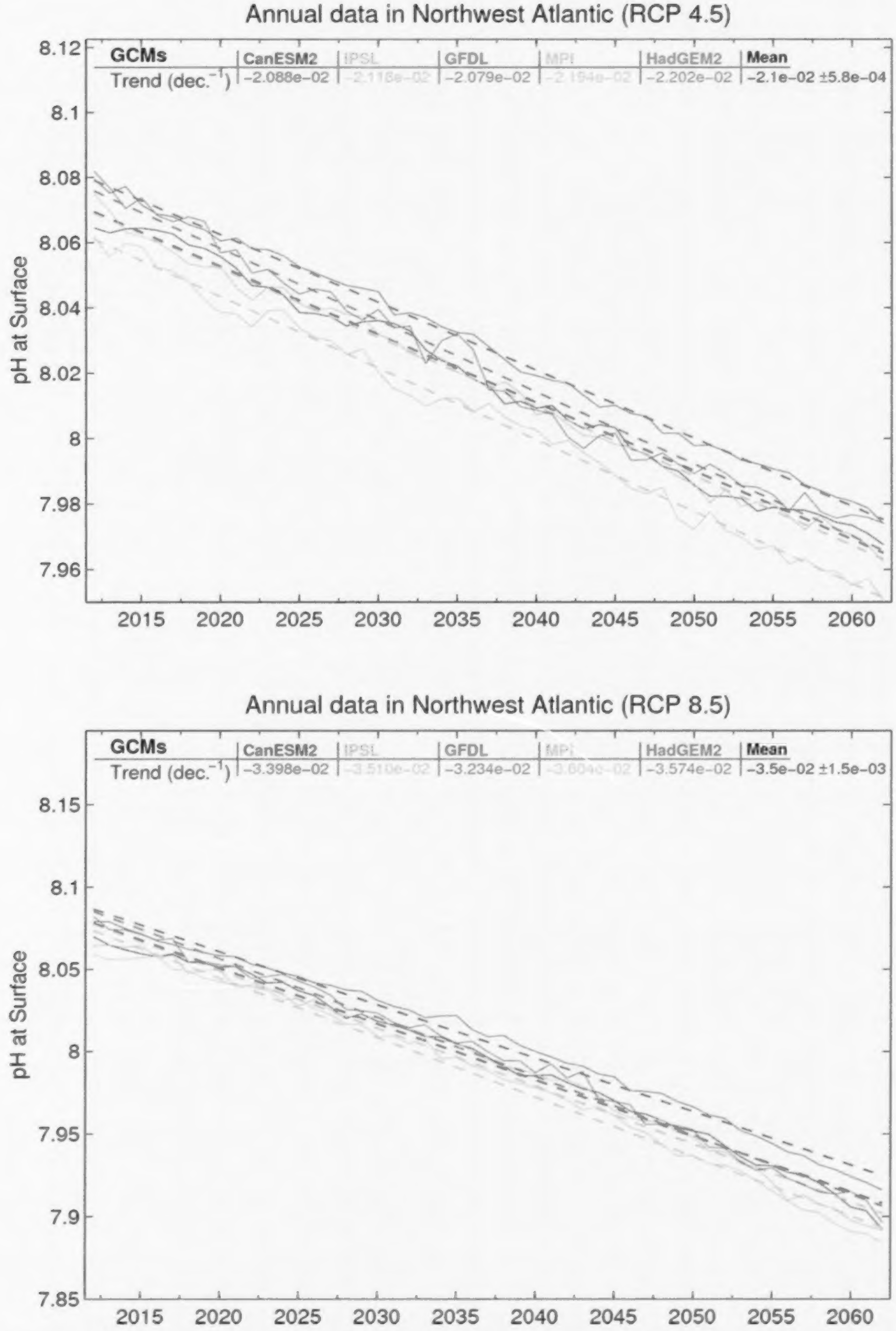

Figure 112. Future pH trends (per decade) at the surface in the AtlNW region for the 2012-2062 period for RCPs 4.5 and 8.5.

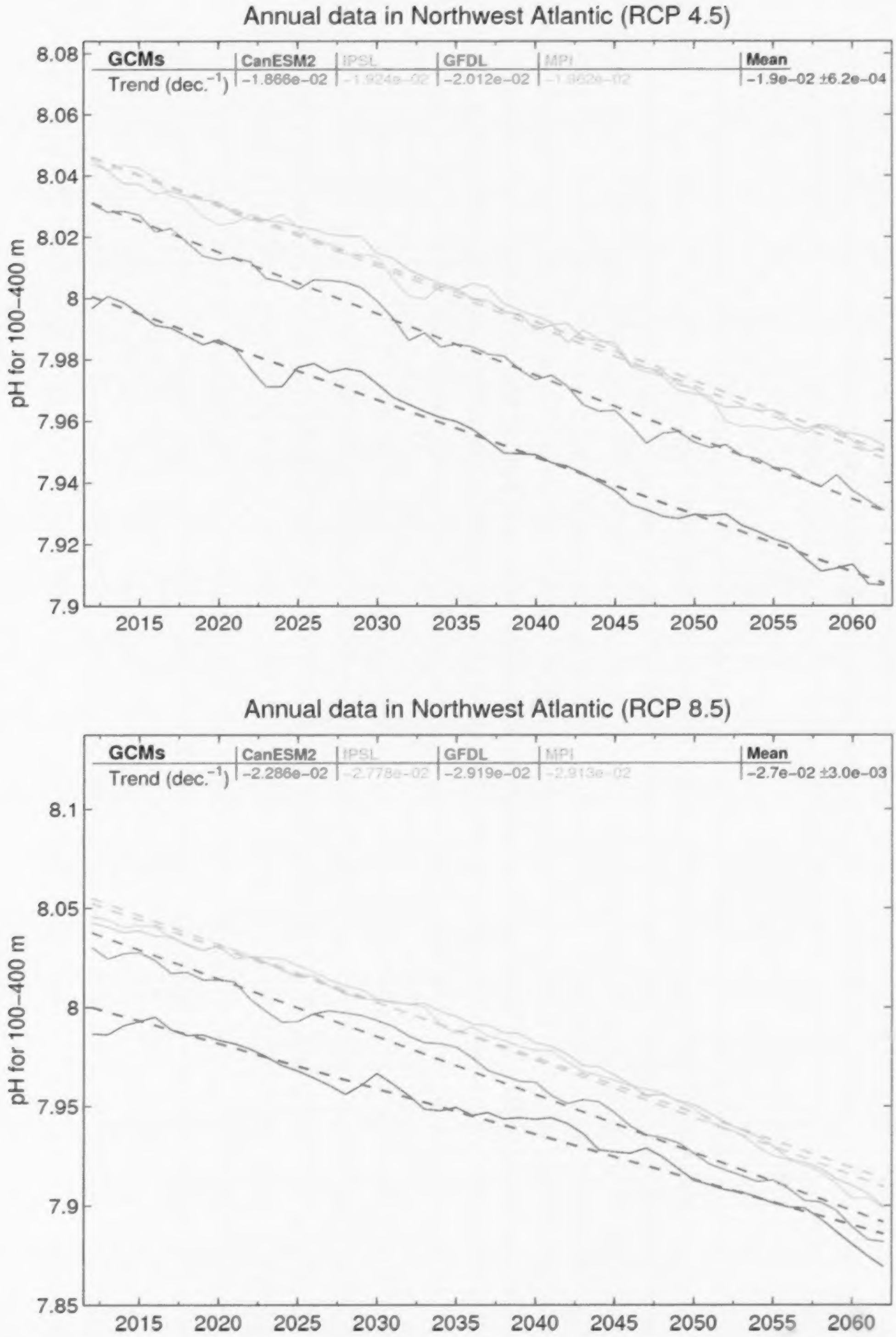

Figure 113. Future pH trends (per decade) at 100-400 m in the AtlNW region for the 2012-2062 period for RCPs 4.5 and 8.5.

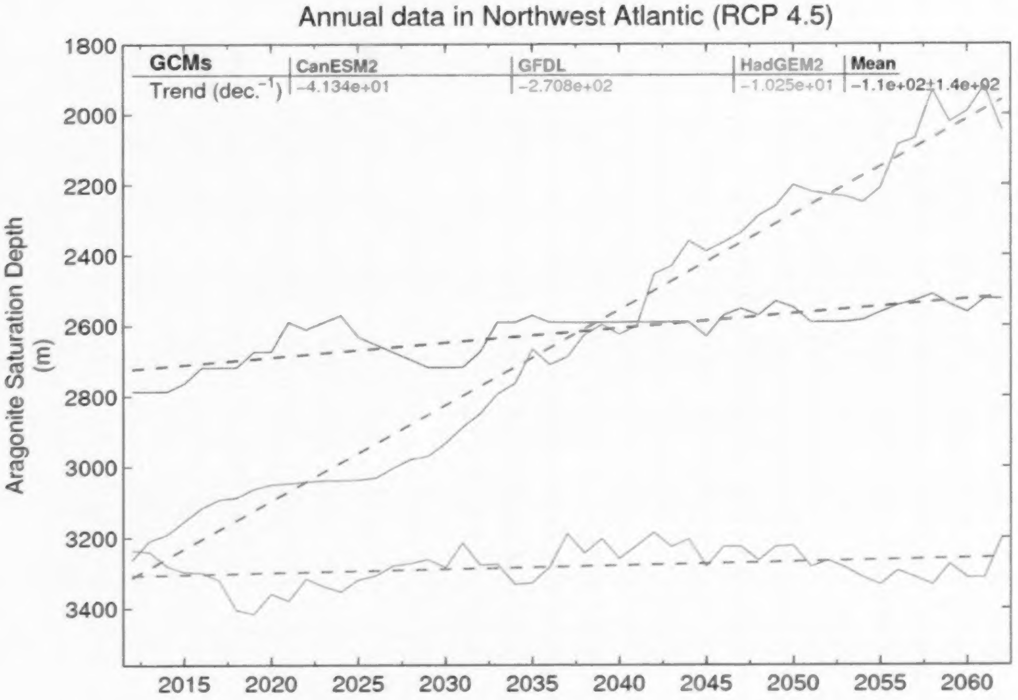

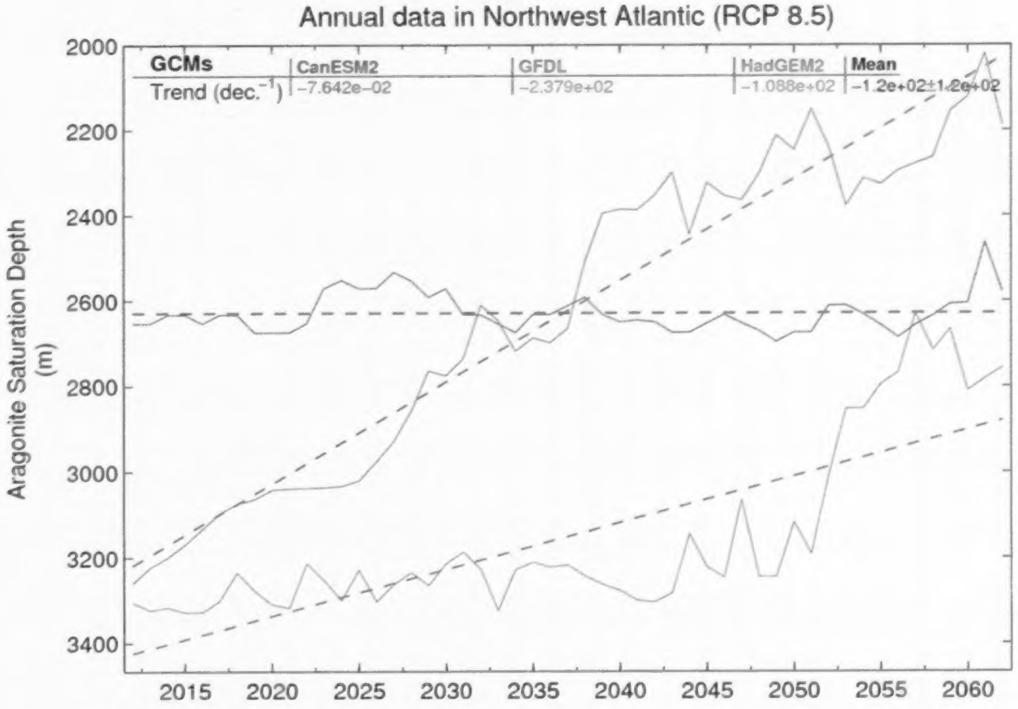

Figure 114. Future aragonite saturation depth trends (m/decade) in the AtlNW region for the 2012-2062 period for RCPs 4.5 and 8.5.

Appendix I

Appendix I-1. Multi-model ensemble mean trends over the next 50 years for the different variables at the surface, in the 50-100 m layer, and in the 100-400 m layer for the two scenarios (RCPs 4.5 and 8.5).

Region		Labrador Sea		Atlantic Northwest	
RCPs		RCP 4.5	RCP 8.5	RCP 4.5	RCP 8.5
SST	Surf.	+0.16±0.13	+0.22±0.13	+0.28±0.10	+0.39±0.12
	50-100m	+0.14±0.14	+0.19±0.14	+0.26±0.11	+0.34±0.12
	100-400m	+0.16±0.08	+0.24±0.09	+0.26±0.11	+0.36±0.13
SSS	Surf.	-0.06±0.10	-0.12±0.11	+0.008±0.032	-0.02±0.03
	50-100m	-0.022±0.017	-0.07±0.06	+0.031±0.026	+0.025±0.021
	100-400m	+0.001±0.033	-0.014±0.019	+0.04±0.02	+0.04±0.03
MLD	mean	-6.0±3.7	-13±14	-0.29±0.59	-3.2±4.5
	max	-4.3±6.8	-11.8±18.5	-0.34±0.79	-3.0±4.9
NO_3	Surf.	-0.11±0.12	-0.19±0.12	-0.05±0.04	-0.08±0.06
	50-100m	-0.10±0.17	-0.21±0.10	-0.08±0.05	-0.19±0.12
	100-400m	-0.06±0.10	-0.08±0.13	-0.12±0.06	-0.20±0.15
Chl a	PP	+0.05±0.15	-0.01±0.17	-0.02±0.20	-0.02±0.19
	Surf.	-0.3e-3±9.8e-3	-0.009±0.010	+0.0007±0.019	-0.010±0.017
	50-100m	+2.8e-3±4.5e-3	+3.8e-3±2.5e-3	-0.004±0.12	+0.3e-3±5.0e-3
	100-400m	-0.3e-3±1.1e-3	-5e-4±1.3e-3	-4e-4±8e-4	-0.3e-3±1.0e-3
O_2	Surf.	-0.6±1.3	-0.9±1.3	-1.4±0.5	-2.0±0.7
	50-100m	-0.7±1.5	-0.7±0.9	-1.3±0.5	-1.5±0.7
	100-400m	-1.2±0.3	-2.0±1.0	-1.2±0.4	-1.5±0.7
DIC	Surf.	+0.28±0.10	+0.39±0.12	+0.008±0.002	+0.012±0.002
	50-100m	+0.26±0.11	+0.34±0.12	+0.010±0.001	+0.0140±0.0008
	100-400m	+0.26±0.11	+0.36±0.13	+0.0095±0.0005	+0.0130±0.0004
pH	Surf.	-0.026 ± 0.002	-0.042 ± 0.003	-0.021 ± 0.0006	-0.035 ± 0.002
	50-100m	-0.025 ± 0.002	-0.038 ± 0.003	-0.021 ± 0.0008	-0.031 ± 0.004
	100-400m	-0.024 ± 0.001	-0.034 ± 0.002	-0.019 ± 0.0006	-0.027 ± 0.003

Appendix II: Figures of bidecadal changes

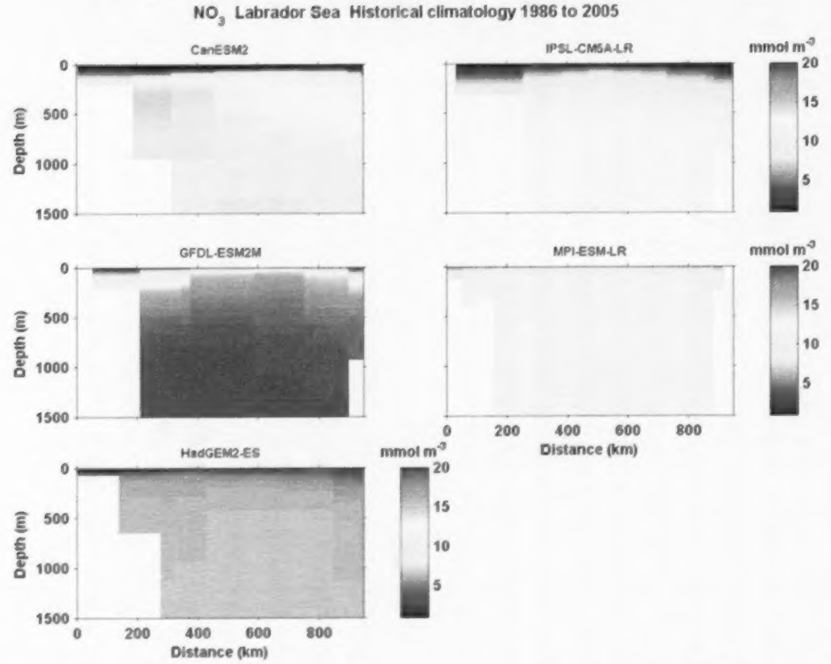

Figure II- 1. Mean simulated nitrate concentration along the Labrador Sea transect for the historical period (1986-2005).

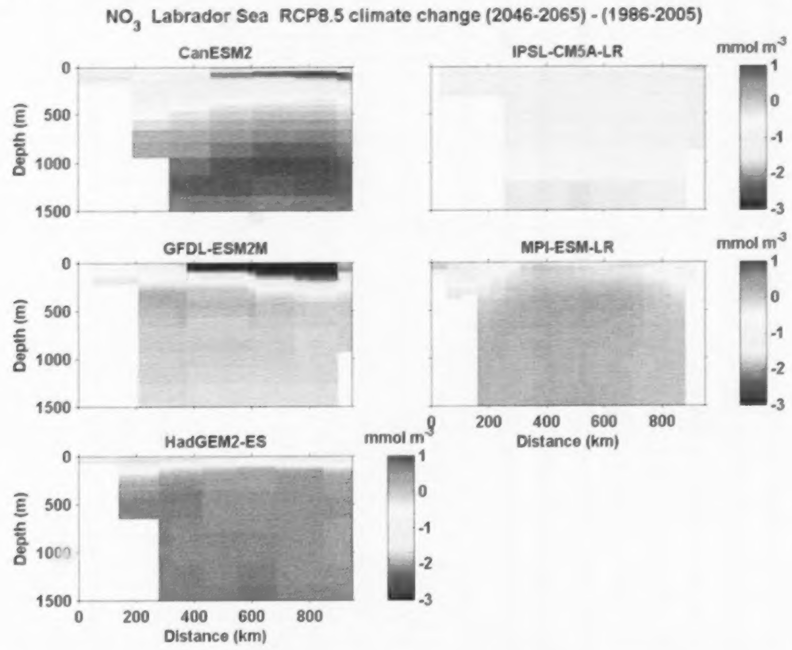

Figure II- 2. Bidecadal changes (2046-2065 average minus 1986-2005 average) in nitrate concentration along the Labrador Sea transect for RCP 8.5.

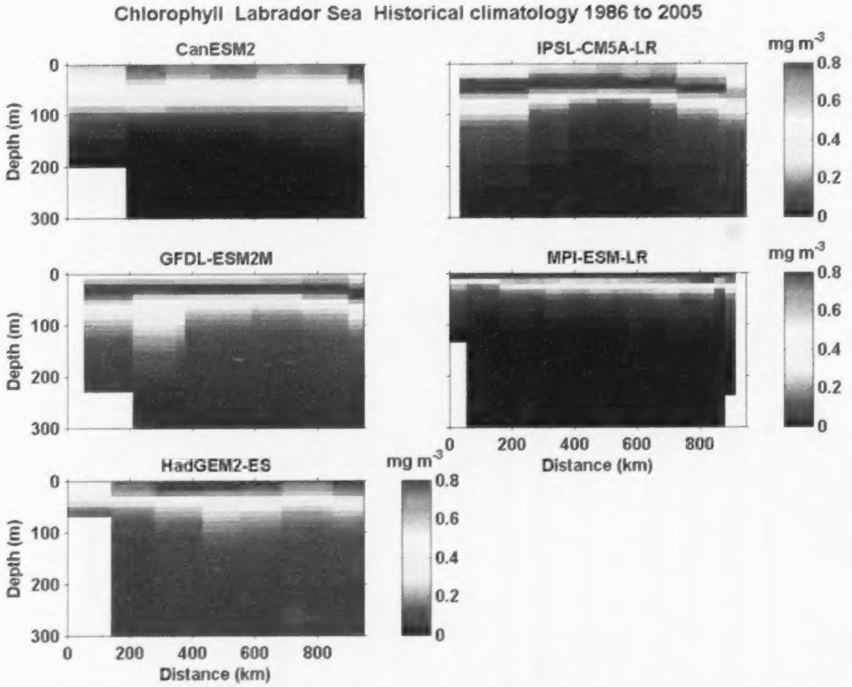

Figure II- 3. Mean simulated Chl a concentration (mg m^{-3}) along the Labrador Sea transect for the historical period (1986-2005).

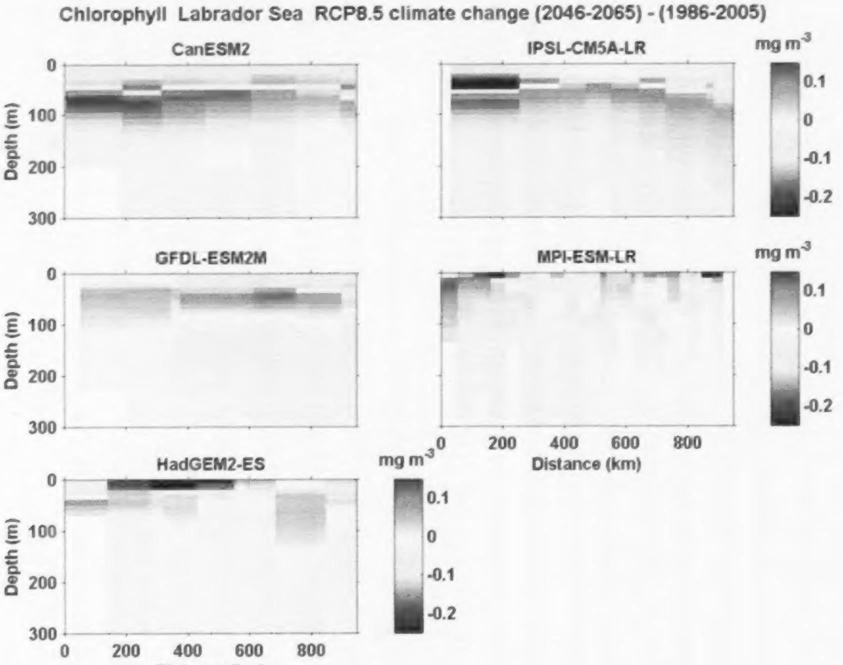

Figure II- 4. Bidecadal changes (2046-2065 average minus 1986-2005 average) in Chl a concentration along the Labrador Sea transect for RCP 8.5.

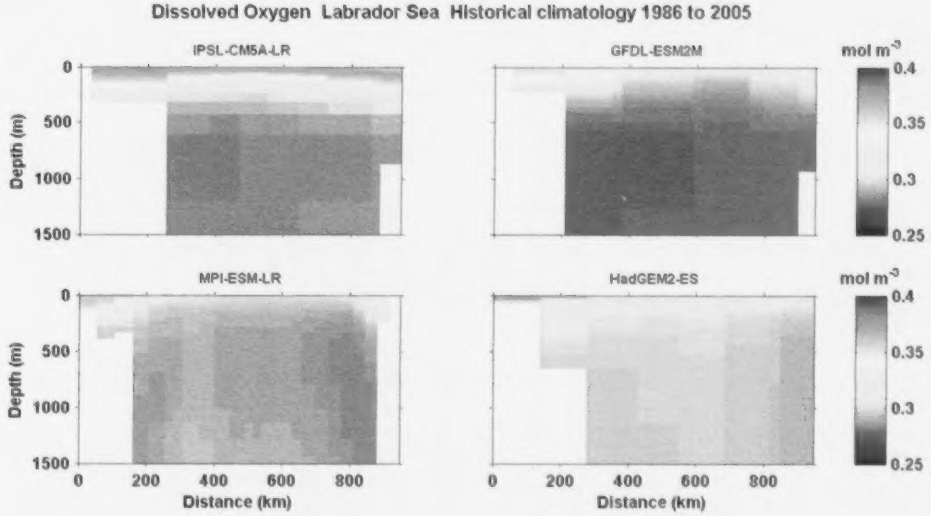

Figure II- 5. Mean simulated dissolved oxygen concentration along the Labrador Sea transect for the historical period (1986-2005).

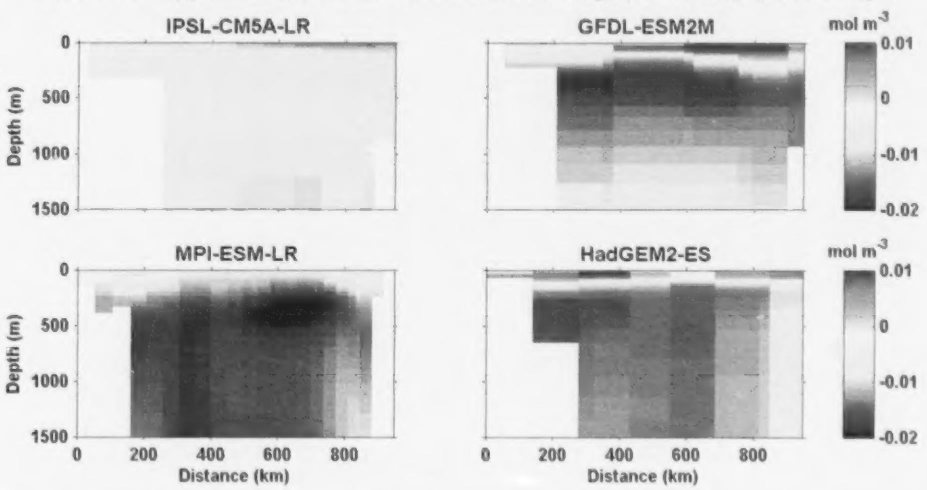

Figure II- 6. Bidecadal changes (2046-2065 average minus 1986-2005 average) in dissolved oxygen concentration along the Labrador Sea transect for RCP 8.5.

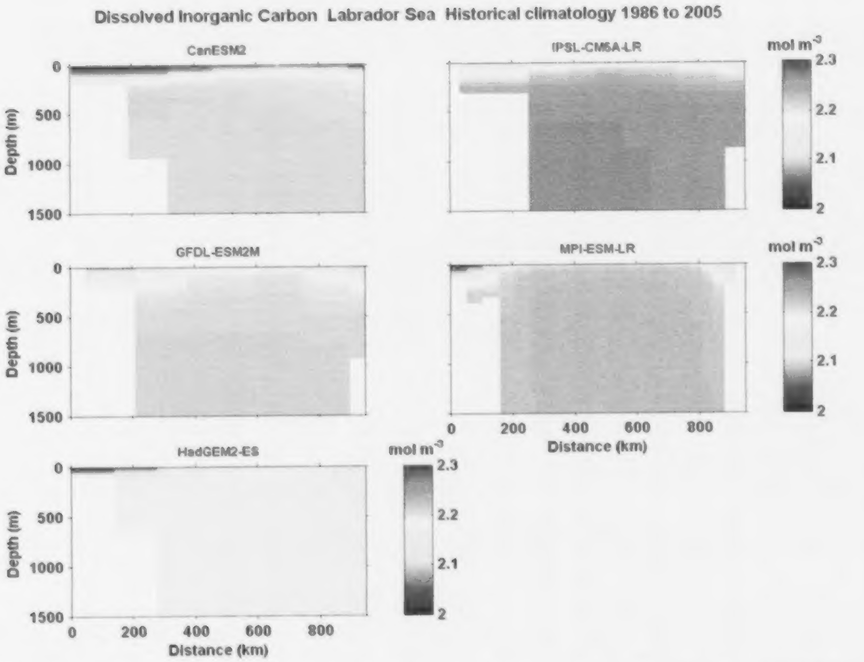

Figure II- 7. Mean simulated dissolved inorganic carbon concentration along the Labrador Sea transect for the historical period (1986-2005).

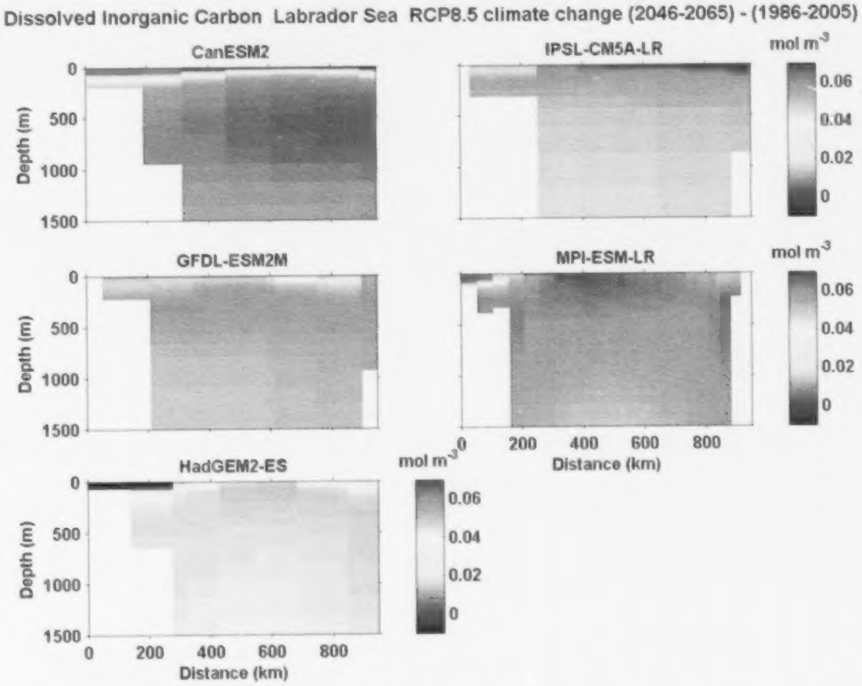

Figure II- 8. Bidecadal changes (2046-2065 average minus 1986-2005 average) in dissolved inorganic carbon concentration along the Labrador Sea transect for RCP 8.5.

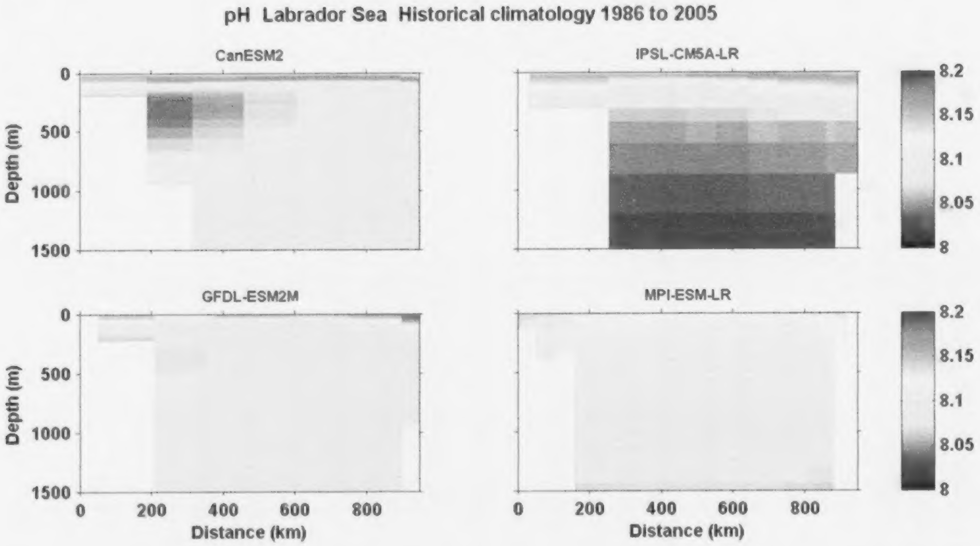

Figure II- 9. Mean simulated pH along the Labrador Sea transect for the historical period (1960-2005).

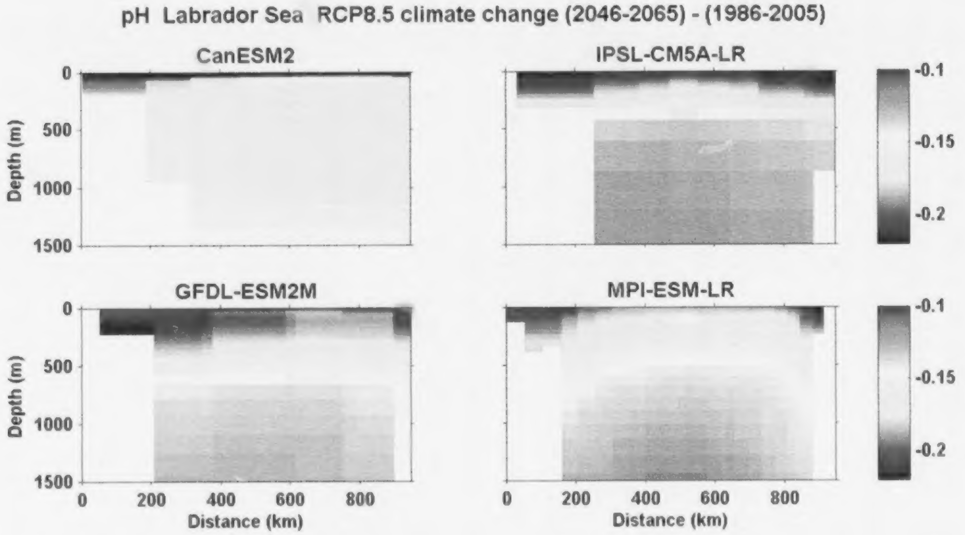

Figure II- 10. Bidecadal changes (2046-2065 average minus 1986-2005 average) in pH along the Labrador Sea transect for RCP 8.5.

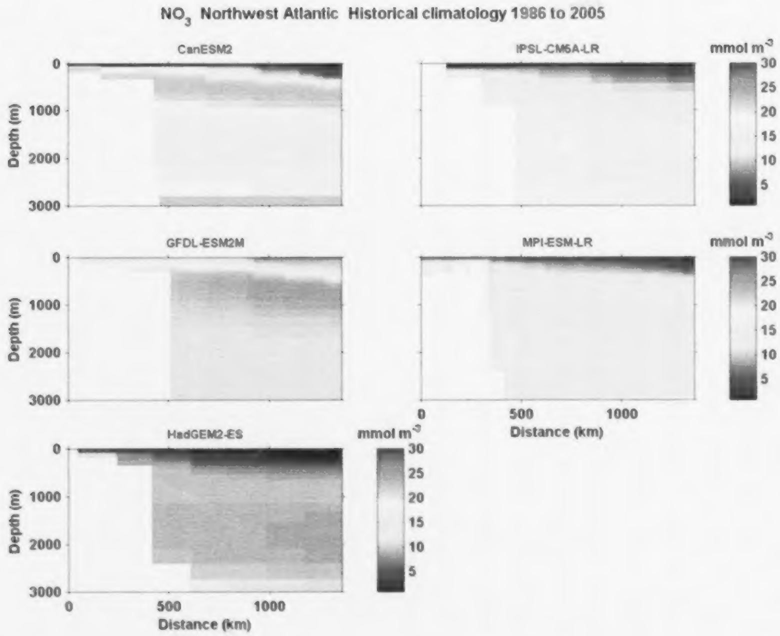

Figure II- 11. Mean simulated nitrate concentration along the AtlNW transect for the historical period (1986-2005).

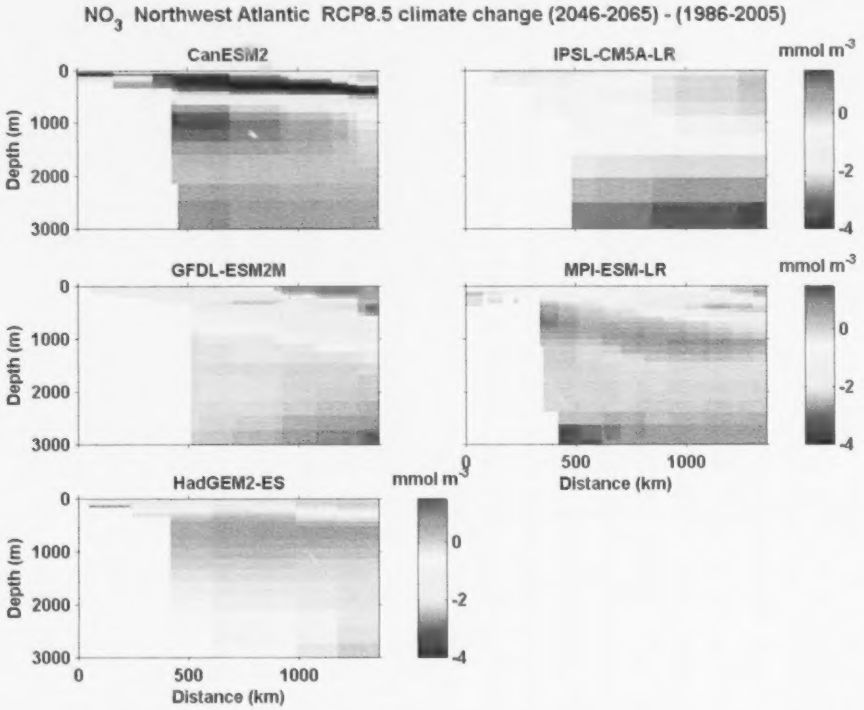

Figure II- 12. Bidecadal changes (2046-2065 average minus 1986-2005 average) in nitrate concentration along the AtlNW region transect for RCP 8.5.

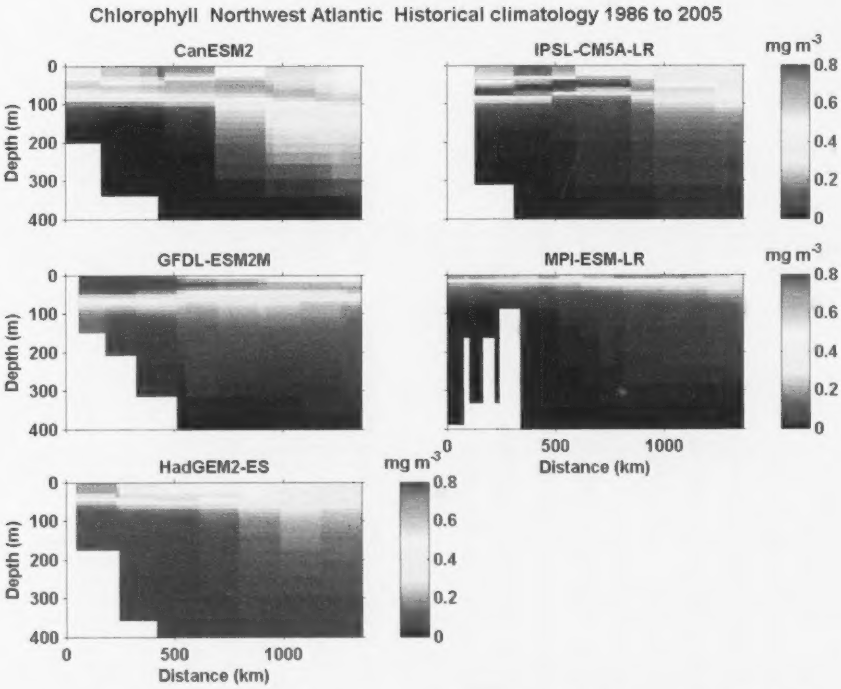

Figure II- 13. Mean simulated Chl a concentration along the AtlNW region transect for the historical period (1986-2005).

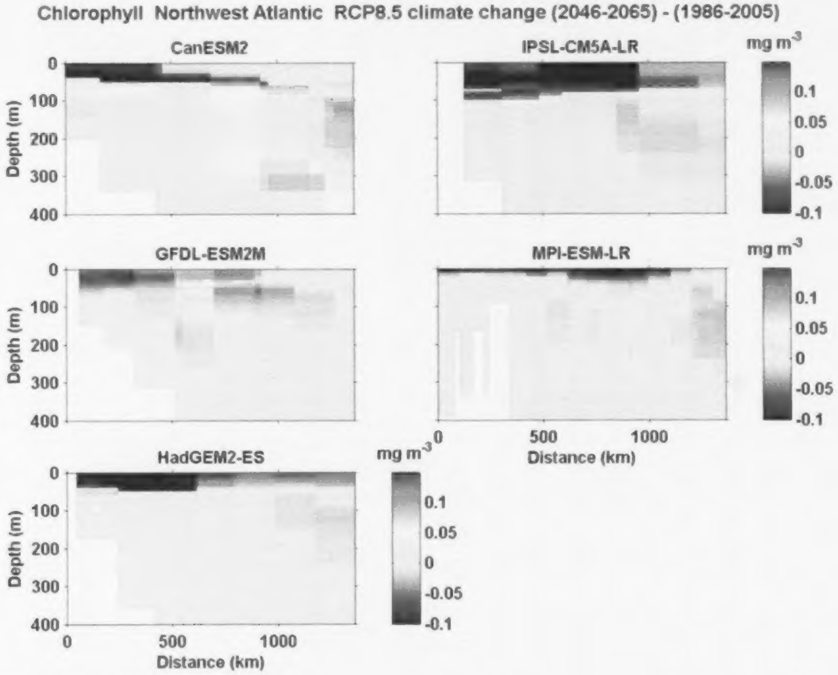

Figure II- 14. Bidecadal changes (2046-2065 average minus 1986-2005 average) in Chl a concentration along the AtlNW region transect for RCP 8.5.

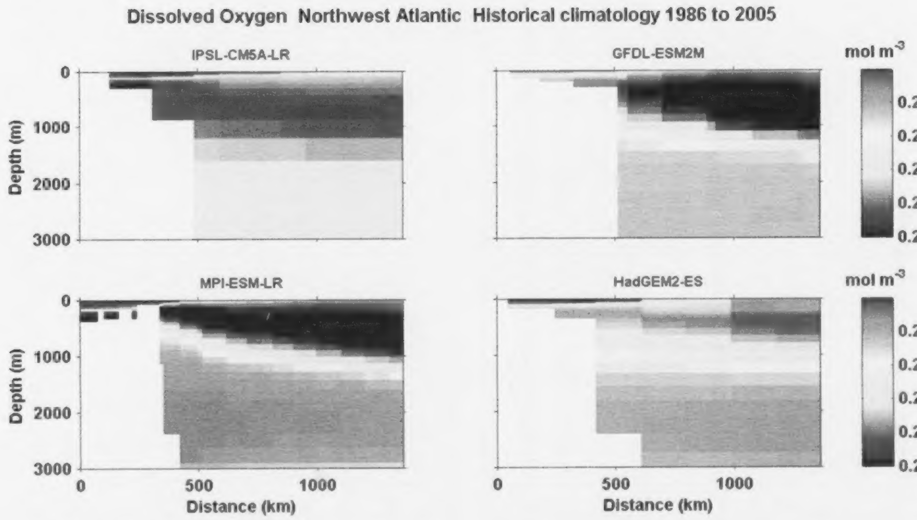

Figure II- 15. Mean simulated dissolved oxygen concentration along the AtlNW transect for the historical period (1986-2005).

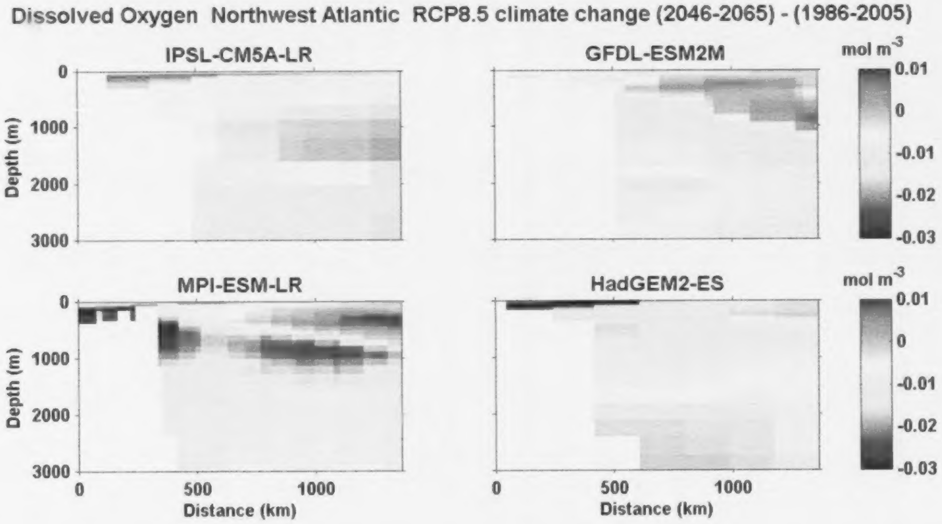

Figure II- 16. Bidecadal changes (2046-2065 average minus 1986-2005 average) in dissolved oxygen concentration along the AtlNW region transect for RCP 8.5.

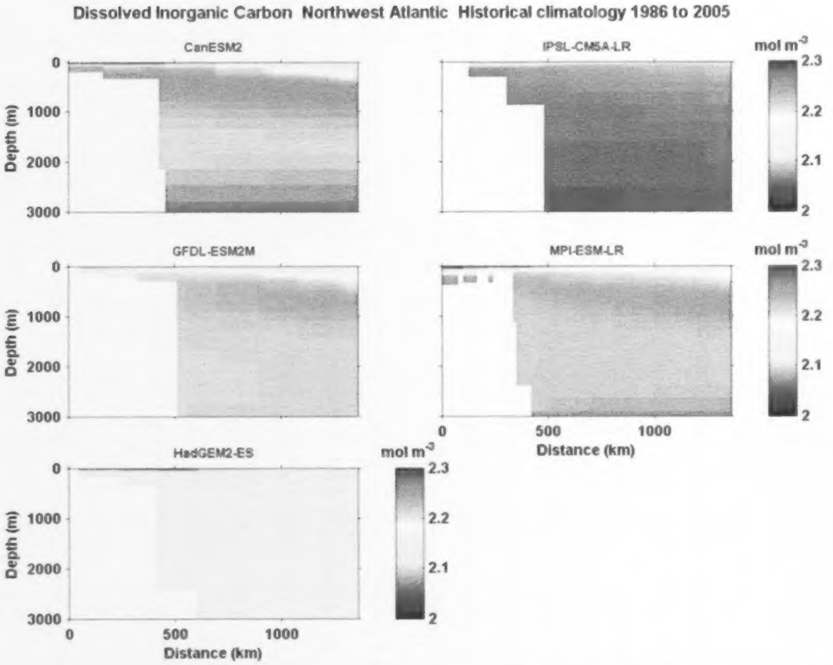

Dissolved Inorganic Carbon Northwest Atlantic Historical climatology 1986 to 2005

Figure II- 17. Mean simulated dissolved inorganic carbon concentration along the AtlNW transect for the historical period (1986-2005).

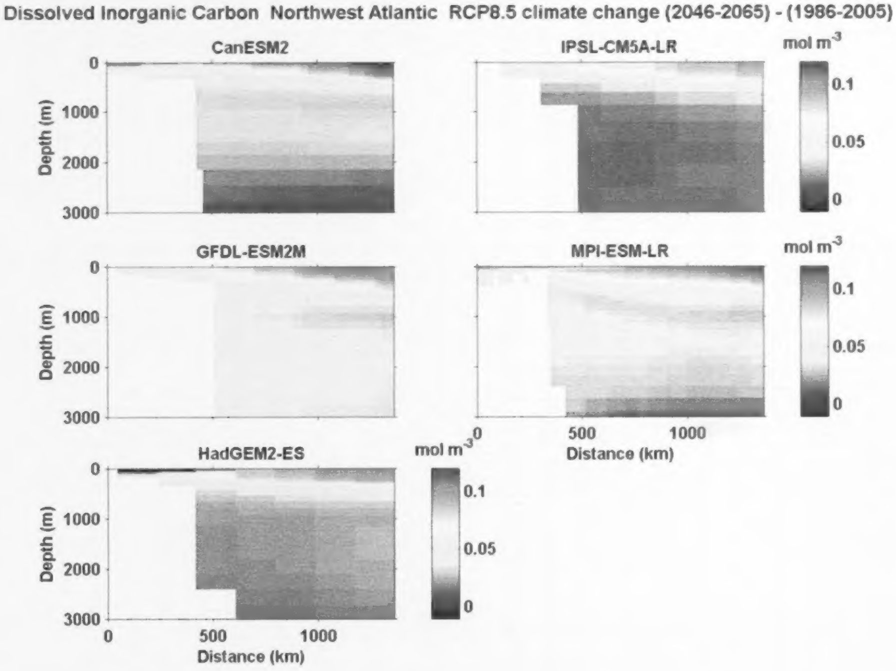

Dissolved Inorganic Carbon Northwest Atlantic RCP8.5 climate change (2046-2065) - (1986-2005)

Figure II- 18. Bidecadal changes (2046-2065 average minus 1986-2005 average) in dissolved inorganic carbon concentration along the AtlNW region transect for RCP 8.5.

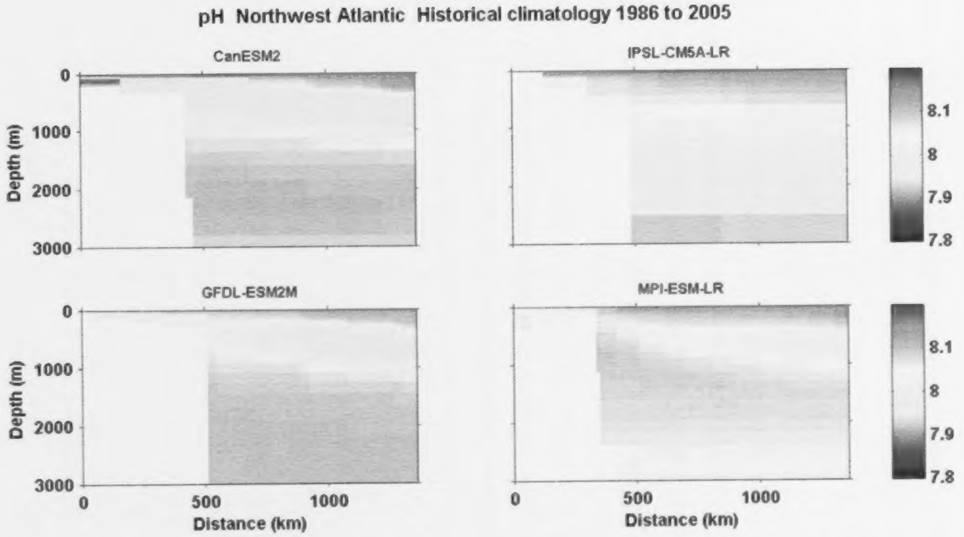

Figure II- 19. Mean simulated pH along the AtlNW transect for the historical period (1986-2005).

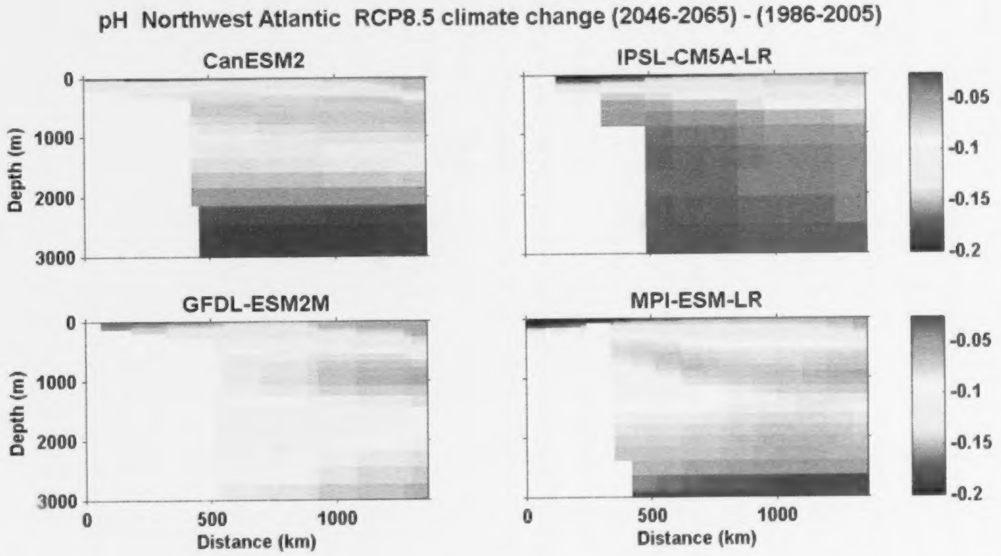

Figure II- 20. Bidecadal changes (2046-2065 average minus 1986-2005 average) in pH along the AtlNW region transect for RCP 8.5.

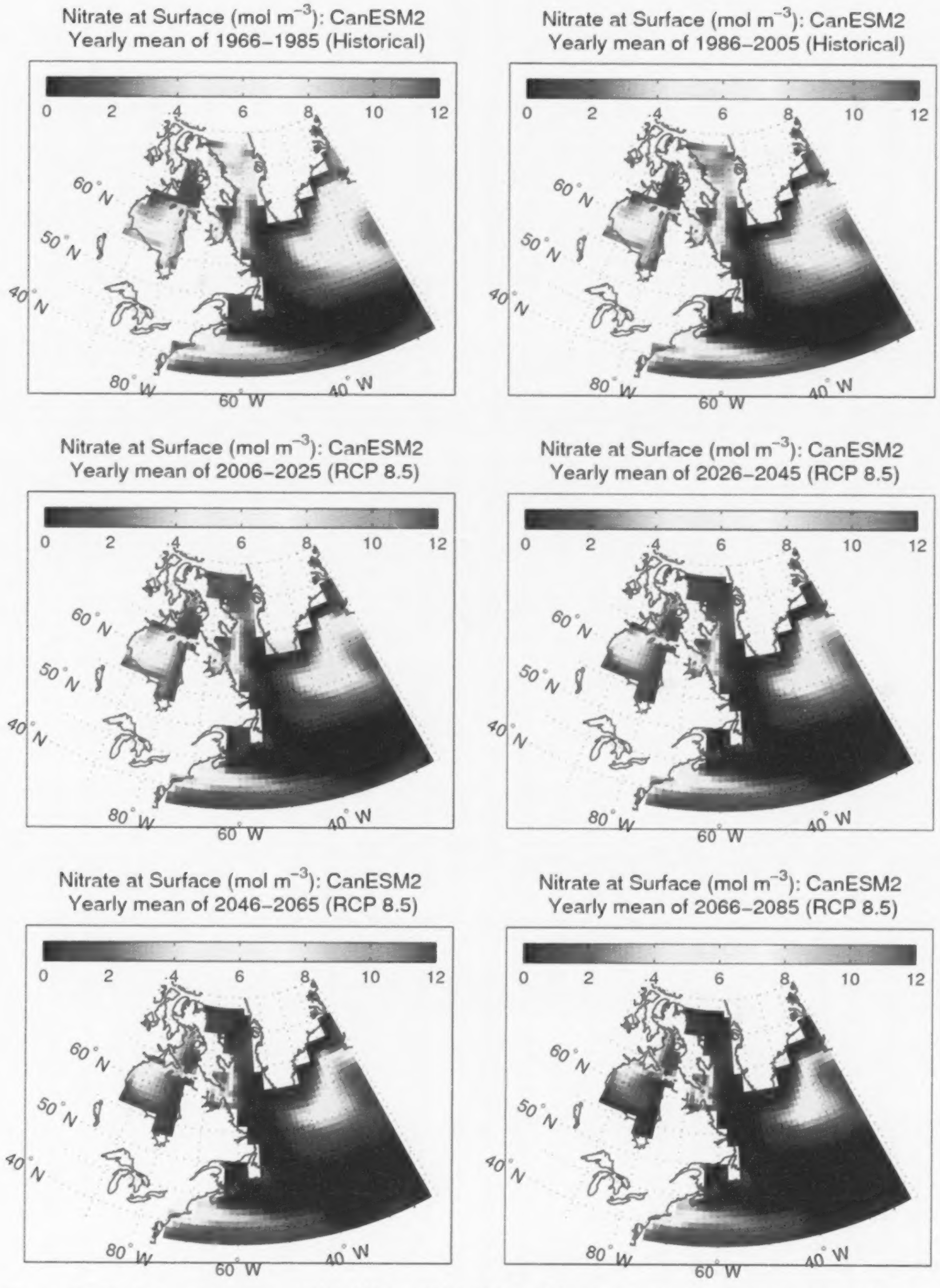
Nitrate at Surface (mol m^{-3}): CanESM2
Yearly mean of 1966–1985 (Historical)
Nitrate at Surface (mol m^{-3}): CanESM2
Yearly mean of 1986–2005 (Historical)
Nitrate at Surface (mol m^{-3}): CanESM2
Yearly mean of 2006–2025 (RCP 8.5)
Nitrate at Surface (mol m^{-3}): CanESM2
Yearly mean of 2026–2045 (RCP 8.5)
Nitrate at Surface (mol m^{-3}): CanESM2
Yearly mean of 2046–2065 (RCP 8.5)
Nitrate at Surface (mol m^{-3}): CanESM2
Yearly mean of 2066–2085 (RCP 8.5)
0
2
4
6
8
10
12
60° N
50° N
40° N
80° W
60° W
40° W

Figure II- 21. Bidecadal means (1966-1985 to 2066-2085) of simulated nitrate concentration at the surface with CanESM2 for the RCP 8.5 scenario.

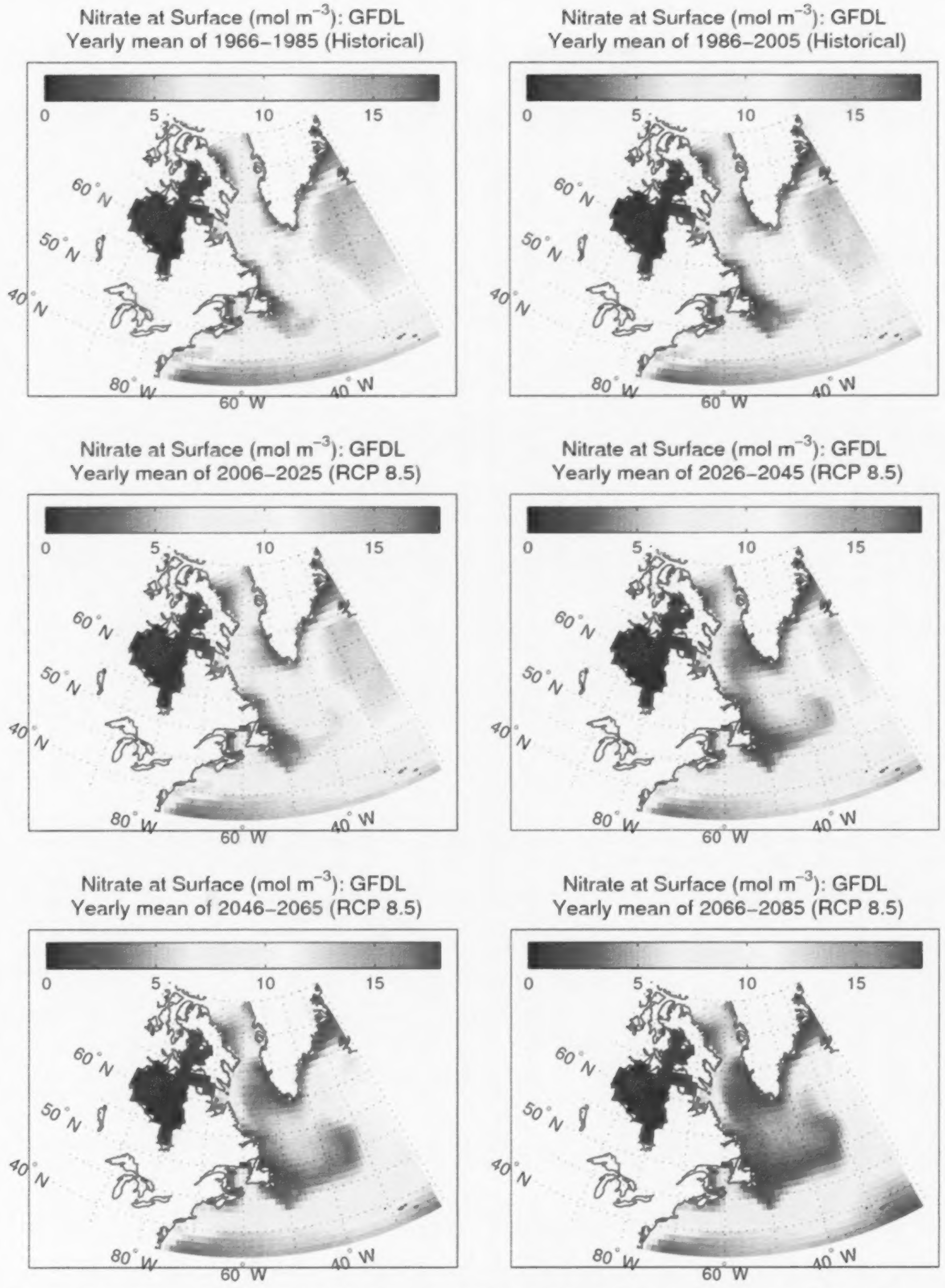
Nitrate at Surface (mol m^{-3}): GFDL
Yearly mean of 1966–1985 (Historical)
Nitrate at Surface (mol m^{-3}): GFDL
Yearly mean of 1986–2005 (Historical)
Nitrate at Surface (mol m^{-3}): GFDL
Yearly mean of 2006–2025 (RCP 8.5)
Nitrate at Surface (mol m^{-3}): GFDL
Yearly mean of 2026–2045 (RCP 8.5)
Nitrate at Surface (mol m^{-3}): GFDL
Yearly mean of 2046–2065 (RCP 8.5)
Nitrate at Surface (mol m^{-3}): GFDL
Yearly mean of 2066–2085 (RCP 8.5)
0
5
10
15
60° N
50° N
40° N
80° W
60° W
40° W

Figure II- 22. Bidecadal means (1966-1985 to 2066-2085) of simulated nitrate concentration at the surface with GFDL for the RCP 8.5 scenario.

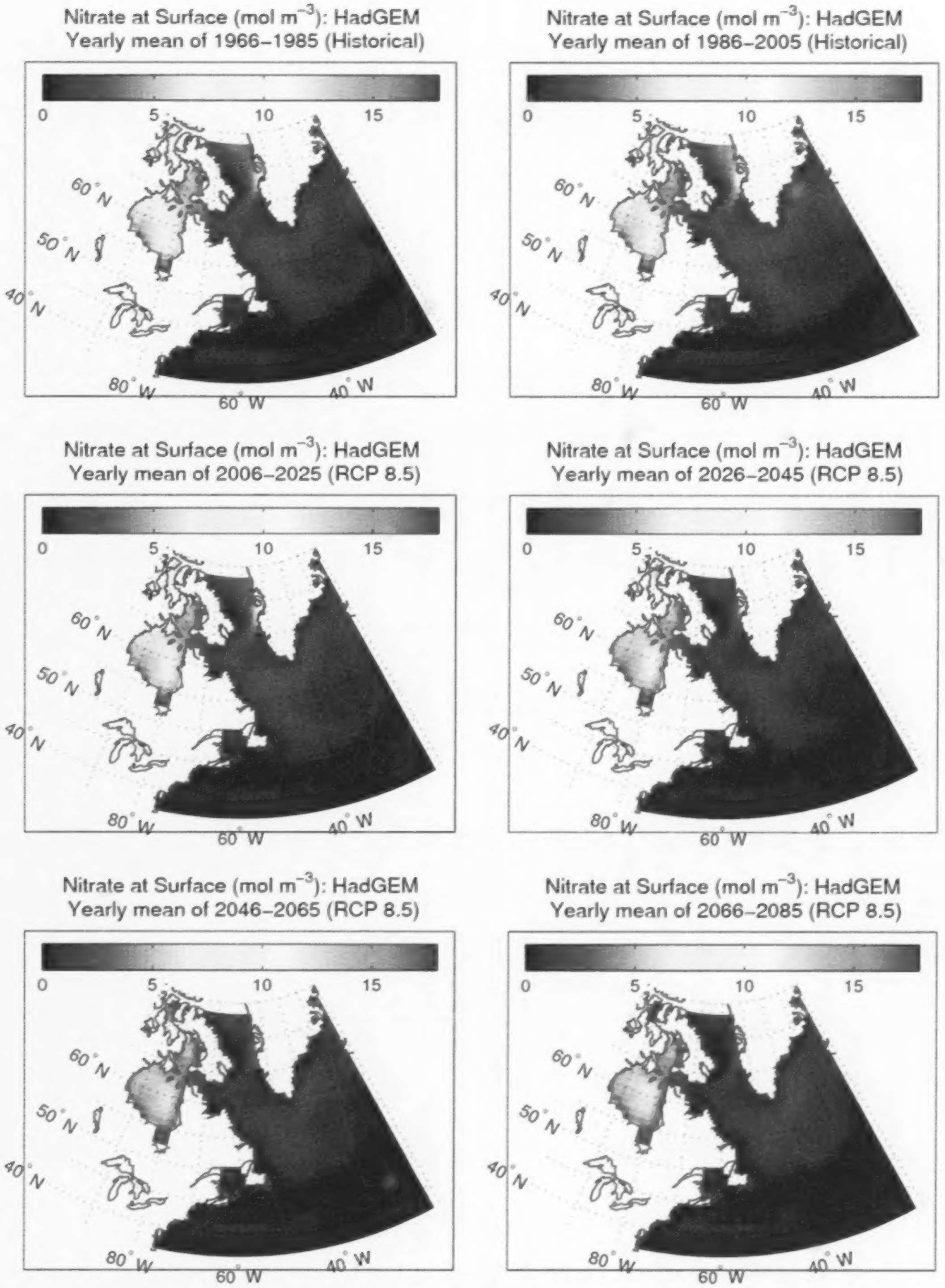
Nitrate at Surface (mol m^{-3}): HadGEM
Yearly mean of 1966–1985 (Historical)

Nitrate at Surface (mol m^{-3}): HadGEM
Yearly mean of 1986–2005 (Historical)

Nitrate at Surface (mol m^{-3}): HadGEM
Yearly mean of 2006–2025 (RCP 8.5)

Nitrate at Surface (mol m^{-3}): HadGEM
Yearly mean of 2026–2045 (RCP 8.5)

Nitrate at Surface (mol m^{-3}): HadGEM
Yearly mean of 2046–2065 (RCP 8.5)

Nitrate at Surface (mol m^{-3}): HadGEM
Yearly mean of 2066–2085 (RCP 8.5)

Figure II- 23. Bidecadal means (1966-1985 to 2066-2085) of simulated nitrate concentration at the surface with HadGEM2 for the RCP 8.5 scenario.

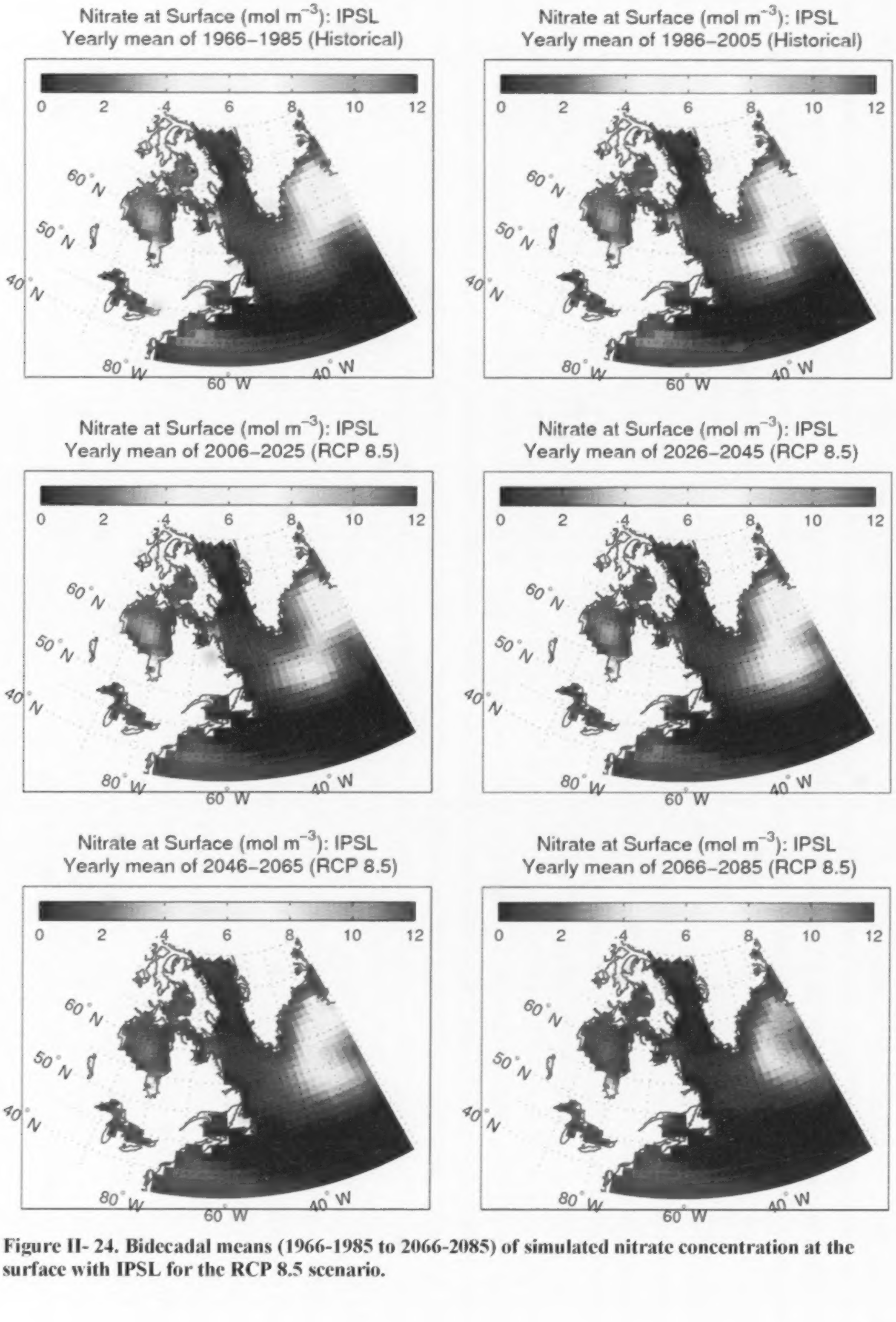

Nitrate at Surface (mol m^{-3}): IPSL
Yearly mean of 1966–1985 (Historical)

Nitrate at Surface (mol m^{-3}): IPSL
Yearly mean of 1986–2005 (Historical)

Nitrate at Surface (mol m^{-3}): IPSL
Yearly mean of 2006–2025 (RCP 8.5)

Nitrate at Surface (mol m^{-3}): IPSL
Yearly mean of 2026–2045 (RCP 8.5)

Nitrate at Surface (mol m^{-3}): IPSL
Yearly mean of 2046–2065 (RCP 8.5)

Nitrate at Surface (mol m^{-3}): IPSL
Yearly mean of 2066–2085 (RCP 8.5)

Figure II- 24. Bidecadal means (1966-1985 to 2066-2085) of simulated nitrate concentration at the surface with IPSL for the RCP 8.5 scenario.

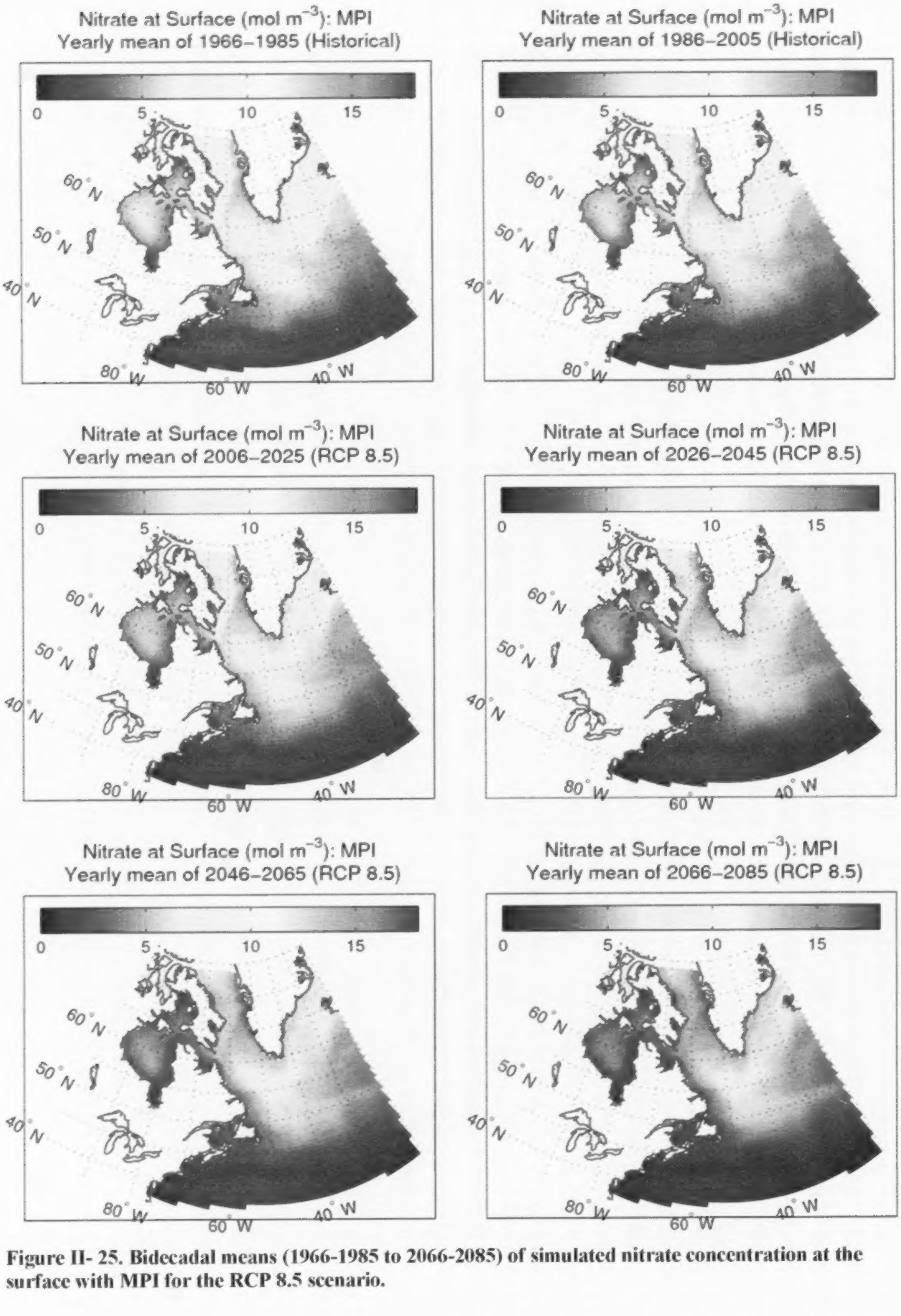

Nitrate at Surface (mol m^{-3}): MPI Yearly mean of 1966–1985 (Historical)

Nitrate at Surface (mol m^{-3}): MPI Yearly mean of 1986–2005 (Historical)

Nitrate at Surface (mol m^{-3}): MPI Yearly mean of 2006–2025 (RCP 8.5)

Nitrate at Surface (mol m^{-3}): MPI Yearly mean of 2026–2045 (RCP 8.5)

Nitrate at Surface (mol m^{-3}): MPI Yearly mean of 2046–2065 (RCP 8.5)

Nitrate at Surface (mol m^{-3}): MPI Yearly mean of 2066–2085 (RCP 8.5)

Figure II- 25. Bidecadal means (1966-1985 to 2066-2085) of simulated nitrate concentration at the surface with MPI for the RCP 8.5 scenario.

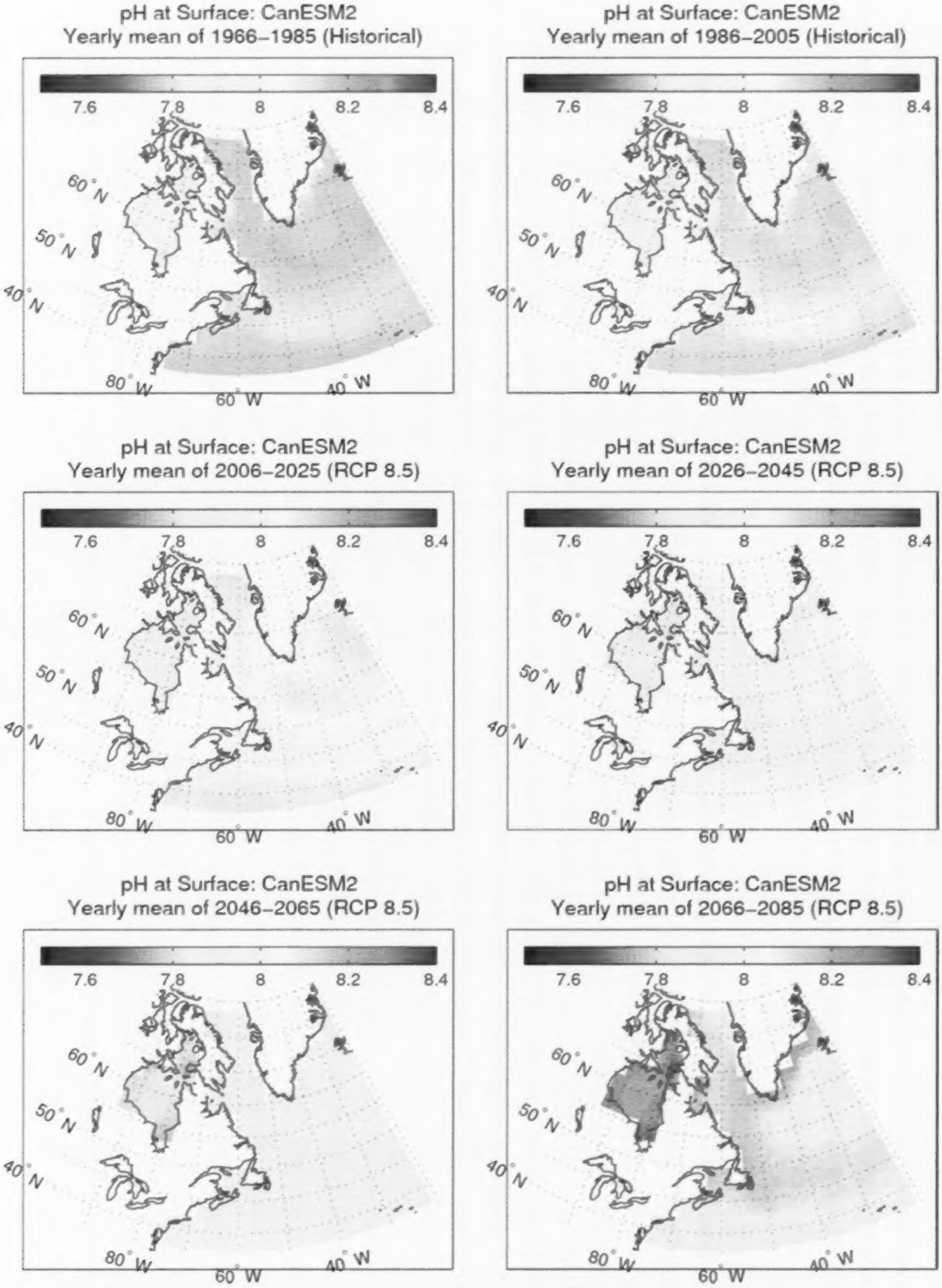
pH at Surface: CanESM2
Yearly mean of 1966–1985 (Historical)
pH at Surface: CanESM2
Yearly mean of 1986–2005 (Historical)
pH at Surface: CanESM2
Yearly mean of 2006–2025 (RCP 8.5)
pH at Surface: CanESM2
Yearly mean of 2026–2045 (RCP 8.5)
pH at Surface: CanESM2
Yearly mean of 2046–2065 (RCP 8.5)
pH at Surface: CanESM2
Yearly mean of 2066–2085 (RCP 8.5)
7.6
7.8
8
8.2
8.4
60° N
50° N
40° N
80° W
60° W
40° W

Figure II- 26. Bidecadal means (1966-1985 to 2066-2085) of simulated pH at the surface with CanESM2 for the RCP 8.5 scenario.

pH at Surface: GFDL
Yearly mean of 1966–1985 (Historical)

pH at Surface: GFDL
Yearly mean of 1986–2005 (Historical)

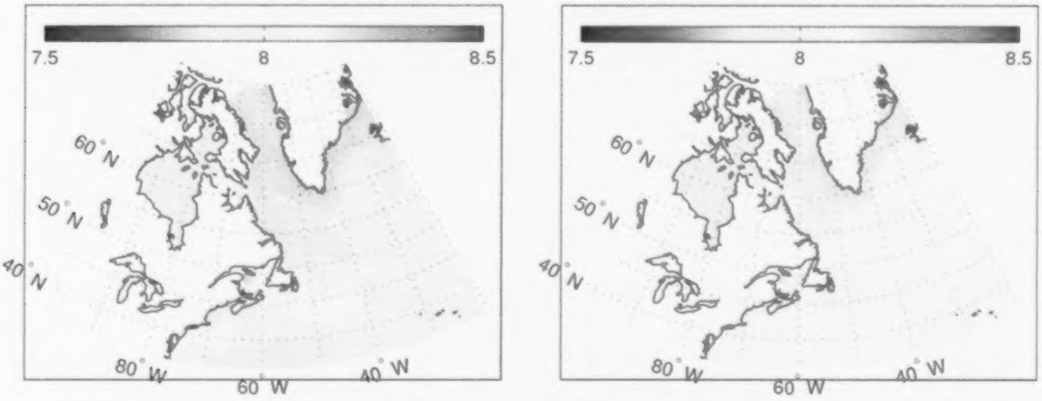
7.5
8
8.5
60° N
50° N
40° N
80° W
60° W
40° W
7.5
8
8.5
60° N
50° N
40° N
80° W
60° W
40° W

pH at Surface: GFDL
Yearly mean of 2006–2025 (RCP 8.5)

pH at Surface: GFDL
Yearly mean of 2026–2045 (RCP 8.5)

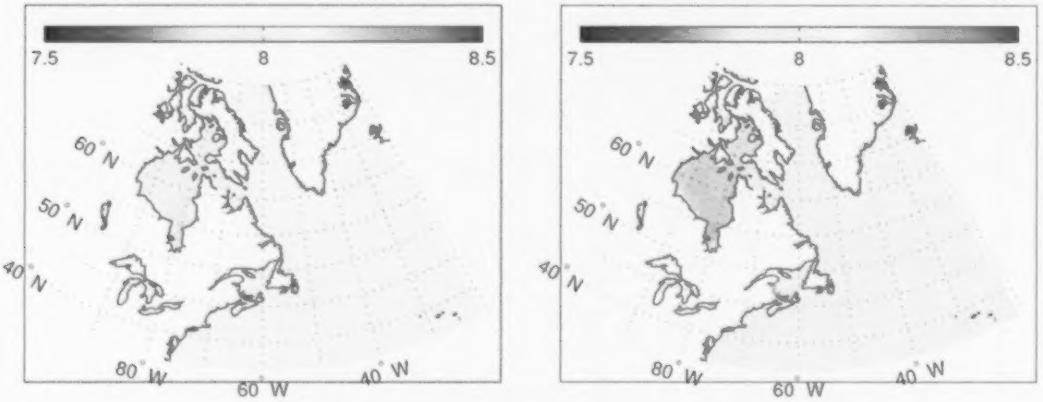
7.5
8
8.5
60° N
50° N
40° N
80° W
60° W
40° W
7.5
8
8.5
60° N
50° N
40° N
80° W
60° W
40° W

pH at Surface: GFDL
Yearly mean of 2046–2065 (RCP 8.5)

pH at Surface: GFDL
Yearly mean of 2066–2085 (RCP 8.5)

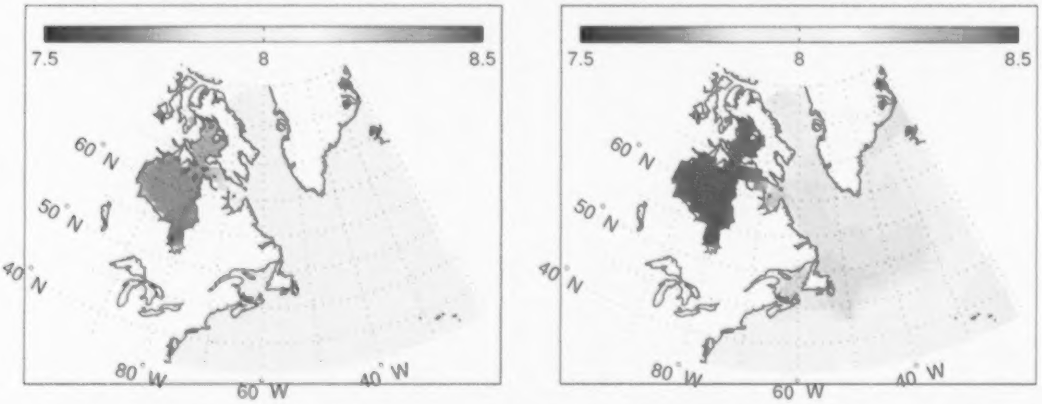
7.5
8
8.5
60° N
50° N
40° N
80° W
60° W
40° W
7.5
8
8.5
60° N
50° N
40° N
80° W
60° W
40° W

Figure II- 27. Bidecadal means (1966-1985 to 2066-2085) of simulated pH at the surface with GFDL for the RCP 8.5 scenario.

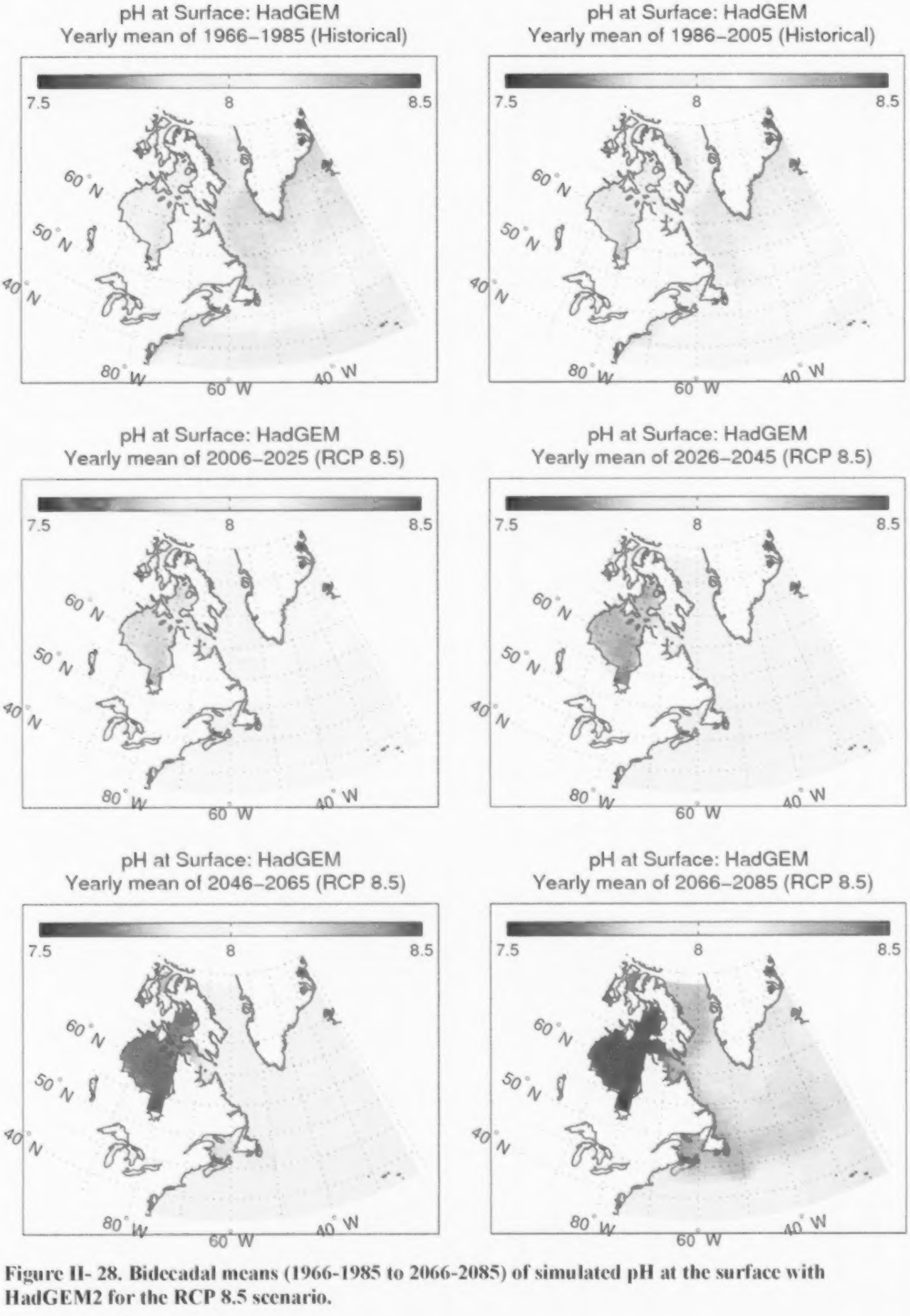
pH at Surface: HadGEM
Yearly mean of 1966–1985 (Historical)
pH at Surface: HadGEM
Yearly mean of 1986–2005 (Historical)
pH at Surface: HadGEM
Yearly mean of 2006–2025 (RCP 8.5)
pH at Surface: HadGEM
Yearly mean of 2026–2045 (RCP 8.5)
pH at Surface: HadGEM
Yearly mean of 2046–2065 (RCP 8.5)
pH at Surface: HadGEM
Yearly mean of 2066–2085 (RCP 8.5)
7.5
8
8.5
60° N
50° N
40° N
80° W
60° W
40° W

Figure II- 28. Bidecadal means (1966-1985 to 2066-2085) of simulated pH at the surface with HadGEM2 for the RCP 8.5 scenario.

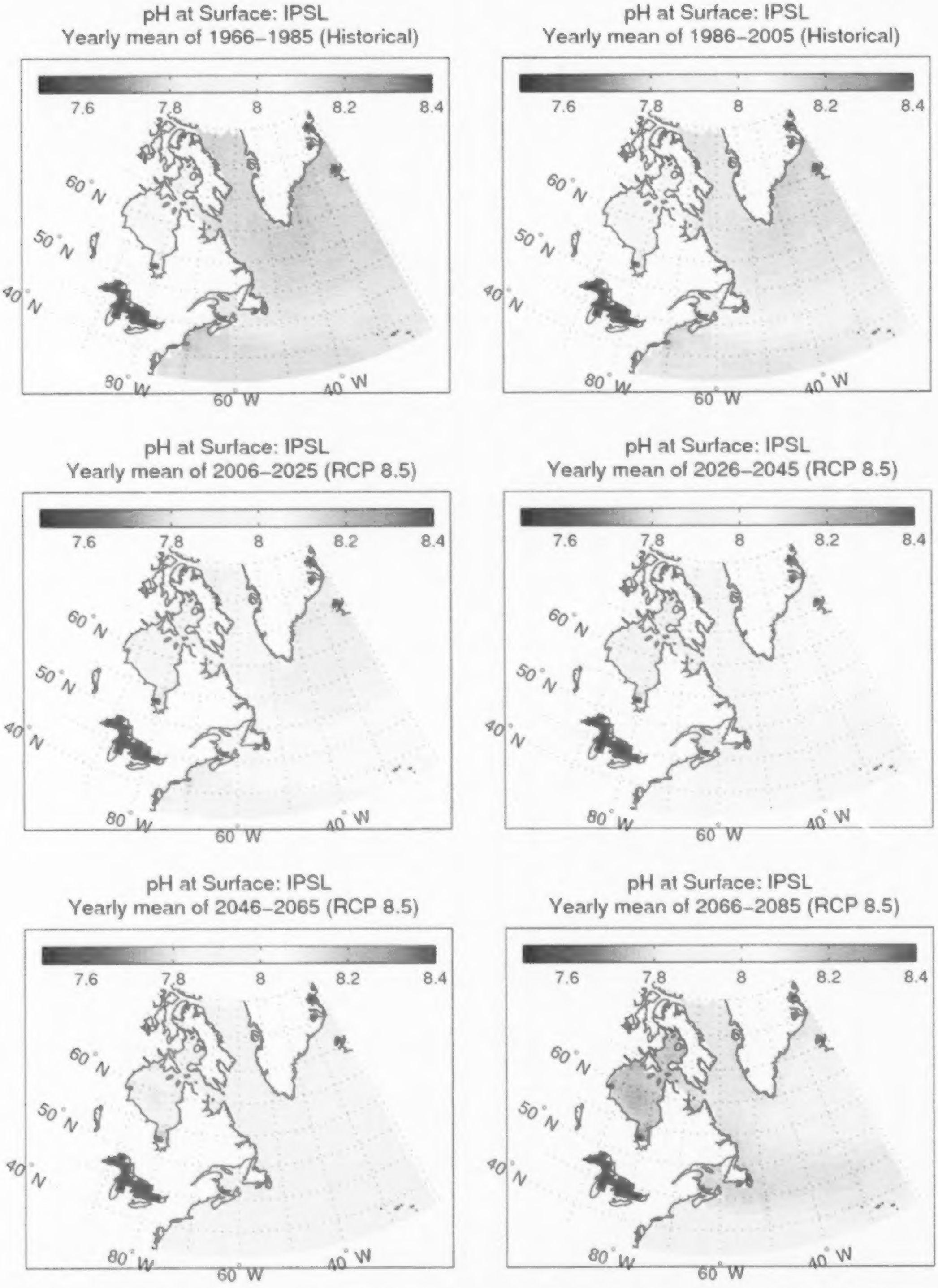

pH at Surface: IPSL
Yearly mean of 1966–1985 (Historical)

pH at Surface: IPSL
Yearly mean of 1986–2005 (Historical)

pH at Surface: IPSL
Yearly mean of 2006–2025 (RCP 8.5)

pH at Surface: IPSL
Yearly mean of 2026–2045 (RCP 8.5)

pH at Surface: IPSL
Yearly mean of 2046–2065 (RCP 8.5)

pH at Surface: IPSL
Yearly mean of 2066–2085 (RCP 8.5)

Figure II- 29. Bidecadal means (1966-1985 to 2066-2085) of simulated pH at the surface with IPSL for the RCP 8.5 scenario.

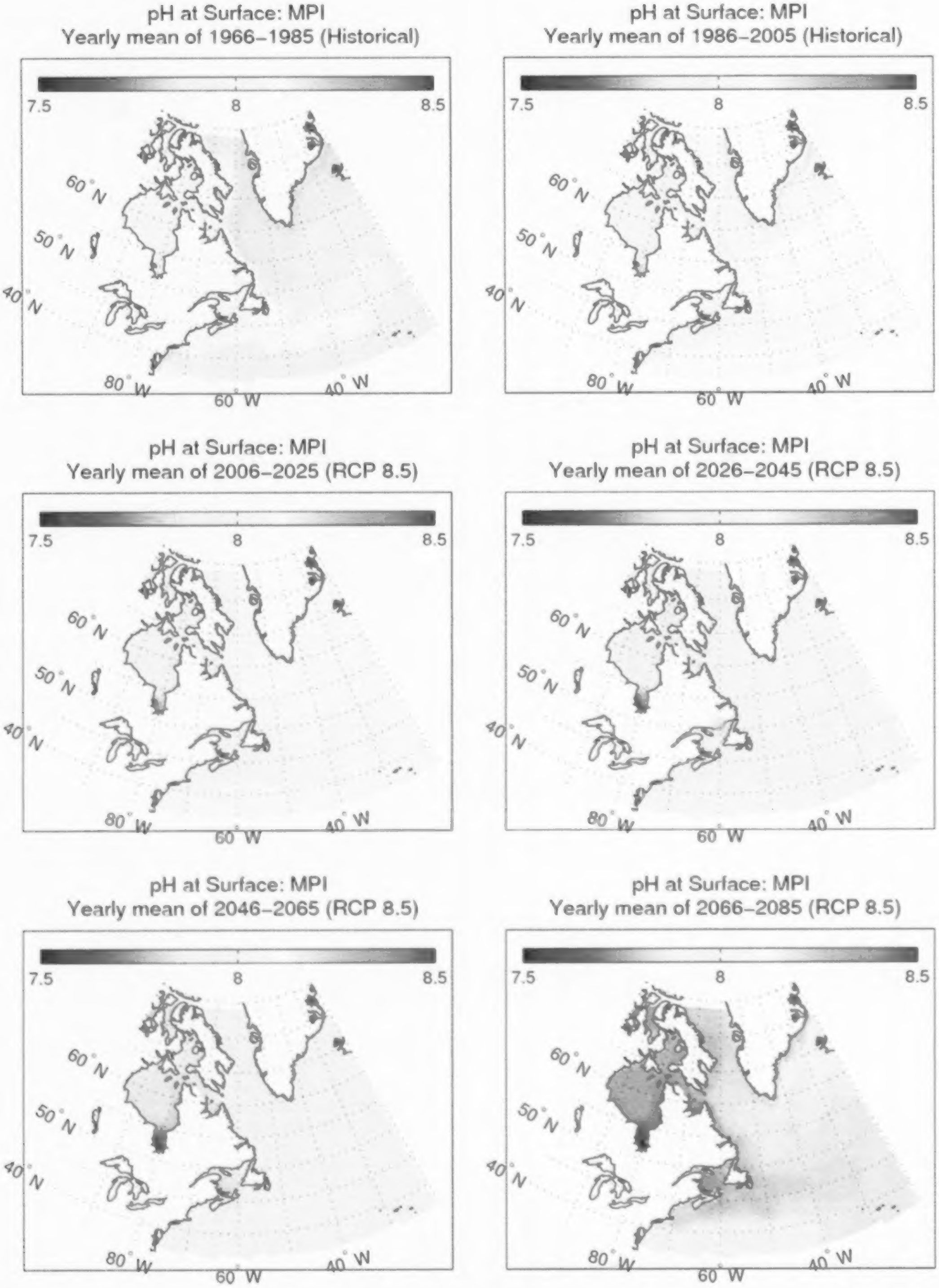

pH at Surface: MPI
Yearly mean of 1966–1985 (Historical)

pH at Surface: MPI
Yearly mean of 1986–2005 (Historical)

pH at Surface: MPI
Yearly mean of 2006–2025 (RCP 8.5)

pH at Surface: MPI
Yearly mean of 2026–2045 (RCP 8.5)

pH at Surface: MPI
Yearly mean of 2046–2065 (RCP 8.5)

pH at Surface: MPI
Yearly mean of 2066–2085 (RCP 8.5)

Figure II- 30. Bidecadal means (1966-1985 to 2066-2085) of simulated pH at the surface with MPI for the RCP 8.5 scenario.

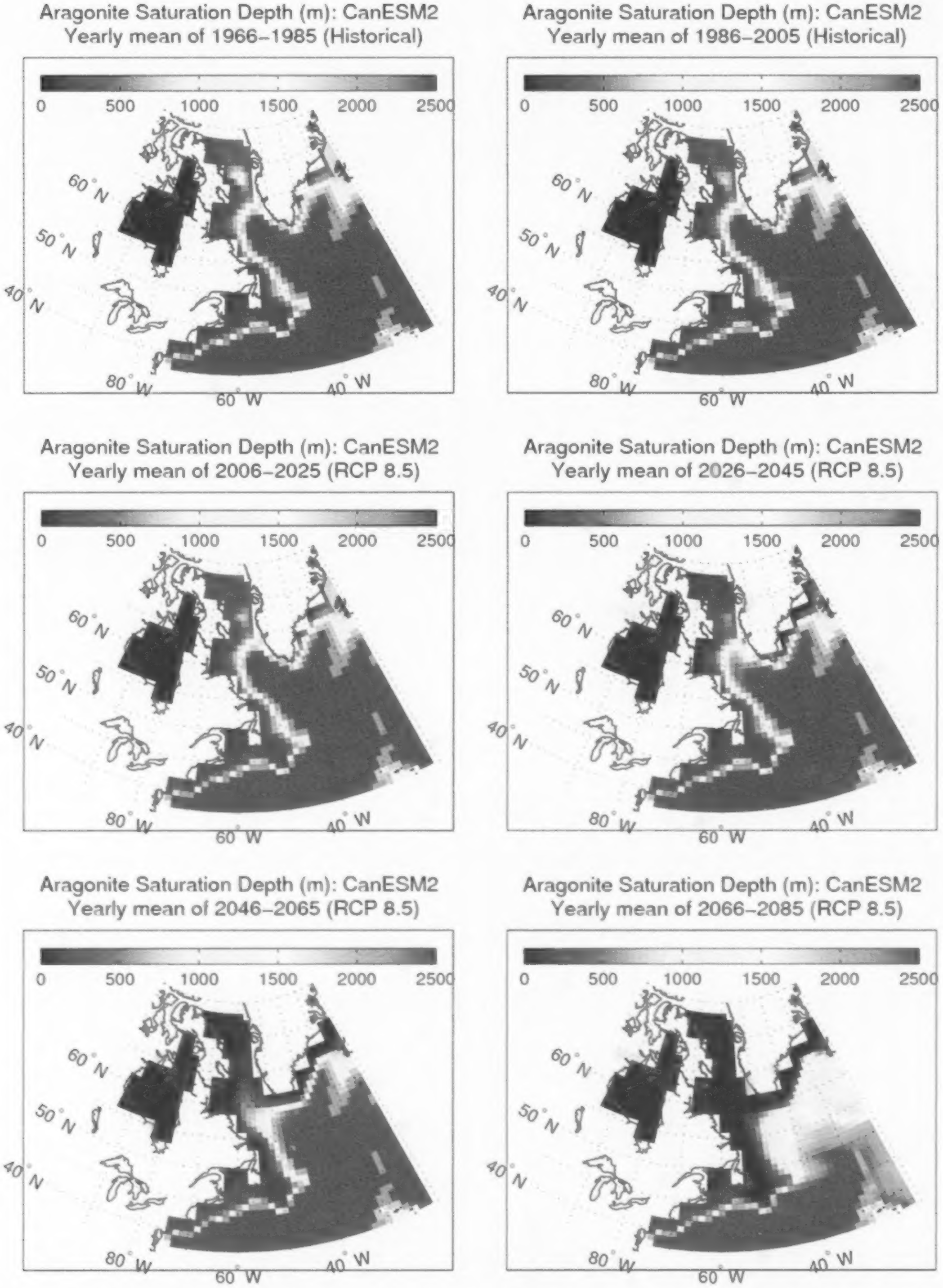
Aragonite Saturation Depth (m): CanESM2
Yearly mean of 1966–1985 (Historical)
Aragonite Saturation Depth (m): CanESM2
Yearly mean of 1986–2005 (Historical)
Aragonite Saturation Depth (m): CanESM2
Yearly mean of 2006–2025 (RCP 8.5)
Aragonite Saturation Depth (m): CanESM2
Yearly mean of 2026–2045 (RCP 8.5)
Aragonite Saturation Depth (m): CanESM2
Yearly mean of 2046–2065 (RCP 8.5)
Aragonite Saturation Depth (m): CanESM2
Yearly mean of 2066–2085 (RCP 8.5)
0
500
1000
1500
2000
2500
60° N
50° N
40° N
80° W
60° W
40° W

Figure II- 31. Bidecadal means (1966-1985 to 2066-2085) of aragonite saturation horizon depth with CanESM2 for the RCP 8.5 scenario.